Evolutionary Many-Objective Optimisation for Pathfinding Problems

DISSERTATION

zur Erlangung des akademischen Grades

Doktoringenieur (Dr.-Ing.)

angenommen durch die Fakultät für Informatik
der Otto-von-Guericke-Universität Magdeburg

von Jens Weise, M.Sc.

geb. am 05.04.1990 in Magdeburg

Gutachterinnen/Gutachter

Prof. Dr.-Ing. habil. Sanaz Mostaghim
Prof. Dr. Kalyanmoy Deb
Prof. Dr. Pascal Kerschke

Eingereicht am: 14.10.2022
Verteidigt am: 06.02.2023

Magdeburg, den 02.03.2023

Weise, Jens:
Evolutionary Many-Objective Optimisation for Pathfinding Problems
Dissertation, Otto von Guericke University
Magdeburg, 2022.

Für meinen Opa, der immer an mich glaubte und zu früh von uns ging,
um diese Worte zu lesen.

Abstract

It has always been challenging to determine a path across an area or within a medium — whether on a road map for route planning, in a 3D CAD model to generate wire paths, or by surgeons on medical scans for treatment planning. In such scenarios, a decision-maker must consider multiple objectives simultaneously to make an informed decision. In multi-objective optimisation, several objectives are considered, and a set of solutions is produced. Such problems can have large search spaces, as they typically consider a well-defined data structure representing the connections between entities. Classic exact optimisation approaches can result in relatively long computation times. To counteract this, metaheuristics, such as evolutionary algorithms, can generate good solutions in a reasonable time. However, pathfinding problems can be deceptive, resulting in relatively poor performance when using such methodologies. This thesis addresses the optimisation of many-objective pathfinding problems using evolutionary algorithms.

In the related literature, several works on multi-objective pathfinding problems have been proposed. They are outlined and categorised in this thesis. Furthermore, various techniques accounting for different aspects of pathfinding optimisation problems have been addressed by other authors. Yet in many works, only specific use-case tailored problems have been considered, with specialised environments.

This thesis proposes methodologies to generate variable and scalable pathfinding benchmark problems and techniques to improve the optimisation process. The result is an increased quality of solutions. The benchmark generator was developed using real-world knowledge and can be employed by the research community to evaluate new algorithms. The techniques to improve the optimisation can be divided into two parts. First, various approaches to represent pathfinding problems for optimisation algorithms are proposed. Second, new techniques that can be used with existing algorithms to increase the quality and maintain the diversity of the solution set are presented. The results show an improvement in the solution set's quality.

Furthermore, this thesis addresses the challenge for decision-makers to choose one solution among many that are all Pareto-optimal. Approaches to identifying interesting paths are presented and evaluated, based on a real-world road network. The results indicate that computing sets of various alternatives or robust solutions can be helpful for human decision-makers in real life.

Zusammenfassung

Es war schon immer eine Herausforderung, einen Weg über ein Gebiet oder innerhalb eines Mediums zu bestimmen - sei es auf einer Straßenkarte zur Routenplanung, in einem 3D-CAD-Modell zur Erstellung von Drahtwegen oder von Ärzten auf medizinischen Scans zur Behandlungsplanung. In solchen Szenarien muss ein Entscheidungsträger mehrere Ziele gleichzeitig berücksichtigen, um eine fundierte Entscheidung zu treffen. Bei der multikriteriellen Optimierung werden mehrere Ziele berücksichtigt, und es wird eine Reihe von Lösungen erstellt. Solche Probleme können große Suchräume haben, da sie typischerweise eine wohldefinierte Datenstruktur berücksichtigen, die die Verbindungen zwischen den Einheiten darstellt. Klassische exakte Optimierungsansätze können zu relativ langen Berechnungszeiten führen. Um dem entgegenzuwirken, können Metaheuristiken, wie z. B. evolutionäre Algorithmen, in angemessener Zeit gute Lösungen erzeugen. Pfadfindungsprobleme können jedoch trügerisch sein, was zu einer relativ schlechten Leistung beim Einsatz solcher Methoden führt. Diese Arbeit befasst sich mit der Optimierung von multikriteriellen Pfadfindungsproblemen durch evolutionäre Algorithmen.

In der einschlägigen Literatur sind mehrere Arbeiten zu multikriteriellen Wegfindungsproblemen vorgeschlagen worden. Sie werden in dieser Arbeit beschrieben und kategorisiert. Darüber hinaus haben sich andere Autoren mit verschiedenen Techniken befasst, die unterschiedliche Aspekte von Pfadfindungsoptimierungsproblemen berücksichtigen. In vielen Arbeiten wurden jedoch nur auf bestimmte Anwendungsfälle zugeschnittene Probleme mit speziellen Umgebungen berücksichtigt.

In dieser Arbeit werden Methoden zur Erzeugung variabler und skalierbarer Pfadfindungs-Benchmark-Probleme und Techniken zur Verbesserung des Optimierungsprozesses vorgeschlagen. Das Ergebnis ist eine höhere Qualität der Lösungen. Der Benchmark-Generator wurde unter Verwendung von Wissen aus der Praxis entwickelt und kann von der Forschungsgemeinschaft zur Bewertung neuer Algorithmen eingesetzt werden. Die Techniken zur Verbesserung der Optimierung können in zwei Teile unterteilt werden. Erstens werden verschiedene Ansätze zur Darstellung von Pfadfindungsproblemen für Optimierungsalgorithmen vorgeschlagen. Zweitens werden neue Techniken vorgestellt, die mit bestehenden Algorithmen verwendet werden können, um die Qualität zu er-

höhen und die Vielfalt der Lösungsmenge zu erhalten. Die Ergebnisse zeigen eine Verbesserung der Qualität der Lösungsmenge.

Darüber hinaus befasst sich diese Arbeit mit der Herausforderung für Entscheidungsträger, eine Lösung unter vielen zu wählen, die alle Pareto-optimal sind. Es werden Ansätze zur Identifizierung interessanter Pfade vorgestellt und anhand eines realen Straßennetzes bewertet. Die Ergebnisse zeigen, dass die Berechnung von Gruppen von verschiedenen Alternativen oder robusten Lösungen für menschliche Entscheidungsträger im Alltag hilfreich sein kann.

"This Is The Way."
THE MANDALORIAN, IN THE MANDALORIAN

Contents

1 Introduction

1.1 Motivation

Pathfinding is one of the most challenging tasks for humans. Since the first explorers set foot on highly unpredictable terrain to the highly detailed maps today, finding the best route between two points has always been equivalent to an optimisation problem. Pathfinding becomes even more difficult when travellers must choose between several options because they have more than one objective to accomplish. Pathfinding is used in many industrial applications with complex requirements as well as in private route planning. Logistics such as delivery services, ambulances, postal services, and other services that use road maps to plan their routes all have specific requirements. For example, animal transports may use routes with relatively few curves to reduce stress on the animals. For ambulances, routes and pathways must be resilient to unexpected events. Pathfinding is not only performed on road maps that show street networks but also in various other applications, such as the automobile industry or the medical field. For example, a doctor may plan a path from the outside of the body to the cancerous cells for liver ablation or other tumour interventions. Typically, the physician makes an educated guess as to where to insert the needle. The methods we develop in this thesis provide an approach to personalised path-planning that can help doctors select the optimal path for surgery or can enable decision-makers (DMs) to locate alternative solutions when planning their routes in logistic applications. It is common for an industry to optimise a route or path based upon several objectives. However, a DM usually establishes a specific weighting of the objectives, based on their experience, yielding a single optimal path. In evolutionary multi-objective optimisation, a number of objectives are simultaneously optimised, resulting in a set of possible alternative solutions.

In pathfinding applications, multi-objective optimisation methods can be applied. Such problems can be considered NP-hard, i.e., not solvable by an algorithm in polynomial time. Although this might not be an issue for small-scale problems and exact algorithms can be used, time is precious and waiting for a result can be costly. The dimensionality of multi-objective optimisation problems is high, resulting in long times to finish an optimisation.

To provide suboptimal solutions in a reasonable time, evolutionary algorithms (EAs) have proven useful. Results can be obtained early that give good insights regarding a problem for a DM. A second advantage of metaheuristics like evolutionary algorithms is their anytime property, which means that the algorithms can be halted at any time and results can be obtained. To see results with exact methods, the optimisation process usually must complete. It is also for this reason that EAs are appropriate for solving multi-objective pathfinding problems. The DM is always able to obtain intermediate results and can see how the optimisation process is proceeding.

In addition, from a real-world perspective, there are several applications that can benefit from pathfinding algorithms to identify more interesting and better solutions [CZKZ22]. We outline a subset of them here.

We also provide different methodologies for pathfinding used in several applications; thereafter, we evaluate and examine those methods.The first and best-known application is pathfinding on road networks. These networks are typically hierarchical [Gei08], which is used by speed-up techniques such as hub-labelling. The second application is pathfinding in medical treatments.

From an abstract point of view, these applications are different but have similarities. While the pathfinding on road networks considers a two-dimensional (2D) space, pathfinding in medical application scales to three dimensions (3D), which increases the complexity of the search space. One of the goals of this thesis is to find generally applicable methods which can be used in several applications. In the following section, we describe the two applications.

1.1.1 Road networks

Pathfinding algorithms are commonly used with road networks. Several companies provide pathfinding (or route planning) services based on the world's street network. A road network is composed primarily of streets and intersections. It can be represented as a graph by making each node represent an intersection (or address) in the network, linked to other intersections by edges which represent the streets. Moreover, typical road networks have a hierarchy since they are constituted of different road types. In Figure 1.1, the hierarchy derived from the speed and movement of traffic and access to property is depicted. These characteristics can be exploited in pathfinding algorithms. In road networks, pathfinding is typically used to determine a route from one address to another. It is possible to restrict the pathfinding methods by accessing only certain types of roads. A goal is often not merely an arbitrary path but rather the shortest route. When the term *shortest* is used, it usually refers to the shortest distance or the shortest time needed to traverse a graph.

In marine vessel logistics, waterways are used instead of roads. In this field, navigation and route planning are essential. However, maritime route planning is a problem consisting of a well-defined network of waterways as well as a grid which separates the ocean into distinct areas. Waterways do not exist in the oceans, which are rather a surface to be navigated. Graphs are used as a representation for waterways, and grids are used to represent oceans for vessel routing.

1.1.2 3D Pathfinding

It is necessary to plan routes from one place to another in numerous industries, including aviation. Vehicles of this type move in a space that can be divided into

Figure 1.1: Road Hierarchy

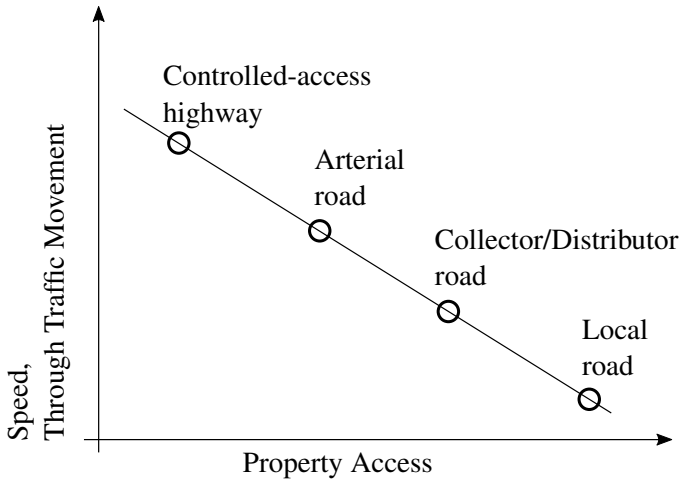

a 3D grid and can be represented as a graph. If one considers the atmosphere of the earth as an example, depending on the grid's resolution (i.e., the size of the grid cells), there could be many grid cells. The number of cells in the graph can be reduced by applying techniques such as *octrees*, which reduces the number of nodes in the graph by sacrificing some accuracy.

Moreover, 3D pathfinding can be beneficial for other applications, such as the routing of wires through mechanical objects. Examples include cars and other mechanically engineered objects which require wiring harnesses.

1.1.3 Coverage Path Planning

Pathfinding techniques can help with coverage path planning. In this task, it is vital to maintain a path that passes over all the points of interest in an area, while avoiding obstacles [GC13].

1.1.4 Medical Applications

This application must be divided into two separate sub-applications. These are derived from the actual medical treatments.

Needle-based Percutaneous Intervention

The first treatment involves a needle-based percutaneous procedure. An ablation treatment or biopsy can be performed using a relatively rigid needle inserted into the body. It is possible to perform a biopsy or ablation in order to examine or treat cancerous cells. It is essential to perform pathfinding to locate an appropriate spot on the skin and the appropriate angle at which to insert the needle. The path in this case refers to the path leading from the outside of the body to the treatment area.

Catheterisation

In the second treatment, a catheter (which is a small tube of medical-grade material) is inserted into the body to support specific tasks, such as draining fluids or performing special operations during surgery. For instance, cardiac or coronary catheterisation is a procedure that can be used for treating myocardial infarctions (heart attacks). In this case, pathfinding can determine a possible route from the outside of the body, through the vessel systems, to the point of interest where the obstruction occurred.

The above two use-cases share the same foundation, namely voxel data from medical imaging techniques such as computed tomography scans (CT) or magnetic resonance imaging (MRI). Once raw data has been acquired, it is preprocessed and segmented. Organs and other structural elements within the data can be extracted and labelled through segmentation. Because of their grid-like structure, voxels can be converted into a 3D lattice graph. Following this step, each voxel is represented as a node which is connected to its six neighbours using edges. It is possible to label each node with the specific tissue type by segmenting the data prior to analysis. The labelled lattice graph can then be used for pathfinding within tissue.

At present, pathfinding methodologies differ for each sub-application. The different methods affect the underlying graph used to compute the paths.

1.1.5 Manufacturing

In the field of manufacturing, many applications benefit from pathfinding methodologies using graphs. For instance, 3D CAD models can be represented as a graph while searching for disassembly, or assembly sequences can be performed using a pathfinding algorithm [WBM18]. Furthermore, finding possible ways for wires and harnesses through a 3D CAD model using a graph-based shortest path technique can support engineers [WBM19]. Identifying functional groups in a CAD model is another application of pathfinding. For each of these problems, multiple objectives are usually considered by the engineer or DM.

1.2 Research Goals and Questions

This thesis assesses and develops methodologies for the multi-objective pathfinding problem in several aspects. Analysis of the various applications indicates that each of them can be represented by a graph, i.e., a data structure to store information about how entities are interconnected. Such entities can be road intersections or blood vessel branches and junctions. In addition, neighbourhood relationships in a CAD model can be expressed with such a structure. It is independent of but does not exclude geometrical or geographical information, and it can represent complex relations. In this thesis, we focus on using such structures to encode a pathfinding problem.

In previous studies, often only three objectives have been considered, regardless of the underlying methodology, such as exact methods or evolutionary algorithms. In reality, problems can have more than three objectives. Additionally, current methodologies often do not consider the objective functions commonly encountered in the real world but use specific well-defined continuous benchmark functions. In this thesis we investigate the Many-Objective (Single-Path) Pathfinding Problem (MaOPF), which is a problem of finding a set of Pareto-optimal paths in a graph concerning more than three objectives. There is little research on the topic of MaOPF, a gap this thesis addresses through meta-heuristics (i.e., evolutionary algorithms). We next describe the goals (G1–G5) of this thesis and the research questions (RQs).

The goals of this thesis are defined as follows and result in five research questions, which are described afterwards:

G 1 Review of state-of-the-art approaches

G 2 Define a scalable and variable test problem to evaluate algorithms for MaOPFs

G 3 Assess representation schemes of the MaOPF

G 4 Develop new methodologies to improve the performance of optimisation algorithms for pathfinding problems

G 5 Evaluate the proposed techniques

The goals listed here also provide a broad outline of this thesis. To achieve these goals, we worked on the following research questions, which arose from the research and corresponding challenges regarding evolutionary many-objective optimisation methods for pathfinding. As a first question, related work is of concern but also whether methodologies from the single-objective domain can increase the performance of multi-objective techniques.

RQ 1 Which techniques exist to solve the MaOPF?

- RQ 1.1 Which environmental classes are used and how do they differ?
- RQ 1.2 Which state-of-the-art algorithms are used in the respective environments?
- RQ 1.3 Can single-objective speed-up techniques be used to support a multi-objective approach?

In this thesis, we develop strategies for the many-objective pathfinding problem. Furthermore, we study different evolutionary operators and search strategies. We modify existing methods and develop new techniques to cope with the identified challenges of such problems and to explore and exploit the search spaces more efficiently.

A question that arises when designing an algorithm for a specific problem is the representation of the problem and its solutions. When using genetic algorithms in particular, the choice can strongly influence the performance. Therefore, we address the following research question:

RQ 2 Is there a significant difference between using problem and solution tailored representations rather than standard encodings?

In addition to the encoding schemes, another aspect to consider when developing methodologies to solve the problem is that the new technique should work well on a variety of similar problems. Therefore, it is necessary to have a well-known test problem to compare different approaches. In this regard, the following research questions were addressed:

RQ 3 How should a scalable and variable benchmark test problem be designed to cover a wide variety of pathfinding problems?

- RQ 3.1 Which real-world related objectives should be considered in the test problems?

A key question is how optimisation can be improved to obtain better results, possibly in less time. A specific characteristic of the MaOPF is that its solutions are actual paths that are eventually traversed by a robot, car or any other entity or

object. The actual expression of a path is of great interest. Furthermore, a large diversity of possible options is beneficial for a DM. Therefore, we concentrate on analysing the geometrical and physical characteristics of a path and thus address the following questions:

RQ 4 How can the geometrical properties of a path be assessed?

RQ 4.1 How can differences from other paths be measured?

RQ 5 How can these properties be exploited for the optimisation process?

RQ 6 Can such properties be used to increase the diversity of the resulting solution set?

A new technique or approach must be evaluated to assess its quality. However, when multiple solutions are presented to a DM, the number of options should be reduced so as not to overwhelm them and to support the decision process. With a large network and with numerous objectives, the number of Pareto-optimal solutions tends to increase. A human DM might be unable to comprehend such a high number. Therefore, we aim to develop and evaluate methodologies to find interesting solutions without sacrificing the diversity of the proposed solution set. Furthermore, we introduce the concept of decision points (DPs). Hence, in addition to the previous questions, the following questions are also of interest:

RQ 7 What performance indicator (PI) can be used to evaluate the algorithm's performance?

RQ 8 How to reduce the number of solutions that are presented to a decision-maker?

In this thesis, we aim to answer these questions. Hence, the findings and new methodologies should enable planners, engineers and similar professionals to find better and more diverse solutions to their problems.

1.3 Structure of the Thesis

This thesis is structured as follows. In Chapter 2, we discuss the relevant scientific fundamentals on topics such as graph theory and EAs. In Chapter 3, RQ 1 is addressed, and we describe related works on the topic of multi-objective optimisation for pathfinding problems and their relevant solution approaches. Furthermore, we identify and summarise characteristics of the works. Different aspects of the pathfinding problem and related techniques are covered. A benchmark suite for the proposed problem is presented in Chapter 4, where RQ 3 is addressed. We propose how a scalable and variable test problem can be generated that incorporates several properties of real-world problems. Chapter 5 addresses RQ 2 and describes the various representations for pathfinding problems. In the same chapter, we present several methodologies for the initial solution generation and how multi-objective techniques can benefit from single-objective speed-up approaches. New methodologies in terms of diversification in the decision space during the search are described in Chapter 6, which addresses RQ 4, RQ 5, and RQ 6. At the end of each chapter, we present an evaluation of the proposed methodologies. To support a DM, in Chapter 7 we address RQ 8 and present techniques to find interesting path solutions. The chapter

also proposes methodologies for reducing the resulting solution set. Moreover, we define DPs. Although RQ 7 is partially addressed in Chapter 2, Chapter 7 covers another crucial aspect of this question with a focus on decision-making. The conclusion of this thesis is given in Chapter 8, and promising future work is covered in Section 8.3.

Due to the vast amount of experiments, we aggregated the results in the evaluations to determine which algorithm outperformed its competitors. To save trees and the environment, we present the raw indicator values in an additional online appendix (Appendix B), which is not included in the printed version of this thesis. More information are presented in Appendix A.2.

2 Scientific Fundamentals

In this chapter, the following points are covered

- Background
- Mathematical definitions

In this chapter, the scientific background is introduced. We describe graph theory, which is used in our proposed approaches (Section 2.1), multi-objective optimisation in general (Section 2.2) and evolutionary optimisation specifically (Section 2.2.1). In Section 2.3.2, we present a holistic definition of the multi-objective pathfinding problem. In Section 2.4, basic principles of pathfinding are introduced. Path similarity measurement methodologies are described in Section 2.5, as they are used in several parts of this thesis. Finally, performance metrics are presented in Section 2.6, which are used to evaluate the quality of solutions. Furthermore, we present the basic concepts of decision-making and clustering techniques.

2.1 Graph Theory

Graphs are used to represent the relations between entities. A graph G consists of a set of vertices that are the representations of such entities and a set of edges that denotes the relations. An edge usually consists of an unordered or ordered set of two vertices. Formally, a directed graph G is a pair $G = (V, E)$, where V denotes the set of vertices and E is the set of edges, where $E \subseteq \{(n, n') \mid (n, n') \in V^2, n \neq n', n, n' \in V\}$. Note that E consists of two-element ordered subset of V^2, which renders a graph *directed*. In undirected graphs, by contrast, E consists of two-element unordered subsets of V^2 [Wil10b].

There are different types of graphs. In *simple graphs*, only one edge between two vertices is allowed, while multiple edges can exist in a *multigraph*. Furthermore, a graph can contain loops, which allow edges that join vertices to themselves.

In bipartite graphs, the vertices are divided into two subsets so that there is an edge from every node in a subset to any other node in the other, but no edge from one vertex to the other inside the subsets.

A hypergraph is a generalisation of a graph where edges can have an arbitrary number of nodes. For every hypergraph, there exists a corresponding graph.

A graph can also be weighted. This means a *weight* is assigned to each edge through a weight function $w : E \to \mathbb{R}$.

In this thesis, we work with specific types of graphs, namely directed or undirected and weighted graphs. We use the following definition of a graph: $G = (V, E, \phi)$, where V is the set of vertices, E is the set of edges, and ϕ is a function that maps every edge to a pair of vertices. Note that ϕ can refer to both a function mapping to ordered or unordered pairs of vertices, depending on the use-case and the available data. Hence, $\phi : E \to \{(n, n') \mid (n, n') \in V^2, n \neq n'\}$. The set notation is used in the case of unordered pairs and, therefore, undirected graphs. In a later section, we extend this definition to represent graph-based pathfinding problems.

There are several approaches to describing a *way* through a graph and thus also several different terms. In [Wil10a], a *walk* is defined as a finite or infinite sequence of edges that joins a sequence of nodes or vertices. Formally, a sequence of edges $(e_1, \cdots, e_{k-1})$ is a finite walk, if there is a sequence of nodes $(n_1, \cdots, n_k)$ with $\phi(e_i) = \{n_i, n_{i+1}\}$, $i = 1, \cdots, k-1$. It is also called the node sequence of the walk. If $n_1 = n_k$, it is a closed walk and an open walk otherwise. In an infinite walk, there is no first and no last node. There are also *trails* that are walks containing only distinct edges and *paths* with distinct edges and nodes. However, several authors do not apply the definitions strictly and simply refer to a *path*, although it may not have a distinct node set [Wil10a].

2.1.1 Properties

The following section is largely based on the publication [WBM18].

A graph structure has several properties, which are outlined as follows.

Direction A graph structure is called directed if the graph's edges have an orientation. It is defined as $G = (V, E)$, where V is the set of nodes and E is a set of ordered pairs of nodes. Directed graphs have ordered pairs of nodes, while undirected graphs have unordered pairs (see above).

Node Degree A node's degree indicates how many connections a node has to other neighbouring nodes. This measure may be considered the most fundamental measurement of a graph [BS09], since several other properties are related to it; the algorithm's complexity is also linked to it. The degree distribution of a graph represents the degree of all nodes and is different in each use-case of a graph-based system (GBS).

Cycles A graph is a cycle if three or more nodes can be ordered such that there is an edge passing from one node to the next and from the last node to the first. Graphs can also contain cycles, which influences several algorithms. This applies to both directed and undirected graphs.

Planarity A planar graph is a graph which can be drawn without intersecting edges. Boyer and Myrwold introduced an $\mathcal{O}(n)$ algorithm to determine the planarity of a graph [BM04]. Often, road networks can be represented as planar graphs. However, bridges or underpasses can render the graph non-planar.

Completeness In a complete graph, there is an edge from each node to every other node. Hence, all possible edges are included in the set of edges.

Connectivity Two unordered nodes are connected if there is a path from one to the other. An undirected graph is connected if there is a path of any node to any other node in the graph. Otherwise, the graph is a disconnected graph. The graph's connectivity in directed graphs is divided into strongly and weakly connected graphs. A pair of ordered nodes is connected if there is a directed path from one node to the other. It is weakly connected if directed edges are replaced with undirected and a path exists. In a strongly connected graph, this applies to all ordered pairs of nodes. Hence for a weakly connected graph it holds when replacing directed edges with undirected edges.

Centrality A node's centrality represents the importance of the node in a network, e.g., how likely it is that information will be transferred through that node when traversing the graph. There are several types of centrality, which have different measurements. The first is degree centrality, which indicates each node's degree. In a directed graph there is an in-degree and an out-degree centrality. Another type is the betweenness centrality, which indicates how many times a node lies on the paths between two other nodes [Fre77]. The closeness centrality indicates the average of the shortest path's length between the node and any other node inside the graph [Sab66].

2.1.2 Methods and Algorithms

This section provides a short overview of the existing methodologies and algorithms designed to extract features or analyse certain properties in graphs.

Pattern Matching and Recognition Pattern matching algorithms find predefined specific patterns in a given data set. The aim of pattern recognition is to find unknown patterns in a data set.

Labelling Labelling is usually a function which maps the nodes or edges to a set of labels. Labels are used to categorise nodes into classes or to further analyse a network structure. An example of graph labelling is graph colouring, where a colour is assigned to every node such that two adjacent nodes do not have the same colour. Use-cases for graph colouring are scheduling problems, where jobs can be executed in parallel but some jobs share the same resources. Two jobs which use the same resource may be connected by an edge, and each execution process is represented by a colour. Graph colouring can be used in pattern matching and Sudoku solving [Lew16]. Furthermore, labelling techniques can be used in a preprocessing stage to speed up path queries in a graph.

Pathfinding Pathfinding algorithms are often executed to find the shortest path between two nodes; these are among the earliest use-cases of graph-based systems. One of the best-known shortest path algorithms is Dijkstra's algorithm, which finds optimal paths for two given nodes [Dij59]. The problem of single-objective shortest path calculation can be divided into four classes: *single-pair shortest path problem (SPP)*, where the objective is to find a shortest path

between two nodes; *single-source SPP*, in which all the paths from a given node must be found; *single-destination SPP*, where all the shortest paths from any node to a given node must be found and *all-pairs SPP*, in which all shortest paths for every pair of nodes must be found.

Clustering The main objective of clustering algorithms is to find groups of entities with a certain similarity or with a certain relationship to each other. There are several kinds of clustering algorithms. Examples include *hierarchical*, *representative-based*, *grid-based* and *density-based* algorithms [EC02].

2.2 Optimisation

Optimisation is the task of finding the best solution to a given problem. Exact approaches always result in the global optimum but require an exponential runtime for NP-hard problems. In addition to these approaches, heuristics are often problem-specific, whereas meta-heuristics can generate good solutions in an acceptable time frame. Usually, meta-heuristics can be applied to a variety of problems.

In this thesis, we use meta-heuristics, specifically evolutionary algorithms (EAs). Such meta-heuristic algorithms have often been inspired by biological processes which can be observed in nature. EAs are an instance of so-called population-based meta-heuristics. To find solutions, a population of different solutions is created and evolved during the optimisation process.

2.2.1 Evolutionary Algorithms

An EA is a type of algorithm which is used to generate solutions to optimisation problems. EAs are based on the principles of natural selection and evolution. Natural selection is the process by which organisms that are better adapted to their environment survive and reproduce, while those that are less adapted die off. This process leads to a gradual change in the characteristics of a population over time. EAs mimic the process of natural selection to find solutions to optimisation problems. EAs typically start with a population of size μ of randomly generated solutions, called chromosomes or phenotypes. These solutions are then evaluated according to a fitness function, and the fittest solutions are selected to produce the next generation of solutions; these are then evaluated again and selected, and so on. The process of selection and reproduction continues until a stopping criterion is met, such as a certain number of generations being reached, or a solution being found with a fitness that is good enough for the problem at hand.

EAs are used to solve a wide variety of optimisation problems, such as finding the shortest path between two points or the lowest energy state of a system. There are several types of EA, which differ in the way that solutions are represented and selected. The most common type of EA is the genetic algorithm (GA), which uses a representation called a chromosome. A chromosome can be a string of bits (ones and zeros) that represents a potential solution to the optimisation problem. Each bit corresponds to a particular decision that needs to be made to find the solution. For example, in the shortest path problem, each bit could represent a decision about which direction to turn at a junction. Other representations are possible and are discussed in Chapter 5.

Figure 2.1: Basic flow of an EA.

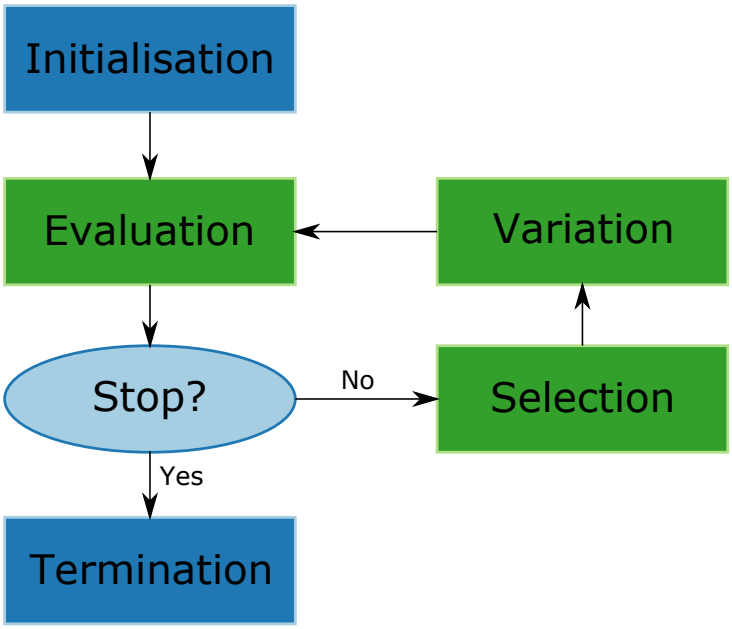

GAs work by selecting the fittest chromosomes from the current generation and producing a new generation of chromosomes through the process of crossover and mutation. Crossover is the process of combining two parent chromosomes to produce a child chromosome. For example, if the two parent chromosomes are 101101 and 100011, the child chromosome could be 101001. Mutation is the process of randomly changing the value of one or more bits in a chromosome. For example, if the chromosome is 101101, a mutation could change it to 101111. The process of selection, crossover and mutation is repeated until a solution with a fitness good enough for the problem at hand is found or a predetermined number of generations has been reached. Figure 2.1 illustrates the basic scheme of an EA.

EAs are powerful optimisation tools that can find solutions to problems that are difficult or impossible to solve using traditional methods. However, EAs are not perfect and there are several limitations, which need to be considered when using EAs. The first limitation is that EAs can only find a solution that is good enough, which is not necessarily the best possible solution. This is because the search space of possible solutions is too large to be searched exhaustively. The second limitation is that EAs can get stuck in local optima, which are regions of the search space where the fitness of the solutions is good, but not as good as it could be. This is because EAs often consider the immediate neighbours of a solution when exploiting the search space for better solutions. The third limitation is that EAs can be slow, particularly when the search space is large. This is because the process of selection, crossover and mutation can take a long time to converge on a good solution. Despite these limitations, EAs remain powerful optimisation tools that can be used to solve a wide variety of problems.

The principles of EAs imitate biological evolution. They are referred to as meta-heuristics, which include several other methods, including particle swarm optimisation and ant colony optimisation, which are biologically based. They also include classic processes such as simulated annealing, which originated in thermodynamic processes. It applies the principles of evolution, such as mutation and selection, to populations of candidate solutions to find a sufficiently good solution to any optimisation problem [KBB+16].

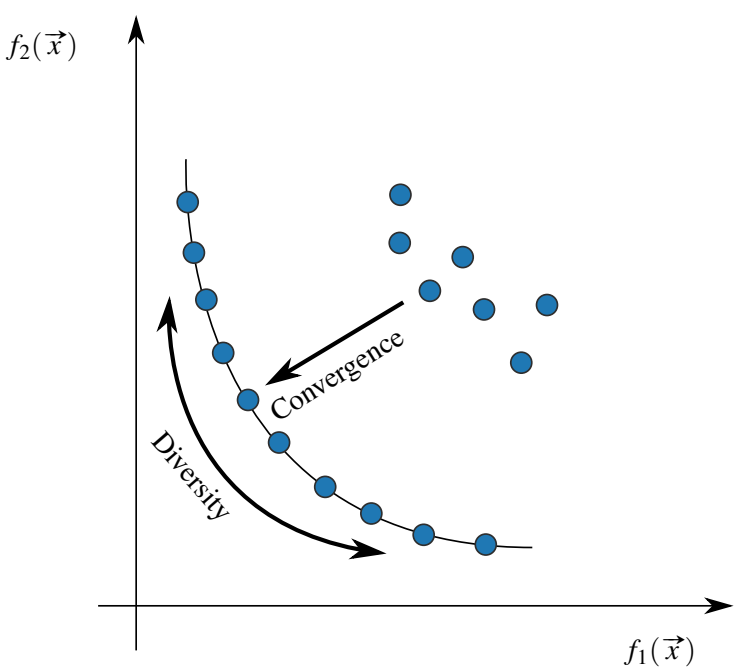

Figure 2.2: Diversity and Convergence of a population-based approach

2.2.2 Multi-objective Optimisation

Multi-objective optimisation (MOO) is the process of finding the best possible solution to a problem that has multiple conflicting objectives. In other words, it is the process of finding a solution that maximises or minimises multiple objectives simultaneously. MOO is a challenging problem because there is often no single *best* solution. Instead, there is a set of solutions, each of which is the best possible solution for a given set of objectives. The challenge in MOO is to find the best possible solution for the overall problem, not just for a specific set of objectives. MOO algorithms are designed to find the best possible solutions to a problem by searching through the space of all possible solutions. The search process is guided by a set of objectives, which are used to evaluate the quality of a solution. The most common type of MOO algorithm is the EA. EAs are a type of optimisation algorithm that uses a population of solutions, which are evolved over time through a process of selection, crossover and mutation. EAs are well suited to MOO because they can simultaneously optimise multiple objectives. EAs can also handle problems with many variables and constraints. MOO algorithms are used to solve a range of problems in fields such as engineering, economics and operations research. There are several MOO algorithms, each with its own strengths and weaknesses. The choice of algorithm depends on the specific problem being solved. MOO is a powerful tool for solving complex problems. However, MOO algorithms can be computationally expensive and they may not always find the best possible solutions [Deb11a, Gol89, Mic96].

In Figure 2.2 the two primary goals of MOO methodology are shown. The first goal is *convergence*, which is the or closeness to the true Pareto-front; the second is *diversity*, which is a measurement for how diverse and spread the solutions are along the Pareto-front.

Real-world problems often contain multiple conflicting objectives. The term *multi-objective problem (MOP)* for such problems has been used in the research community. Equation (2.1) shows a mathematical formulation.

In MOO one is confronted with several conflicting objectives $f_i(\vec{x}), i = 1, \cdots, m$ which are to be optimised (without loss of generality, we take minimisation):

$$\begin{aligned} Z: \quad & \min \vec{f}(\vec{x}) = (f_1(\vec{x}), f_2(\vec{x}), \ldots, f_m(\vec{x}))^T \\ & \text{s.t. } \vec{x} \in \Omega \end{aligned} \tag{2.1}$$

where $\vec{x}$ corresponds to a decision variable in n-dimensional feasible decision space Ω. The solution of this problem is a set of so-called Pareto-optimal solutions denoted by P. Pareto-optimality refers to a situation (or solution) where an objective value cannot be improved without worsening at least one other. The concept is used to introduce a partial ordering on a set of solutions to rank them. To compare two solutions, it must be determined if one of them *dominates* the other in the Pareto-sense, which is defined below. This is resolved by using the Pareto-dominance criteria, described in Equation (2.2). In Figure 2.3a an example is shown. It follows for the set of Pareto-optimal solutions that for each $\vec{x} \in P$, there is no other $\vec{y} \in \Omega$ which dominates $\vec{x}$ (denoted by $\vec{y} \prec \vec{x}$):

$$\begin{aligned} \vec{y} \prec \vec{x} : & f_i(\vec{y}) \leq f_i(\vec{x}), \forall i = 1, \cdots m \\ & f_j(\vec{y}) < f_j(\vec{x}), \exists j \end{aligned} \tag{2.2}$$

Hence, the solutions in P are all Pareto-optimal and indifferent from each other. Pareto-optimality is defined as follows:

$$\vec{x}^* \in \Omega \text{ is Pareto-optimal} \iff \nexists \vec{x} \in \Omega \mid \vec{x} \prec \vec{x}^* \tag{2.3}$$

These solutions are usually represented in the so-called decision space Ω (also called the *search space*), which represents the decision variables. The optimal solutions in this space construct the Pareto-set (PS). The image of these solutions in the objective space constitutes a Pareto-front (PF). Formally, the PS is defined as the set of all Pareto-optimal solutions:

$$\text{PS} := \{\vec{x} \mid \vec{x} \text{ is Pareto-optimal } \} \tag{2.4}$$

The PF is the set of points that is obtained by applying the objective function vector to a Pareto-optimal solution:

$$\text{PF} := \{\vec{f}(\vec{x}) \mid \vec{x} \in \text{PS}\} \tag{2.5}$$

The goal of MOO algorithms is to find several Pareto-optimal solutions which can provide a good representation of the Pareto-front.

In an MOP, the n-dimensional decision space Ω is mapped to the m-dimensional objective space $\mathscr{M}$. There are m fitness functions that compute the objective values of a solution. The optimisation of an MOP aims to minimise or maximise these functions simultaneously. Such fitness functions are also called objective functions. Chapter 5 presents different encoding schemes of the pathfinding problem, which change the definition of Ω. The decision space can be constrained to implement a feasibility measurement. In this thesis, the particular optimisation in the field of pathfinding problems is discussed. Therefore, we assume Ω to be a subspace of all possible paths from the start to the end points, denoted by $\mathbb{S}$. The space $\mathbb{S}$ can be further constrained by a number of inequali-

ties expressed by some function $\vec{g}(p)$, where p is a solution path. The decision vector $\vec{x}$ is, in the scope of this thesis, a path p; hence $p = \vec{x}$.

$$\begin{aligned}\mathbb{S} = \{p = (n_i, \cdots, n_k) \mid n_i \in V, i = (1, \cdots, k) \wedge \\ \exists \phi\,(e_{i,i+1}) = (n_i, n_{i+1}) \in E, i = 1, \cdots, k-1\}\end{aligned} \tag{2.6}$$

Equation (2.6) shows the mathematical definition of the search space. Therefore, $\Omega = \{p \in \mathbb{S} \mid \vec{g}(p) \leq 0\} \subseteq \mathbb{S}$. However, direct constraint handling is outside the scope of this thesis and is not addressed. Constraints in pathfinding problems are often set in the environment; furthermore, in this thesis we consider only minimisation problems.

Aside from the mentioned Pareto-dominance, other dominance criteria can be implemented, as follows. Figure 2.3 illustrates three such criteria.

ε-Dominance The ε-dominance introduces a factor $\varepsilon \in \mathbb{R}^{>0}$ which enlarges the area that is dominated by a solution. Applying it to a Pareto-front results in a set of ε-optimal alternatives with a limited number of solutions. Figure 2.3b shows a visual example, and it is defined as follows [PY00]:

$$\begin{aligned}\vec{y} \preceq_\varepsilon \vec{x} : f_i(\vec{y}) - \varepsilon_i \leq f_i(\vec{x}), \forall i = 1, \cdots, m \\ f_j(\vec{y}) - \varepsilon_j < f_j(\vec{x}), \exists j\end{aligned} \tag{2.7}$$

Cone-Dominance In [KWZ84], a cone-shaped domination relation is described. With such a relation, specific features of a Pareto-front can be found. For instance, solution candidates that are inferior to other solutions in one objective, yet non-dominated, can be dominated if cone-dominance is used [IKK01, BCGR11]. In other words, with cone-dominance, a cone (defined by an angle) defines the area that is dominated. Cone-dominance is also known as α-dominance. Figure 2.3c shows a visual example, and it is defined as follows (using angle φ):

$$\begin{aligned}\vec{y} \preceq_\alpha \vec{x} : \omega_i(\vec{y}) \leq \omega_i(\vec{x}), \forall i = 1, \cdots m \\ \omega_j(\vec{y}) < \omega_j(\vec{x}), \exists j\end{aligned} \tag{2.8}$$

where

$$\begin{aligned}\omega_i(\vec{x}) = f_i(\vec{x}) + \sum_{j=1, j\neq i}^{m} a_{ij} f_j(\vec{x}), i = 1, \cdots, m \\ a_{ij} = \tan \frac{\varphi - 90}{2}, \forall i, j, i \neq j\end{aligned} \tag{2.9}$$

An advantage of the cone-dominance relation is its ability to find knee-points [BDDO04] in a Pareto-front, which can be of great interest to DMs. The reason is that a neighbouring solution to the knee-point on the front often has an unfavourable trade-off [AD13, DG11].

Typically, problems with $m > 1$ are called multi-objective problems, whereas problem instances with $m > 3$ are called many-objective optimisation problems.

In many-objective optimisation, various challenges arise [DS05, GFPC09, ZZN+19]. One of them derives from the fact that as the number of objectives in-

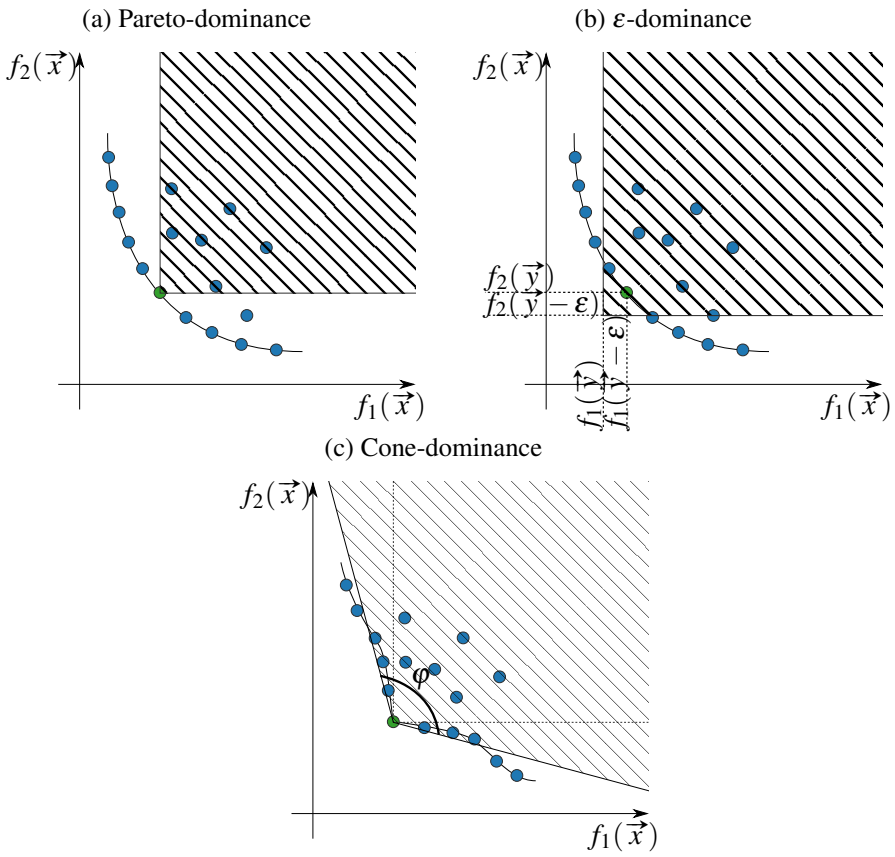

Figure 2.3: Different Dominance Relations

creases, so does the proportion of non-dominated solutions [Deb11b, GFPC09]. This characteristic makes methodologies based solely on Pareto-dominance less suitable for many-objective optimisation. It can happen that a large proportion of the solution set is non-dominated and focusing on those solutions is not beneficial to the search process as there is little room for new solutions [DJ14]. This is known as the loss of selection pressure [ZZN+19]. Another challenge is that measuring the diversity becomes computationally more expensive in high-dimensional spaces. Moreover, recombining solutions to generate new ones can be inefficient, as a few randomly chosen solutions from the population can be distant from each other, resulting in distant offspring solutions. Deb and Jain in [DJ14] stated that it is also difficult to represent the trade-off surface, as more points are needed with more dimensions. Furthermore, the computational costs of performance indicators can be high if there are many objectives. For instance, the computational effort of computing the hypervolume increases exponentially with the number of objectives [FPLI06, WHBH06a, DJ14]. Finally, presenting a solution set with many objectives visually is difficult.

Various methodologies have been developed to overcome these challenges. For instance, decomposition-based approaches, can divide the objective space into equally spaced regions that enable the algorithm to focus on solutions along those vector lines. Such approaches divide the problem into several single or multi-objective problems that are solved simultaneously by the algorithm. Aside from these kinds of algorithms handling many-objective problems, there are also domination-based approaches that improve either the dominance regulation or the sorting mechanism. Moreover, indicator-based algorithms use a particular indicator to measure the quality of solutions during the optimisation, and objective-reduction-based approaches use a subset of objectives during the evaluation [ZZN+19]. Increasing convergence and diversity in the decision space

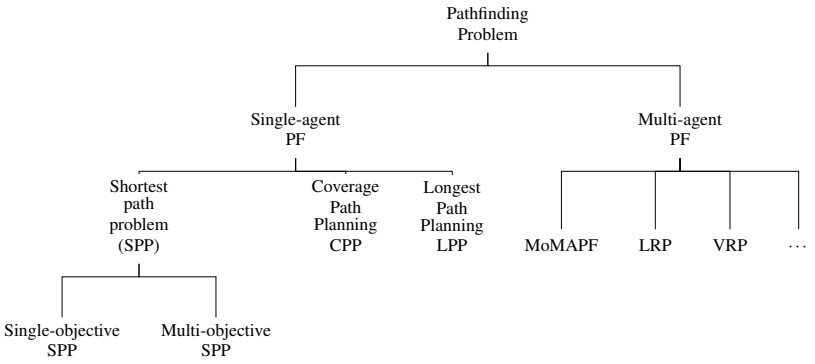

Figure 2.4: Pathfinding problem classes.

can be beneficial for the performance measured in the objective space, since close solutions in one space can be distant from each other in the other space, a likely case in multi-objective pathfinding problems. For instance, focusing solely on the objective space can result in a large uncovered area in the decision space. Problems such as the multi-objective pathfinding problem are problems where the quality of solutions benefits from these approaches.

2.3 Pathfinding Problems

There is a wide range of pathfinding problems, with the *(multi-objective) shortest path problem* discussed in this thesis being only one of the variants.

2.3.1 General Overview

In Figure 2.4, an overview of different pathfinding problems is shown. This tree represents a subset of pathfinding problems; a complete analysis appears in [ZH21]. In general, pathfinding problems can be characterised with respect to the number of agents or entities for which a path should be computed. It can either be a *single-agent* problem, where one path for one moving entity is to be found, or *multi-agent*, where a set of paths P for a set of agents A is to be found. The multi-agent variant can be further divided into several subproblems, including the location routing problem (LRP), vehicle routing problem (VRP), and the multi-objective multi-agent pathfinding problem (MoMAPF) [WMZM20]. On the other side, single-agent pathfinding also has sub-classes, such as coverage path planning (CPP) or the shortest path problem (SPP). The goal of the former is to find a route through a space that includes all points of interest while simultaneously averting traversing through obstacles [GC13]. Regarding the latter, it can be subdivided into the single-objective shortest path problem, where one objective function is considered and one path is computed. In the multi-objective shortest path problem, multiple objective functions are considered and optimised simultaneously. This problem is examined in this thesis. It should be noted that several of the other problems can be transferred to an SPP and solved using different methodologies. For instance, for CPP, the coverage can be defined as an objective and maximised during the optimisation.

2.3.2 The Multi-objective Pathfinding Problem

The multi-objective route planning problem, hereafter called the *pathfinding problem*, can be defined as a network flow problem [RE09, PMPDLC15]. The goal is to find a set of optimal paths (routes) $P* = \{p_1, \cdots, p_L\}$ in a graph

$$G = \left(V, E, \phi, \vec{f}, \iota_V(\mathfrak{P}), \iota_E(\mathfrak{P}), n_s, n_e\right) \tag{2.10}$$

where V is the set of vertices or nodes, E represents the set of edges and ϕ represents a function mapping every edge to a ordered pair of nodes n and n'; hence $\phi : E \to \{(n,n') \mid (n,n') \in V^2\}$. A path p_i is the sequence of nodes from a starting node $n_S \in V$ to a predefined end node $n_{End} \in V$, i.e., $p_i = (n_i, n_{i+1} \cdots, n_k)$, where $n_S = n_i$ and $n_{End} = n_k$ and $n_i \in V$ for $i = 1,2,\cdots,k$ and $\exists\phi(e_{i,i+1}) = (n_i, n_{i+1}) \in E$ for $i = 1,2,\cdots,k-1$. Such a path p is called a path of length $k-1$ from n_1 to n_k. A path p_i is here represented as a list of nodes in a graph. Another representation is a list of edges to traverse; hence $p_i = (e_1, \cdots, e_{k-1})$ where $n_S = \phi(e_1)(1)$ and $n_{End} = \phi(e_k)(2)$ and $e_i \in E$ for $i = 1,2,\cdots,k$. Following the definition of a MOP, the decision variable $\vec{x}$ is a path p in search space Ω (cf. Section 2.2.2 and Equation (2.6)). The vector $\vec{f}$ represents the objective functions that are to be optimised; hence $\vec{f} = (f_1, \cdots, f_m)$. The graph's nodes and edges can have further properties, e.g., an assigned location information, such as a coordinate or height. For edges traversals, the properties can be, e.g., constraints, such as maximum velocity. Assigning properties to the graph's entities is also known as the *property graph data model* [RN10]. Two functions $\iota_V(\mathfrak{P})$ and $\iota_E(\mathfrak{P})$ take a set of predefined property functions as an argument and return the node's or edge's respective property values. A property set $\mathfrak{P}$ is defined as a set of property functions taking a node or edge as an argument; hence $\mathfrak{P}(\cdot) = \{g_i(\cdot)\}$, where $(\cdot)$ is either a node or an edge, and therefore $i = 1,2,\cdots,|V|$ or $i = 1,2,\cdots,|E|$. The function g_i, represents a specific property that assigns the value of the property to a node or edge. Given m real-valued function mappings from $f_i : \Omega \to \mathbb{R}$ for $i = 1,2,\cdots,m$, i.e., $\vec{f}$, the multi-objective shortest path from n_S to n_{End} is the set of Pareto-optimal paths $P*$ which minimises all $f_i(p)$ for $i = 1,2,\cdots,m$ in a multi-objective sense. In the course of this thesis, we also use the simplified definition of a graph for pathfinding problems, that is $G = (V,E)$.

All points which are represented by nodes in a graph usually have an assigned coordinate, and all edges represent actual traversal paths. The methods discussed in this thesis are primarily for coordinate-based pathfinding and thus are *geometric path planning*. However, using different measurements and metrics, the proposed methodologies can be applied to non-geometric pathfinding too.

In contrast to several other approaches discussed in the related work (cf. Chapter 3), we use a graph-based problem representation and genetic algorithms for the actual optimisation. Therefore, we use a variable-length chromosome representation for the solutions when using the proposed methodologies. However, pathfinding problems and their solutions can be defined in different ways, with a graph being one of several possibilities (cf. Chapters 3 and 5). We define the multi-objective pathfinding problem that includes the many-objective pathfinding problem. The methodologies presented in this thesis can be applied to both types but are more tailored to the many-objective variants which optimise more than three objectives.

The multi-objective pathfinding problem can be a multi-modal problem, i.e., there can be more than one solution resulting in the same objectives [Jin21].

The problem we work on in this thesis has different names in the literature (see Chapter 3) and is also used with differing definitions in the research community. Some authors use the terminology of both path planning and trajectory planning. Nevertheless, there is a clear difference. A geometric path is to be found in path planning, which indicates *how* to move — through via-points — from a start point to an endpoint. By contrast, in trajectory planning, a computed geometric path is used and enriched with time information about *when* an entity traversing the path should be at which point [GBLV15]. Moreover, in this thesis, the focus is on pathfinding in general. The shortest path problem is a sub-problem, since pathfinding can include the *longest path problem*, *coverage planning*, *round trip planning* and other pathfinding methodologies, such as *cycle detection* [AMO93].

2.4 Pathfinding Techniques

There are various pathfinding methodologies available. It should be noted that such techniques are usually tailored to a specific pathfinding problem. This fact makes meta-heuristics — such as EAs — suitable for these problems, as they can solve a broad range of such problems. Pathfinding techniques are a major feature of this thesis, and different approaches are described in Chapter 3. Here, we only outline the most known exact approaches and relevant speed-up techniques that are used in some methodologies proposed in this thesis.

2.4.1 Exact Approaches

One of best-known algorithms to solve the shortest path problem is Dijkstra's algorithm, proposed in [Dij59]. It is a correct greedy algorithm to compute either a single-pair SPP (given start and end node) or can be used to compute a single-source SPP, i.e., given the start node, the shortest paths to all other nodes are computed. When exploring the graph from a starting node it always follows the edge with the current minimum summed-up costs. In that way it will always result in the shortest possible path if there is one. It should be noted that the algorithm only works with positive edge weights.

Another well-known algorithm to solve the shortest path problem is the A* algorithm. In its basics it has the same pattern as Dijkstra's algorithm but uses a heuristic to estimate the cost to the goal node from the current position. Therefore, it is an informed search and usually performs better than the former. Instead of following the edge with the least cost, it adds the value computed with the heuristic function and then follows the most promising edge [HNR68].

2.4.2 Speed-up Techniques

It is well known that Dijkstra's algorithm is often impractical for large graphs. Therefore, techniques that pre-process the graph to speed up the subsequent path search have been developed. For instance, contraction hierarchies, proposed in [Gei08], create shortcuts to avoid nodes during the expansion that are considered unnecessary. Creating shortcuts works especially well on hierarchical networks, such as street networks. For instance, the fastest route from one major city to another one often leads to a highway. The shortcuts, including shortcuts between other shortcuts, are created during a preprocessing phase and can be unpacked in the query and retrieval phase. During the latter phase, the search

only expands the set of shortcut edges, which has a much lower cardinality than the edge set of the actual graph.

2.5 Path Similarity Measurements

Path or curve similarity measurement are found in several fields; e.g., in handwriting recognition, curves are compared to match letters or words [SKB07]. Other fields include morphing [EGHP+02] and protein structure alignment [JXZ08,WM21b]. Although related, these methodologies have not been used to support an MOO process in maintaining and increasing the solution set's diversity.

In general, such a measurement or distance metric assigns a real value to two arbitrary curves, A and B. A distance metric $d : X \times X \to \mathbb{R}$ where X is a set, satisfies the following conditions for $x, y, z \in X$:

$$d(x,y) \geq 0, d(x,y) = 0 \textit{ iff } x = y \text{ (Non-negativity)} \tag{2.11}$$

$$d(x,y) = d(y,x) \text{ (Symmetry)} \tag{2.12}$$

$$d(x,z) \leq d(x,y) + d(y,z) \text{ (Triangular inequality)} \tag{2.13}$$

However, we also propose to use measurements that do not fulfil all requirements of a metric, e.g., dynamic time warping (DTW). It should be noted that there are different metrics or measurements available that take different curve definitions into account. For instance, the original Fréchet distance [EM94] computes the distance between two continuous curves, while the Hausdorff metric [AG95] and dynamic time warping [Mül07] take discretised curves and their inputs. Paths that are computed using techniques proposed in this thesis are discretised curves and can be used as inputs for the presented similarity metrics. In Chapter 6 a detailed description of the metrics and measurements is given.

2.6 Performance Measurement

For assessing the quality of an EA, various performance indicators (PIs) can be used. It has to be noted that each indicator describes different characteristics of the solution set. For instance, a metric can be used for convergence or diversity of the solution set to a known true Pareto-front. However, certain indicators can be used without any knowledge of the true optimal solutions. In this section, the indicators used in this thesis are explained in detail. Formally, a performance indicator maps the set of solutions $A = \left\{ \vec{a}_1, \cdots, \vec{a}_\mu \right\}$, where each $\vec{a}_i$ is an objective vector $\vec{a}_i = (f_1(p_i), \cdots, f_m(p_i))$, to a single performance value. Hence, a PI is defined as a unary operator, $I : \Omega \to \mathbb{R}$ [TI20]. Nevertheless, as outlined, there are also PIs that map the obtained set of decision vectors to a single performance value, $I : \mathscr{M} \to \mathbb{R}$.

Because PIs are based on different factors, one algorithm may have an advantage when a particular indicator is used but might be outperformed by another algorithm when a different indicator is used. Other issues of fair comparisons of MOO algorithms are termination condition, population size μ, and test problems [IPS22].

An algorithm's performance can be measured in different spaces, i.e., the objective and the decision space. The PIs measure properties of the set of solutions,

such as diversity or convergence to the real Pareto-front or set, or the number of non-dominated solutions, and a PI may also reflect a combination of such characteristics.

Performance indicators can be classified as either *not*, *weakly* or *strongly Pareto-compliant* [HJ98]. A PI I is strongly Pareto-compliant if the order it imposes on $\mathscr{M}$ follows the Pareto-dominance relation. Formally, given two solution sets A and B, a PI I is $\triangleright$-compliant (Pareto-compliant) if $A \triangleright B \Rightarrow I(A) < I(B)$, assuming a lower indicator value as better, without loss of generality. An example of a strong Pareto-compliant PI is the *hypervolume* indicator. A PI is weakly Pareto-compliant if it determines at least equal performance for two reference sets if one set is better in the sense of Pareto-dominance but never determines that the better set is worse in the sense of the indicator. Formally, a PI I is weakly $\triangleright$-compliant if $A \triangleright B \Rightarrow I(A) \leq I(B)$. When comparing two sets with a PI that is not Pareto-compliant, the outcome can be that the better set (Pareto-dominance) is determined to be worse [IPS22, FCEC19]. There are several approaches to make weakly Pareto-compliant PIs strongly Pareto-compliant, such as shown in [FCEC19].

In the following section, several PIs are explained that were used for evaluating the methodologies proposed in this thesis.

2.6.1 Objective Space

To measure the quality of a set of candidate solutions, a researcher can apply a PI in the objective space, i.e., the space of the objective functions $\mathscr{M}$. In this thesis, we apply three PIs. The inverted generational distance (IGD) and IGD$^+$ use a reference point set, denoted as $Z = \{z_1, \cdots, z_k\}$, which contains reference solutions; hence $z_i \in \mathscr{M}$, for $i = 1, \cdots, k$. Using the PIs, we compute this distance from the reference set Z to the approximation set $A = \{a_1, \cdots, a_\mu\}$.

Inverted Generational Distance

The IGD, which is a non-Pareto-compliant PI, measures the average distance from the reference set to the approximation set [CCRS04]:

$$\mathrm{IGD}(Z,A) = \frac{1}{|Z|} \sum_{i=1}^{|Z|} \min_{j=1}^{|A|} d(z_i, a_j) \tag{2.14}$$

The distance function $d(\cdot,\cdot)$ measures the Euclidean distance between a reference point and a point from the approximation set.

Inverted Generational Distance$^+$ (IGD$^+$)

In [IMTN15a], the distance function of IGD was changed to incorporate the dominance relation between the reference and approximation points. The authors stated that the new distance can be seen as a measurement of inferiority of the solution compared to the reference point. This IGD$^+$ indicator is weakly Pareto-compliant. The distance function $d(\cdot,\cdot)$ in Equation (2.14) is altered as follows:

$$d_{IGD^+}(z,a) = \sqrt{\sum_{k=1}^{m} \left(\max\{z_k - a_k, 0\}\right)^2} \tag{2.15}$$

Therefore, the IGD$^+$ indicator is computed as follows:

Figure 2.5: Hypervolume

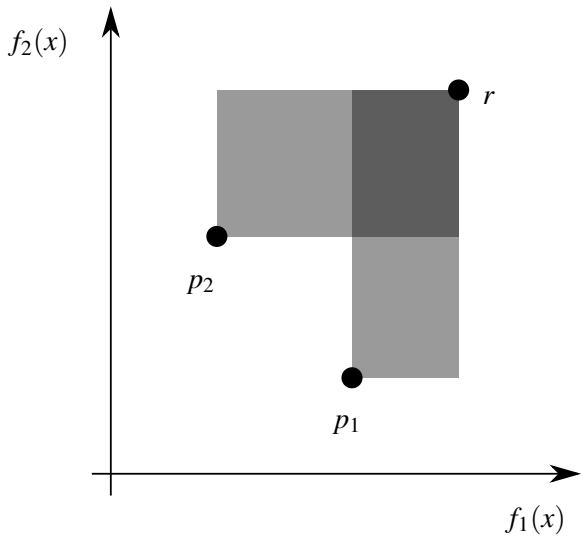

$$\mathrm{IGD}^{+}(Z,A) = \frac{1}{|Z|}\sum_{i=1}^{|Z|}\min_{j=1}^{|A|} d_{IGD^{+}}(z_i,a_j) \tag{2.16}$$

Hypervolume (HV)

In real-world problems, a reference front is not always given. Furthermore, evaluating the results using PIs that are not Pareto-compliant can lead to the wrong final solution choice. The only known Pareto-compliant PI is the hypervolume (HV) indicator [IMTN15a, IPS22]. However, for many-objective optimisation problems, it becomes impractical as it requires a relatively large computational effort.

The HV indicator computes the combined volume of all non-dominated points in a set of points $S \subset R^d$ and is defined by Equation (2.17), where $r \in R^d$ is a volume limiting point. The term $[p,r]$ denotes the volume limited by a point $p \in S$ on the lower side and r on the upper side [ZT98, GFP20]. The term Λ refers to the Lebesgue measure. In Figure 2.5, a visual example of the HV indicator is shown. The indicator measures the size of the surface (or volume in higher dimensions) of the grey areas. In other words, it indicates the size of the area that is dominated by the approximation restricted by a reference point r.

$$HV(S,r) = \Lambda\left(\bigcup_{\substack{p\in\mathbb{S}\\ p\leq r}}[p,r]\right) \tag{2.17}$$

In addition to indicators in the objective space, some performance indicators are computed in the decision space.

2.6.2 Decision Space

Inverted Generational Distance X (IGDX)

The inverted generational distance X (IGDX) indicator measures the distance of the true Pareto-set (reference set) to the set of candidate solutions [AQY09]. It is adapted from the IGD indicator, which measures the quality of the solution set in the objective space. Usually, the distance between a reference point and a candidate solution is computed using the Euclidean distance. However, in

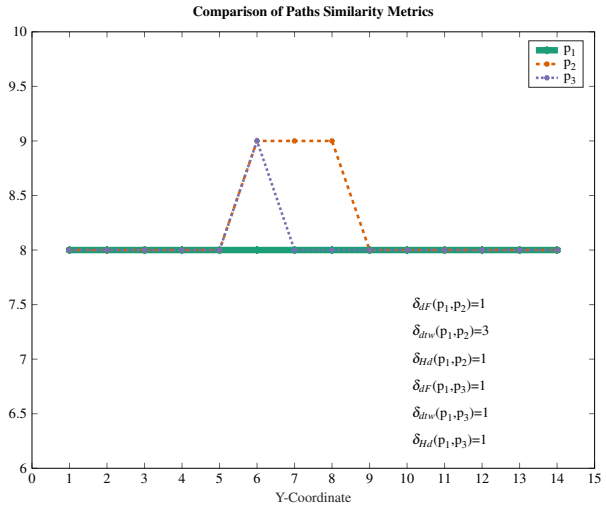

Figure 2.6: Similarity measurement comparison.

the decision space of the graph-based multi-objective pathfinding problem, the Euclidean distance cannot be used. Therefore, we propose using a path similarity metric to measure the distances in the decision space. However, different metrics can result in different results, as shown in Figure 2.6. The figure shows three different paths: p_1 in green as a baseline, p_2 in orange and p_3 in violet. Path p_2 differs in only one node compared to the baseline path, whereas p_3 differs in three nodes. Intuitively, p_3 is more different from p_1 than is p_2. However, computing $\delta_{dF}(p_1, p_2)$ and $\delta_{dF}(p_1, p_3)$ results in the same value, i.e., $\delta_{dF}(p_1, p_2) = \delta_{dF}(p_1, p_3) = 1$. By contrast, using the dynamic time warping distance results in different similarity values, as shown in the respective figure. Therefore, to evaluate small differences between several paths, analysts should use dynamic time warping rather than the Fréchet distance. We also show the respective values for using the Hausdorff distance.

2.7 Decision Support

A decision support system can support a DM to find a Pareto-optimal solution that is the best choice accoording to the DM's preferences [Mie08]. The need for such a system arises from the challenge in multi-objective optimisation that multiple criteria must be considered and a set of Pareto-optimal solutions cannot be totally ordered. In Chapter 7, we propose a methodology to reduce the number of Pareto-optimal solutions.

There are four major types of decision-making methodologies in multi-criteria decision making (MCDM) [Mie08]. An *a priori* technique requires the DM to select their preferences before a multi-objective optimisation algorithm computes a solution set. However, often a DM is not fully aware of their preferences as they lack knowledge about the problem. In *a posteriori* methods, an approximation of the Pareto-front is computed first, and a DM has to choose the preferred solution afterwards. When more than two objectives are optimised, a visualisation of the non-dominated solutions is not trivial and DMs can find it difficult to understand the information. A third type is *no-preference* methodologies, where assumptions are made and a neutral trade-off solution is found, e.g., a point that is identified using the average values of the nadir and utopian point. The fourth type, *interactive* methodologies, involve the DM in the optimisation

process. Here, the DM is provided with indermediate solutions and can identify their preferences [Mie08].

2.8 Clustering

Often, for analysing a data set consisting of data points, a technique called *clustering* is used to divide the set into different categories or classes according to the data points' similarity. Depending on the kind of data, various methodologies to achieve this grouping are employed. The technique can be used during a decision-making process. A clustering process divides an n-dimensional population into κ sets, which results in a set of clusters C_i, $i = \{1, \cdots, \kappa\}$, $i \in \mathbb{N}$ [Mac67]. Since we only examine a subset of methodologies from the large field of cluster analysis, the interested reader is referred to [TSKK19]. In the following, we explain the most relevant techniques employed in Chapter 7.

2.8.1 Clustering Types

There are various types of clustering methodologies. In *partitional* clustering, a set of data points is divided into κ groups, where κ is known before. However, if a cluster C can contain a set of sub-clusters, it is considered to be *hierarchical* clustering. A prominent example of the partitional type is the k-means algorithm [Mac67, Llo82]. Hierarchical clustering can be divided further into a divisive or an agglomerative approach.

Divisive At the beginning of a divisive clustering, each object or data point is assigned to the same cluster. During the process, the cluster is split until each object belongs to a dedicated cluster.

Agglomerative In agglomerative clustering, a bottom-up approach is realised. At first, each data point belongs to its own cluster, and the clusters are merged with respect to predefined metrics until a single cluster left.

The result of both approaches is a hierarchy of clusters, which can be visualised using a dendrogram or a nested cluster diagram.

In this thesis, we use agglomerative clustering during the decision support process. We explain the necessary characteristics in this section.

During the fusion of clusters, a linkage criterion is needed to determine the merging clusters. Various criteria are typically used to compute cluster proximity. In *single* linkage, cluster proximity is defined as the proximity between the two closest points of two different clusters. In contrast, in *complete* linkage, the farthest two points are used. For both techniques, a distance metric is needed (cf. Equations (2.11) to (2.13)), which assigns a real positive value to two objects.

2.8.2 Evaluation of κ

For assessment of the clustering, internal or external methodologies can be used. The former is a measurement with respect to inter-cluster distance and variance of a cluster. However, for the latter, ground-truth data is needed to compare the obtained clustering. Due to the nature of the problem, there is no benchmark data for path clustering available. Therefore, we describe only such methods that do not require ground-truth data. However, we can compare the clustering

results while gaining little information about the overall quality. Each of the following indices reflects the relationship between the compactness of a cluster and its separation from other clusters. Each index has a different approach.

Silhouette coefficient

To measure the quality of a clustering technique, Rousseeuw proposed the use of a so-called *silhouette*, i.e., a graphical representation of a cluster [Rou87]. The silhouette coefficient displays the validity of a clustering. Its computation requires two things: the partitioning of a data set into κ clusters and a dissimilarity matrix that contains the distance between all objects. To compute the silhouette value $s(i)$ for an object i, one must compute $a(i)$, i.e., the average distance to all other objects in the same cluster C_I ($i \in C_I$), which is defined by:

$$a(i) = \frac{1}{|C_I| - 1} \sum_{j \in C_I, i \neq j} d(i, j) \tag{2.18}$$

Furthermore, we must compute the minimum of the mean dissimilarity to all other clusters, i.e., the mean distance to all other objects $j \in C_J$, $C_I \neq C_J$, and then determine the minimum value. This value $b(i)$ is defined as:

$$b(i) = \min_{J \neq I} \frac{1}{|C_J|} \sum_{j \in C_J} d(i, j) \tag{2.19}$$

Here, $d(i, j)$ is the distance between the two data points i and j, which can be any distance metric. Finally, we compute the silhouette value $s(i)$ for an object i as follows:

$$s(i) = \begin{cases} 1 - a(i)/b(i), & \text{if } a(i) < b(i) \\ 0, & \text{if } a(i) = b(i) \\ b(i)/a(i) - 1, & \text{if } a(i) > b(i) \end{cases} \tag{2.20}$$

The value is $-1 \leq s(i) \leq 1$ and its mean value $\tilde{s}$ over all objects i is a measurement of how effective a clustering is, or how closely all points within a cluster are grouped. Using this value, Kaufmann and Rousseeuw proposed the silhouette coefficient, which maximises the mean $s(i)$ when computing it for each $\kappa = 2, \cdots, n-1$ where n is the number of objects in the data set [KR90]. The coefficient is defined as follows:

$$SC = \max_{\kappa} \tilde{s}(\kappa) \tag{2.21}$$

It results in the value for κ, which is the maximum mean $s(i)$, and is, therefore, a good choice for the number of clusters.

Dunn Index

Dunn proposed a measure that is the ratio of the minimum inter-cluster distance and the maximum cluster diameter [Dun73]. It is defined as follows:

$$DI_m = \frac{\min_{1 \leqslant i < j \leqslant m} \delta(C_i, C_j)}{\max_{1 \leqslant k \leqslant m} \Delta_k} \tag{2.22}$$

The function δ represents the inter-cluster distance, whereas Δ_k is the cluster diameter. However, computing these values is not predefined and is adapted to the underlying data set. A higher Dunn index represents a better clustering.

Davies-Bouldin Index

Davies and Bouldin developed a measure to compute the similarity of clusters. For each cluster C the maximum similarity to any other cluster is computed, and the average of all maximum values is referred to as the *Davies-Bouldin Index* [DB79]. It is defined as:

$$\bar{R} \equiv \frac{1}{N} \sum_{i=1}^{N} R_i \tag{2.23}$$

where $R_i \equiv max_{i \neq j} R_{ij}$. The value of R_{ij} is defined as the ratio of the sum of the dispersion measures S_i of two clusters and their Minkowski distance M_{ij} and is calculated as follow:

$$R_{ij} \equiv \frac{S_i + S_j}{M_{ij}} \tag{2.24}$$

where a dispersion measure S_i is defined as

$$S_i = \left(\frac{1}{T_i} \sum_{j=1}^{T_i} \left\| X_j - A_i \right\|_p^q \right)^{1/q} \tag{2.25}$$

where T_i is the number of objects in cluster C_i, and A_i is its centroid. Therefore, S_i is the qth root of the qth moment of the objects in a cluster C_i about the cluster's representative point. If $q = 1$, the dispersion measure equals the average distance of objects in the cluster to the centroid, whereas $q = 2$ represents the standard deviation of the distances of the objects to the cluster's centroid.

The Minkowski distance is defined as follows:

$$M_{i,j} = \left\| A_i - A_j \right\|_p = \left(\sum_{k=1}^{n} \left| a_{k,i} - a_{k,j} \right|^p \right)^{\frac{1}{p}} \tag{2.26}$$

that is, the distance between the centroids of the clusters C_i and C_j. In Equations (2.25) and (2.26), if $p = 2$, distances equal the Euclidean distance, while they equal the Manhattan distance if $p = 1$. A lower index value indicates a better clustering.

2.9 Summary

In this chapter, we have presented the necessary scientific background for the following chapters. We have described graph theory, MOO in general and specifically evolutionary MOO. Moreover, we have discussed the background of pathfinding methodologies and various path similarity measurements that are used in this thesis. Another point was the definition of the multi-objective pathfinding problem that is addressed in this work. With an increasing number of objectives, more solutions are non-dominated, and a DM needs to select a solution. Therefore, we have described a subset of clustering analysis methodologies that are used for determining interesting solutions in a decision support methodology that is described later.

3 Related Work and State-of-the-art

In this chapter, the following points are covered

- Literature Review
- Classification

In this chapter, we present various algorithms and approaches that have been proposed in the literature. We furthermore classify and discuss the methodologies. In the literature, there are different names for similar problems. For example, some authors discuss the *multi-objective path planning problem* or *multi-objective shortest path problem*, but other names are *multi-objective path optimisation* or *multi-objective route optimisation*. Many articles have addressed such problems. It should be noted that the definitions of these problems also differ in the literature because some researchers use them for trajectory planning instead of pure path planning.

There are specific approaches for pathfinding in the literature, which usually work on graphs to find paths between two nodes. Besides the exact single-objective methods which solve the shortest path problem (e.g., the well-known Dijkstra's algorithm [Dij59]), there are several optimisation methods for these algorithms, such as contraction hierarchies [Gei08, DSSW09]. Another example of such speed-up methods is hub labelling. They are used because the performance of Dijkstra's algorithm is inversely related to the size of the underlying graph. The larger the graph, the longer the time required to obtain a result.

Speed-up techniques bypass this limitation by preprocessing the graph to find shortcuts between certain nodes. The preprocessing time can itself be extensive but the procedure only needs to be done once if the environment does not change. As in general optimisation, there are exact methods for the multi-objective (single-path) pathfinding problem, as well as meta-heuristic methods, e.g., EAs to solve it [AD13, DPMH13, FC14, NN11, XS18, CTM07, ORK14, CPS11, JQ10, AD11]. A few articles address the multi-objective perspective of pathfinding using exact methods [WYMW19, SnC19, LVEJ16, DMS08, FS13, LPLH12, SM13, GKS10].

Combining approaches from both fields by creating hybrid strategies could lead to faster and better results, since EAs can be stopped or paused at any stage to obtain results.

In general, many studies have been based on a form of the multi-objective pathfinding problem. However, they usually evaluate the methodologies on unique and highly specialised environments, tailored to a specific use-case, with path planning for robots or unmanned aerial vehicles (UAVs) being among the most popular use-cases. Hence, application-specific methodologies are carried out on the respective problem and they improve the quality of results for these particular problems.

More general analysis or propositions of generally applicable methodologies are scarce. One of the reasons is that pathfinding problems are often inherently application-specific. This circumstance implies the non-triviality of generalising pathfinding problems and finding an algorithm for various path planning problems. Moreover, each environment has different characteristics and must be analysed thoroughly.

In the following chapters, we aim to provide methods that can cover a variety of pathfinding tasks. Furthermore, many pathfinding problems can be translated (transferred) into a shortest path problem, which is the main focus of this thesis. In our analysis of the related work landscape, we have classified the works according to the research questions that we address in this thesis. This includes various aspects of the studied environments, algorithms, operators and search methodologies. Diversification and initialisation techniques are additional key points.

3.1 Classification of Literature

We identified 17 characteristics on which we could build a classification. The primary classification is based on the number of objectives optimised by the respective algorithm and the number of nodes in the graph being studied. Figure 3.1 summarises the characteristics and their relation or hierarchy.

Figure 3.2 illustrates the existing approaches to solve the multi-objective pathfinding problem regarding the number of objectives, the number of nodes $|V|$ and the respective graph's density ρ. The x-axis shows the number of optimised objectives. The left y-axis shows the number of nodes, whereas the right (red) y-axis shows the density. For each objective, each work is assigned a marker that can be found up to two times for the respective number of objectives. For instance, there is only one work with a relatively high number of nodes and a comparable small density for the case of one objective. Both types of information are depicted by the diamond marker ($\diamond$), referring to the same work. However, there were also works for which we could not determine the density; there is only one blue marker for such cases, showing the number of nodes. Furthermore, we estimated the number of edges for a few grid-based works by analysing how a respective agent can move on the used grid.

Figure 3.3 shows the relation between the number of nodes and the density, both on a log scale. It is evident that the two properties have an inverse log-log linear relationship, i.e., as the number of nodes increases, the density decreases.

Tables 3.1 and 3.2 summarise the most important related literature. These articles address multi-objective pathfinding problems in various environments

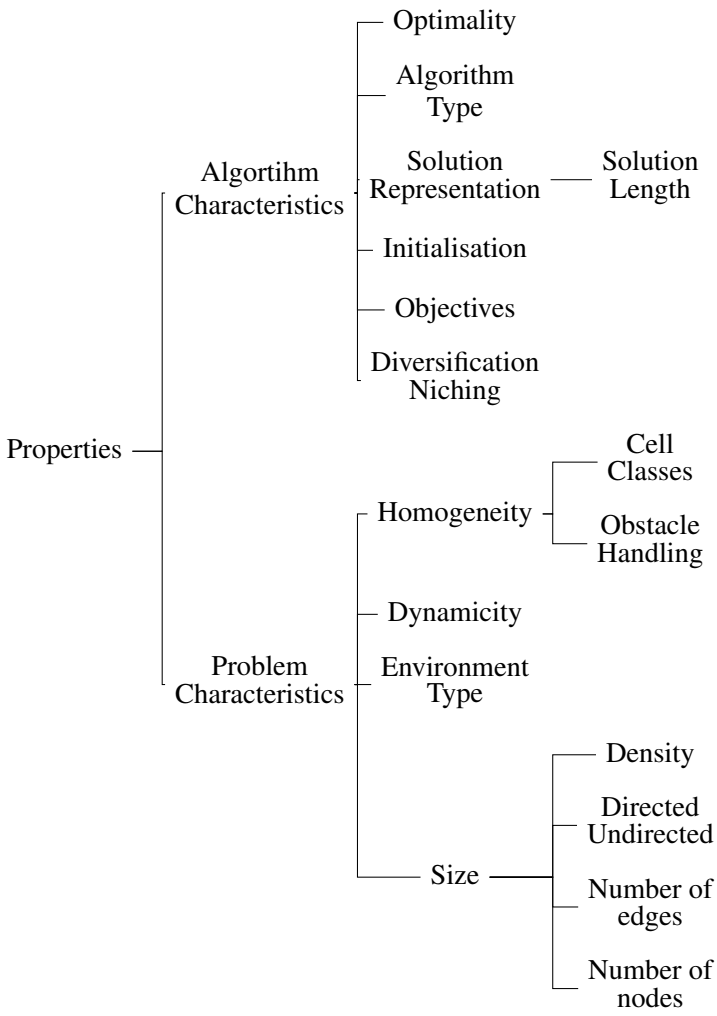

Figure 3.1: Properties of the identified related work.

and use different algorithms. In the table, each column corresponds to one of the identified characteristics. However, we could not determine the value of each property in all works, and in several cases the property was not relevant for the approach used. For instance, optimal approaches usually do not need a diversification strategy. We assigned *N/A (not applicable)* for such entries. If the property value could not be determined, we assigned a dash (–). The table shows the type of environment that was explored, and if applicable its size and the number of different cell classes that defined the environment. Some works included an obstacle handling technique that increased the number of cell classes. In addition, we determined the dynamicity of the environment and its homogeneity, as well as the number of nodes and edges. If possible, we computed the resulting density.

Several works proposed special diversification and niching strategies or initialisation methodologies. For the proposed solving techniques, we determined the type of algorithm, the corresponding representation scheme and, if applicable, whether it was a fixed- or variable-length representation. In the penultimate column, we show the marker that is used in the corresponding objective value (see Figure 3.2. The last column in Table 3.2 presents additional relevant information.

As visible in the two figures, only a few articles have addressed many-objective pathfinding problems. The maximum number of nodes in these analyses (accounting only for $m > 3$) was 487 500 [DPMH15].

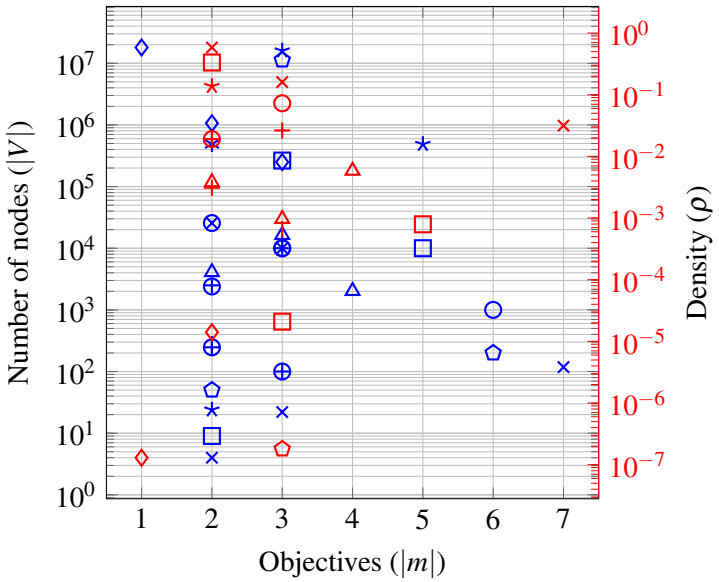

Figure 3.2: Related Work Landscape.

The reader should note that we do not cite the respective works in the following sections again if a property is relevant to many articles; the references are given in Tables 3.1 and 3.2. Next, we summarise the characteristics and their expressions.

3.1.1 Problem characteristics

In the related works, different problems are used. A pathfinding problem's environment represents its basis and has several properties. The problems, then, can be classified concerning their representation or the actual environment's size, dynamicity, homogeneity or solution representation. The problem characteristics are presented in Table 3.1.

Size

Figure 3.2 shows that the environment's size often inversely correlates with the number of objectives. Defining an environment's size is not trivial. Imagining a graph with five nodes, representing five intersections on a road map: Connecting them can be done using a few edges, representing streets, resulting in, e.g., three streets per intersection. If the nodes represent roundabouts a larger number of streets can end in such intersections. Doing so would result in more edges while retaining the five initial nodes. Therefore, the size of an environment should be always given with its complexity, such as *density* in graph-based environments; see Equations (3.1a) and (3.1b). Therefore, we use density in our analysis, and it is defined as follows for undirected graphs [Bol79]:

$$\rho_{G_U} = \frac{|E|}{\binom{|V|}{2}} = \frac{2|E|}{|V|(|V|-1)} \tag{3.1a}$$

Figure 3.3: Relation of $|V|$ and ρ.

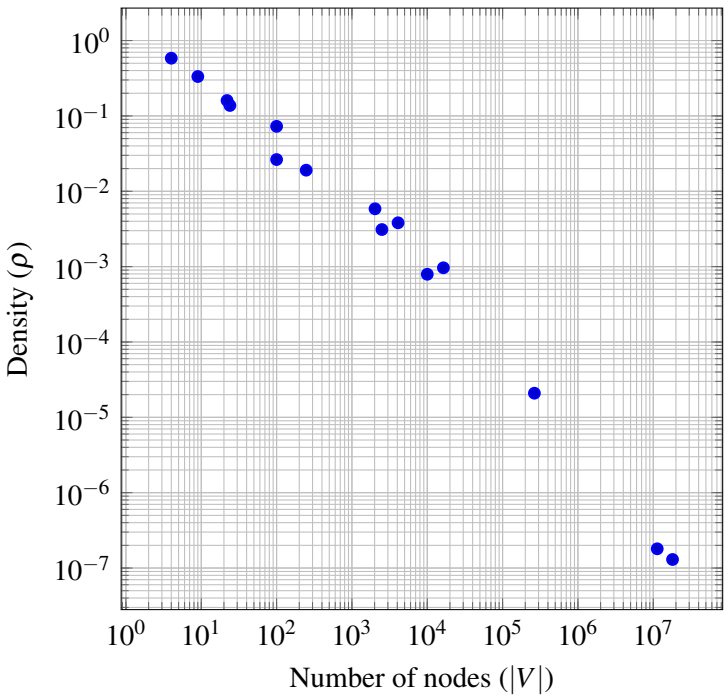

In other words, the density is the ratio of the actual number of edges $|E|$ and the possible number of edges, i.e., $\binom{|V|}{2} = \frac{|V|(|V|-1)}{2}$. For directed graphs, the number of possible edges is as twice as large, since there can be two edges between any arbitrary set of two nodes; hence $2\binom{|V|}{2}$. Therefore, the density of a directed graph is defined as:

$$\rho_{G_D} = \frac{|E|}{2\binom{|V|}{2}} = \frac{|E|}{|V|(|V|-1)} \tag{3.1b}$$

Another point in the size property is the environment's shape. Often, grid-based environments have a rectangular shape. Other shapes are possible but are not found in the literature regarding grid-based approaches. Graph-based environments inherently have no shape; they have only a size and complexity that is defined by their number of nodes $|V|$, number of edges $|E|$ and the density ρ.

Problem representation

The representation is usually performed using a grid or a graph, while homogeneous environments — such as road maps — are often encoded as a graph. These environments can also be discretised into a grid, which can be beneficial to reduce computational effort while sacrificing some accuracy. Moreover, some studies have employed directed graphs, implying that a hypothetical agent cannot move freely. As this property is one of the primary aspects in this thesis, we discuss it in detail in a separate section (see Section 3.1.3).

Dynamicity

An environment can be of a static, dynamic or stochastic nature. The most trivial case is a static grid or graph, where the cost of a traversal does not change and is deterministic at any point in time. Total deterministic environments were used in the majority of the analysed works. Deterministic but unknown environments were worked on in two articles [OP16, QYS21]. In such ap-

Table 3.1: Related Work - Problem characteristics

Grid size	Type	Cell classes	|V|	|E|	Directed	Obstacles	Density	Homogenety	Dynamicity	Reference	Marker
–	Graph	1	$1.8 \cdot 10^7$	$4.22 \cdot 10^7$	Yes	No	$1.3 \cdot 10^{-7}$	–	Deterministic	[Gei08]	◊
64x64	Grid	2	4,096	32,006	–	Yes	$3.82 \cdot 10^{-3}$	–	Deterministic	[AD11]	△
3x3	Graph	1	9	24	Yes	No	0.33	–	Dynamic (time-dependent)	[HLZ+18]	□
–	Graph	1	24	76	Yes	No	0.14	He	Stochastic	[ZCS04]	⋆
50x50	Grid	2	50	–	No	Yes	–	He	Stochastic	[ZGZ13]	⬠
60x40	Grid/Graph	2	2,400	–	No	Yes	–	He	Deterministic	[MS10]	○
–	Graph	1	4	7	Yes	No	0.58	Ho	Deterministic	[Wak02]	×
50x50	Grid	3	2,500	19,404	Yes	Yes	$3.11 \cdot 10^{-3}$	He	Stochastic	[Mou12]	+
–	Graph	1	247	1,158	Yes	No	$1.91 \cdot 10^{-2}$	Ho	Dynamic (time-dependent), stochastic	[CNT05]	⊕
160x160	Grid	5	25,600	–	No	Yes	–	He	Deterministic, but unknown	[OP16]	⊗
700x700	Grid	3	$4.9 \cdot 10^5$	–	No	Yes	–	He	Deterministic, but unknown	[QYS21]	✳
28x10	Grid	2	280	–	No	Yes	–	He	Deterministic	[ZXL+15]	ı
1124x948	Grid	1	$1.07 \cdot 10^6$	$7.99 \cdot 10^6$	No	No	$1.41 \cdot 10^{-5}$	He	Deterministic	[HBAO21]	◊
128x128	Grid	2	16,384	$1.3 \cdot 10^5$	–	Yes	$9.65 \cdot 10^{-4}$	–	Deterministic	[AD13]	△
–	Graph	1	$2.64 \cdot 10^5$	$7.3 \cdot 10^5$	No	No	$2.09 \cdot 10^{-5}$	–	Deterministic	[PMPDLC15]	□
4000x4000	Grid	2	$1.6 \cdot 10^7$	–	–	Yes	–	–	Deterministic	[XS18]	⋆
–	Graph	1	$1.13 \cdot 10^7$	$2.29 \cdot 10^7$	Yes	No	$1.8 \cdot 10^{-7}$	–	Deterministic	[FS13]	⬠
10x10	Graph	1	100	360	No	No	$7.27 \cdot 10^{-2}$	Ho	Stochastic	[RBSMBA15a]	○
–	Graph	1	22	37	No	No	0.16	He	Stochastic	[ZJWW10]	×
10x10	Grid/Graph	2	100	261	Yes	Yes	$2.64 \cdot 10^{-2}$	He	Deterministic	[JQ10]	+
100x100	Grid	2	10,000	–	No	Yes	–	He	Deterministic	[HPVRFP15]	⊕
100x100	Grid	2	10,000	–	No	Yes	–	He	Deterministic	[HPVRFP17]	⊗
N/A	N/A	–	–	–	–	–	–	He	Deterministic	[Mou04]	✳
100x120	Grid	2	12,000	95,484	Yes	Yes	$6.63 \cdot 10^{-4}$	He	Deterministic	[DPMH13]	ı
500x500	Grid	2	$2.5 \cdot 10^5$	–	No	Yes	–	He	Deterministic	[HA20]	◊
45x45	Grid/Graph	4	2,025	12,000	No	Yes	$5.86 \cdot 10^{-3}$	–	Deterministic	[MML+08]	△
100x100	Graph	1	10,000	39,600	No	No	$7.92 \cdot 10^{-4}$	–	Deterministic	[PMPDLC15]	□
650x750	Grid	2	$4.88 \cdot 10^5$	–	No	Yes	–	He	Deterministic	[DPMH15]	⋆
10x20	Grid	2	200	–	–	Yes	–	–	Stochastic	[TMS17]	⬠
–	Graph	1	1,000	–	Yes	No	–	Ho	Dynamic (time-dependent), stochastic	[OMH06]	○
–	Grid/Graph	2	118	218	No	No	$3.16 \cdot 10^{-2}$	He	Deterministic	[Jin21]	×

proaches, the algorithm must not know the complete environment and thus cannot exploit it upfront. A dynamic environment can change depending on the time [HLZ+18]; however, the network's state is also deterministic. In a stochastic environment, the traversal costs are stochastic, which must be considered by a pathfinding algorithm when minimising, e.g., the variance of an objective. These kinds of networks have been used by [ZCS04, ZGZ13, Mou12, RBSMBA15a, ZJWW10, TMS17]. Some works consider both stochastic and dynamic networks [CNT05, OMH06]. Designing an algorithm capable of handling all dynamicity types is not trivial. Methodologies for static problems can be applied to stochastic environments by adapting their respective objective functions to cope with variances. However, problem-tailored approaches usually outperform transferred methodologies.

Homogeneity

Environments can consist of different cell classes, where the trivial classes are *obstacles* and *free space*. However, several works — and therefore also algorithms — take multiple classes into account. The real world can be seen as a multiclass environment depending on the use-case. Furthermore, an environment entity can have properties that describes the entity in more detail, such as height information, movement constraints or safety measurements. Entity properties can be discrete or continuous. The related articles examined homogeneous and heterogeneous environments. A heterogeneous environment resembles the real world best, as different kinds of representative points are usually found. Furthermore, approaches for heterogeneous environments can also work on homogeneous ones. Table 3.1 indicates which works used a homogeneous or heterogeneous environment.

Table 3.2: Related Work - Algorithm characteristics

Divers. & Niching	Objectives	Initialisation	Representation	Length	Algorithm type	Optimal	Reference	Marker	Comment
N/A	1	N/A	Direct node list	F	Graph Search	Yes	[Gei08]	◊	–
NSGA-II	2	–	Splines	F	Genetic Algorithm	No	[AD11]	△	–
N/A	2	N/A	Direct node list	V	Ripple-spreading algorithm	Yes	[HLZ+18]	□	–
Mutation, by finding random path from mutation point	2	STOCH algorithm, random neighbour selection	Direct node list	V	Genetic Algorithm	No	[ZCS04]	*	Simulation-based
Altered probability to select infeasible solutions	2	Random	Coordinates	F	Swarm Intelligence	No	[ZGZ13]	⬠	Continous space
Probabilistic Road Map	2	Random (sensor distance of robot)	N/A	N/A	Swarm Intelligence	No	[MS10]	○	Weighted sum
N/A	2	N/A	Direct node list	N/A	Policy improvement procedure	Yes	[Wak02]	×	Single-objective + Constraints on other obj.
N/A	2	N/A	Direct node list	N/A	Vector-Value Markov Decision Process	Yes	[Mou12]	+	Preference-based
N/A	2	N/A	Direct node list	V	Graph Search	Yes	[CNT05]	⊕	–
N/A	2	N/A	Direct node list	N/A	Graph Search	No	[OP16]	⊗	–
N/A	2	RRT	Direct node list	N/A	Graph Search	No	[QYS21]	*	–
Domain specific Operators	2	Random	Obstacle Vertex indicies	V	Memetic algorithm	No	[ZXL+15]	I	–
Custom Step size crossover, extended log-normal rule mutation	2	equidistant Point sampling between start and goal, and addition of single-objective optimal paths (biased)	Splines	F	Evolutionary Strategy	No	[HBAO21]	◊	–
NSGA-II	3	–	Integer-coded (among others)	F	Genetic Algorithm	No	[AD13]	△	–
N/A	3	–	Direct node list	N/A	Graph Search	Yes	[PMPDLC15]	□	Took 6h to complete
Domain specific Operators	3	Only feasible, also local minimum of each objective added	List of turning points	V	Genetic Algorithm	No	[XS18]	*	–
N/A	3	N/A	Direct node list	F	Graph Search	Yes	[FS13]	⬠	Weighted sum
NSGA-II	3	Random neighbour Selection	Direct node list	V	Genetic Algorithm	No	[RBSMBA15a]	○	–
MOPSO	3	Node priority	Indirect, node priority	F	Swarm Intelligence	No	[ZJWW10]	×	–
Domain specific operators	3	Visibility Graph and Chaos Sequence	Coordinates	V	Genetic Algorithm	No	[JQ10]	+	–
Domain specific operators	3	Selection Window	Coordinates (Grid cells)	V	Shuffled Frog-Leaping Algorithm	No	[HPVRFP15]	⊕	–
Domain specific operators	3	Selection Window	Coordinates (Grid cells)	V	Swarm Intelligence	No	[HPVRFP17]	⊗	–
N/A	3	N/A	Direct node list	N/A	Markov Decision Process	Yes	[Mou04]	*	Theoretical paper, Preference Based
Domain specific Operators	3	fixed number of different Waypoints for each initial solution	Coordinates (Grid cells)	V	Genetic Algorithm	No	[DPMH13]	I	–
N/A	3	One initial path is found using Voronoi-visibility points	Coordinates	V	Region of Sight	No	[HA20]	◊	Constraints on obj. and then shortest path
ACO	4	–	Direct node list	N/A	Swarm Intelligence	No	[MML+08]	△	–
N/A	5	–	Direct node list	N/A	Graph Search	Yes	[PMPDLC15]	□	–
Domain specific Operators	5	fixed number of different Waypoints for each initial solution	Coordinates (Grid cells)	V	Genetic Algorithm	No	[DPMH15]	*	–
N/A	6	–	Direct node list	V	Reinforcement learning	No	[TMS17]	⬠	–
N/A	6	N/A	Direct node list	N/A	Graph Search	Yes	[OMH06]	○	Returns one solution
N/A	7	N/A	Direct node list	N/A	Graph Search	Yes	[Jin21]	×	Multi-modal

3.1.2 Algorithm Characteristics

Various algorithmic approaches have been leveraged to solve the pathfinding problem. In this section , we describe specific characteristics of the methodologies found in the literature, as outlined in Table 3.2.

Number of objectives

As shown in Figure 3.2, most of the examined literature was concerned with optimising two or three objectives. There were relatively few studies on more than three objectives [TMS17, PMPDLC15]. For instance, [TMS17] identified only three works, including theirs, that dealt with four or more objectives [PMPDLC15, MML+08]. Only one work in our analysis considered seven objectives by working on a comparable small graph. For five objectives, the highest number of nodes or grid cells was 487 500 [DPMH15]. The same study employed a GA, as we have done in this thesis. In one work, multiple objectives were considered, but the computation resulted in only one solution that had the best trade-off

according to a metric [OMH06]. The exact computation of the complete Pareto-optimal set for such a high number of objectives is often time-consuming, as the problem is NP-hard.

Types

Different algorithm types have been employed to solve pathfinding problems. For example, there are GAs [AD11, ZCS04, AD13, XS18, RBSMBA15a, JQ10, DPMH13, DPMH15]; memetic algorithms [ZXL+15]; and swarm intelligence techniques, such as *ant colony optimisation* [MML+08] or *particle swarm optimisation* [ZGZ13, MS10, ZJWW10]. In the realm of swarm intelligence techniques, the firefly algorithm has been employed in pathfinding [HPVRFP17]. Other methodologies have been employed, such as direct graph searches [Gei08, CNT05, QYS21, PMPDLC15, FS13, PMPDLC15, OMH06], including A* algorithms and variations of it [OP16, Jin21] as well as reinforcement learning [TMS17], or other nature-inspired methodologies such as *ripple-spreading* [HLZ+18] or a *frog-leaping* algorithm [HPVRFP15]. The *region of sight* technique was used in [HA20]. In three works, a Markov model was proposed [Wak02, Mou12, Mou04]. Finally, most of the works employed a direct graph-search algorithm. However, the distinction implies other properties of an approach too, such as the *anytime* property, which means that suboptimal results can be obtained before the termination criteria of the algorithm is met. Usually, population-based approaches have this property, whereas direct graph searches such as A* must run to completion to yield a result. Algorithms without the anytime property usually obtain optimal solutions, but exceptions exist.

Precomputation

Depending on the underlying pathfinding problem and the requirements in the final application, precomputation can be employed before the actual pathfinding algorithm is run to reduce the time to obtain results [FS13]. Usually, a lookup table or a similar data structure is built up to decrease the time until a solution is obtained. Only a few works used precomputation for multi-objective pathfinding problems, as this process is time-consuming and often memory-consuming. However, when the environment is static and several pathfinding queries will be set on this environment, precomputing a lookup table can be beneficial in the actual real-world execution of the algorithm. There are also several speed-up techniques, such as *contraction hierarchies*, that use extensive preprocessing to accelerate shortest path queries on a graph [Gei08].

Optimality

There are several optimal and deterministic methodologies to solve single-objective and multi-objective pathfinding problems. There are also optimal approaches with the precomputation characteristic, making them suitable for applications with a static environment and many executions afterwards. However, techniques have been proposed which may consume vast time to obtain a result. For pathfinding on graphs, there are optimal methods available that usually count to the class of *greedy* algorithms. A well-known algorithm is Dijkstra's shortest path algorithm [Dij59]. The algorithm can be seen as a specialisation of the A* algorithm, as it uses a heuristic equal to 0. Due to a chosen heuristic function, A* can often solve the problem in less time. Dijkstra's worst-case time complexity is $\mathcal{O}(|E|+|V|\log|V|)$, whereas the complexity of A* is $\mathcal{O}(|E|)$.

Additionally, a multi-objective variant of Dijkstra's algorithm was proposed in [Mar84].

Initialisation

In the literature, different initialisation techniques have been employed. They can substantially influence the performance of the algorithm and the quality of results. The majority of works that use an initialisation method employ a random strategy [ZGZ13, ZXL+15, MS10, RBSMBA15a]. Here, the population-based approaches' decision values are initialised randomly within their respective intervals. However, infeasible solutions can be generated, as they do not always constitute a valid solution. Nevertheless, these solutions can be helpful during the search process, as promising solutions can occur at the border between feasible and infeasible solutions [RSIS09]. Some works employ an informed search to generate the initial solution set using domain-specific knowledge. However, injecting specific individuals into an initial population can bias the search, which can be unhelpful. For instance, in [XS18] only feasible solutions were generated and the global minimum of each objective was predetermined and added to the set; the same was done in [HBAO21]. Other techniques, such as the STOCH algorithm — which is an optimised Dijkstra's algorithm [ZCS04] — and rapidly-exploring random trees (RRT) [QYS21] have been employed. In [ZJWW10], the *node priority* methodology was used, which was also utilised in the representation scheme. Jun and Qingbao used a visibility graph and the chaos sequence technique to generate the initial population [JQ10]. A waypoint-based approach was similarly proposed and used by [DPMH13, DPMH15]. Using this technique, a different set of randomly generated waypoints is used for each solution and is connected in a second step. Hidalgo et al. proposed a selection window approach, i.e., the search space for the next point on the path was within a small window that was shifted accordingly during the generation process [HPVRFP15, HPVRFP17]. In one work, the authors used Voronoi-visibility points [HA20]. The authors in [HBAO21] used equally spaced points between the start and end points to generate the initial paths.

Diversification and Niching

The identified works used various diversification and niching methodologies. While there is no such technique for most optimal approaches, the authors using an evolutionary approach implement them. Often, domain-specific operators are used to (a) ensure the feasibility of the solution and (b) diversify the solution set. In general, diversification and niching methodologies in the literature are placed in the objective space. Because such techniques are a major aspect of this thesis, we provide more detail in a separate section (see Section 3.1.4).

3.1.3 Representation Schemes

Pathfinding problems have to be distinguished according to the representation of the pathfinding problem and the solution. For the former, we identified grid-based and graph-based approaches. For the latter, classification into fixed or variable-length solution representations can be made, with further sub-categories. We describe the related works in terms of these two classes.

Figure 3.4: Grid to Graph conversion [WM21b]

(a) Superimposed graph on a grid

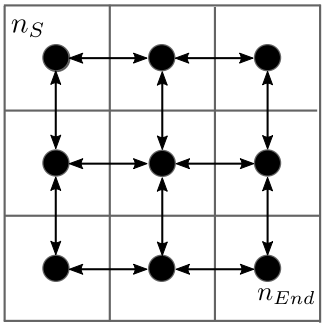

(b) Two paths p_i and p_{i+1} that go along nodes and edges.

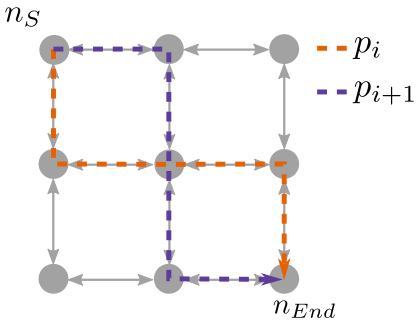

Problem Representation

There is extensive literature in the field of route planning and pathfinding in general, and especially for vehicle route planning, which uses EAs [AD13, CTM07, AKC+13, AD11]. Because EAs are considered as a meta-heuristic, a problem needs to be represented in a data structure to enable the algorithm to evaluate solution candidates.

Various representations have been suggested for the pathfinding problem. These include graph-based [CXCG10, QL16, TMS17, PMPDLC15, RBSMBA15b, WBM18] and grid-based representations [AD13, YBH15].

Grid-based representations for pathfinding problems have proven to be highly practical for EAs [AD13, AD11]. Such grid representations can be refined depending on the required resolution of the problem, as a search space can be defined as either coarse- or fine-grained. The resolution of a problem is the granularity of its representation. Moreover, grids are often used for benchmarking purposes [Stu12, KPK+14], and they can represent real-world problems by discretising the problem representation [Ang11]. Grids typically consist of units with adjustable size [Anb13]. Considering grids, several constraints for movements on specific paths by defining an upper limit for movements (such as speed) on each grid unit can be introduced. In this way, various linear and non-linear constraints on each unit, representing the speed, ascent, obstacles and others can be incorporated [WM21b].

It is comparatively easy to convert a grid into a graph by considering units as nodes and their contact-edges as the graph's edges. Grid-to-graph transfer is performed in several applications, e.g., the game industry. Regarding pathfinding, a grid is superimposed over an area and graph-search algorithms are used [Yap02]. The A* algorithm can be used for pathfinding on a grid which is transferred to a graph, where the heuristic function is the distance between grid cells [Yap02, Stu12].

In general, graph-based representations allow higher flexibility in representing real-world problems which are heterogeneous than do the typically homogeneous grids. However, other grid forms are also possible [WM22b].

Figure 3.4 depicts a graph which is superimposed on a grid (lattice graph) in the left panel and two paths p_i and p_{i+1} in the right panel.

Solution Representation

In most cases, two approaches are used. In the first approach, solutions are represented with a variable-length chromosome, which may be used in conjunction with a graph-based problem representation [EAA04, JQ10, MDSK07, DPMH13]. A solution is represented as a list of nodes, the length of which is variable when calculating a path. Another approach involves a fixed-length chromosome that is made up of a list of nodes in a graph or grid cells with indications of the direction of traversal [BPdlTMRM13, QXA13, AD13].

In [JQ10,LLHL13,JKC11], the authors proposed a graph-based approach, where each path consists of a list of variable length of nodes in a graph. Other variable-length approaches include techniques that use indices of obstacle vertices to encode a path [ZXL+15].

Regarding the genetic representation of paths, Beke et al. compared direct variable-length and direct fixed-length encodings [BWC20]. Variable-length encodings were introduced in [MTS98], where chromosomes consisted of the IDs of nodes in a graph. A random chromosome would probably end up in an infeasible path since two arbitrarily chosen nodes are not connected by an edge. Due to the variable length, this approach needs specialised operators to ensure its feasibility. Fixed-length encodings were influenced by the work of Inagaki [IHK99]. Here, the chromosome length equalled the number of nodes in a graph and a gene's locus, and the allele defines the next node in a path. However, besides direct representations containing node IDs, indirect representations also exist. A decoding function constructs the corresponding path. Gen et al. also proposed a random-key-based encoding, where the prioritisation was performed using real-valued priorities [GRD97]. The node with the highest priority among the current node's neighbours is attached to the last node to construct the path. Therefore, a chromosome's decoding will result in a valid path. Several existing crossover and mutation operators can work with such a fixed-length representation. Gen also proposed a random-key-based encoding, where the prioritisation was done using real-valued priorities [GL06]. Such real-valued and fixed-length representation schemes enable most operators to work on these problems. Other approaches for fixed-length chromosomes include the representation using splines [AD11, HBAO21].

In conclusion, in most of the literature, coordinate-based techniques were used, in which the coordinates that a path covered were encoded in the chromosome. It should be noted that several authors consider the variable-length representation to be unhelpful for solving and optimising pathfinding problems [ZJWW10, ZXL+15].

3.1.4 Diversification Methodologies

In the literature, various diversification and niching techniques are used. However, depending on the actual approach, several algorithms inherently lack this kind of measurement to maintain or increase the diversity of the solution set, such as optimal approaches. Shir stated that standard EAs tend to lose diversity within the population, resulting in landing in local optima [Shi12]. To address this issue, niching methods support maintaining diversity. Various methodologies in current state-of-the-art algorithms implement techniques to increase or maintain diversity. One example is to use crowding distance to identify crowded areas in the objective space. This measure reflects the average distance of the two neighbouring solutions of an individual [DPAM02]. During the replacement

and selection phase of the NSGA-II algorithm, this measurement can be used to emphasise solutions in less crowded areas. Other techniques involve the use of reference vectors. Solutions along these vectors are usually preferred, and as they are distributed in the objective space, diversity can be maintained [DJ14]. The latter methodology is often used with many-objective problems, optimising more than three objectives. However, studies have shown that the performance is impacted by the type of problem, resulting in the need for careful consideration when choosing an algorithm and not relying only on the number of objectives [CSF18,WM22b].

Furthermore, for specific problems, especially multi-modal ones where two or more solutions can map to the same objective values, other diversity measurements can be useful, such as combining different metrics in the objective and decision space [JRAM20]. For example, the many-objective pathfinding problem is a problem where close solutions in objective space can be far from each other in decision space, and vice versa. Therefore, using a diversity-maintaining measurement in decision space can be beneficial to an algorithm's performance [WM21b]. However, it is not trivial to compute a measurement of diversity in the decision space, especially if the solution's representation is of variable length. For fixed-length chromosomes, crowding distance or another metric — such as the harmonic mean — can be employed [JM21].

In the related work, genetic operators were often used to explore and exploit the search space. We mention such techniques in this subsection as they contribute to a diverse solution set. In several works, domain-specific operators were used [ZXL+15, XS18, JQ10, HPVRFP15, HPVRFP17, DPMH13, DPMH15]. In such cases, the authors incorporated problem knowledge into their algorithm, as the operators worked on various path representations, partially ensuring feasible solutions. Some works also used special operators to optimise specific objectives. Furthermore, domain-specific operators, such as mutation by finding a random path from a random point to the endpoint, have been proposed [ZCS04]. Altered probabilities and the use of probabilistic road maps were also employed [ZGZ13]. The authors of [HBAO21], who used evolutionary strategy, employed a custom step size crossover and extended log-normal rule mutation.

To our knowledge, diversification and niching (explicitly and by using operators) has been performed in the objective space in most studies that consider the pathfinding problem. It must be noted that domain-specific operators are not necessarily applied in the decision space but can also be applied in the objective space. This approach works for the problems that were examined, but it can be detrimental if properties of the environment change or other objective functions are used. In Chapter 6 we propose various methodologies that work in the solution space of the problem and therefore also work directly on the cause.

Furthermore, in several works, e.g., [DPMH15] it has been shown that paths can be highly similar to each other in the decision space yet distant in the objective space. However, a DM should choose from a diverse solution set in both spaces, since their criteria for satisfaction cannot always be objectified. Hence, a dominated solution with specific characteristics in the decision space can be the final choice by a DM.

3.1.5 Objectives

In the literature, several objective functions have been defined. In most cases, the length of the path is of interest and should be minimised. In [RMHS17] three objectives were optimised using a modified multi-objective A* algorithm, i.e.,

horizontal and vertical distance as well the maximal slope of a path. Machuca and Mandow used distance and time [MM12] as two objectives. Kanoh and Kenta additionally included a third objective, called *total penalty*, in which they aggregated various negative aspects of a path on a road network [KH08]. In Tozer et al., six objectives — such as distance, signal loss to a communication station, observability of an agent, travel time and the amount of used energy — were proposed [TMS17]. Other objectives, such as the smoothness of a path or some form of safety distance, are often used [RMHS17]. In contrast to its commonly known definition, the smoothness is often minimised to comply with other objectives. Criteria such as interestingness [SK21] or amenities of driving [Kan07] also appear in the literature.

3.1.6 Discussion

Some of the works claimed to propose a multi-objective approach that turned out to be a weighted sum or purposely found a single solution as a result. This approach does not comply with the definition of MOO. However, authors from other fields may follow a different concept of the term. Some authors proposed solutions where a set of objectives was first ensured and then, in a second step, another objective was optimised, using the comparable smaller search space from the first step. All proposed methodologies are valid approaches that work for the respective problems. According to the *no free lunch theorem* [WM97], no methodology outperforms another concerning all possible problems. Hence, the proposed techniques are all good solutions for their respective problems. However, the proposed problems have several characteristics in common. This commonality enables creating a more abstract pathfinding problem and the respective methodologies to solve them.

3.2 Applications

Pathfinding problems are found in several industrial applications. A trivial application is route planning on road networks for logistic applications or leisure purposes and so on. Besides road networks, vessels or aircraft such as airplanes, helicopters or drones need pathfinding techniques to reach their goals. The key is to transfer their respective medium of movement into a graph or grid.

Various other applications can also be represented as a pathfinding problem. For instance, surgeons plan paths when performing catheterisations or an ablation. In both cases, the tissue can be scanned with medical imaging methodologies and then transferred into a graph using a technique such as voxel representation and connecting them by edges. Furthermore, several other problems, such as job shop scheduling, can be transferred or reduced to a shortest path problem [SSBK21].

Another interesting application of the shortest path problem is the detection of negative cycles to find arbitrage opportunities [AMO93]. Such an opportunity can happen due to the inefficiencies on the stock market, and a trader may use differences in prices for the same asset in different markets. By detecting such a cycle, traders can make a profit. Other applications include project management, facility layout planning and DNA sequence alignment [AMO93]. The topic of this thesis is pathfinding methodologies using EAs, which each application can benefit from. To conclude, shortest path problems are found in various industries, medical applications, management and social sciences.

3.3 Benchmarks

For testing optimisation approaches and pathfinding algorithms, a ground-truth data set is needed to evaluate the quality of results compared to a known set of optimal solutions. Benchmarks meet this need by providing different classes of problems that algorithms can be applied to. In addition, so-called frameworks often provide generators to create problems that incorporate different characteristics.

There are several existing benchmark frameworks and test problems, such as [FCAM19, DTLZ05], for MOO algorithms in general. Additionally, there are several benchmark sets for the shortest path problem with multiple objectives, e.g., [Stu12, DGJ09]. The *DIMACS Implementation Challenge — Shortest Paths* [DGJ09] presents road maps for several states in the United States, combining different independent data sets. Various articles have used these graphs and a multi-objective approach, e.g., [MM12]. Other benchmark data sets operate on grid-based approaches, e.g., [Stu12, TMS17]. Usually, the data sets and graphs provided in these data sets are large, making it difficult to compute the true Pareto-front for given objectives [WM22b].

Nevertheless, in the related work, unique problems are mentioned in almost every article. Furthermore, reimplementing these problems is often an impossible task due to the lack of definitions of obstacle positions or specific height values. Moreover, it is often a challenge for researchers to understand a given code, especially if it is a language the researcher does not know. These facts are common barriers to working on the same problem as other authors.

In 2021, at the IEEE Congress on Evolutionary Computation, a multi-modal multi-objective pathfinding challenge was held. The challenge authors published several predefined scenarios to apply different algorithms. The problems resembled different roadmap designs and were imposed with different characteristics, such as traffic congestion or mandatory via-points through which a route had to pass. The maps also varied in size. Throughout the scenarios, up to seven objectives had to be taken care of. However, the authors did not provide the true Pareto-fronts and sets. In [Jin21] an exact algorithm was proposed to compute the true Pareto-optimal solutions.

The work of Hu et al. describes a benchmark test toolkit for multi-objective path optimisation [HZZ+19]. The authors propose a toolkit for discrete combinatorial problems and especially multi-objective path optimisation problems. In the study, a bottom-up approach is performed because the network in which paths are to be found is constructed by providing a model with certain information, such as the number of nodes and links. Furthermore, the user has to provide a set of Pareto-optimal objective vectors from which the network is created in a two-step process. In this work, the number of optimal paths is known beforehand as they are used to construct the test problem. Therefore, the work offers an approach to construct arbitrary large test problems. However, the authors stated that environmental characteristics, such as the direction of a network edge or the number of links of a node, are not adjustable. They mentioned that their model produces abstract transportation models that do not refer to any real-world application. The authors proposed a test problem-generating methodology that is based on the Pareto-optimal solutions instead of environmental characteristics that define a test problem.

3.4 Decision Support Systems

To our knowledge, there is only one work on decision support systems which is specifically tailored to the multi-objective pathfinding problem, but not to its many-objective variant. Such work is nonetheless important since with an increasing number of objectives, more solutions are non-dominated and therefore lie within the resulting solution set. In addition, pathfinding problems have real-world expressions and characteristics that an objective or a constraining function may not cover but are important to the DM. However, certain generally applicable methodologies in decision-making can be applied to pathfinding problems. Such techniques usually take information about objective values and other meta information into account that has been obtained from the DMs.

3.4.1 Application-specific Approach

Partes [Par21] proposes different methodologies to reduce the solution set to find interesting paths. First, the author presents a technique that involves different dominance criteria to identify an approximation of the solution set. The cardinality of this approximation set is likely smaller than the original set. Such approximation includes the computation of solutions that are not ε-dominated or knee-points on the non-dominated solution set. Furthermore, the author proposes to use clustering in the decision space to find similar paths according to a path similarity metric. Finally, the medoids of the computed clusters are presented as interesting solutions, as they represent a class of paths. In addition, a combined approach was proposed by first approximating the solution set in the objective space and clustering the remaining solutions in the decision space afterwards.

3.4.2 General Applicable Approaches

In the literature, several methodologies are presented to help a DM identify the most satisfying solutions concerning their aspirations. In this section, a subset of such methods is presented. In [RA15], the authors reviewed several articles covering different approaches. The interested reader is referred to that work, as we merely outline the most widely used techniques here.

Multi-Attribute Utility Method

The multi-attribute utility method can be a weighted sum approach, but other combining functions are also possible [Jan11]. With this methodology, for each objective that is considered an attribute of a solution, the importance is determined by interaction with the DM. The most trivial approach to compute the value $v(x)$ of an alternative x is a linear combination of the different attributes:

$$v(x) = \sum_{i=1}^{n} w_i v_i(x_i) \tag{3.2}$$

Here, w_i is the importance or weight of the value v_i of attribute i of x, namely x_i [Jan11]. Eventually, the alternative with the highest value will be the one that is chosen.

Analytic Hierarchy Process

The analytic hierarchy process involves determining the values representing the importance of a criterion over other criteria [Saa08]. After the resulting importance matrix has been obtained, the same methodology is applied to the values of each criterion. Then, they are ranked in a pairwise comparison. Finally, matrices containing inter-criteria importance rankings and intra-criteria importance rankings are computed. The principal eigenvector is computed for each criterion by determining the eigenvector centrality. This calculation yields a measure of the overall importance of the criteria. The jth solution's priority p_j can then be computed by:

$$p_j = \sum_i w_{ij} \cdot w_i \tag{3.3}$$

Here, w_i is the importance weight of criteria i, and w_{ij} is the importance weight of solution j of criteria i.

Other Approaches

Another approach, ELECTRE, eliminates alternative solutions from the solution set. Choosing, ranking and sorting methodologies are used throughout the process to iteratively result in recommendations [Tri00]. TOPSIS is another approach where distances from the best and worst alternatives are used to calculate the merits of an alternative. Using these distances, it is quantified how beneficial an alternative is [HY81]. Both these techniques require the input of the DM as solutions are compared in terms of their different attributes.

3.5 Summary and Conclusion

In this chapter, we have shown that the extent of previous research related to the topic of this thesis is vast, yet such work has not covered all aspects of the proposed problem. We have also shown that a general, scalable and variable pathfinding benchmark problem appears to be lacking. Furthermore, a methodology that is problem-specific, application independent and diversity preserving and enhancing does not exist. A study exploring the advantages and disadvantages of different representation schemes is required. Finally, given the nature of many-objective optimisation problems and the fact that a hypothetical DM must select from a large solution set, we have shown that the existing work on decision support systems can be extended in this area.

Although other works cover a wide range of aspects, there is still room for improvement and more in-depth analysis. In the following chapters, we address the drawbacks of the current approaches and present solutions to increase the performance of pathfinding algorithms.

4 Benchmarking Pathfinding Algorithms

In this chapter, the following points are covered

- Benchmark Construction
- Baseline Evaluation

The following chapter is largely based on the publication [WM22b].

Testing new algorithms is a challenging task. The literature on specific test problems for pathfinding and, specifically, multi-objective shortest path problems is scarce. In this thesis, we develop a novel scalable many-objective pathfinding benchmark, which can be considered a suite because many different instances can be generated. This chapter provides an in-depth description and analysis of the test suite. The benchmark itself is highly variable and scalable, as it can be adjusted in terms of size and hence the search space size; it can also be adjusted with respect to various constraints which influence the complexity.

4.1 Grid and Graph-based Benchmarking

Benchmarks can be based on grids to resemble an environment where a shortest path is to be found. Another approach is to create tests based on graph structures, as they often resemble real-world maps in a better way. In contrast to [HZZ+19] (cf. Section 3.3), our proposed test toolkit follows a top-down approach, i.e., we propose well-defined functions that are used to create test problems of arbitrary size. Furthermore, we suggest five objective functions that can be used to evaluate MOO algorithms.

This benchmark is aimed at representing environments for pathfinding algorithms on maps. Hence, we construct the instances by defining a cartesian grid with a specific size, where the cells have the same dimensions, also known as integer lattice. The variable properties of the benchmark influence the properties of each cell in the lattice [WM22b].

4.1.1 Benchmark Problem Construction

The multi-objective pathfinding problem can be defined as described in Section 2.3.2 and Equation (2.10). Before constructing the problem-related graph, we model a grid which is used as a map for the pathfinding problem. We assume that we have a two-dimensional search space defined by a given size (i.e., size of the map) denoted by the range $[1, x_{max}]$ in x-direction and $[1, y_{max}]$ in y-direction, $x_{max}, y_{max} \in \mathbb{N}$. This search space is divided into grid cells, which define the resolution of the path planning and therefore the size of the search space. Finally, the grid has x_{max} number of grid cells in the x-direction and y_{max} number of grid cells in the y-direction accordingly. We define different types of grid cells denoted by the position (x, y). These types impose constraints on the velocity of movements indicated by $v_{max}(x, y)$, which represents different road types as well as obstacles (denoted by $g_{LA}(x, y)$ and $g_{CH}(x, y)$ in Section 4.3.1). On obstacles a movement cannot occur. The cells with a velocity of zero define infeasible areas which can add further non-linear constraints.

We define an elevation function $h(x, y)$ with a variable number of hills, which can be defined by using either a peak-function or a combination of hill functions. This elevation function can be mapped to the cells in the map. Two additional features concern the neighbourhood and backtracking. The neighbourhood property restricts the number of possible neighbour cells an agent can move to. We use the 2^k-neighbourhood, similar to [SSF+19]. For instance, $k = 2$ means that it is possible to go to one of the four neighbours located in the cardinal directions. This neighbourhood is known as the *von Neumann neighbourhood*. If $k = 3$, there are eight possible neighbours, taking the diagonal cells into account. This neighbourhood is known as the *Moore neighbourhood*. The backtracking property of the benchmark defines whether an agent can go backwards or only forward. For instance, if backtracking is allowed and the goal is to go from the north-west corner of the grid to the southern-east corner, the agent can go in any direction specified by the 2^k-neighbourhood from any cell on a certain path. If backtracking is not allowed, the agent can only move in the directions of east, south and south-east (if $k = 3$). An 8-neighbourhood with enabled backtracking is also known as *king-moves*, derived from chess. A summary of the above adjustable features is shown in Table 4.1.

In the following, we propose a graph-based representation of the benchmark grid. As stated in Section 2.3.2, we describe all objectives for the evaluation of a solution represented as a path p of variable length j consisting of a list of adjacent nodes in a graph: $p = (n_1, \cdots, n_j)$. However, for the evaluation on the grid (as described above), each node n_i, $i = 1, \cdots, j$ can be replaced by their respective coordinates (x_{n_i}, y_{n_i}).

To transfer the grid to its corresponding graph, each cell c_i of the grid with its respective coordinates (x_i, y_i) is considered as a node in the graph. In our implementation, we assign properties to the graph's elements in the form of key-value pairs (see Section 2.3.2). Therefore, we assign the coordinates as a property to each node, making it possible to evaluate the objectives. Additionally, the various cell types, velocity constraints, characteristics about obstacles and elevation values are assigned to the properties of the node. Depending on the 2^k-neighbourhood and backtracking property, the corresponding nodes are connected to their respective neighbours using edges. The resulting graph is also known as *lattice graph*. Figure 4.1 shows an example of the transfer from a grid to a graph [WM22b].

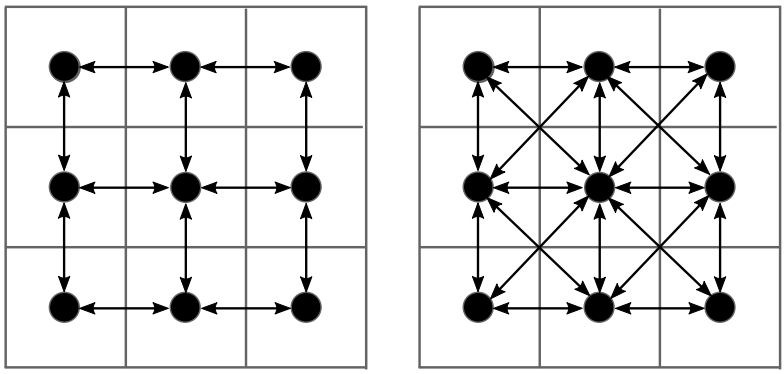

Figure 4.1: Superimposed graphs on grids for $k = 2$ (left) and $k = 3$ (right) instances. [WM22b]

Table 4.1: Adjustable properties of the proposed benchmark [WM22b]

Property	Values
Size	$\{x,y\}_{max} \in \mathbb{N}$, $1 < \{x,y\}_{max}$
Movement per cell	v_{max}
Expected delay	$delay(n_i, n_{i+1})$
Elevation Function	$nh \in \{1,2,3,M\}$
Neighbourhood	2^k, $k \in \{2,3\}$
Backtracking	$\{True, False\}$

4.1.2 Objective Functions

In this section, we define five objective functions by which a solution path p of length K is evaluated.

Objective 1: Euclidean length. The Euclidean length represents the distance between the start n_S and the end n_{End} of a path. It is calculated by the sum of the Euclidean distances $d(n_{i-1}, n_i)$ between the neighbouring vertex pairs n_{i-1} and n_i in a solution path p, as follows:

$$f_1(p) = \sum_{i=1}^{K-1} d(n_i, n_{i+1}) \tag{4.1}$$

Here, $i = 1$ corresponds to the starting point n_S, and the last node of a path n_K maps to the endpoint denoted n_{End}. Figure 4.2 illustrates an example. In real-world applications, this objective can additionally be used to estimate fuel consumption [WM22b].

Objective 2: Expected delays. The second objective is meant to measure the expected delay in a given path. In real-world applications, delays are caused by accidents or traffic. Therefore, a delay is the likelihood of having an accident or encountering other blockages on each node of the path. However, in our proposed approach, we do not take draws from the probability distribution, making it deterministic. The expected delay per path segment between the nodes n_i and n_{i+1} is defined by the differences between the corresponding velocity values of the two adjacent nodes (cf. Equation (4.12)). Our proposed second objective f_2 calculates the sum of $delay$ for all the edges on a given path p [WM22b]:

$$f_2(p) = \sum_{i=1}^{K-1} delay(n_i, n_{i+1}) \tag{4.2}$$

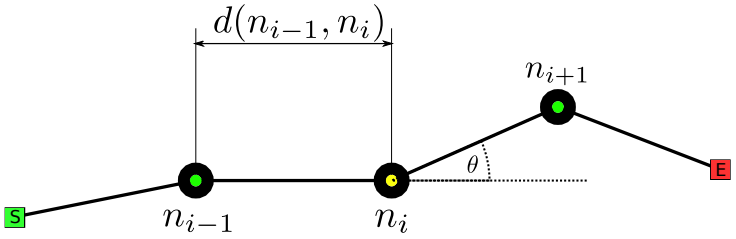

Figure 4.2: Objectives (1) and (5) on an example path modelled by a graph [WM22b]

Objective 3: Elevation. The aggregated ascent of a solution path is represented by the third objective. Our proposed benchmark contains various possibilities for defining the elevation function $h(n_i)$ which is defined on a node n_i. The ascent is calculated between two nodes in the graph $e(n_i, n_{i+1})$. The third objective $f_3(p)$ is the sum of the elevations between all the nodes in a path p:

$$f_3(p) = \sum_{i=1}^{K-1} e(n_i, n_{i+1})$$
$$e(m,n) = \begin{cases} h(n) - h(m), & \text{if } h(n) > h(m) \\ 0, & \text{otherwise} \end{cases} \tag{4.3}$$

This objective accounts to the amount of fuel consumption in a real-world application [WM22b].

Objective 4: Travelling time. The fourth objective represents the travelling time. For this calculation, we utilise the average velocity of two subsequent nodes defined by $\frac{v_{max}(n_i)+v_{max}(n_{i+1})}{2}$ for each node n_i and use the length of the path utilised in Objective 1 [WM22b]:

$$f_4(p) = \sum_{i=1}^{K-1} \frac{2d(n_i, n_{i+1})}{v_{max}(n_i) + v_{max}(n_{i+1})} \tag{4.4}$$

Objective 5: Smoothness. The smoothness or curvature of a path is modelled in the fifth objective. We measure smoothness by calculating the angle between three nodes on a path, as shown in Figure 4.2. The angle θ is obtained by extending the line between two nodes and measuring the angle to the third node. Similar to [ORK14, JQ10, HPVRFP15, DPMH15], we invert $a \cdot b = \|a\|\|b\|cos(\theta)$:

$$f_5(p) = \sum_{i=2}^{K-1} arccos\left(\frac{\overrightarrow{n_i n_{i-1}} \cdot \overrightarrow{n_{i+1} n_i}}{|\overrightarrow{n_i n_{i-1}}| \cdot |\overrightarrow{n_{i+1} n_i}|}\right) \tag{4.5}$$

Because we intend to minimise the objective values, the smaller smoothness value represents a straighter path [WM22b].

4.2 Benchmark Test Suite

In the following, we propose various examples for a test suite by selecting specific features for the defined variables of the benchmark. We set $n_S = (1,1)$ as the start and $n_{End} = (x_{max}, y_{max})$ as the end nodes. This means a path starts in the north-western corner and ends in the south-eastern corner. We set four kinds of cells with velocity values v_{max} of 130, 100, 50 and 0. For obstacle cells with $v_{max} = 0$, we propose two different forms: 1) the checkerboard pattern is

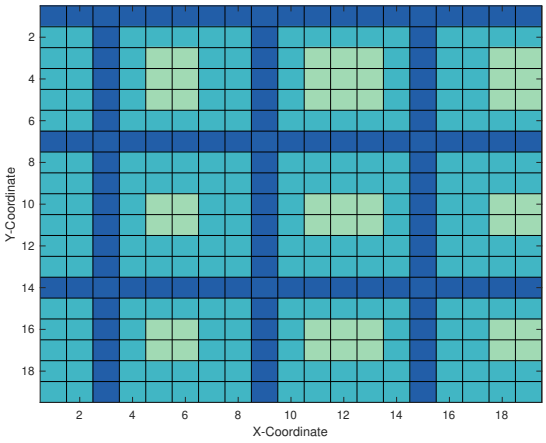

Figure 4.3: Three types of cells [WM22b]

(a) *lake* obstacle (b) *checkboard*-obstacles

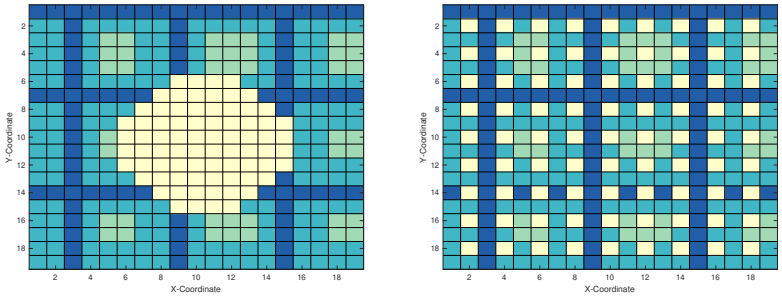

Figure 4.4: Examples of grid cell properties (dark to light colours represent high to low speed values) [WM22b]

designed to simulate block-like environments, and 2) the lake obstacle denotes a larges region which is not passable (Figure 4.4). For the checkerboard obstacles, we define every second cell to be an obstacle in both x and y directions. The lake obstacle is defined as a circle on the grid. The circle radius is defined by a fraction of the x-size of the grid. We represent the checkerboard and lake obstacles as a variant of the square wave function and circle function, respectively (see Equations (4.8a) and (4.10)). In the tested instances, the lake obstacles are defined by a radius of $x_{max}/4$. Figures 4.4a and 4.4b show the two obstacle types on an example instance of the benchmark problem. Figure 4.3 shows an example instance of size 19 [WM22b].

The corresponding equations are provided in Section 4.3.1.

For the elevation, we take four hill functions in the domain $[-3,3]$, which will be scaled when applied to the grid with cell coordinates (x,y) represented by the node n in the path segment. For determining the corresponding height value $h(x,y)$, the two cell coordinates must be scaled to the interval $[-3,3]$, hence $[\{1,1\},\{x_{max}+1,y_{max}+1\}] \rightarrow [-3,3]$ and $(x,y) \rightarrow (x_s,y_s), \{x_s,y_s \in \mathbb{R} | -3 \leq x_s,y_s \leq 3\}$. In the equation, we refer to (x_s,y_s) to represent the scaled coordinates:

$$\begin{aligned} h_m(x_s,y_s) =& 3(1-x_s)^2 e^{-x_s^2-(y_s+1)^2} - 10e^{-x_s^2-y_s^2} \\ & (-x_s^3+x_s/5-y_s^5) - 1/3e^{-(x_s+1)^2-y_s^2} \\ h_1(x_s,y_s) =& 5e^{-(x_s+1.5)^2-(y_s+1.5)^2} \\ h_2(x_s,y_s) =& 5e^{-(x_s-1.5)^2-(y_s-1.5)^2} \\ h_3(x_s,y_s) =& 5e^{-(x_s-1.5)^2-(y_s+1.5)^2} \end{aligned} \tag{4.6}$$

Figure 4.5: Different elevation profiles of the proposed benchmark [WM22b]

(a) Elevation profile for $nh = M$

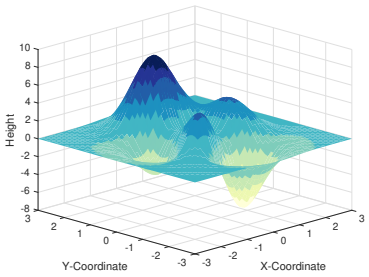

(b) Elevation profile for $nh = 1$

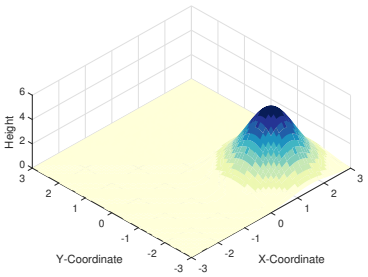

(c) Elevation profile for $nh = 2$

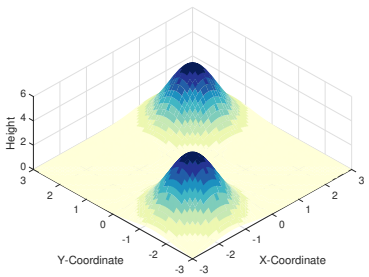

(d) Elevation profile for $nh = 3$

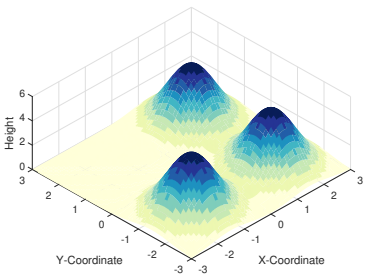

We chose these functions to represent different height settings on the grid. Equation h_m, also known as the *peaks* function, has various hills and valleys. Since this function is defined in the interval of $[-3,3]$, we define the other three functions in the same interval. Each of the three other equations represents a hill on the landscape. In Figure 4.5, the linear combinations of the functions are depicted. Combining them yields various elevation characteristics of the problem instances. Finally, an instance can have h_m *or* a linear combination of the others as its elevation function. Therefore, we define h as:

$$h(x,y) = \begin{cases} \sum_{i=1}^{nh} h_i, & \text{if } nh \in \{2,3\} \\ h_3, & \text{if } nh = 1 \\ h_m, & \text{if } nh = M \end{cases} \tag{4.7}$$

For the third objective, we aggregate positive slopes, as we want to focus on flat routes. Taking negative elevations into account too can result in a path containing a hill with a steep gradient, which is not beneficial for a bulky transportation. The fourth objective, expected delay, is defined by v_{max} of two subsequent cells (see evaluation section Equations (4.11) and (4.12).)

All these variations of the properties are used in the name of a benchmark instance. The name starts with *ASLETISMAC* for the five objectives to be minimised: ascent, length, time, smoothness and accidents (expected delay). Thereafter, the name includes the obstacle type, followed by the size (in X and Y directions), the elevation function (PM stands for the peaks function h_m and the combination is set to Pnh), followed by the 2^k-neighbourhood and finally the backtracking (B) property (T for true or F for false). For example, *ASLETISMAC_CH_X10_Y10_P1_K2_BF* defines an instance with the checkerboard obstacles, sized 10x10, $nh = 1$ as the elevation function (one hill), four possible neighbours (K2), but no backtracking (BF) [WM22b]. For the values of delays (caused by accidents) in the second objective, we refer to real-world

Table 4.2: Integer sequences of possible number of paths from the north-western corner to the south-eastern corner one with no obstacles on oeis.org for the size of nxn [WM22b].

Benchmark type	Integer sequence
K3,BF	A001850
K3,BT	A140518
K2,BF	A000984
K2,BT	A007764

statistical data (see Equation (4.2))[1]. We adopt the likelihood of encountering an accident from real-world data, depending on the v_{max} of a certain cell. For instance, one is far more likely to have an accident when driving on streets located in a city, i.e., with a lower v_{max}, than on highways or country roads. Therefore, we assume a smaller likelihood of encountering an accident with higher velocities. We also assume a large likelihood when the type of street changes, such as travelling on an access road or an exit road [WM22b].

4.2.1 Obtaining the True Pareto-front

We performed an exhaustive search on 272 benchmark instances with different obstacle types, sizes, elevation functions and neighbourhood metrics. To obtain the fronts, we performed a depth-first search (DFS) from the cell at the northern-west corner to the south-east corner cell. The larger the instances, the longer the DFS takes to complete. The most complex in terms of the number of possible paths we evaluated was the instance *ASLETISMAC_NO_X14_Y14_PX_K3_BF*, which had a size of 14x14, 4-neighbourhood and no backtracking. For this instance, there were 1 409 933 619 possible paths.

The number of possible paths is represented by specific integer sequences, obtainable at oeis.org. The numbers are shown in Table 4.2.

4.2.2 Benchmark Characteristics

The proposed benchmark has several specific characteristics. Regarding the decision space, we can define a fixed- or variable-length encoding of solutions. Fixed encodings are suggested especially for the *K2,BF* instances, as the allowed paths have the same length $f_1(p)$, i.e., $f_1(p) = ((x_{max} - 1) + (y_{max} - 1))$. Using a variable-length approach can represent the problem as a combinatorial one. For this purpose, one can use graph, real-value or integer-value representations. In this case, the true Pareto-fronts of the test instances are disconnected and degenerate due to the discrete search space. In addition, the fronts are irregular and the different objectives have different scales. An interesting characteristic of this benchmark is that similar paths on the grid are not necessarily close in the objective space, implying that paths which differ in most of their nodes can lead to similar objective values. In the *K2,BF* instances, the challenges for algorithms depend on the chosen representation to find a feasible path, as the ratio of infeasible to feasible solutions is relatively high. In Section 4.3.4 and Appendix A.1.2, Figures 4.10 and A.2 to A.5 show several examples of obtained true Pareto-sets and fronts as well as algorithmic results [WM22b].

1. https://www.destatis.de/EN/Themes/Society-Environment/Traffic-Accidents/_node.html

4.3 Evaluation

The suite of test problems is a baseline for the methodologies and approaches proposed in the following chapters. Therefore, we evaluate standard algorithms on various instances. We set specific obstacle and velocity configurations (i.e., *environmental settings*) for the mentioned problems and use four algorithms. Furthermore, the benchmark characteristics are transferred to a real-world map and the same algorithms are applied.

4.3.1 Environmental Settings

Obstacles on the map

The following equations are defined for the lake g_{LA} and checkerboard g_{CH} obstacles. These equations are mapped to the grids with the grid cell positions of (x,y). With these functions, cells of the grid can be identified where obstacles will be positioned, hence cells with $v_{max} = 0$. The two provided obstacle functions can be used as a constraining function when running an optimisation algorithm. They take the cell's coordinate as an input and output a true or false value, which determines whether the specified cell is an obstacle. For all obstacle functions holds: $\{x \in \mathbb{N} | 1 \leq x \leq x_{max}\}$ and $\{y \in \mathbb{N} | 1 \leq y \leq y_{max}\}$ [WM22b].

The checkerboard obstacle is defined as follows:

$$\begin{aligned} g_{CH}(x,y) =& \operatorname{sign}\left(\sin\left(\frac{\pi}{2}+\pi x\right)\right) + \operatorname{sign}\left(\sin\left(\frac{\pi}{2}+\pi y\right)\right) \\ & - 2\Pi(x-x_{max})\,\Pi(y-y_{max}) < 2 \end{aligned} \tag{4.8a}$$

$$\Pi(a) = H\left(a+\frac{1}{2}\right) - H\left(a-\frac{1}{2}\right) \tag{4.8b}$$

where $H(\cdot)$ is the so-called Heaviside step function with:

$$H(x) := \begin{cases} 1, & x > 0 \\ 0, & x \leq 0 \end{cases} \tag{4.9}$$

The lake obstacle is defined as follows:

$$\begin{aligned} & g_{LA}(x,y) = \\ & \left(x-1-\frac{x_{max}}{2}\right)^2 + \left(y-1-\frac{y_{max}}{2}\right)^2 - (r x_{max})^2 < 0 \end{aligned} \tag{4.10}$$

where r denotes the radius ratio.

Velocity functions

To determine the velocity v_{max} of each cell except obstacle cells with $v_{max} = 0$, we used the following equation, representing the three street types of highways, country roads and city streets. The data is derived from the usual speed limits in Germany. The function takes the cell's coordinates as an input and outputs the respecting v_{max} for that cell. The provided values can be exchanged or extended

to represent other road networks. For all velocity function the following holds: $\{x \in \mathbb{N} | 1 \leq x \leq x_{max}\}$ and $\{y \in \mathbb{N} | 1 \leq y \leq y_{max}\}$ [WM22b].

$$v_{max}(x,y) = \begin{cases} 130, & \text{if } w(x,y) > 0.9 \\ 50, & \text{if } w(x,y) < -0.4 \\ 100, & \text{else} \end{cases} \tag{4.11}$$

where $w(x,y) = \max(sin(x-1), cos(y-1))$.

Derived from this property, the expected delay per path segment is also defined:

$$delay(n_i, n_{i+1}) = \begin{cases} 2 & \text{if } v_{max}(n_i) \neq v_{max}(n_{i+1}) \\ 3 & \text{if } v_{max}(n_i) = v_{max}(n_{i+1}) = 50 \\ 1 & \text{if } v_{max}(n_i) = v_{max}(n_{i+1}) = 100 \\ \frac{1}{5} & \text{otherwise} \end{cases} \tag{4.12}$$

4.3.2 Experimental Settings

In the experiments, we investigated the degree of difficulty of the proposed benchmark problem. We applied four state-of-the-art EAs to several instances to evaluate the complexity of the benchmark. Furthermore, we present a custom mutation operator which can operate on a variable-length chromosome consisting of a list of nodes.

In our proposed benchmark, we consider a solution to be a sequence of nodes $p = (n_1, \cdots, n_K)$ with a variable-length K. We take this representation for the encoding in EAs. The variable-length chromosome poses difficulties for the algorithms but can be highly efficient when using realistic data, since intersections and endpoints are not homogeneously distributed and paths usually have different lengths. This representation was used by [LBE18, TY12, LZY+06] and studied by [BWC20].

We used a one- or two-point crossover for this encoding, as follows. If two selected solutions had intersection points except for the start and end nodes, these points could be used as possible cut-off points. If there were fewer than two intersections, we used a one-point crossover. Additionally, we defined the so-called *perimeter mutation operator*. From a given path which is to be mutated, we took two arbitrary points within a maximum network distance $d_{max} = \frac{|p|}{2}$ and computed their middle point. Then we searched for a random point within a maximum distance of r_{max}, using an R-tree index [Gut84], which was generated upfront. We performed a random search (local search) from the first and second points to it. Depending on the benchmark instance, we either considered all neighbouring nodes within the radius in positive cardinal and diagonal directions (instances of type *K3,BF*) or a subset of them, namely, nodes in positive cardinal directions for *K2,BF* [WM22b]. In Section 6.1.2, the operator is described in more detail.

In the experiments, we used the NSGA-II [DPAM02], NSGA-III [DJ14] and DIR-enhanced NSGA-II (d-NSGA-II) [CSF18] algorithms. The d-NSGA-II employs a diversity indicator based on reference vectors [CSF18], making it suitable for many-objective optimisation problems. Additionally, we used an indicator-based algorithm, the $I_{SDE}+$ algorithm [PMS19]. For all four algorithms, we set the population size to $\mu = 212$ as in the original NSGA-III study.

We set the probabilities for crossover and mutation to $\mathbb{P}_c = 0.8$ and $\mathbb{P}_m = 0.2$, the number of divisions for NSGA-III to 6, the maximum number of generations to 500, and the number of runs to 31 for statistical analysis. The task of the pathfinding algorithm was to find a path from the north-west corner to the south-east corner.

To compare the algorithms, we calculated the IGD^+ indicator [IMN15,IMTN14]. The results were compared and tested for statistical significance using the non-parametric Kruskal-Wallis test and Bonferroni correction for multiple independent samples, as suggested by Knowles et al. [KTZ06]. The null hypothesis states that that the distributions of the four samples have equal medians. Statistical significance of the difference in performance was assumed for p-values smaller than 0.01 [WM22b].

Real-World Data

OpenStreetMap (OSM)[2] provides the GPS coordinates for a graph representation, which can be used to measure the path length for the first objective. For the second objective concerning the delay (number of accidents), we used the publicly available accident statistic data from 2018[3] and mapped the data to the imported network. The coordinates of the accidents generally differed from the available nodes in the network. Hence, we defined an R-tree index [Gut84] on the network and performed a nearest node search for each accident to align each accident to a node in the network.

The third objective was measured using the Google Maps Elevation API[4]. The elevation is obtained in metres above mean sea level and written to the node's properties. For the smoothness, we simplified the network to straight connections between nodes, which meant that smoothness was obtained in the same way as in the proposed benchmark.

From the OSM network, we obtained information about speed limits per street segment. We calculated the time needed per segment as the ratio of distance and speed. Summing the values of each segment resulted in the total travelling time (Objective 5). For the experiments, we used the same parameter settings as above with only one-point crossover [WM22b].

4.3.3 Results

Artificial Instances

In the first part of our analysis, we counted the number of successful runs in which the algorithms could obtain the entire Pareto-front. A front was found if the IGD^+ was 0 in all 31 runs of the algorithms. Given 272 valid instances, NSGA-II, NSGA-III, d-NSGA-II and $I_{SDE}+$ were unable to find the complete true Pareto-fronts for 234, 233, 240 and 221 instances. This indicates the difficulty of the benchmark for specific instances. For 15 instances, the algorithms did not find a result. This outcome occurred mostly on the small *X3_Y3* instances. The reason was the customised operators, which can fail on relatively short paths. It can occur that the mutation operator cannot find a suitable node in the given radius.

2. https://www.openstreetmap.org
3. https://web.archive.org/web/20200704125405/https://unfallatlas.statistikportal.de/_opendata2019.html
4. https://developers.google.com/maps/documentation/elevation/start

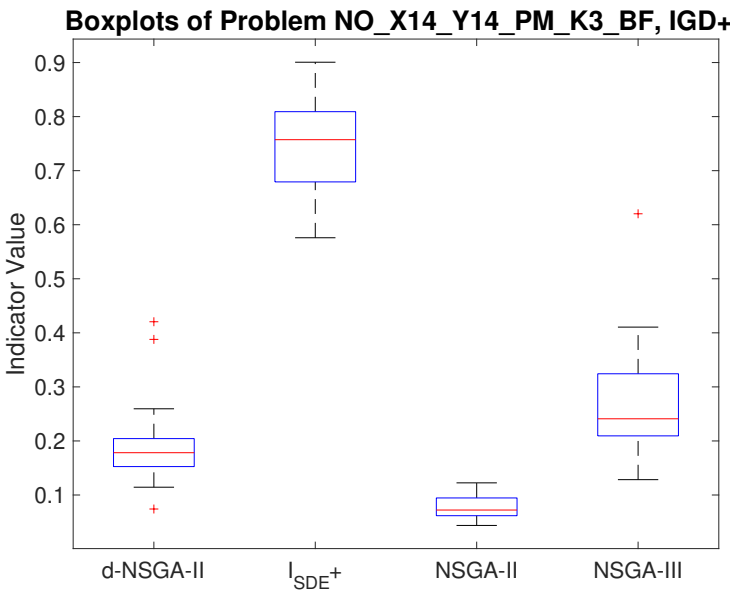

Figure 4.6: Obtained IGD$^+$ Values for the instance NO_X14_Y14_PM_K3_BF [WM22b]

Table 4.3: Wins, losses and ties of each algorithm pair (rows vs. column) with statistical significance at $p < 0.01$, Bonferroni correction applied, IGD+ indicator. [WM22b]

	$I_{SDE}+$	NSGA-II	NSGA-III
d-NSGA-II	167/31/59	22/183/52	66/45/146
$I_{SDE}+$		26/213/18	41/158/58
NSGA-II			179/39/39

After running the experiments, we obtained complete results for 257 instances. By 'complete' we mean the results from all 31 runs for an instance for all four algorithms. Figure 4.6 shows the obtained IGD$^+$ values for the instance NO_X14_Y14_PM_K3_BF, for which none of the algorithms found the whole Pareto-front, indicating the complexity of the problem. We noted that NSGA-II obtained the best result, although NSGA-II is not usually considered the best option for many-objective problems. In Table 4.3, the wins, losses and ties are shown for each of the algorithms.

Overall, NSGA-II performed the best in the IGD$^+$ indicator in most instances, with a statistically significant difference ($p < 0.01$, see Figure A.1). This could be due to the crowding distance estimation to maintain diversity, which is beneficial to irregular Pareto-fronts [CSF18]. However, the results of the $I_{SDE}+$ algorithms indicate that more algorithms of this class should be tested on the benchmarks, as they yielded the most completely solved instances. Five other instances, including their Pareto-set and results for the four algorithms, are presented in Section 4.3.4 and Appendix A.1.2 in Figures 4.10 and A.2 to A.5. The $I_{SDE}+$ algorithm showed the most diverse results in the decision space. When analysing the algorithms' progress, we often saw in the *K2,BF* instances that some algorithms converged to paths that only went down and then right. We surmised that it can be challenging for algorithms to explore these instances' search spaces because they may fall into local optima. The proposed benchmark suite generated instances in which the closeness of paths did not reflect closeness in objective space. In conclusion, size, neighbourhood and backtracking increased the search space size; conversely, changing the latter two to values which decreased the search space would also increase the ratio of infeasible to feasible solutions. The convergence to local optima is visible in Figure A.5 in the appendix (see Appendix A). From a visual perspective, it seems that the $I_{SDE}+$ algorithm is less prone to these challenges [WM22b].

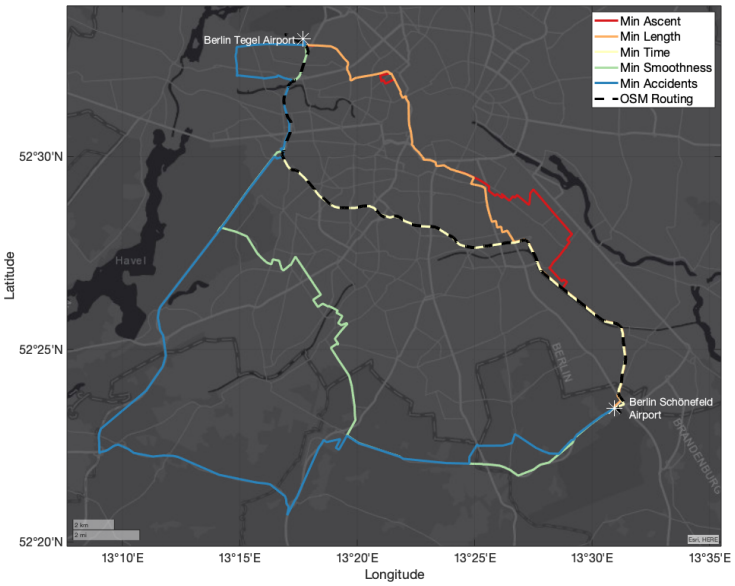

Figure 4.7: Map of Berlin showing the best path in terms of each objective. — Min Ascent, — Min Length, — Min Time, — Min Smoothness, — Min expected delay. The dashed black line represents the path from the original OSM Routing Service [WM22b]

Real-World Data

In the following, we transfer the problem from the proposed benchmark to a real-world application. We use the data on the map of Berlin and compute a set of paths between the two airports *Berlin-Tegel* and *Berlin-Schönefeld*. For this purpose, we use OSM data, which is imported and converted to an undirected graph via the *osmnx* library [Boe17]. We simplify the network by removing nodes which do not represent an intersection. The resulting graph has 63 731 vertices and 84 912 edges. For merged edges, we take the maximum values of the merged partners and aggregate the distances. Our computed path is thus an approximation but can be used to analyse the algorithm's performance on real-world data. Figure 4.7 shows the layout of the map and depicts the start and end points [WM22b].

Because this is a real-world problem, we do not know the true Pareto-front. To approximate the performance of the algorithms, we combined all results from all four algorithms and all 31 runs and calculated the non-dominated solution set. We obtained 1422 non-dominated solutions. Figure 4.7 shows a subset of the obtained non-dominated solutions and the path obtained from the OSM routing service. For clarity, we do not illustrate the whole set but only five non-dominated paths from one airport to the other, representing the best solution per objective. It is evident that the paths differ. Furthermore, the paths with the fewest accidents mostly traverse highways, indicating that the algorithms could explore the search space. Interestingly, our obtained path with the least time is the same as that obtained from the OSM routing service. All depicted paths could be recommended to a hypothetical driver, representing different possible requirements. The blue route is probably the most reliable one as it contains the least expected delay, despite being relatively long. The red route is suitable for vehicles with relatively low power [WM22b].

With the obtained reference from all runs, we calculated the IGD^+ indicator for the four algorithms. Figure 4.8 shows the respective values of the obtained results, and Figure 4.9 shows the parallel coordinates plot of the best solutions per objective. In this experiment, NSGA-III obtained the best median; however, it significantly outperformed d-NSGA-II and $\text{I}_{SDE}+$ [WM22b].

Figure 4.8: Obtained IGD$^+$ values on the real-world problem [WM22b]

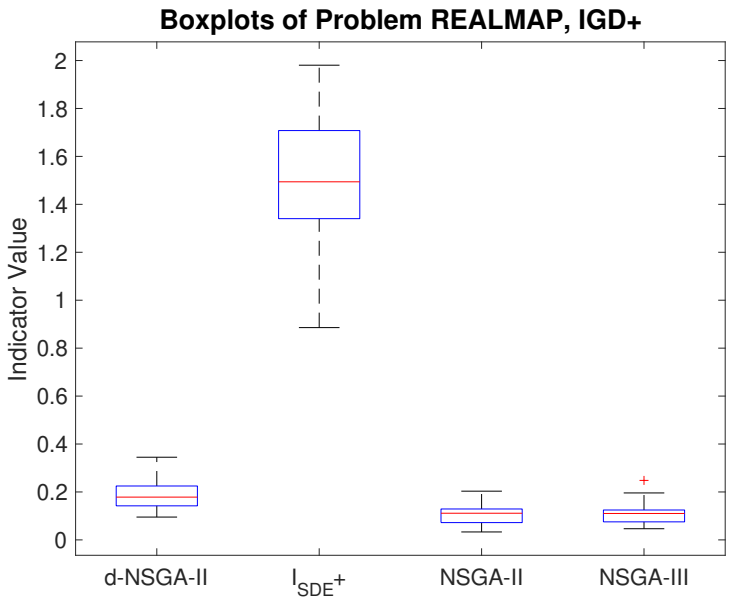

Figure 4.9: Parallel coordinates plot of the best paths for each objective [WM22b]

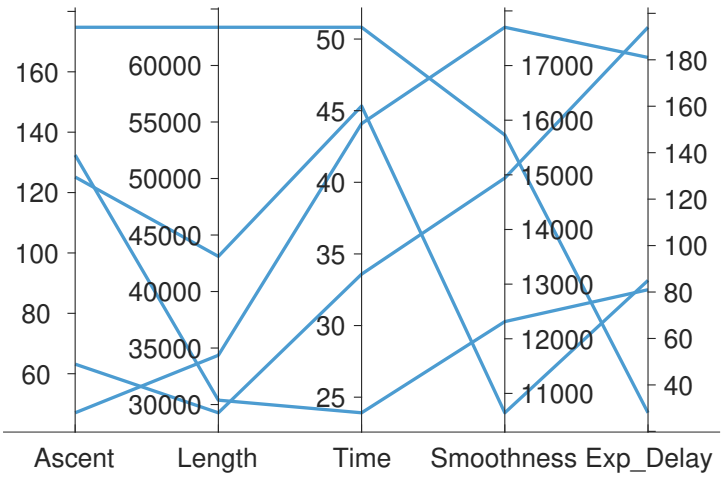

The experiments show that while the NSGA-II performed the best on the majority of the benchmark instances, the NSGA-III was at least equally good on the real-world example. The artificial instances are distinguishable from the real-world example because the former are ordered as a grid, whereas real-world data is usually more heterogeneous. An algorithm's performance can depend on the underlying structure. The artificial instances reflect the properties of real-world street networks to a certain extent while being scalable and variable [WM22b].

4.3.4 Detailed Path Visualisations

Figure 4.10 show true Pareto-fronts, sets and results from the algorithms for the instance NO_X5_Y5_P3_K3_BF. Figures A.2 to A.5 in the appendix (see Appendix A.1.2) show true Pareto-fronts, sets and results from the algorithms for four other different instances. Furthermore, Figure A.1 illustrates the obtained IGD+ values regarding the different types of problem instances. For the smoothness objective, values are given in degrees.

4.4 Summary

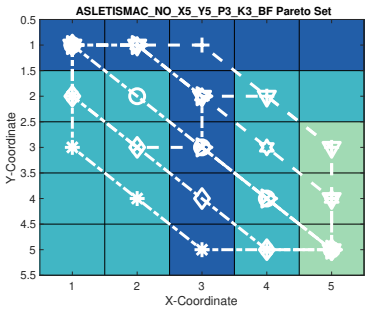

(a) Pareto-set of instance NO_X5_Y5_P3_K3_BF

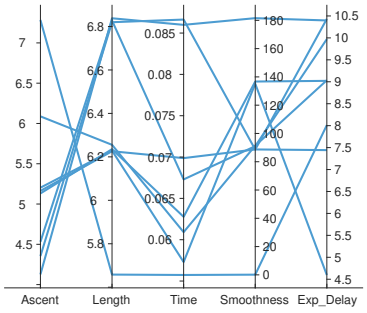

(b) Pareto-Front of instance NO_X5_Y5_P3_K3_BF

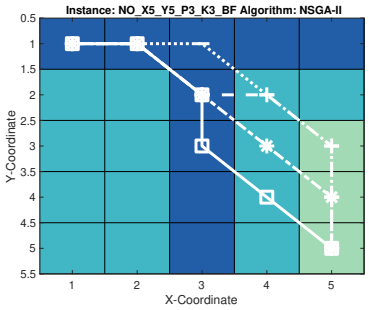

(c) Result set of algorithm NSGA-II

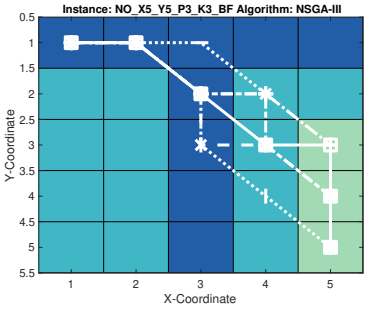

(d) Result set of algorithm NSGA-III

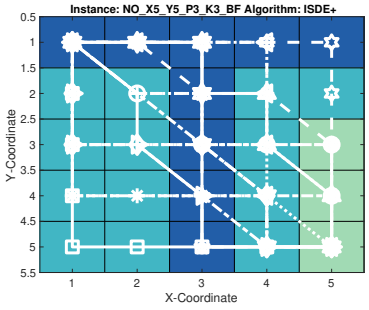

(e) Result set of algorithm $I_{SDE}+$

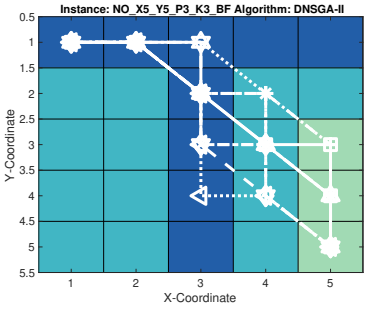

(f) Result set of algorithm D-NSGA-II

Figure 4.10: Pareto-set and front of instance NO_X5_Y5_P3_K3_BF and result sets of all algorithm (median run with respect to IGD^+ value) [WM22b]

In this chapter, we have presented a scalable many-objective pathfinding benchmark problem representing a real-world related navigation problem on actual map data. The benchmark is scalable and can be used to analyse many-objective optimisation techniques for path and route planning and navigation. Different obstacle types, as well as elevation functions, neighbourhoods and backtracking properties, can be adjusted according to the required complexity. We have proposed five objective functions for the benchmark related to real-world goals when planning a route. Furthermore, we have obtained the true Pareto-fronts for several benchmark instances, which we provide in the appendix. Additionally, we have used four existing EAs to minimise five objectives and compared the results with the obtained true Pareto-fronts of several benchmark instances. Moreover, we have transferred the benchmark's characteristics to real-world data by adding further information to an OSM data graph that we had downloaded. We have also applied the algorithms with the same parameters and obtained promising results. In the following chapters, we use the proposed

problem generator to evaluate our approaches and methodologies for different problem sizes and complexities.

5 Representation Schemes and Performance Considerations

In this chapter, the following points are covered

- Comparison of Encodings
- Initial Solution Generation
- Performance Considerations

In this chapter, different representation schemes of the many-objective pathfinding problem and its respective solutions are discussed and evaluated. Furthermore, various approaches for generating an initial solution set are proposed. Additionally, considerations regarding the size of the problem graph are examined, and several performance-enhancing techniques are proposed.

5.1 Representation Schemes

The following section is largely based on the publication [WZM21].

In EAs, a problem and its respective solutions can be represented by various approaches. For many problems, a fixed-length representation is used, where the chromosome is an n-dimensional vector of real-valued numbers. A problem then has n decision variables. Several existing state-of-the-art operators, e.g., crossover and mutation operators, work on these fixed-length chromosomes. For instance, a crossover operator can create new offspring chromosomes by dividing two parent chromosomes at the same decision variable and concatenating the different respective parts again. In the other approach, i.e., variable-length representation, new challenges occur because chromosomes can vary in length, and this renders the division not trivial. In this section, we describe these two main approaches and propose suitable representation schemes tailored for the multi-objective pathfinding problem. The representation scheme or encoding is often chosen regarding a specific problem. We thus evaluate our approaches on the ASLETISMAC benchmark proposed in Chapter 4.

5.1.1 Fixed Length

In contrast to the encoding used in the original work (Chapter 4, [WM22b]), which used a variable-length encoding, most algorithm frameworks are — by

default — configured with fixed numbers of variables. Here, we propose a real-valued and a binary representation scheme, respectively.

Moreover, in the original graph representation of the problem, obstacles in the map were avoided by removing their nodes from the graph. However, in our approach, coordinates in the map could be created that contained obstacles (which render a path infeasible). Hence, we propose two different ways of handling infeasible solutions in our encodings [WZM21].

Real-valued Encoding

For the real-valued encoding, each variable represents one step of movement on the grid-based map. Based on the chosen neighbourhood, obstacles and other parameters, different directions of movement are possible from any given location in the grid. As a result, each variable represents the direction to move in during the next step while traversing the path. Because we define a fixed-length encoding, using this pattern, only a fixed number of steps is possible. The maximum number of direction changes for a path from one corner to the opposite corner is defined by the map's size, i.e., $d_{max} = x_{max} + y_{max} - 2$. We propose multiplying this number by a certain factor δ because of the benchmark's ability to represent maps where backtracking is allowed. Hence, the destination can be reached even if directions are used, which increase the distance to the end coordinates in suboptimal solutions or when obstacles have to be avoided. In the experiments, we evaluate the impact of different values of δ. The total number of decision variables is defined as $D = \lceil d_{max} \cdot \delta \rceil$.

Decoding is implemented from the real-valued vector $\vec{r}$, which translates the real values into coordinates in the grid, i.e., a list of nodes. This list is then used in the original evaluation functions of the problem, as shown in Chapter 4.

For each decision variable r_i, we define the domain $r_i \in [0,1]$. During the evaluation, this interval is divided into the number of possible neighbours of a cell; therefore, each sub-interval maps to another direction in the following way. For each variable r_i, determine the neighbours $n_{neighbours}$ of the current grid cell. Then, divide the interval $[0,1]$ into $n_{neighbours}$ parts. The value of r_i determines which neighbour is used and which step is added to the path [WZM21].

Binary Encoding

The binary encoding uses a number of bits necessary to express the possible neighbouring nodes according to the chosen neighbourhood structure for every decision. One individual consists of a binary vector $\vec{b} = (b_1, \cdots, b_D)$, where $b_i \in \{0,1\}$, for $i = 1, \cdots, D$. In the same way as in the real encoding, we employ the factor δ to increase the likelihood of reaching the goal. The number of decision variables with this encoding is defined by $D = \lceil (\lfloor log_2(n_{neighbours}) \rfloor + 1) \cdot d_{max} \cdot \delta \rceil$. The value of $n_{neighbours}$ depends on the benchmark's setting regarding the 2^k-neighbourhood and the backtracking setting. Since we need $\lfloor log_2(n_{neighbours}) \rfloor + 1$ bits to encode one change in direction, we map the respective number of bits to a number in the interval of $[0,1]$ and decode the path using the same methodology as in the real-value encoding [WZM21].

Neighbour Calculation

In both proposed encodings, the number of existing neighbours $n_{neighbours}$ must be computed for each grid cell. The number of neighbours is influenced by the

problem's parameters, i.e., the neighbourhood ($k = 2$ or $k = 3$), and by whether backtracking is allowed on paths. For instance, if $k = 2$ and backtracking is allowed, there are four possible neighbours: east, south, west and north. By contrast, without backtracking, the traversal is allowed only to the east and the south. On the other hand, with a $k = 3$ neighbourhood, the diagonal directions would also be allowed. Furthermore, cells at the edges of the map may possess fewer neighbouring cells. In addition, the existence of obstacles in the map can lead to smaller numbers of neighbours for the cells next to the obstacle cells.

In our encoding, the movement towards a neighbouring cell is always computed with only the available neighbours. This means that in cases where backtracking is not allowed and the current position lies on the right border of the map, the only remaining neighbour is the cell below. Hence, no matter which value the following real or binary-encoded movement contains, the outcome is always the same neighbour [WZM21].

Constraint Handling

Constraint handling methodologies are necessary for the fixed-length encodings to tackle two separate challenges: (1) the produced paths do not necessarily arrive at the designated destination position, i.e., (x_{max}, y_{max}) in the map, and (2) the encodings may be able to produce paths that traverse through grid cells with obstacles on them.

While the original implementation reported in [WM22b] always operated on feasible paths with a fixed start and destination, the proposed fixed-length encoding does not guarantee arrival at the destination. Instead, the decisions on which direction to take in each grid cell can, independent of binary or real-valued encoding, result in a path that stops at arbitrary coordinates.

To account for this circumstance and enable arbitrary algorithms to produce optimal paths, we utilise penalty values to decrease the quality of incomplete paths. More precisely, if the target destination is not reached within the length of an individual (i.e., the fixed number of steps), a penalty value of twice the Manhattan distance from the current position to the destination is added to the first objective value f_1, which represents the length of the path. This value is chosen because it represents a longer distance than the longest distance necessary to reach the goal from the current position; therefore, the objective function value for f_1 is worse for a solution that does not arrive at the destination than for the worst solution that does arrive. Other approaches have used different constraint handling techniques [Deb00], which are not accounted for in this implementation.

The second issue concerns obstacle handling. In this thesis, we compare two methods of dealing with obstacles. The first is not to allow obstacles on the paths, which means removing the neighbouring cells from the list of possible neighbours if they contain obstacles. This version is most similar to the original implementation of ASLETISMAC , as it does not allow obstacles on the path. The second approach allows our encoding to produce arbitrary paths even if they contain obstacle cells. Such paths are not beneficial for the underlying pathfinding application. Therefore, a cell containing obstacles in a path is penalised by adding the number of obstacles contained to the first objective function f_1.

For the analysis, we consider solutions that do not arrive at the destination or traverse obstacles as infeasible [WZM21].

5.1.2 Variable Length

A variable-length representation [RADG17, RADG19] can be considered a relatively natural encoding, because in reality paths often have different lengths. Encoding a path using a variable-length representation is suitable for graph-based problem representations, where a solution can be a sequence of nodes, and for grid-based problem representations, where a solution is represented as a sequence of coordinates to traverse.

A node-list-based representation is usually interpreted as a sequence of intersections one has to pass to reach the destination. Each pair of consecutive intersections is connected by a street segment, represented as an edge in a graph. No other intersections are on this segment.

Following the definition of a pathfinding problem graph $G\left(V, E, \phi, \vec{f}, \iota_V(\mathfrak{P}), \iota_E(\mathfrak{P}), n_s, n_e\right)$ from Section 2.3.2, a path p is a sequence of nodes of variable length: $p = (n_s, \cdots, n_e)$. Each node n has a set of properties assigned by applying $\iota_V(\mathfrak{P})$ to the set of nodes V. Properties can be any value and are always chosen and defined with respect to the underlying problem. A trivial example is coordinates that are assigned to each node, which are used to measure distances between the nodes. Other examples include height information, or movement constraints such as maximum velocities, or safety information. Using $\iota_V(\mathfrak{P})$, for each node, we can derive its set of node-properties: $\mathfrak{P}(n) = \{g_i(n) \mid i \in \mathbb{N}, 1 \leq i \leq |V|\}$, where $g_i(n)$ is a function that maps the node to a value. However, this value can be real-valued, categorical or any other data type. The properties are used during the evaluation of a path to compute its objective values.

The variable-length chromosome poses difficulties for the algorithms; however, it can be highly efficient when using realistic data, because intersections and endpoints are not homogeneously distributed and paths usually have different lengths. In [MSG08,LG09], it was found that a variable-length encoding was not suitable for large networks. A key argument was that the respective crossover operator can produce many infeasible solutions. However, in this thesis, new methodologies are explored to make this encoding more suitable for large networks. Furthermore, we demonstrate that the encoding outperformed a fixed-length representation in several experiments. In general, the encoding can be used for problems of arbitrary sizes and does not need to be adapted to the problem size. Nevertheless, other approaches exist that use a fixed-length representation and are also suitable for problems independent of their size. However, other issues can occur because a path is not represented as a whole.

When using EAs, the operators have to fit the selected encoding and therefore also the representation scheme. In many studies, fixed-length schemes have been preferred over variable-length schemes since the latter impose additional challenges when designing the operators. In the evaluation section of this chapter (Section 5.4.1), we compare the two major encoding schemes, namely fixed-length and variable-length.

5.2 Initial Solution Generation (ISG)

Before a GA such as NSGA-II begins its loop, a certain number of solutions is generated, which serve as a seed for the optimisation. For various benchmark problems, a real-valued encoding is used. Therefore, random numbers can be

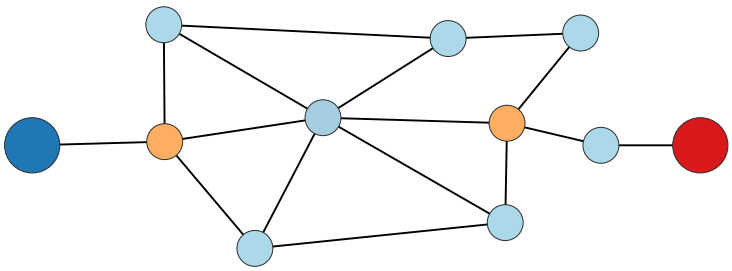

Figure 5.1: ● Start, ● Goal, ● Other, ● Gateways

employed to generate an initial solution set. However, when using a variable-length node-list-based encoding, it is not trivial to generate this set rapidly. A naive approach is to find μ random paths, where μ is the population size. On large graphs, finding random paths can be time-consuming, since the probability of finding an arbitrary path decreases with increasing graph size. The following three proposed techniques can be used.

5.2.1 k-shortest path finding

In k-shortest path finding (KSPF), algorithms are employed which can compute an arbitrary number k of shortest paths. No coordinate-based graph is needed for these algorithms, as they can be applied to the general graph structure. Various k-shortest path algorithms exist, such as *Yen's k-shortest paths* which can employ any shortest path algorithm. In the first step, the 1st-shortest path is determined, and in the following steps the other $(k-1)$-shortest paths are computed by iteratively removing links between nodes that have been obtained in the previous searches [Yen70, MP03]. Other algorithms, such as Eppstein's algorithm for finding the k-shortest path, can be employed if loops are allowed [Epp98]. Although these methods can find k-shortest paths, these paths can be still — in terms of similarity — comparatively close to each other, which is not unlikely in large real-world road networks [CBG+20]. For instance, after the shortest path is found from Place A to Place B in a road network, the second shortest path is probably almost the same, with only a few roads being changed, analogous to detours around construction sites. Suurballe's algorithm is used if k *edge-disjoint* shortest paths should be found [Suu74]. A more diverse set of initial paths can be found with this method since all found paths do not share any edge. However, it can happen that only one road is available to the terminal destination or from the starting destination in specific road networks. In these cases, the algorithm must search between the nodes with more than two edges. These gateway nodes can be identified by traversing a directed graph G_D from the respective start or end node until a node with a degree of $deg^{+}_{G_D}(n_{start}) > 1$ for the start node, or $deg^{-}_{G_D}(n_{end}) > 1$ for the end node. For an undirected graph G_U, a degree of $deg_{G_U}(n_{start}) > 2$ is required to qualify a node as a gateway node. However, more requirements may be necessary depending on the graph's structure, since the method described above does not guarantee finding distinct paths in any case. Figure 5.1 displays a visual example of such gateway nodes.

An enhancement of the KSPF is to introduce a rolling objective shortest path. Yen's k-shortest path is computed with respect to a single objective. By generating $k = \mu$ solutions for the initial population, the population's diversity might end up comparatively low in the objective and in the decision space. This happens due to the nature of the algorithm, as it creates small deviations in the paths. The probability of obtaining significantly different objective values is therefore low. However, if μ is large enough, a sufficient diverse set of solutions can be obtained; this depends naturally on the properties of the underlying

graph, i.e., V, E and ρ. However, introducing a rolling objective mechanism can increase the diversity. Before the solution generation starts, we created a corresponding graph for each edge weight we wanted to consider. It should be noted that the edge weights have to be computed beforehand, which is not possible for every objective. For instance, the smoothness objective which is used in the benchmark instances cannot transferred to an edge weight (see Section 6.6.3). For each subgraph, we can run Yen's k-shortest path algorithm to compute the k shortest paths. Thereafter, we unify the sets of paths and select μ random solutions to use as the initial solution population. Approaches other than the random choice are similarly suitable. For instance, the objective-wise best paths can be added. In our implementation we chose the random approach to avoid bias in the search.

5.2.2 Random Paths

Through random path generation, random edges are traversed until the designated goal has been found. In large networks, this approach can result in serious performance issues, because the probability of finding a random path can — depending on the size of the network — be rather low due to its stochastic nature. However, guided random path walks can be employed, such as a weighted random walk, where edge weights are considered to decide which edge is taken in the next step. Nevertheless, this approach is quite uncertain and should not be used when quick results are a requirement.

5.2.3 Random point connection RPC

In RPC, n_{RPC} points are generated with random coordinates that refer to their nearest node in a graph. These points are then connected in the order in which they were generated, starting with the starting node of the pathfinding problem and ending with its respective ending node. Finally, $n_{RPC}+1$ paths have to be computed for a single initial solution. A variety of shortest path algorithms can be used to connect these points. One of the best known is Dijkstra's algorithm for finding the shortest path between two nodes in a graph [Dij59]. However, as the graph size increases, so does the runtime, since the time complexity of the algorithm is $O(|V|\log(|V|)+|E|)$. Therefore, a different approach must be used to obtain an initial solution set when the algorithm is applied to large road maps. From the domain of single objective shortest path algorithms, a speed-up technique called *contraction hierarchies* can be used to increase the performance of a RPC search (cf. Section 5.3.2). With RPC paths with loops can be generated. Also note that for the random coordinates, an area must be specified where the points are to be placed.

Usually, graphs for pathfinding problems have coordinates assigned to their nodes to assign a random coordinate to a specific node in a graph. However, other methods for finding random nodes can be employed if this is not the case, such as picking random nodes from the graph's set of nodes. Finally, the approaches have the same outcome, but the coordinate-based method uses problem knowledge and can narrow the search space. Similar to KSPF, one can diversify the set of initial solutions by introducing the rolling objective.

5.3 Performance Considerations

The multi-objective pathfinding problem is an NP-hard problem [GBR06], which implies that an algorithm's runtime increases exponentially with increasing graph size. Meta-heuristics are methods that do not guarantee optimality but can find good solutions in a reasonable amount of time. However, the runtime increases with a larger graph, and longer paths are found in the multi-objective pathfinding problem. Often, DMs cannot wait indefinitely before obtaining a solution and searching for it can be time-critical [GPN+11]. On real-world street maps, paths can be considerably long. However, due to the hierarchical nature of such maps and structures, paths can have a significant length even on a small geographical area if the number of nodes in a path is seen as representing the path length. From a computational perspective, this is of interest.

The proposed representation schemes have various disadvantages and advantages. Function evaluations of candidate solutions for variable-length representations can require considerable time, since the length of the solution's path is uncertain at the outset. However, in a way-point-based approach, the computational cost of finding the paths between these points has to be considered. Nevertheless, integer and permutation-based encoding are primarily suitable for environments with a fixed path length, i.e., well-defined pathfinding benchmark instances, which can be considered a white-box problem as most properties are known upfront. Working on real-world maps and structures to find paths can be considered grey-box; usually, some properties are known, but others – such as path length – can be highly dynamic.

Several techniques can increase the algorithm's performance through sacrificing its ability to explore and exploit the solution space. However, a DM can be in favour of obtaining a solution quickly instead of obtaining a close-to-optimal solution more slowly.

5.3.1 Path Simplification

Reducing the number of nodes in a path can help to decrease the computational effort and better utilise the available computational budget. The performance of the various proposed methods relies strongly on the number of nodes in a path and therefore on its length. For instance, computing the path similarity between two paths is computationally expensive for long paths; hence, computing dissimilarity matrices (see Section 6.4) takes considerable time. An algorithm to simplify a path and reduce the number of nodes is the *Ramer-Douglas–Peucker algorithm (RDPA)* [DP73]. It originated in geo computer science as a technique for map generalisation. The algorithm smooths a curve by removing certain vertices that are inside a certain area spanned by two other vertices. Using approximations of curves to determine their similarities can significantly improve the performance, since fewer calculations are required.

In the first step, a polygonal curve p, defined by its points $p = (x_1, \cdots, x_k)$ ($x_i \in \mathbb{R}^n$, $i = 1, \cdots, k$), is examined to find the point x_m of p with the maximum distance to the direct line connecting x_1 and x_k (denoted by $\overline{x_1 x_k}$), which is the first approximation of the curve:

$$d_{\max} = \max_{i=2\ldots k-1} d\left(x_i, \overline{x_1 x_k}\right) \tag{5.1}$$

The distance function d can be any distance metric. If $d_{\max} \leq \varepsilon_{\text{RDPA}}$, where $\varepsilon_{\text{RDPA}}$ is a predefined threshold, all other points between x_1 and x_k are discarded and the remaining line between the two points is the found approximation.

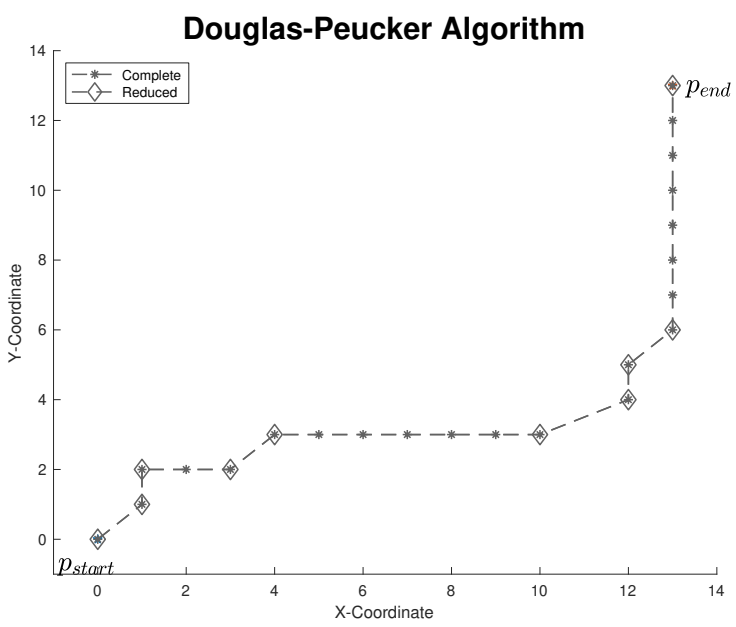

Figure 5.2: Example of the Douglas-Peucker agorithms.

If $d_{\max} > \varepsilon_{\text{RDPA}}$, the new approximation is considered to be (x_1, x_m, x_k). Then, $d_{\max}$ is to be found in the two segments, and the approximation is refined until $d_{\max} \leq \varepsilon_{\text{RDPA}}$ is met.

This technique significantly reduces the number of nodes in a path. Considering a path with 10 nodes on a straight line, it can be reduced to two nodes by the algorithm. Figure 5.2 provides an example. The original path is denoted by the $*$-marker, whereas the simplified path is denoted by the $\diamond$-marker. In this example, $\varepsilon_{\text{RDPA}} = 0$ is used, and only knickpoints are retained.

However, simplification often means sacrificing some quality. For instance, two mostly similar paths with very small differences can result in the same simplified path, which results in a Fréchet distance (see Section 6.3.2) of 0 between the paths. In the algorithm design, the value of $\varepsilon_{\text{RDPA}}$ must be chosen carefully.

Our experiment demonstrated (see Section 5.4.3) how simplification could influence the quality of the results.

5.3.2 Single-objective Speed-up Techniques

There are numerous techniques in the domain of single-objective shortest path problems which can help to increase performance. Often, these methodologies require extensive precomputing. However, they can be helpful during the initial phase of a GA and its reproduction phase. In Section 5.2, we described various existing shortest path algorithms which can be used in the initial solution generation. The same algorithms can also be used during the reproduction phase. However, a speed-up in time is always connected with sacrificing the ability to explore, as these algorithms are deterministic and reduce randomness during the search. The randomness, however, is needed to find new and promising solutions.

Similarly, during the algorithm's reproduction phase, speed-up techniques can be utilised. In Section 6.1.2, the proposed mutation operator finds possible nodes in the surrounding – or perimeter – of a predetermined node. In the following step, the node at the beginning of the mutation segment is connected to a random node in the vicinity, which is then connected to the node at the end

of the segment. The connection mechanism can be a single-objective shortest path algorithm or a random path generation. We thus used the same speed-up techniques as in the proposed RPC method in the initial solution generation (see Section 5.2). However, depending on the network size, it can be beneficial to employ a random search to determine the two paths to be found, as this approach exploits the solution space more thoroughly. If runtime is crucial, a simple pathfinding method such as Dijkstra's algorithm can be utilised, or a speed-up methodology such as *contraction hierarchies* is applicable. Choosing the right connection mechanism largely depends on the underlying network, its characteristics and requirements for the optimisation. Besides the mutation operator, the crossover can also utilise such speed-up methodologies. In cases when the two chromosomes do not share common points, we randomly chose one on each path and connected them using a path search (cf. Section 6.1.1).

5.4 Evaluation

In the following, we evaluate the different encodings and ISG approaches in terms of algorithmic performance.

5.4.1 Evaluation of Representation Schemes

In this section, we address the following research questions:

- How does the encoding of the problem impact the algorithm's performance?
- How do existing large-scale algorithms perform on high-dimensional instances of ASLETISMAC?
- How are the performance and feasibility rate impacted by different overlength settings?
- In what way are the results influenced by the choice of handling obstacles?

Parameter Settings

For the experiments, we evaluated various encodings and several algorithms with the proposed benchmark in Chapter 4 [WM22b]. Each of two different encodings, namely *real-valued* and *binary*, was adapted to the respective benchmark instance type. From the benchmark suite, we used a variety of problems incorporating various characteristics. All three available obstacle configurations from the benchmark were used: 1) no obstacles, 2) the lake obstacle and 3) the checkerboard pattern. In addition, we applied the algorithms to different benchmark instance sizes, starting with small maps of 5×5 cells up to map sizes of 200×200 in various step sizes [WZM21].

We conducted several experiments to answer the research questions. In Table 5.1, the general experimental settings are shown. We used the NSGA-II [DPAM02], NSGA-III [DJ14] and GLMO [ZIMN16a] algorithms with 106 000 function evaluations, as this resulted in 500 generations for a population size of $\mu = 212$. The values were taken from the original NSGA-III study. Although NSGA-II is usually not suitable for many-objective optimisation problems, it had outperformed NSGA-III in another study on the multi-objective pathfinding problem [WM22b]. Therefore, we used it in our comparisons. To evaluate

Table 5.1: General experimental settings [WZM21]

Parameter	Value
Algorithms	NSGA-II, NSGA-III, GLMO
Encodings	binary, real
Sizes	5,10,14
Neighbourhood	K2,K3
Backtracking	True/False
Allow Obstacles On Path	False
Population Size (μ)	212
Max. Function Eval.	106000
δ	1.5

Table 5.2: General experimental settings (large scale)

Parameter	Value
Algorithms	NSGA-III, GLMO, WOF, LCSA
Encodings	real
Sizes	50,100,200
Neighbourhood	K2,K3
Backtracking	True/False
Allow Obstacles On Path	False
Population Size (μ)	212
Max. Function Eval.	212000
δ	1.5

algorithms for large-scale problems, we additionally employed the algorithms WOF [ZIMN16b, ZIMN18, ZM17] and LCSA [ZM19, Zil19] on benchmark instances with map sizes 50, 100 and 200. In these runs, we set the number of function evaluations to 212000 (Table 5.2). Furthermore, we employed a dedicated experiment to evaluate the influence of allowing obstacles on the path and another experiment to evaluate the impact of δ [WZM21].

As the true Pareto-front is not available for instances over the size of 14, we estimated the worst solution to have a reference point for the hypervolume indicator [WHBH06b, ZT99]. The estimation relies solely on the Manhattan distance, namely $x_{max} + y_{max} - 2$ from the start point $(1,1)$ to the endpoint (x_{max}, y_{max}). For the first, second and fourth objectives, to take possible detours due to backtracking into account, we multiply the length of the chromosome by a factor of $\delta = 1.5$. The worst solution for the elevation objective is estimated by the underlying elevation profile, given by h_i, which is defined by the benchmark's *nh* parameter (cf. Section 4.2). The function determines the number of hills and is therefore used as a factor. Moreover, due to possible backtracking moves, we multiply it by the factor mentioned above and by 5, which was the highest elevation of each hill, to allow for possible multiple upward and downward movements. The number of steps estimates the smoothness objective from the start to the end point, multiplied by $\frac{\pi}{2}$, i.e., a turn of 90°. We divide this value by 2, estimating that the worst path cannot have a higher smoothness value. However, the worst solution is merely an approximation. Future research should indicate more accurate estimations. As the true Pareto-front is available for instances without backtracking and for sizes $x_{max}, y_{max} \leq 14$, we use the IGD^+indicator [IMTN15b] to compare it with the variable-length encoding from the original study [WM22b]. Each combination of an algorithm, an encoding and a benchmark instance is run 21 times for statistical analysis. To test the pairwise performances (each algorithm compared to NSGA-III), we

use the Mann-Whitney U-test for the null hypothesis that the two samples had equal medians. The results were statistically significant at $p < 0.05$ [WZM21].

Impact of Encoding

Figures 5.4 and 5.5 depict the results for two particular instances without obstacles, the third elevation profile and no backtracking. Figure 5.4 shows the results of the instance with $k = 2$ neighbourhood, whereas Figure 5.5 shows results of the instance with $k = 3$ neighbourhood. Shown in blue are the original study results concerning a variable-length encoding for different instance sizes, with comparable results from this study shown in green. The variable-length algorithms are denoted by *VL*, whereas the fixed-length approach is denoted by *FL-R* for the real-valued encoding and *FL-B* for the binary encoding. We compared sizes up to $14x14$ since that was the maximum size used in the original study [WM22b, WZM21].

For the $k = 2$ neighbourhood instance, the variable-length algorithms outperformed the fixed-length approach. In contrast, on the $k = 3$ neighbourhood instance, for sizes 5 and 10 the fixed-length NSGA-II achieved better results than the variable length in the original study. For size 14, our proposed encodings were outperformed by the original study's.

Comparing the binary and real-valued encoding, the algorithms using the binary representation outperformed their counterparts on most instances. This finding was relevant to both $k = 2$ and $k = 3$ instances. An explanation lies in how a change in the decision variables affects the choice of the neighbouring cells. In the binary encoding, for the $k = 2$ instances, only 1 bit is used to encode each movement step. A change in a decision variable leads directly to the choice of a different neighbour. It is noteworthy that this increased exploitation behaviour enables the algorithms with binary encoding to outperform the real-valued ones even in the $k = 3$ instances [WZM21].

Interestingly, NSGA-II outperformed NSGA-III on the larger neighbourhood. Moreover, due to the discrete Pareto-front and different distributions of Pareto-optimal solutions, NSGA-II outperformed NSGA-III, which is usually more suitable for many-objective algorithms. This behaviour was studied by Cai et al. [CSF18].

Next, we examined how the algorithms dealt with the two encodings. We compared various instances of the benchmark with different parameter settings. In Tables 5.3 and 5.4, we show the winning rates of the algorithms compared to each other. For the four methods listed in the table, the numbers indicate how often these algorithms performed significantly better, worse or on par with the reference method NSGA-III. Table 5.3 shows the data for real-valued encodings, and Table 5.4 shows the data for the binary encoding. A dash indicates that the specific combination of algorithm and instance size was not tested [WZM21].

For the real-valued instances, NSGA-II and NSGA-III had the same performance and outperformed the respective other in multiple instances. The GLMO generally performed superior to or on par with NSGA-III. This picture changed when binary encoding was used, as the number of instances where GLMO performed significantly more poorly than NSGA-III increased substantially. It should be noted that the GLMO was configured with its standard parameters given in the framework and therefore used NSGA-III internally as an optimiser. GLMO seems to perform more poorly when binary encoding is used because the standard grouping mechanism uses ordered grouping. Algorithms, such as

Table 5.3: Wins, losses, and ties of each algorithm compared to NSGA-III using real-valued encoding [WZM21]

Map size	NSGA-II	GLMO	LCSA	WOF
5	1/10/13	3/1/20	-	-
10	7/10/7	9/0/15	-	-
14	6/8/10	7/0/17	-	-
50	-	3/0/3	0/0/6	3/2/1
100	-	6/0/0	1/2/3	5/0/1
200	-	6/0/0	3/1/2	6/0/0

Table 5.4: Wins, losses, and ties of each algorithm compared to NSGA-III using binary-valued encoding [WZM21]

Map size	NSGA-II	GLMO
5	3/12/9	3/9/12
10	6/10/8	5/11/8
14	4/9/11	3/15/6

GLMO, employ a group-wise mutation which changes large portions of the decision variables at once. For such low-dimensional instances, this behaviour is not beneficial since it results in more exploration than exploitation. In contrast, the real-valued encoding allows for mutations to change the variables without an immediate change in the chosen neighbour of a cell, which in turn eases the small variations in the path [WZM21].

Higher Dimensional Instances

Table 5.3 displays the wins, losses and ties on the large-scale instances. We compare the NSGA-III algorithm to the large-scale algorithms GLMO, LCSA and WOF on real-valued instances. With increasing dimensionality, each of the three algorithms outperformed NSGA-III in more instances. GLMO outperforms NSGA-III in all six instances from size 100 onwards, while the same happens for the WOF only at the size of 200. From the three large-scale algorithms, LCSA performs the worst compared to NSGA-III. However, as expected, the large-scale algorithms perform better the larger the instances become [WZM21].

Feasibility Rate regarding Encoding Length δ

Concerning the feasibility rate, we found that in most of the tested algorithms and benchmark instances, each converged to a completely feasible solution set. Our proposed constraint handling penalises the fitness if paths do not end at the designated goal coordinate or paths traverse through obstacles, as such infeasible solutions could occur. However, there were certain exceptions, such as the two examples shown in Figures 5.3a and 5.3b. Figure 5.3a shows the feasibility rate (number of solutions in the population that are feasible) of the three algorithms NSGA-II, NSGA-III and GLMO for one instance with the checkerboard obstacle, the first elevation profile, $k = 3$ neighbourhood with the binary encoding. In this example, obstacles were not allowed on a path and $\delta = 1.0$, meaning there was no room for longer paths in the chromosome. After the maximum of function evaluations was reached, the GLMO feasibility rate was below 1.0, i.e., a portion of the population resulted in infeasible paths.

It is noteworthy that the feasibility rate of the initial population seldom lay over 0.0 for any algorithm, which is not visible in the diagrams. Due to its grouped mutation mechanism, a quarter of the decision variables — and therefore also directions — were changed at once, while only one was changed using NSGA-II or NSGA-III. Changing a direction may lead to moving in the opposite direction.

Figure 5.3: Feasibility rates of the algorithms for different instances [WZM21]

(a) Checkerboard obstacle, K3, no obstacles allowed on path

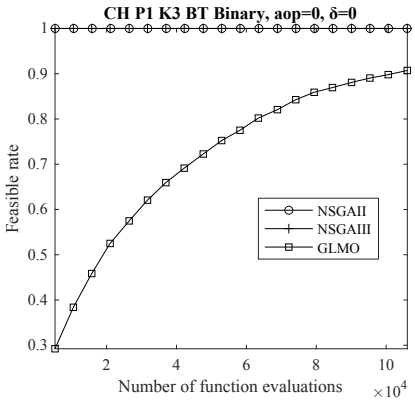

(b) Checkerboard obstacle, K3, obstacles allowed on path

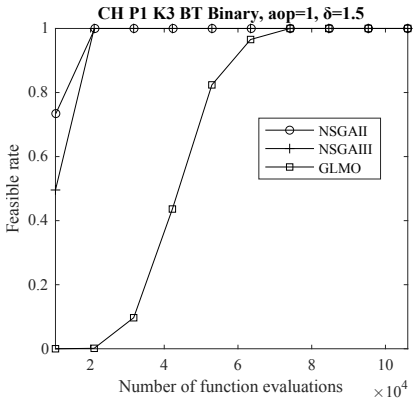

Table 5.5: Median and IQR of the hypervolume indicator for NSGA-III, Problem CH P1 K3 BT, $\delta = 1.5$. Statistically significant differences between the two columns are shown in bold [WZM21].

Map size	Obstacles not allowed	Obstacles allowed
5	1.7586e-01 (8.1125e-05)	1.7583e-01 (9.0567e-05)
10	**3.0499e-01 (1.7423e-03)**	2.3519e-01 (2.8475e-02)
14	**2.9737e-01 (6.0812e-03)**	2.3117e-01 (2.4072e-02)

When several directions are changed, and $\delta = 1.0$, there is no room left for arriving at the designated goal.

In Figure 5.3b, the feasibility rate for the same instance type is shown. However, in this evaluation, obstacles were allowed on the path (while penalising the objective f_1 when traversing through them), and $\delta = 1.5$, leaving room to reach the goal while increasing the dimensionality of the problem. All three of the compared algorithms needed several thousand evaluations to converge to a completely feasible solution set, i.e., they reached a rate of 1.0 (see Figure 5.3b). The chosen pattern, the checkerboard, had well distributed obstacles located on the map and a path was thus relatively likely to encounter an obstacle when traversing through the grid. However, after the maximum of function evaluations had been reached, each algorithm converged to a complete feasible solution set, i.e., they found paths that avoided obstacles and arrived at the destination [WZM21].

Obstacle Handling

In Table 5.5, a comparison between the two obstacle handling techniques regarding the hypervolume indicator for the NSGA-III algorithm is shown. A single benchmark instance with the checkerboard pattern, $k = 3$ neighbourhood, and enabled backtracking is assessed here. Except for map size 5, the algorithm achieved a significantly higher hypervolume if obstacles were not allowed on the path. As a result, it is beneficial to use problem knowledge when executing the algorithm, as it can decrease the size of the search space, especially in environments with several obstacles. However, pruning neighbours adds computational effort as non-visitable neighbours must be identified upfront. In other networks with numerous neighbouring cells, this can negatively impact the algorithm's performance. Nevertheless, as shown by [MMC05], it can be beneficial to maintain infeasible solutions to find feasible solutions on the boundaries of the feasible area [WZM21].

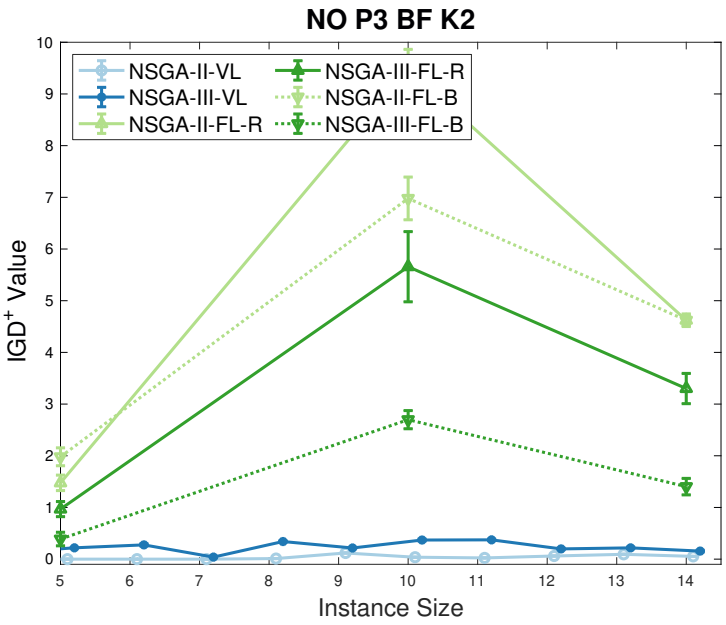

Figure 5.4: Comparison of the original variable-length encoding with the proposed fixed-length for an instance with $k = 2$ neighbourhood. [WZM21]

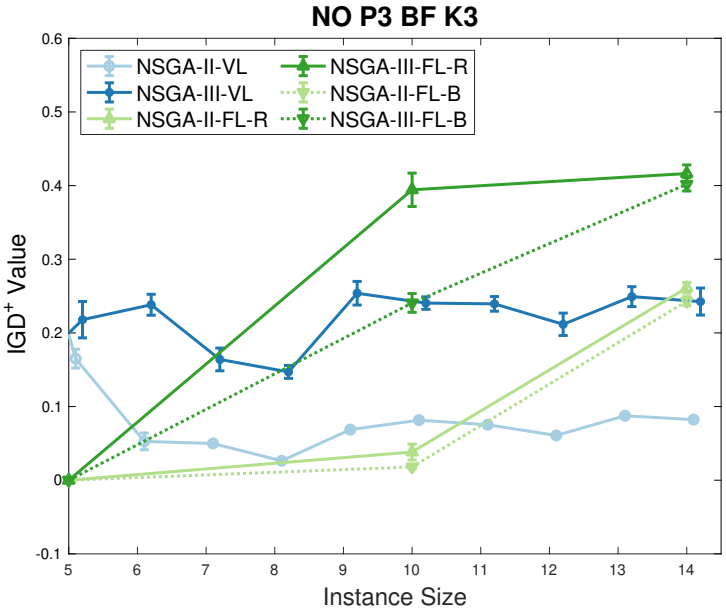

Figure 5.5: Comparison of the original variable-length encoding with the proposed fixed-length for an instance with $k = 3$ neighbourhood. [WZM21]

5.4.2 Evaluation of ISG approaches

To evaluate the different approaches of the initial solution generation, we observed the respective values of both indicators, IGD^+ and IGDX, over the generations. We thus evaluated whether there was a benefit in the first generation and whether it led to an overall performance gain, after all available function evaluations had been exhausted and the termination criteria were met. However, biasing the solution set can be detrimental to the optimisation process, as other promising areas of the fitness landscape may not be evaluated. We decided to evaluate the KSPF incorporating the rolling objective approach.

Table 5.6 outlines the general experiment settings. Finally, we tested the two approaches on 240 different problem instances, ranging from a small size up to size 30×30. Furthermore, we used the length, time and smoothness objectives as the set of rolling objectives.

Table 5.6: General experimental settings for ISG experiment

Parameter	Value
Algorithms	NSGA-II
Encoding	direct node list
Sizes	10,15,20,24,30
Neighbourhood	K2,K3
Backtracking	True/False
Population Size (μ)	212
Max. Function Eval.	106 000
No. of runs	31
Indicators	IGD^+ & IGDX

Table 5.7 presents the results after the initial population had been evaluated (after gen. 1) as well as the results after 500 generations had been evaluated. When evaluating the initial population only, we noted a discrepancy in comparing IGDX and IGD^+ values. In terms of the IGD^+ indicator, the KSPF methodology, i.e., *Yen's shortest paths*, outperforms the random search in most cases. However, for the comparison of results using the IGDX indicator, it was evident that the two approaches equally outperformed each other and also yielded several ties. The effect is due to the way Yen's algorithm works: For each objective, the best path was found, as were paths that were direct predecessors in terms of the respective objective but were thus better regarding other objectives. In this manner, we followed a form of weighted sum approach. However, as we decided to randomly take μ paths, we loosened the weighted sum approach. When analysing the indicator values after all available function evaluations were exhausted, we saw that in terms of IGD^+, initialising the population with Yen's algorithm remained beneficial. Only a few instances were won by the random approach, while the rolling objective initialisation outperformed the other in most cases. When analysing the IGDX indicator, we noted that the random approach outperformed the biased approach in a few instances while also resulting in many ties. Figure 5.6 illustrates how the indicator values developed over the number of generations. We present the median indicator value per generation over all solved problem instances as well as the IQR in the same manner. As evident in Figure 5.6a, the ISG approach using Yen's algorithm started out better and continued to be superior over the course of the generations. The values from Table 5.7 align with this finding, as the random approach was outperformed in 219 problem instances and even in 182 instances after the experiment ended. In terms of the IGDX indicator (Figure 5.6b), most problem instances resulted in a tie, comparing the initial solutions. After all function evaluations had been exhausted, the two approaches ended with highly similar values; however, Yen's algorithm overall resulted in better values in 116 of 240 cases.

Table 5.7: Wins, losses and ties of each algorithm pair (rows vs. column) with statistical significance at $p < 0.01$, Bonferroni correction applied, IGDX and IGD^+ indicator. Three rolling objectives.

		Yen's Algorithm (three rolling objectives)	
		After gen. 1	After gen. 500
Random	IGDX	18/34/188	23/116/101
	IGD^+	9/219/12	6/182/52

In the first experiments, we used three objectives to generate three different graphs on which Yen's algorithm is used. However, more objectives resulted in a higher effort to generate graphs. Therefore, we also examine the impact of

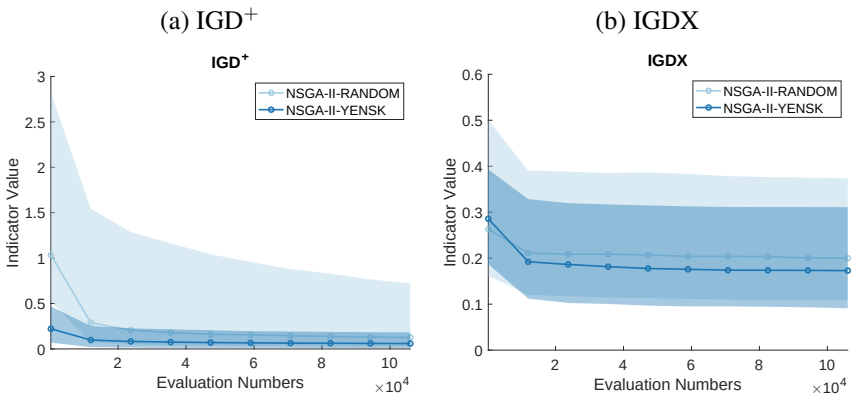

Figure 5.6: The IGD$^+$ and IGDX indicator over the number of generations.

the number of rolling objectives. In Table 5.8 we present the values using only two objectives. Evaluation of the initial solution set resulted in different values compared to using three objectives. For instance, the rolling objective approach outperformed the random approach in a few instances, while also resulting in many ties when comparing the IGDX values for the three-objective variation. Using only two objectives resulted in only 35 ties (compared to 188) and more wins for both algorithms. Furthermore, the random approach outperformed the rolling objective in more cases. Additionally, it was outperformed more often when we compared the IGD$^+$values. After all function evaluations had been exhausted, the results were similar, indicating that using only two objectives yielded an equal performance to using three when all available evaluations were exhausted.

Table 5.8: Wins, losses and ties of each algorithm pair (rows vs. column) with statistical significance at $p < 0.01$, Bonferroni correction applied, IGDX and IGD$^+$ indicator. Two rolling objectives.

		Yen's Algorithm (two rolling objectives)	
		After gen. 1	After gen. 500
Random	IGDX	106/99/35	34/112/94
	IGD$^+$	3/231/6	12/181/47

In this experiment we demonstrated that a biased initial population can be beneficial to the overall performance of an algorithm. Particularly when a rolling objective is used, several Pareto-optimal and near Pareto-optimal solutions were injected into the initial set. However, this approach requires a greedy algorithm to be applied to the graph. Depending on its size and density, this can result in severe performance degradation. Furthermore, the number of objectives taken into the rolling mechanism must be chosen carefully. For some objectives, a transferred graph needs to be generated, potentially resulting in substantially more nodes and edges and adding to the time needed for execution.

In the appendix, we report each value of the experiment (Tables B.3 and B.4).

5.4.3 Path Simplification

We assess the aforementioned path simplification methodology, i.e., the RDPA, by running the same algorithm configuration and either simplifying the paths during the process or not. In next chapter, we propose techniques to maintain and increase the diversity in the decision space and perform specific computations where a path simplification can be applied. We apply the Fréchet distance metric to compute the distance between two paths. In this experiment, before computing the distance, we simplify the paths using the RDPA with $\varepsilon_{\text{RDPA}} = \{0, 2\}$. This results in paths containing only knickpoints or even further simplified paths,

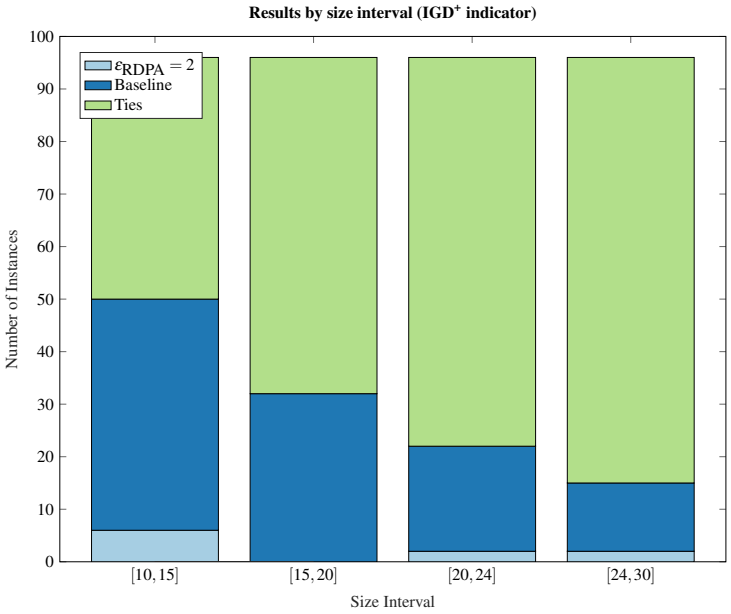

Figure 5.7: Wins and Ties of the proposed approach by different instance size ranges concerning the IGD$^+$ indicator.

besides the obligatory start and end points. Using a higher $\varepsilon_{\text{RDPA}}$ reduces the computational effort of computing the Fréchet distance, as it results in fewer path segments. We use the same general experiment setting as we did in the ISG experiment, presented in Table 5.6.

Table 5.9: Wins/Losses/Ties of each algorithm pair (rows vs. column), statistical significance $p < 0.01$, Bonferroni corrected, IGDX and IGD$^+$ indicator.

		$\varepsilon_{\text{RDPA}} = 0$	Baseline
$\varepsilon_{\text{RDPA}} = 2$	IGDX	7/44/189	6/52/182
	IGD$^+$	7/60/173	6/65/169
$\varepsilon_{\text{RDPA}} = 0$	IGDX	-	3/14/223
	IGD$^+$	-	6/16/218

Table 5.9 shows the results. A comparison of $\varepsilon_{\text{RDPA}} = 0$ with the baseline approach (i.e., using no simplification) indicates that it resulted is numerous ties. However, 5.8% of the problem instances were won regarding the IGDX indicator and approximately 6.6% when comparing the IGD$^+$ indicator. Comparing $\varepsilon_{\text{RDPA}} = 2$ with the baseline, we note that as many as 21.6% and 27% of the problem instances were won by the baseline. The difference is also evident when comparing $\varepsilon_{\text{RDPA}} = 0$ and $\varepsilon_{\text{RDPA}} = 2$.

Analysing the different problem instances in more detail, we note from Figure 5.7 that an increasing instance size is associated with a decrease in the number of instances won by the baseline approach. Therefore, we conclude that longer paths are less prone to performance impacts arising from simplification. The longer the path, the smaller the differences between path similarity measures that use non-simplified paths and those that use simplification techniques. However, when the technique is applied to small size instances, a simplification approach should not be used.

5.5 Summary

In this chapter, we have discussed various solution encodings that are used in genetic algorithms optimising a pathfinding problem. We have shown that a fixed-length representation has some advantages, depending on the data type.

However, the variable-length encoding outperforms the fixed-length in most cases, especially as the problem sizes increases. Additionally, we have proposed different methodologies for the initial solution generation. We have evaluated the approaches using a variety of problem instances that were generated using the aforementioned benchmark generator. To assess the quality of the algorithms, we have used metrics in both spaces, i.e., the objective and the decision space. In addition, we have examined what impact on the performance is associated with path simplification strategies that decrease the computational effort of the diversification methodology. This topic is further explained in the next chapter.

6 Diversification for Pathfinding Problems

In this chapter, the following points are covered

- Genetic Operators
- Path Similarities
- Diversification in the Decision Space

The following chapter is largely based on the publications [WM20, WM21b, WM21a, WM22a].

In this chapter, various new techniques for diversifying the population are introduced and discussed. First, we propose genetic operators tailored specifically for the multi-objective pathfinding problem. Thereafter, we discuss various approaches to increase the diversity during the search process in the objective space and the decision space respectively.

6.1 Operators

In evolutionary multi-objective optimisation (EMO), several operators are applied to the population at different steps during the optimisation process. In Section 2.2.1, it was shown that during the reproduction phase of the algorithm, a *crossover* and a *mutation* operator are used to find new solutions. Other operators also select the candidate solutions to be transferred to the next generation and those that are crossed and mutated in the reproduction phase.

For the algorithm's reproduction phase, we propose a customised crossover and a customised mutation operator. Furthermore, we propose to use a deletion operator that simply removes cycles in a path and is executed before a solution is evaluated. The reason is that no path can be better, for any objective, if we compare a path to the same path with an added arbitrary circle. This holds for our proposed objectives when backtracking is not allowed, but the situation may differ depending on the computation of the objectives. For instance, circles can become beneficial if the pathfinding is constrained in terms of the curvature of the path. It can be better to traverse through a circle instead of turning to the desired direction. A real-world example is flight trajectories, where aircraft have to follow a certain airfield traffic pattern. Specific problem knowledge

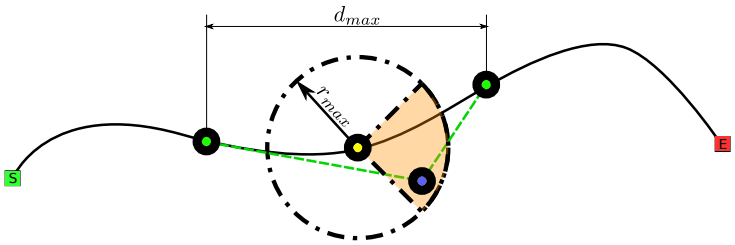

Figure 6.1: Perimeter Mutation Operator (PNM)

is needed to determine whether a repairing operator, such as loop deletion, is suitable and needed.

6.1.1 Crossover

When variable-length representation is used, specialised operators are needed [MTS98]. Therefore, we implemented the crossover operator by performing a n-point crossover if two paths had intersections, where $n \in \mathbb{N}$ [WM20]. In all our experiments throughout this thesis we used $n = 2$ if not stated otherwise. However, it can happen that two paths are disjunct and do not share any edges or nodes except the start and end nodes. In such cases, we selected two random points from each path, determined the shortest path using Dijkstra's algorithm in terms of length and connected the points through that path. The operator is usually executed with a probability of $\mathbb{P}_c = 0.8$.

6.1.2 Mutation

For the mutation operator, we implemented several variants. In this thesis, we mostly use a variable-length chromosome representation; hence, we needed specialised operators to ensure the validity and feasibility of the generated paths. The possible alele of each gene depends on its predecessor. Unlike fixed-length representation, where each gene is often mutated with a probability of $\frac{1}{\text{number of genes}}$, we chose a fixed probability $\mathbb{P}_m = 0.2$, which determines whether a path is mutated. We next describe two approaches to designing a mutation operator for such a problem.

Perimeter Mutation Operator (PNM) We propose an operator for variable-length chromosomes. From a given path which is to be mutated, we took two arbitrary points within a maximum network distance d_{max} and computed their middle point. We then searched a random point in the network within a maximum distance of r_{max}, using an *R-tree*, from that point, and performed a Dijkstra search from the first point to it and to the second point from it. Hence, we performed a local search. Figure 6.1 depicts the operator graphically. An *R-tree* is a data structure that serves as an index for spatial data [Gut84]. Such a method needs precomputation to build the index, but recent algorithms can build indexes — also for large data sets — relatively fast. In Figure 6.1, the set of possible nodes which are candidates for the new node is shown in orange. Generalising this approach would mean, that the whole circle is considered as the set of candidate nodes.

Hierarchical mutation In addition to the PNM approach, we propose a second variation which uses the importance of different network entities and is thus particularly useful for graphs and networks representing road maps. Using that operator, streets that are higher in the hierarchy, e.g., highways in contrast

to residential streets, are mutated with a lower probability (see Section 1.1.1). Simultaneously, r_{max} is adjusted in accordance with a higher hierarchy (higher priority). The actual values are depended strongly on the underlying network. A hyperparameter optimisation can support identifying good values; therefore,

$$\begin{aligned} \mathbb{P}_m(e) &\sim 1/\operatorname{prio}(e) \\ r_{max}(e) &\sim \operatorname{prio}(e) \end{aligned} \tag{6.1}$$

where e refers to and edge, which represents a street in the graph and $\operatorname{prio}(e)$ refers to the edge's priority in the network.

6.2 Objective and Decision Space

In EMO, there are usually two spaces in which solutions are represented: 1) the objective space $\mathscr{M}$ where each solution is assigned a vector of its objective values, and 2) the decision space Ω where a solution is represented by its variables. In both spaces, one can apply methodologies to diversify the solutions. Often, distant solutions in one space can be narrow in the other and vice versa [WM21a].

As Shir noted, genetic algorithms typically suffer from loss of diversity within populations, resulting in a local optimum [Shi12]. Niching methods address this problem by preserving diversity. In state-of-the-art algorithms, there are various methods for increasing or maintaining diversity. Crowding distance is an example of using the objective space to identify crowded areas. In the next section, we describe the approaches performed in both spaces.

6.2.1 Objective Space

Since the goal of an optimisation task is to find solutions with optimal objective values, diversification is performed in the objective space. During the search process, an EA can result in local optima. Furthermore, it can happen that the search becomes stuck there. To overcome this challenge, researchers have proposed various techniques. The goal of diversification is to obtain a set of solutions that covers the Pareto-front. Another methodology to support the search process is called *niching*. With niching, unexplored areas that are not yet covered by a solution are emphasised during the optimisation to be explored [Shi12].

One of the best-known niching techniques is the so-called *crowding distance (CD)*. Individuals are measured by the distance between their two neighbouring solutions [DPAM02]. Relatively isolated solutions can be emphasised by using this measurement during the NSGA-II algorithm's replacement and selection phase. Another technique is to use reference vectors. The solutions along such vectors are generally preferred, and their distribution within the objective space allows diversity to be maintained [DJ14]. When optimising more than three objectives, the latter methodology often serves as a good solution to problems with many objectives. However, research results indicate that performance can be affected not only by the number of objectives but also by the type of problem, requiring careful consideration when choosing an algorithm [CSF18,WM22b].

For multi-modal optimisation problems, such as the multi or many-objective pathfinding problem (specific problems), there are various other techniques

to approximate the Pareto-front. Several alternative distance metrics can be employed. For such problems, measurements in the decision space can be performed [DT05, JRAM20].

6.2.2 Decision Space

If more than one solution can map to the same objective values in specific problems, i.e., multi-modal problems, other diversity measurements can be useful. An example is combining different metrics in the objective and decision spaces [JRAM20, DT05]. For instance, the many-objective pathfinding problem can have close solutions in the objective space, although they are far apart in the decision space. The use of diversity-preserving measurements in the decision space can thus improve an algorithm's performance [SPNE09,WM21b]. Shir stated that diversity along the Pareto-front does not necessarily result in the same diversity in the decision space among the Pareto-set. Furthermore, a decision space-diverse set is of interest for a potential DM [SPNE09, UBZ10]. In their work, Ulrich et al. proposed a methodology to integrate the decision space diversity into a hypervolume-based search [UBZ10]. Particularly if a variable-length encoding represents the solution and the distance between two of them cannot be computed using the Euclidean distance. The CD, in addition to other metrics such as the harmonic mean, can be used when the chromosomes are fixed-length and located in an Euclidean space [JM21]. Other spaces require specialised distance metrics.

In the following sections, we describe metrics and methodologies that can be performed in the decision space to preserve and increase the solution set's diversity. These methods can also overcome the challenges associated with problem-specific encoding.

6.3 Path Similarities

Path or curve similarity measurement is found in several fields. For instance, in handwriting recognition, curves are compared when the letters or words are matched [SKB07]. Other fields include morphing [EGHP+02] and protein structure alignment [JXZ08].

There are different methods of path similarity measurements. This analysis evaluates three different metrics, namely the Hausdorff distance, the Fréchet distance and dynamic time warping (DTW). With Hausdorff distance, the distance of two subsets (curves) in a metric space can be measured [Mun00], while Fréchet distance also takes the flow of curves into account. Fan et al. used the Fréchet distance on road networks to measure the resemblance of road tracks [FLZ11]. Assuming two subsets are in the same metric space, they can have a short Hausdorff distance but a rather large Fréchet distance. Originating from signal theory, DTW finds a warping path between two curves or signals, to align them, and the path's length determines the similarity between the signals and therefore the curves. In the following, we describe each of the distance metrics in more detail [WM22a].

6.3.1 Hausdorff Distance

The *Hausdorff distance* can be used to compute the distance between two sets of points without taking their flow into account. The formula is shown in

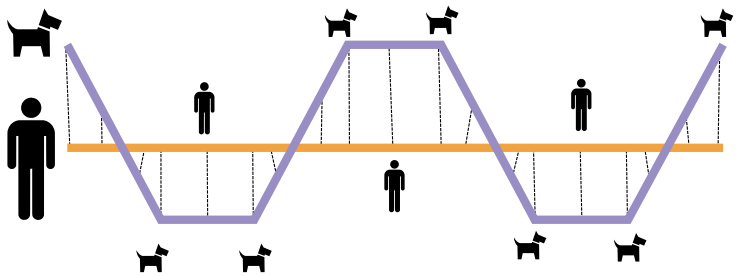

Figure 6.2: An example of a dog walk. [WM21b]

Equation (6.2). This measure is the greatest of all distances between points in one set and their nearest points in the other set.

$$\begin{aligned} D(x,K) &:= \min\{d(x,k) \mid k \in K\} \\ \delta_{hd}(A,B) &:= \max\{\max\{D(a,B) \mid a \in A\}, \max\{D(b,A) \mid b \in B\}\} \end{aligned} \tag{6.2}$$

6.3.2 Fréchet Distance

The Fréchet distance is a measurement of similarity for curves in a metric space. Eiter and Mannila described it through a dog walk analogy [EM94]. A dog and its owner walk on two different paths, and both entities can vary their speed but cannot backtrack. Since there is a leash attached to both entities, the Fréchet distance is defined as the shortest length of a leash which is required for both of them to follow their paths, as shown in Figure 6.2. The dashed lines indicate the leash.

The Fréchet distance [EM94] is mathematically defined as follows:

$$\delta_F(A,B) = \inf_{\alpha,\beta} \max_{t\in[0,1]} \left\{ d\Big(A(\alpha(t)), B(\beta(t))\Big) \right\} \tag{6.3}$$

Here, A and B are curves as a continuous mapping in a metric space $\mathbb{M}$, defined as $A : [0,1] \to \mathbb{M}$ and $B : [0,1] \to \mathbb{M}$. The re-parameterisations α and β are non-decreasing functions from $[0,1]$ to $[0,1]$. In other words, $A(\alpha(t))$ and $B(\beta(t))$ are the positions of the owner and the dog in time-step t, and they are non-decreasing as the two entities cannot move backwards. The function d is the distance metric on $\mathbb{M}$, e.g., the Euclidean distance, which describes the length of the leash between the dog and the owner. Finally, the Fréchet distance is obtained by computing the infimum (greatest lowest bound) of all re-parameterisations α and β of $[0,1]$ of the maximum over all t of the distance d in $\mathbb{M}$ between $A(\alpha(t))$ and $B(\beta(t))$. Alt and Godau studied the computational properties of the measurement [AG95] initially introduced by [Fré06]. They specified an algorithm to compute the distance δ_F in time $\mathcal{O}(ab \log ab)$, where a and b are the number of segments of two curves [EM94]. Eiter and Mannila proposed a variation of the distance metric, i.e., the coupling distance or discrete Fréchet distance δ_{dF}, which provides a good approximation of δ_F in time $\mathcal{O}(ab)$. They also showed that δ_{dF} is an upper bound of δ_F. They approximated the two curves A and B by polygonal curves, which is, intuitively, a list of supporting points. Those points specify the endpoints of line segments. The sequence of segment endpoints of a polygonal curve P is denoted as $\sigma(A) = (u_1, \cdots, u_a)$. A *coupling* L between A and B is defined as a sequence $L = (u_{c_1}, v_{d_1}), (u_{c_2}, v_{d_2}), \cdots, (u_{c_m}, v_{d_m})$ of distinct pairs of $\sigma(A) \times \sigma(B)$, with respect to $c_1 = 1, d_1 = 1, c_m = a, d_m = b$. The coupling respects the order of points.

Finally, the length of the coupling is defined as $||L|| = \max_{i=1,\cdots,m} d(u_{c_i}, v_{d_i})$; hence the longest connection in L. The equation of the discrete Fréchet distance is shown in Equation (6.4) [EM94].

$$\delta_{dF}(A,B) = \min\{||L|| \mid L \text{ is a coupling between } A \text{ and } B\} \tag{6.4}$$

In more recent works, subquadratic algorithms were developed to approximate the discrete Fréchet distance [BM16]. The authors developed an algorithm that runs in $\mathcal{O}(n\log n + \frac{n^2}{\alpha})$, where n is the number of points and $\alpha \in [1,n]$ is the approximation. The two curves must have the same number of nodes. In [CR18], an approximation algorithm resulting in $\mathcal{O}(n\log n + \frac{n^2}{f^2})$ was proposed, where f denotes the approximation and is $f \in [1,n]$. In this analysis, we use all points of the two curves. We can therefore employ the original methodology of [EM94]. Using the more recent approaches with all points would result in $\alpha = f = n$, resulting in $\mathcal{O}(n\log n)$. However, the polygonal curves in this thesis are not constituted of the same number of nodes. Therefore, we use Eiter and Mannila's approach [WM22a].

The Fréchet distance accounts for the flow of the curves, whereas the Hausdorff distance measures the distance from one point in one curve to the closest on the second curve. For the remainder of the analysis, we refer to the discrete Fréchet distance. As we define a path in this thesis as $p_i = (n_s, \cdots, n_{End})$, we can represent it by analogy to the definition of δ_{dF}; hence $p_i = \sigma(A)$ and $(n_s, \cdots, n_{End}) = (u_1, \cdots, u_a)$, where $n_s = u_1$, $n_{s+1} = u_2$, $n_{End} = u_a$. In other words, A represents a continuously defined curve and $\sigma(A)$ are the segment end points. Since a path in a graph is defined by its nodes, every node $n_i \in p_i$ is, in fact, a segment endpoint.

6.3.3 Dynamic Time Warping

Although the Fréchet distance is a metric that results in a dissimilarity measurement of two curves, DTW (which is a measure) can find the best match between two signals and determine their distance [Mül07]. The measure reflects similarities between temporal sequences. However, one can use the approach to determine a distance between two paths which are sequences of locations. In Equation (6.5) the formal definition of the DTW distance is shown. For its computation, a local cost measurement $d(a,b)$ is needed that describes the similarity between two points $a \in A$ and $b \in B$, such as the Euclidean distance. A cost matrix $C(A,B)$ can be built by computing $d(a,b)$ for each pair of a and b. The goal is to find an optimal warping path p^* of the two curves A of length R and B of length l such the overall cost (Equation (6.5a)) of a warping path p is minimal (Equation (6.5c)). An (R,l)-warping path p is a path in the cost matrix that runs along a *valley* of low cost [Mül07]. As the matrix's values represent cost, the warping path is the one obtaining the least combined costs if it passes through the matrix's cells (Equation (6.5c)). In this path, the element $a_{r_\ell} \in A$ is assigned to the element $b_{s_\ell} \in B$. To compute δ_{dtw}, we used dynamic programming [WM22a].

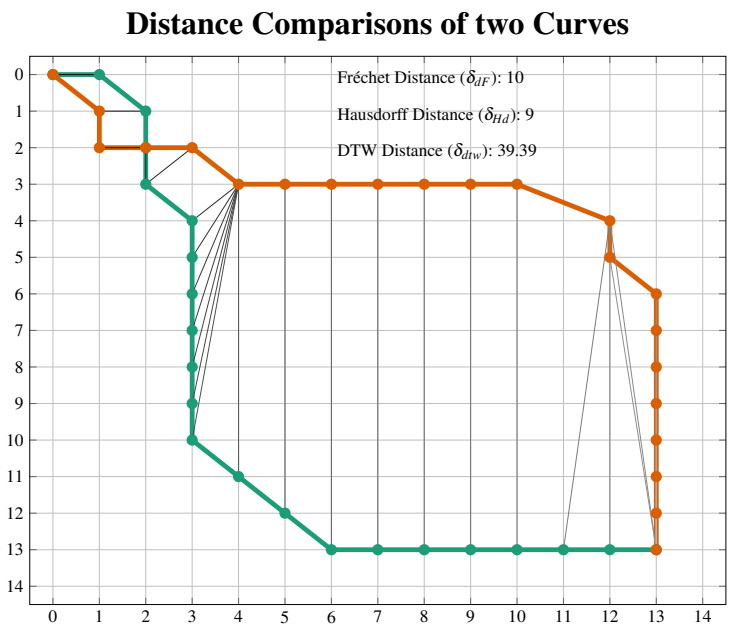

Figure 6.3: Comparison of Distance Metrics. Lines show path couplings [WM22a]

$$c_p(A,B) := \sum_{\ell=1}^{L} d\left(a_{r_\ell}, b_{s_\ell}\right) \tag{6.5a}$$

$$\delta_{dtw}(A,B) := c_{p^*}(A,B) \tag{6.5b}$$

$$\delta_{dtw}(A,B) = \min\left\{c_p(A,B) \mid p \text{ is an } (R,l)\text{-warping path}\right\} \tag{6.5c}$$

Figure 6.3 shows two curves and their respective distance values using each of the three proposed metrics. In all three measures, the function $d(\cdot,\cdot)$ represents the Euclidean distance between two points.

6.3.4 Network Distance

Each of the shown curve similarity metrics is based on a distance metric $d(\cdot,\cdot)$ in the respective space of the curves to measure the distance between two distinct points of the curves. Usually, this is the Euclidean distance between points, i.e., $d_e(p,q) = \sqrt{(q_1-p_1)^2+(q_2-p_2)^2}$ for the two-dimensional case. However, other *inter-point distance metrics* can be used. The pathfinding problem to which we apply our proposed methodology is based on a graph-based representation; hence, the network distance can be employed, which represents the number of minimum number of edges between two nodes in an unweighted graph. This distance is also known as the *geodesic distance* d_g between two nodes in a graph. Furthermore, d_g can also be defined as the total weight of the shortest path in a weighted graph between two nodes.

It should be noted, that the difference of d_e and d_g depends strongly on the underlying graph G. The distances can be equal or similar to each other if G is a Euclidean graph. Therefore, the grid graphs proposed in the ASLETISMAC benchmark can be classified as Euclidean graphs. However, in the following experiments, we used Hausdorff, Fréchet and DTW only. The reason was that we observed in a preliminary study that computing the network distance often required a large computational budget.

Figure 6.4: Different discrete Fréchet distance values [WM21b].

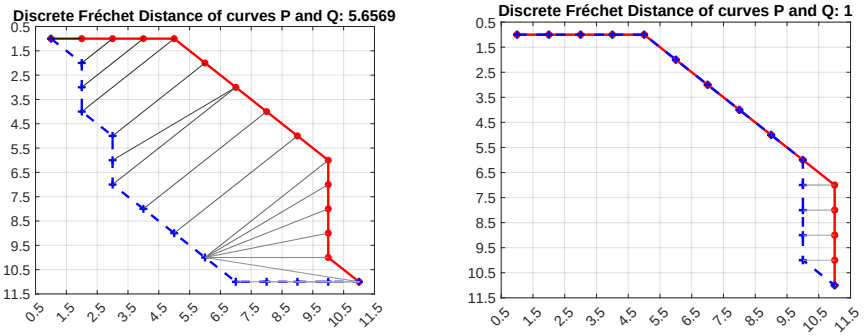

(a) Distinct paths

(b) Close paths

6.4 Diversification Within the Search Process

Within the optimisation process, the proposed methodologies can be implemented. We present here an approach for how such techniques can be used throughout the optimisation.

6.4.1 Incorporating Path Similarity Measurements

To preserve the diversity of solutions (paths) in the decision space, we now use each of the proposed path similarity measurements in the well-known NSGA-II algorithm [DPAM02]. Although NSGA-II has some drawbacks for many-objective problems, our previous study [WM22b] indicated that it outperformed NSGA-III [DJ14] in most problem instances. The problem's Pareto-fronts are usually irregular and degenerate. Due to the use of crowding distance, NSGA-II is more robust to these types of problems, as evenly distributed reference vectors which are used in NSGA-III can lead to the same solution [CSF18]. Furthermore, the pathfinding problem is partially deceptive, which can lead the algorithms to get stuck in local optima. In our experiments, we used several variations of incorporating the path similarity metric into the GA. In another study, we used the three proposed distance metrics to explore their impact on the algorithm results [WM22a].

In our algorithm's approach, we replace the crowding distance used in the NSGA-II algorithm with the proposed distance metric in the decision space. In other words, when the next parent population is filled and the last front cannot be added completely, we compare the solutions by using δ_{hd}, δ_{dF}, or δ_{dtw}. Moreover, we use this distance metric in the selection process. For this purpose, we implement a path similarity sorting method. We compute a dissimilarity matrix for μ paths in a population and assign either the lowest distance of all $\mu - 1$ values to each path or the median distance to $\mu - 1$ paths as described in Algorithm 1. The function ψ describes whether to use $min(\cdot)$ or $median(\cdot)$ as the crowding measurement [WM22a].

In this approach, paths with less similarity have a higher distance value. Figure 6.4 illustrates an example with several possible paths on a benchmark instance. Figure 6.4b shows two of the paths and their respective discrete Fréchet distance of 1, whereas Figure 6.4a shows two rather distinct paths with large distance values of 5.65. After every pair is computed, the paths are sorted by their distance value in descending order. This algorithm is called *NSGA-II-CR-δ-ψ*, where δ and ψ are exchanged with their respective implementation when running the algorithm. For instance, if $\delta = \delta_{FD}$ and $\psi = min()$, then the algorithm is called *NSGA-II-CR-FD-MIN* [WM22a].

Input: List of Paths $P = \{p_1, \cdots, p_\mu\}$
// Map is a key-value store. A path p is the key with the minimum distance as its value.
Result: Map(Path,minimum distance)
// Every Path $p_i \in P$ gets ∞ assigned
Map results = Map(Paths,Infinity);
// The distance δ from every path to every other is computed
// $\{(p_i, p_j) | p_i, p_j \in P, p_i \neq p_j\}$
for *i=1 to* μ **do**
  for *j=i+1 to* μ **do**
    $\delta_{old}(p_i)$ = results(p_i);
    $\delta_{current}(p_i)$=$\delta(p_i,p_j)$;
    results(p_i)=$\psi(\delta_{old}(p_i),\delta_{current}(p_i))$;
  end
end

Algorithm 1: Crowding Path similarity [WM21b], adapted [WM22a]

6.4.2 Using an Archive

In the second approach, we use a limited archive for storing non-dominated solutions and prune solutions by using the proposed discrete Fréchet distance. In this method, we apply the pruning strategy in decision space rather than in objective space. A variant of this approach is used in the context of multi-modal MOO [JZM19, DT05]. In this case, the discrete Fréchet distance metric represents a niching method. We call this variant *NSGA-II-FDAO* (Fréchet distance archive-only). We selected the archive-based approach as it has been shown that using an archive to store the non-dominated solutions can significantly improve the performance [Pat20]. Patil analysed several archive architectures, such as a limited archive which contains a maximum number of solutions. After each reproduction phase, all solutions of the population are added to the archive. A new solution S_{new} is checked for domination with the solutions already in the archive. If S_{new} is dominated by all solutions $S_{i,archive}$, S_{new} is not added. If S_{new} dominates any solution in the archive, the dominated solutions are removed from the archive. For the case where S_{new} is non-dominated, and the maximum number of archive members is reached, a solution in a dense area is removed; this is done based on clustering, nearest-neighbour or crowding distance [WM21b].

The third approach combines the two other approaches, resulting in *NSGA-II-FD*. In this variation, we replaced the crowding distance with the proposed Fréchet distance (as in the first approach), and the algorithm used an archive (as in the second approach) [WM21b].

6.5 Curve Ordering

Computing path similarities is an approach to identify areas in the decision space that are already covered by a majority of the population members. However, in contrast to computing a distance matrix and finding the minimum or median values, as was done in [WM21b, WM22a], imposing an order on a set of curves would open the possibility of finding neighbourhood relationships. With this approach, it is possible to find less covered areas with less computational effort.

When the crowding distance mechanism [DPAM02] is used as an example, it is evident that computing the degree of isolation for a solution – by analysing the distance to its neighbours – can yield benefits. In the crowding distance mechanism, solutions are ordered concerning the objectives being optimised. Then, the distance between the two neighbours is computed per objective and summated. This methodology allows a more focused niching, since less crowded sections are found and can be explored more. In the current analysis, we apply this concept to a set of paths in decision space. However, there is no natural total order on a set of paths or curves in a metric space [WM21a].

To order a set of paths, one can impose a binary relation on it. A relation $\leq$ on a set M is a total order if the following requirements are fulfilled for all $a, b, c \in M$:

$$\begin{aligned} a \leq b \wedge b \leq a &\Rightarrow a = b \text{ (Antisymmetric)} \\ a \leq b \wedge b \leq c &\Rightarrow a \leq c \text{ (Transitive)} \\ a \leq b \vee b &\leq a \text{ (Connected)} \end{aligned} \tag{6.6}$$

Our approach to impose a total order on a set of curves is to contract every curve to a single point and then compute the signed length of an orthogonal vector from a predefined line to these contraction points. Using a *contraction metric* f_{cm}, we then transfer each path from its metric space into the *contracted space*, where each path is represented as a single point [WM21a].

6.5.1 Contraction Metrics

Definition 1 (Contraction Metric)**.** A *contraction metric* can be, but is not limitedistad to, a measure of central tendency on a set of m points $\{x_1, x_2, \cdots, x_m\}$, where each $x_i \in \mathbb{R}^n$. It can be used to contract a path, defined by its set of nodes to a single point, which can be used for further computations. Let P be a set of k paths $P = \{p_1, p_2, \cdots, p_k\}$, where each path $p_i = (x_1, x_2, \cdots, x_m)$ is of a variable length $m \in \mathbb{N}, m \geq 1$, where each $x_i \in \mathbb{R}^n$. Then a contraction metric f_{cm} maps each path to a point, which serves as the path's representative, in the previously mentioned *contracted space* $\mathbb{R}^n$; hence, $f_{cm} : P \to \mathbb{R}^n$. This space has the same number of dimensions as do the points in the respective path.

For the contraction, the following metrics (measures of central tendency) can be used. We employ the set notation because all these metrics are based on sets of points and not on n-tuples. It should be noted that this list is not exhaustive, since other measurements can be used.

Definition 2 (Centroid)**.** The centroid C of a set X of m points $\{x_1, x_2, \cdots, x_m\}$ with each $x_i \in \mathbb{R}^n$ is defined by:

$$\mathbf{C}(\mathbf{X}) = \frac{\mathbf{x}_1 + \mathbf{x}_2 + \cdots + \mathbf{x}_m}{m} \tag{6.7}$$

The centroid, also known as the *centre of mass* of a polygon, is the point where the polygon can be balanced when placed on the tip of a needle.

Definition 3 (Geometric Median)**.** The geometric median of a set of m points $\{x_1, x_2, \cdots, x_m\}$ with each $x_i \in \mathbb{R}^n$ is defined by:

$$\arg\min_{y \in \mathbb{R}^n} \sum_{i=1}^{m} \|x_i - y\|_2 \tag{6.8}$$

Here, a point y is to be found which minimises the sum to all x_i in the set of nodes. This problem is also known as the *Fermat-Weber problem* [CLM+16]. We use *Weiszfeld's* algorithm, which iteratively computes the geometric median [Wei37].

6.5.2 Imposing an Order

After computing the contraction point $x_{cm} = f_{cm}(P)$ for each path $p_i \in P$ and $p_i = (x_1, \cdots, x_m)$, we can impose an order on the resulting set of points. As follows, we use the notation of $\vec{xy}$ for a vector from point x to point y. Hence, $\vec{xy} = \begin{pmatrix} y_0 - x_0 \\ \vdots \\ y_n - x_n \end{pmatrix}$ for two points $x, y \in \mathbb{R}^n$. We take the vector $\vec{v_{se}} = \vec{x_1 x_m}$ from the start to the endpoint and find an orthogonal vector $\vec{w_{se}}$, so that $\langle \vec{v_{se}}, \vec{w_{se}} \rangle = 0$, $\langle \vec{a}, \vec{b} \rangle$ denotes the dot product. This equation holds if $\vec{v_{se}} = \begin{pmatrix} x \\ y \end{pmatrix}$ and $\vec{w_{se}} = \begin{pmatrix} y \\ -x \end{pmatrix}$. We construct the orthogonal vector accordingly. Then, we compute the vector from x_{cm} to x_1, i.e., $\vec{r} = \vec{x_{cm} x_1}$. To determine the signed distance $d_{cm} = f_{distCm}(x_{cm})$ of the point x_{cm} to the line from x_1 to x_m, we compute the dot product of $\vec{-r}$ and $\hat{w_{se}}$, where $\hat{w_{se}}$ is the normalised vector $\vec{w_{se}}$, hence $f_{distCm}(x_{cm}) = \langle \vec{-r}, \hat{w_{se}} \rangle$. This value is also known as the *scalar projection* of the vector $\vec{-r}$ in the direction of the vector $\hat{w_{se}}$. In other words, it is the signed length of the projection of $\vec{-r}$ onto $\vec{w_{se}}$, hence $\vec{-r}_{\vec{w_{se}}}$. This value can be negative or positive, depending on which side of the vector $\vec{v_{se}}$ the point lies. In Figure 6.5, the used vectors and their relations are shown in a two-dimensional metric space.

Proof. Let $\vec{r} = \vec{p_{cm} p_{start}}$, and $v_{se} \perp w_{se}$. So,

$$
\begin{aligned}
cos\theta &= \frac{\|r_{w_{se}}\|}{\|r\|} \\
cos\theta \, \|r\| &= \|r_{w_{se}}\| \\
cos\theta \, \|r\| \, \|w_{se}\| &= \|r_{w_{se}}\| \, \|w_{se}\| \\
\langle w_{se}, r \rangle &= \|r_{w_{se}}\| \, \|w_{se}\| \\
\frac{\langle w_{se}, r \rangle}{\|w_{se}\|} &= \|r_{w_{se}}\| \\
\langle w_{se}, r \rangle &= \|r_{w_{se}}\|
\end{aligned}
$$

□

After computing f_{distCm} for every contraction point of each path $p_i \in P$, we order the values in ascending or descending order. We thus impose a total order on the set of paths by ordering their respective f_{distCm}-values. Figure 6.6 shows an example map, in which different markers denote the different paths. Furthermore, the respective contraction points are shown using the same markers. In addition, the contraction point's distance is colour coded. Paths on the left side of the dashed centre line have a negative distance, whereas paths on the right side have positive distances. In this example, we used the geometric median as the contraction metric [WM21a].

This methodology is independent of the path's orthogonal coordinate system and can be applied to any set of paths. The reason behind this is that both the centroid

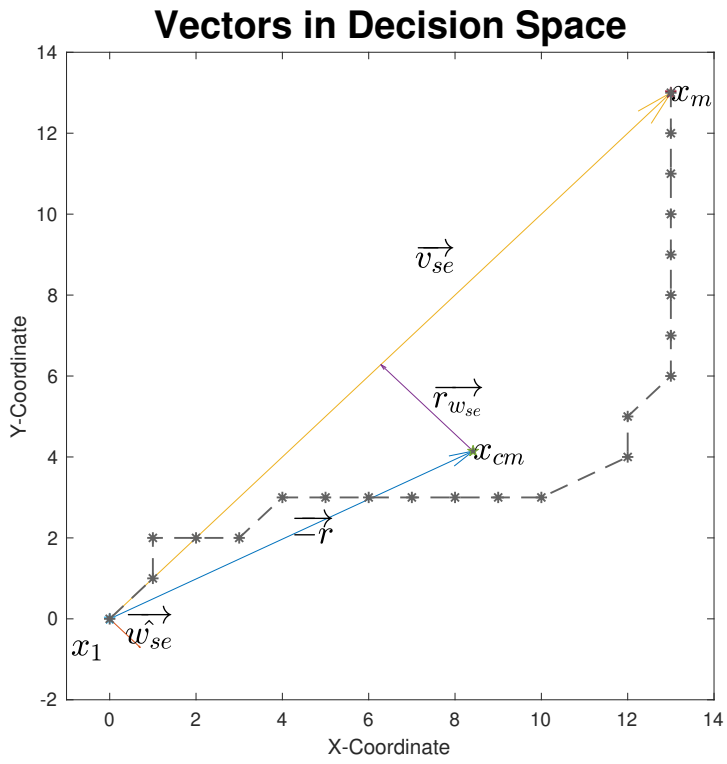

Figure 6.5: Vectors used for measuring the distance between x_{cm} and the vector v_{se}. The dashed line represents an example path. [WM21a]

and the geometric median are equivariant under Euclidean transformations. Only pairwise distances account for a change in their values [Eft15, Kim94].

6.5.3 Path Density-Based NSGA-II

In [WM21b], the authors used the well-known NSGA-II algorithm [DPAM02] and changed the replacement mechanism by employing their *Fréchet sorting method* instead of using crowding distance. When the population cannot be filled with the following front during the replacement process, the solutions are usually ordered using crowding distance to find solutions in less dense areas. The authors in [WM21b] instead computed the distance matrix of all solutions and then assigned the respective minimum value of the distances to the respective solution. Through this approach, they performed the niching in decision space instead of the objective space. The solution with the highest minimum distance was then brought into the next generation. They applied the same technique during the selection process [WM21a].

In our novel approach, instead of computing the distances to all other paths in the respective front and taking the minimum, we compute the distance between the two neighbours of a specific solution, which reduces computational cost and increases the niching. The solutions are ordered according to their respective contraction points, and the Fréchet density values are computed by taking the average distance to the two neighbours of a solution. The two outer solutions are assigned with an infinite distance, as is done in crowding distance. In Figure 6.7, a small example is shown. Three paths are depicted in white, while the paths' respective couplings are shown in black. The middle path is the one whose degree of isolation is computed. The algorithm determines the distances to its two neighbours, and the average is then assigned as its isolation value. For

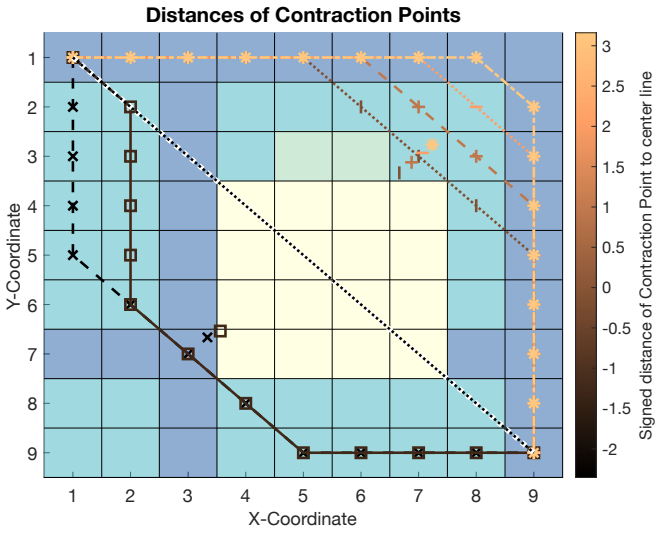

Figure 6.6: Paths and their respective contraction points (geometric median, denoted by the same marker as in the paths) [WM21a]

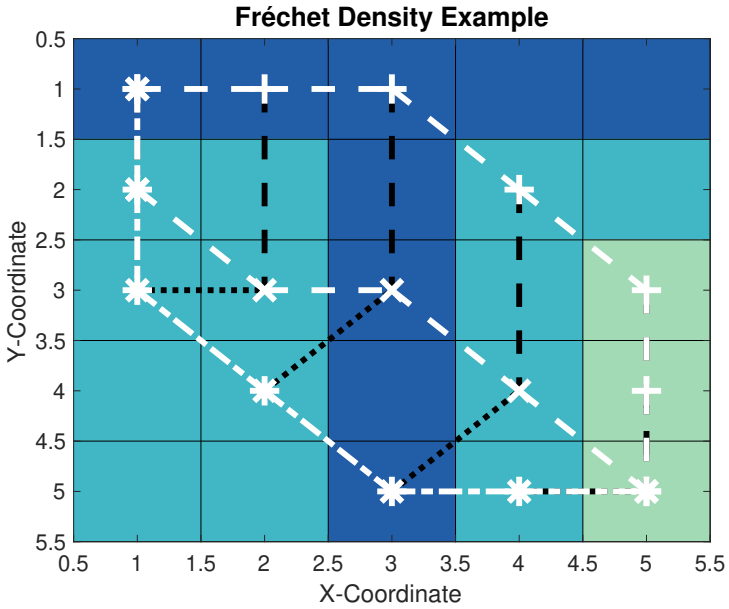

Figure 6.7: Three paths, in white. Black: The paths' couplings. [WM21a]

a path p_i in an ordered set of paths $P = \{p_1, \cdots, p_k\}$, and using one of the above-mentioned contraction metrics, the *Fréchet density value* is defined by:

$$FDV(p_i) = \frac{\Sigma_{j=-1}^{1} \delta_{dF}(p_i, p_{i+j})}{2} \tag{6.9}$$

where $\delta_{dF}(p_i, p_j)$ is the discrete Fréchet distance between the paths p_i and p_j. It should be noted that other similarity metrics can be used here as well.

For the sake of clarity, the algorithm from [WM21b] is denoted as *NSGA-II-CRFD*, whereas our approach is denoted as *NSGA-II-DEFDXX*. Here *XX* refers to the contraction metric used; *CT* means *centroid*, *GM* means *geometric median*, *DE* means *density*, and *FD* means *Fréchet distance*. The solutions with a higher Fréchet density value are thus brought into the next generation and selected if they are non-dominated during the selection phase.

6.6 Evaluation

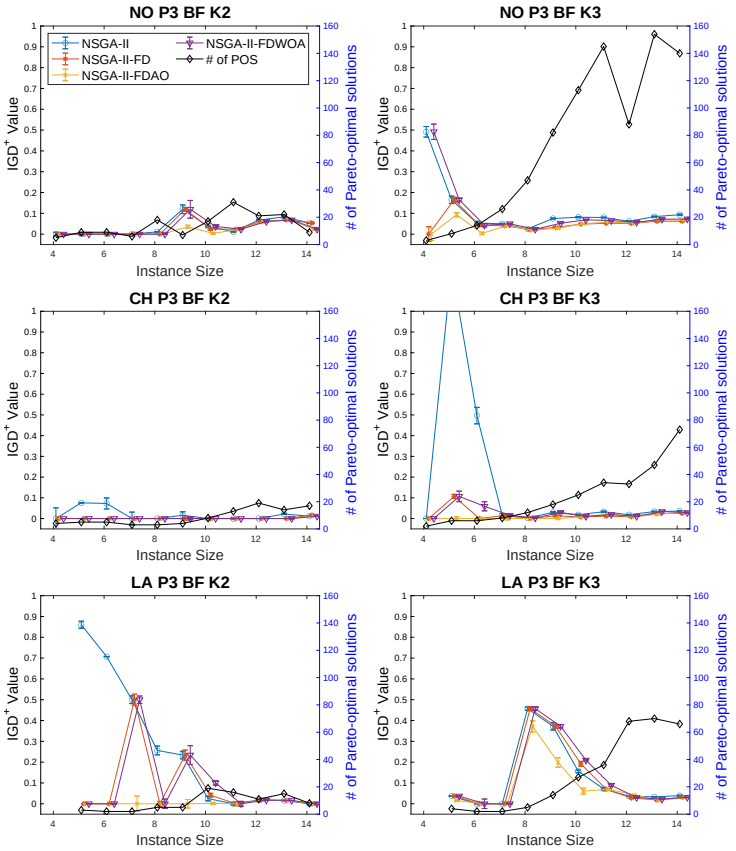

Figure 6.8: IGD$^+$ over instance sizes. Top, middle and bottom rows illustrate NO, CH and LA obstacles. Right and left columns show the K2 and K3 neigbourhoods. [WM21b]

In the previous sections, we proposed different methodologies to maintain and increase the solution set diversity in the decision space. Here, we evaluate each of the approaches described.

6.6.1 Distance Matrices

As follows, we evaluate the proposed methodology, which uses distance matrices for the diversification of the population.

Using an archive

Figure 6.8 illustrates the median value and the standard error of the IGD$^+$ indicator regarding the instance size.

We additionally report the number of Pareto-optimal solutions (indicated by # of POS) for each problem instance. From a graphical perspective, it is evident that the results vary depending on the type and size of the problem instance. In most cases, the NSGA-II-FDAO (archive-only) obtained the best median value and the lowest standard error. Counting the number of experiments where an algorithm was outperformed by at least one other algorithm confirmed that NSGA-II-FDAO was outperformed the least. Comparing this variant solely with the baseline algorithm indicates that the baseline algorithm was outperformed 152 times, whereas the proposed variant was never outperformed. Table 6.1 shows the wins, losses and ties of each algorithm on all 256 problems [WM21b].

The variant with Fréchet distance only (NSGA-II-FDWOA, no archive), also performed well compared to the baseline algorithm alone. The proposed variation of the algorithm was outperformed 76 times (concerning the value of the IGD$^+$ indicator) for the 256 chosen problems, whereas the baseline algo-

Table 6.1: Wins, losses and ties of each algorithm pair (rows vs. column) with statistical significance at $p < 0.01$, Bonferroni correction applied, IGD+ indicator [WM21b].

	NSGA-II-FD	NSGA-II-FDAO	NSGA-II-FDWOA
NSGA-II	0/132/124	0/152/104	0/85/171
NSGA-II-FD		0/45/211	25/34/197
NSGA-II-FDAO			51/33/172

rithm was outperformed 369 times. In the remaining experiments, there was no statistically significant difference.

The mixed variant NSGA-II-FD was never outperformed when compared only to the baseline algorithm. The baseline, by contrast, was outperformed 108 times with respect to the IGD^+ indicator.

When analysing the results, we noted that the high number of ties indicates room for improvement. This could be due to the fact that the Fréchet distance sorting, given two subsets of distinct paths with relatively short distance values inside the subset, results in a short distance value for each path even if the two sets are apart from each other . Nonetheless, the results show an improvement over the baseline algorithm since the proposed variants won in more problems and lost in fewer. The archive-only algorithm obtained the most promising results, supporting Patil's statement that only the use of an archive can significantly affect the results [WM21b].

Comparison of different metrics

Settings In the experiments, we examined the proposed approaches on the benchmark test suite ASLETISMAC [WM22b] (cf. Chapter 4). We consider a two-dimensional space with three obstacle types (NO, LA and CH), with K3 neighbourhood, enabled backtracking and grid sizes of $\{15, 20, 24, 26, 28, 30\}$. NO indicates no obstacles, whereas LA and CH introduce bulk and checkerboard obstacles, as shown in Figure 4.4. In this way, CH constrains the decision space to a few feasible paths. The K3 neighbourhood restricts the number of possible neighbours to eight, i.e., all surrounding cells. All these combinations result in 84 test instances. Given a solution represented by a path p as $p = (n_i, n_{i+1} \cdots, n_k)$ (a list of nodes), we evaluate it by five objectives to be minimised: 1) Euclidean length, 2) Delays, 3) Elevation, 4) Travelling time and 5) Smoothness (Curvature) (see Chapter 4).

We use the same operators for pathfinding as in [WM22b] i.e., a one-point crossover, which creates new offspring chromosomes by crossing two parent paths at one common point. We also use the proposed perimeter mutation for the mutation operator, which mutates the middle point of two arbitrary points within a specific network distance inside a given maximum radius and reconnects the paths afterwards. We thus compare the algorithms using the three incorporated distance metrics. Although the problem is a many-objective optimisation problem, we consider a smaller computational budget than our previous studies did. The reason is that we observed that the quality of results changed only marginally after 100 generations. This decision means we want to take time performance considerations into account by sacrificing quality. Furthermore, we use a population size of $\mu = 100$ to further account for fewer function evaluations. In real-world applications, obtaining results in a short time is often a requirement. For the experiments, we calculate the IGD^+ indicator that is a distance measurement between the obtained front of non-dominated solutions and the known true Pareto reference front [IMN15]. Furthermore, we

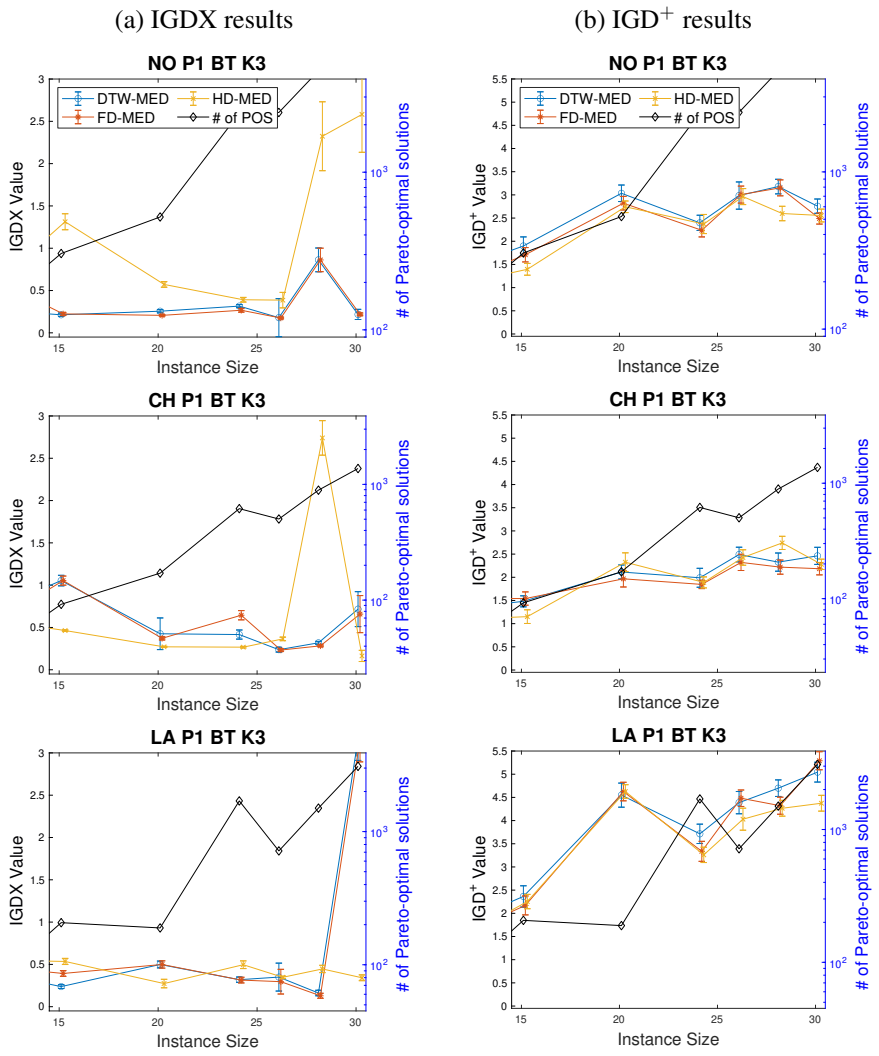

Figure 6.9: IGD$^+$ and IGDX over instance sizes. Top, middle and bottom rows illustrate NO, CH and LA obstacles [WM22a].

report the respective wins, losses and ties of each algorithm for all problem instances [WM22a].

To assess the quality of solutions in the decision space, we also employ the IGDX indicator [AQY09], which measures the distance between the known Pareto-set and the found solutions. Again, we compare the results of the algorithms to each other and test for statistical significance using Bonferroni correction (because we perform multiple comparisons). Our null hypothesis states that the populations have equal medians [WM22a].

Results Figure 6.9 illustrates the median values and standard error of the IGDX and IGD$^+$ indicators, respectively, for the instance sizes and obstacle settings. Each row in the figure shows a different obstacle profile: *NO*, *CH* or *LA*.

We also report the number of Pareto-optimal solutions for each problem instance on the right axis, which we obtained using the exact approach. From a graphical perspective, it is evident that the results vary depending on the type and size of the problem instance. It is noteworthy that in the instance of LA P1 BT K3 (bottom left) of size 28, the algorithms using Fréchet and DTW distance obtained a small IGDX value, whereas the IGD$^+$ value was relatively high. This indicates that solutions near the optimal solutions in the decision space were found, but they were of a low quality in the objective space. For the

Table 6.2: Wins, losses and ties of each algorithm pair (rows vs. column) with statistical significance at $p < 0.01$, Bonferroni correction applied, IGDX and IGD$^+$ indicator [WM22a].

		FD-MED	HD-MED
DTW-MED	IGDX	3/6/75	23/16/45
	IGD$^+$	0/0/84	0/6/78
FD-MED	IGDX		23/14/47
	IGD$^+$		0/2/82

multi-objective pathfinding problem, we have shown that solutions close to the optimum in decision space are not necessarily close to the optimum in terms of the respective objective values. However, the same two algorithms obtained a worse IGDX value on instance of size 30 for the same map type, whereas the algorithm incorporating the Hausdorff distance could still obtain a low value. Nevertheless, in the other two obstacle settings, using the Hausdorff distance was not as stable as the other two distance metrics regarding IGDX values as backtracking was allowed. This meant the metrics that took the flow of a curve into account yielded better results. If a path gets closer to its origin, whereas another path does not, the Hausdorff distance does not always reflect their similarity correctly, in the sense of their flow. As a result, the Hausdorff distance can be small although the Fréchet and DTW distances give higher values, as the paths are more distinct.

Concerning the IGD$^+$ indicator, all three algorithms obtained similar values. The indicators' results show that using the proposed niching methodology improves the quality of solutions in terms of closeness to the true Pareto-set. However, there is room for improvement regarding the objective values. Because we limited the search to 10000 function evaluations (which is relatively low for many-objective optimisation problems), the results regarding IGD$^+$ were expected. In this study, the search process focused on employing measurements in the decision space to minimise the objective functions. Therefore, there was little improvement in the objective space that was measured by IGD$^+$. The underlying problem is deceptive, which can result in paths that are close to an optimal solution in the decision space (measured by IGDX) but far from the optimum in the objective space. For a real-world application, the impact would be that a slight perturbation when executing or traversing a path can result in a severe deterioration in terms of objective functions. Future research could develop more advanced methodologies to focus on local optimisation. Often, only a small portion of the path needs to be changed to result in better objective values [WM22a].

Table 6.2 shows the wins, losses and ties of each algorithm on all 84 test problems. Again, the differences concerning the two performance indicators is evident, as most outcomes regarding IGD$^+$ were ties. Several instances had a definite winner when the IGDX values were compared [WM22a].

Figure 6.10 shows a comparison of two variants of the algorithm using δ_{dF}, i.e., (1) taking the median value of all distances to other paths, denoted by *FD-MED*, and (2) taking the minimum value of the distances, denoted by *FD-MIN*. The two variants are again compared concerning IGDX (Figure 6.10a) and IGD$^+$ (Figure 6.10b). Interestingly, regarding IGD$^+$, *FD-MED* either won or was of the same quality as *FD-MIN*, whereas the latter won in several instances regarding IGDX. The reason is that the $min()$ approach works better for local optimisation since the closest paths are used as a reference [WM22a].

A more detailed view is provided in Figure 6.11, where the respective indicator values over different sizes for a specific instance type are depicted. Clearly,

(a) IGDX results (b) IGD$^+$ results

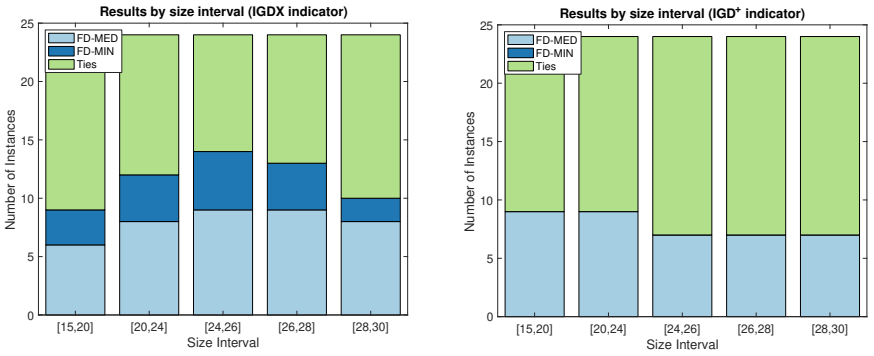

Figure 6.10: Wins/Losses/Ties of the algorithm incorporating Fréchet distance with respect to the IGD$^+$ and IGDX indicators over different instance size intervals [WM22a].

(a) IGDX results (b) IGD$^+$ results

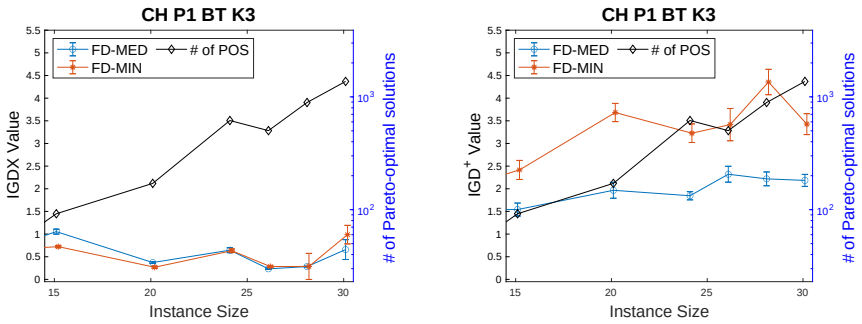

Figure 6.11: Indicator values of the instance CH P1 K3 BT for different sizes, comparing FD-MED *and* FD-MIN *[WM22a].*

FD-MIN obtained better or similar values in terms of the IGDX values but was outperformed by *FD-MED* with respect to IGD$^+$.

When analysing the results, we noted that the high number of ties indicates room for improvement. The many ties are a result of the path similarity sorting. Sorting with two subsets of distinct paths that have relatively short distance values inside the subset will result in a short distance value for each path, although the two sets may be apart from each other [WM22a].

6.6.2 Curve Ordering

In this section we evaluate the proposed curve ordering technique using contraction metrics.

Experiment Settings

To test our approach, we used the proposed five objective benchmark suite from [WM22b]. We generated 240 different instances with different sizes, obstacle and neighbourhood configurations, and elevation functions. Drawing from the same work, we used the provided true Pareto-fronts and sets to evaluate our methodology. Figure 6.6 shows an example map which represents the *lake* obstacle configuration on an instance of size 9, while in Figure 6.7 the map is of size 5 and there are no obstacles. For the experiments, we used instance sizes in the interval $\{5,6,\cdots,14\}$, all four proposed elevation functions, 2^k-neighbourhoods for $k \in \{2,3\}$ and disabled backtracking. In addition to the benchmark instances, we applied the algorithm on a real-world data set to compute the set of paths between two airports in Berlin. The same approach was followed in [WM22b].

The problem instances are defined on grids of various sizes with different constraints. However, they are represented as a graph $G = (V,E)$, where each

node $n \in V$ has various properties, including their respective coordinates, a height value and constraints concerning possible movements when this node is traversed (see Chapter 4). The problem has five objectives, i.e., path length, the time needed to traverse the path, expected delay, total positive ascent of a path, and curvature (smoothness).

To compare our results, we used the proposed algorithm in [WM21b] as our baseline. We used the same implementation but changed the Fréchet sorting method to our proposed ordering and neighbourhood relation identification method. The two contraction metrics are used in dedicated algorithms. The reason for using NSGA-II for a many-objective problem is that in the original study, it outperformed many-objective algorithms such as NSGA-III [WM22b]. We ran the algorithms 31 times with a population size of $\mu = 212$ for 500 generations, totalling 106 000 evaluations. The crossover and mutation rates were set to 0.8 and 0.2, respectively. For performance comparison, we used the IGD^+indicator [IMN15] and the IGDX indicator [AQY09] to measure the distance in the decision space. The distance from the Pareto-set to the candidate solutions are, again, measured using the Fréchet distance. To compute a reference front for the real-world example, we combined the results from all runs of all algorithms and computed the non-dominated set. The statistical evaluation was performed using the Kruskal-Wallis test and applied Bonferroni correction for multiple comparisons, as suggested in [KTZ06], and statistical significance was set at $p < 0.01$. In pairwise comparisons, we assumed the null hypothesis held, namely that the distributions of the two samples had equal medians [WM21a].

The algorithms were implemented in Java using the *jMetal* framework [NDV15] and the jGraphT library [MKNS19].

Results

Figure 6.12 shows the results of the algorithms. Depicted are the IGD^+values and their corresponding standard errors for different instance sizes. It is evident that the proposed method performed better for larger sizes. Mainly from the size of 10 and above, the new method outperformed the other in most instances. This trend indicates that the proposed niching methods should not be used with small instance sizes. The reason for the poor performance on smaller instances is that the contraction points are comparatively close to each other or may even exist at the same coordinates, which makes it hard for the algorithm to find less dense areas; this holds for both variations employing different contraction metrics. However, the geometric median approach performed slightly better. The approach in [WM21b], by contrast, was better on smaller instances, as it determined crowded areas using a distance matrix, which gives a better estimation of densities [WM21a].

The results also showed that the proposed approach outperformed the original method when the Pareto-optimal solutions were comparatively dense in decision space. The former approach has various drawbacks in such a situation, since the values in the distance matrix are mostly the same. This makes it hard for the algorithm to determine the solution with the lowest degree of isolation [WM21a].

In Figure 6.13, different size intervals are grouped, and the respective wins of each algorithm are shown. It is evident that with increasing size, the proposed method won most benchmark instances. In the diagram, each interval contains 48 benchmark instances. For example, the interval $[5,6]$ contains instances with

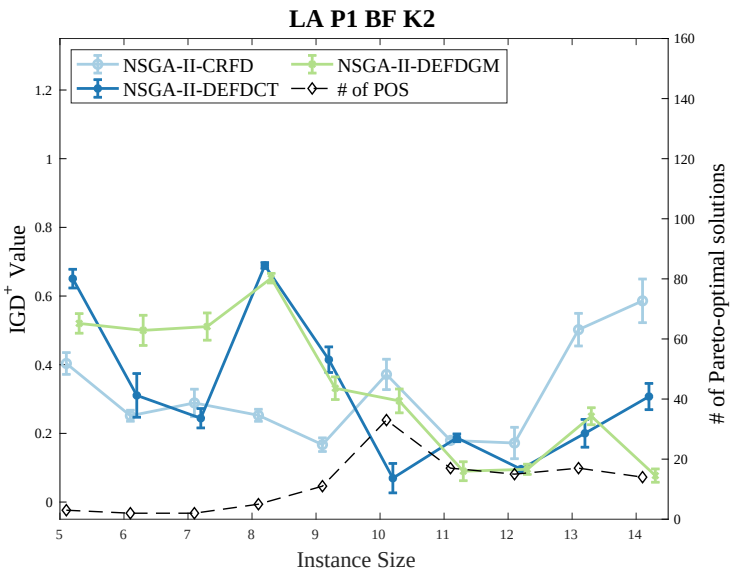

Figure 6.12: Results of the algorithms (IGD$^+$ indicator) by size of the instance type LA P1 K2 BF*. [WM21a]*

all different obstacle, neighbourhood and elevation configurations, but only those of size 5 and 6 [WM21a].

In Table 6.3, the wins, losses and ties concerning the two used indicators are shown. The table numbers indicate the respective number of benchmark instances. With respect to IGD$^+$, our proposed methods won most of the instances. Moreover, using the geometric median as the contraction metric can yield benefits over using the centroid approach. The reason is the characteristics of the geometric median, which by nature is more robust to outliers (cf. *mean* and *median*). If a path is mutated so that a few nodes are shifted, the centroid's position is impacted more than the geometric median's coordinates. In this approach, the geometric median can still provide a good estimate of the path's relations to its neighbours, compared to the centroid. In other words, using the centroid approach, a neighbourhood relation can change more quickly if only a few nodes change their positions [WM21a].

However, there are still several losses and also ties, indicating room for improvement. Figure 6.12 illustrates a direct comparison of the obtained IGD$^+$indicator values concerning the instances' sizes. Our proposed methods achieved better results with increasing map size [WM21a].

A different outcome was obtained by analysing the results using the IGDX indicator, which measures the distance to the true Pareto-set in the decision space. When the method from [WM21b] was compared to our approach, our methodology was outperformed more often than it won an instance. Furthermore, there were many ties between the methods. The reason is that the older method uses a dissimilarity matrix to determine crowded areas and is therefore more sensitive to differences in paths. The path comparison in [WM21b] uses the complete path information, whereas our technique uses a single point of representation. We also compared the centroid-based methodology to the geometric median-based approach. They won similar cases against each other, and the comparison also resulted in numerous ties [WM21a].

The results of the real-world example indicated that the proposed method was superior to the original approach. This conclusion is supported by the IGD$^+$ indicator, shown in Figure 6.14, depicting the indicator value over the number of evaluations. Here, a faster convergence can be observed. Finally, the proposed approach outperformed the reference methodology regardless of the chosen

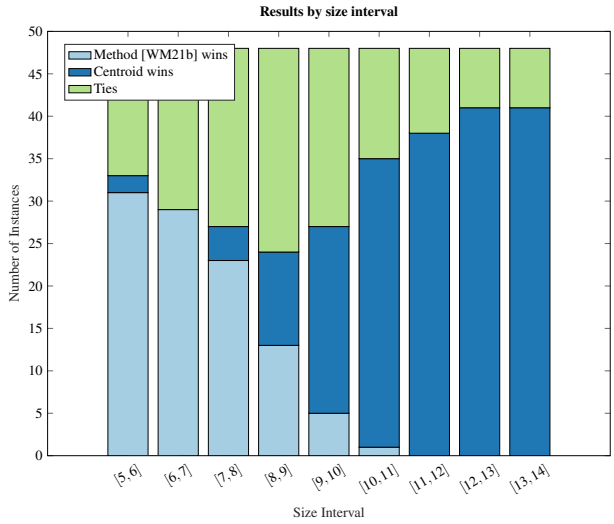

Figure 6.13: Wins and Ties of the proposed approach by different instance size ranges (using the centroid method) concerning the IGD$^+$ indicator. [WM21a]

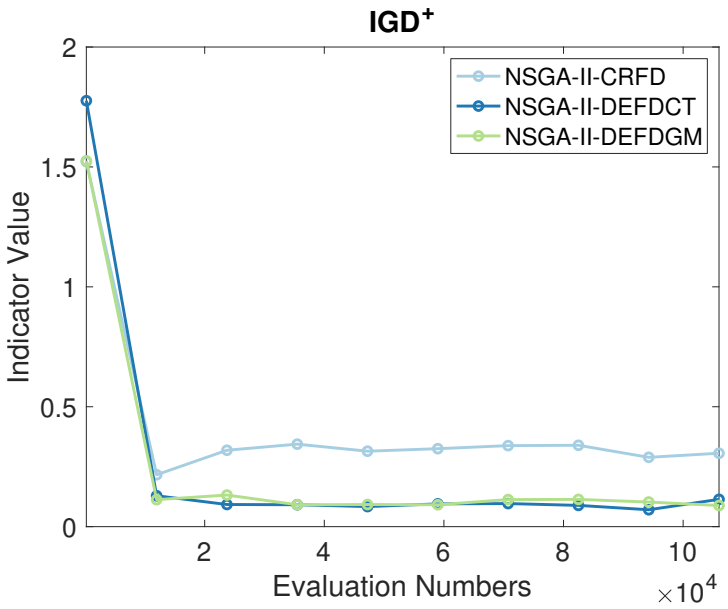

Figure 6.14: IGD$^+$ indicator over function evaluation for the real-world problem. The run, with the median value at the end of the experiments, is depicted. [WM21a]

contraction metric. The two metrics had no statistically significant difference regarding the values of the IGD$^+$ indicator [WM21a].

A comparison of the computational costs indicated the benefits of using our proposed method. In [WM21b] a distance matrix was used, resulting in $\mu - 1$ distance computations for each solution, where μ is the population size. In our approach, after ordering the set and determining neighbourhood relations, we needed to compute only two distances for each solution. The algorithms' run time was lower than in the baseline approach. However, the computation of the contraction points must also be considered. Computing the centroid of a set of points needs less computational effort, since the points' coordinates are averaged. There is no analytic solution for the geometric median, because this is a computationally challenging task and an iterative algorithmic approach has to be used. There are newer approaches to solve the problem of finding the geometric median which achieve lower computational complexity than Weiszfeld's algorithm, i.e., [CLM$^+$16], which achieved a nearly linear time complexity of $O\left(nd \log^3 \frac{n}{\varepsilon}\right)$ for a $(1-\varepsilon)$-approximate geometric median. In contrast to our study, n denotes the number of points and d the number of dimensions.

Table 6.3: Wins, losses and ties of each algorithm pair (rows vs. column) with statistical significance at $p < 0.01$, Bonferroni correction applied, IGDX and IGD$^+$ indicator [WM21a].

		Centroid	Geom. Med.
[WM21b]	IGDX	66/54/120	76/67/97
	IGD$^+$	51/93/96	47/109/84
Centroid	IGDX		54/56/130
	IGD$^+$		20/50/170

6.6.3 Comparison with Exact Approaches

We compared our approach in terms of performance to an exact approach, i.e., the multi-objective Dijkstra shortest path algorithm [Mar84]. A comparison with exact methods is not trivial, since algorithms such as Dijkstra or A* typically use edge weights to evaluate a path's cost. In the classical multi-objective shortest path problem, a path p of length k is defined by a sequence of edges in the graph, i.e., $p = (e_1, \ldots, e_k)$, where $e_i \in E$, for $i = 1, \ldots, k$ and the path's cost is defined by the sum of the edges' weight vectors, i.e., $z(p) = (z_1(p), \ldots, z_m(p))$, where $z_j(p) = \sum_{l=1}^{k} w_j(e_l)$ and $\overrightarrow{w(e)} = (w_1(e), \ldots, w_m(e))$, where m is the number of cost values or objectives [GBR06].

Graph Transfer

In the benchmark of [WM22b], the objectives *cannot* be represented as a weight vector $\overrightarrow{w(e)}$ on each edge $e \in E$. The reason is the smoothness objective, which depends on the location of three nodes in a sequence. In Equation (4.5), it is evident that this objective takes three nodes as its input parameters. Therefore, it cannot be expressed as a weight value assigned to an edge connecting only two nodes. It always depends on three nodes. An edge's weight vector $\overrightarrow{w(e_i)}$ thus depends on the previous edge on the path, i.e., $\overrightarrow{w(e_{i-1})}$. To apply conventional multi-objective pathfinding methodologies to these problems, one must reduce the problem to a regular multi-objective pathfinding problem by transferring the graph $G = (V, E)$ to a new graph $G' = (V', E')$. A node is denoted by $(\cdot)$, and a directed edge between two nodes is denoted by an arrow, i.e., $(\cdot) \to (\cdot)$. In graph G', each pair of nodes, i.e., $(q, r), q, r \in V$, with $(q) \to (r) \in E$ in graph G, is represented by a new node $(q, r) \in V'$. Furthermore, an edge from $(q, r) \to (r, s)$ is added to E', which represents the traversal from r to s, assuming q was the traversed node before r. The pathfinding problem has predetermined start and target nodes, i.e., $s, t \in V$. Therefore, we added the nodes $s^+ \in V'$ and $t^+ \in V'$ and edges $\gamma = (s^+) \to (s, q) \in E'$, with $w_i(\gamma) = f_i(s, q)$, for $i = 1, \ldots, 4$, but $w_i(\gamma) = 0$, for $i = 5$, and $\eta = (q, t) \to (t^+) \in E'$ with $\overrightarrow{w(\eta)} = \vec{0}$, i.e, the zero vector [WM22a].

The graph transformation enables conventional multi-objective shortest path algorithms to solve the problem. However, the number of nodes and edges in graph G' can be substantially higher than those in G, depending on the specified problem instance. For K3 instances with enabled backtracking, the number of nodes is defined by $|V'| = 4(x_{max} - 1)(2x_{max} - 1) + 2$ and the number of edges $|E'| = 4(x_{max} - 1)(16x_{max} - 23) + 6$. Given these functions, it is clear that the number of nodes and edges grows quadratically and influences the algorithm's performance. Figure 6.15 illustrates an example, showing the original graph G in Figure 6.15a and the transferred graph G' in Figure 6.15b [WM22a].

To set the edges' weight vectors, we can employ the objective functions from the benchmark to compute the weights for each $e \in E'$. The proposed functions are path-based and have an arbitrary path p of length $k > 1$ as an input, where k is

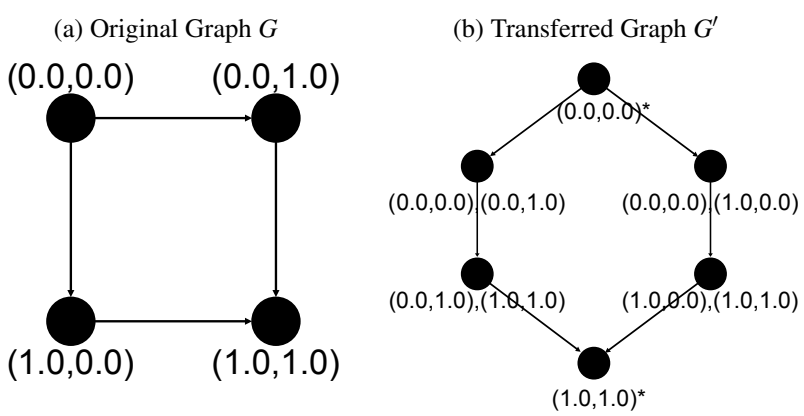

Figure 6.15: Comparison of the original problem graph G and the transferred graph G'. In parentheses: the respective grid coordinates [WM22a].

the number of nodes in p_i. Again, all objective functions, except the *smoothness* objective, need two consecutive nodes to be computed. However, the *smoothness* (f_5, Equation (4.5)) is based on three nodes to compute the angle between them. The edge's weight vectors are set as shown in Equation (6.10), where the inputs of the objective functions are node lists [WM22a].

$$\vec{w}((q,r) \to (r,s)) = (f_1((r,s)), f_2((r,s)), f_3((r,s)), f_4((r,s)), f_5((q,r,s))) \tag{6.10}$$

We employed the multi-objective Dijkstra for various instances of different sizes and properties, to find the true Pareto-fronts and sets.

In conclusion, the cost of reducing an arbitrary graph of a multi-objective pathfinding problem to a standard multi-objective shortest path problem (where each edge's weight vector represents the objective functions) can be large, depending on the actual computation of the objective functions. The more nodes that are considered for an objective, the costlier the transfer, and the costlier the computation of an optimal method. Nevertheless, in a real application, it should always be considered how performant and costly an exact approach would be, as such an approach can be beneficial [WM22a].

Naturally, it is not trivial to compare an exact algorithm to a meta-heuristic. However, since the running time of the multi-objective Dijkstra is directly related to the number of nodes and edges, we decided to combine running times with the quality of results of the algorithms to compare them. We therefore used the indicator values. Our comparison metric was $\lambda_I = median(t_I) \cdot (1 + median(\mathrm{I}))$, i.e., the median run time t_I of an algorithm on a problem multiplied by the median indicator value I added to 1. This metric takes the suboptimality of meta-heuristics into account. However, the indicator value I for the optimal algorithm is inherently 0, where I is the IGD^+ or IGDX indicator [WM22a].

Performance Comparison

We also compared the performance of the algorithms on the original graph to an exact approach on the transferred graph in order to evaluate the quality and running time when allowing a small computational budget of 10000 evaluations. Figure 6.16 shows the values of the proposed λ-performance for the two employed quality indicators. The y-axis is on a logarithmic scale. In the left graph, λ_{IGDX} shows that the proposed approach has a better value from instance sizes of 26 onwards, whereas the values are lower from size 28 for λ_{IGD^+}, compared to the exact approach. Nevertheless, a trend is evident in which lower λ

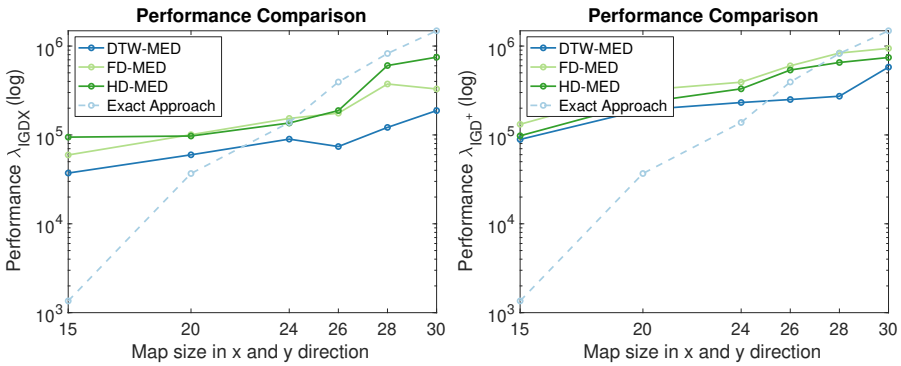

Figure 6.16: Results of the λ performance measurement (IGD^+ & IGDX) [WM22a].

values for the metaheuristic approach than for the exact approach are associated with larger map sizes. That is to be expected, as the running time for the exact approach grows quadratically. Interestingly, the DTW approach achieved the best performance in most of the runs. Although the DTW is computationally expensive, it can diversify the solution set well since it is sensitive to path differences. Nevertheless, the λ indicator is an approximation and cannot be used to make decisions about significant differences between algorithms [WM22a].

6.7 Summary

In this chapter, we have proposed various techniques and methodologies to diversify the set of solutions during the search process. Without special techniques, an optimisation can get stuck in local optima, as the many-objective pathfinding problem can be deceptive. Most of the presented approaches take place in the decision space, because other methods (such as CD) do not obtain accurate solutions in terms of the objective values. Nevertheless, for some approaches, we have shown that focusing solely on diversification and niching in the decision space can result in close-to-optimal objective values — but also in solutions that are distinct from optimal solutions in the decision space. As a result, if a path is traversed in the real world, and if small perturbations happen, the eventual objective values can be much worse than the computed ones. Combining techniques in both of the spaces can result in good objective values and closeness to optimal solutions in the decision space, resulting in more robust solutions. This topic is addressed in the next chapter.

7 Decision Support and Large Road Networks

In this chapter, the following points are covered

- How to support a decision-maker (DM) using reduction approaches
- Definition of DPs
- Pathfinding on large road networks

In many-objective optimisation, the result is usually a large set of solutions. However, in a real-world process, only a single solution can be chosen. This principle also holds for the pathfinding problem: from all paths found, only one can be executed or traversed. According to Miller, only 7 ± 2 so-called *chunks* of information can be processed by humans [Mil56]. It should be noted that recent research indicates that this number is even lower, at approximately 3 to 4 chunks [RMC+08]. To find an appropriate number of solutions from the result of a multi-objective algorithm, researchers need an additional methodology. A *decision support system* can help in identifying interesting solutions from the complete solution set.

Usually, with many objectives, a large fraction of the solution set is Pareto-optimal [DJ14]. On large road maps, for instance, thousands of solutions can be Pareto-optimal, which no human DMs can comprehend at once. In this chapter, we present methodologies that reduce a large solution set to a small and comprehensible subset that is specifically developed for pathfinding problems. Again, we intend to find a set of final solutions from which a DM can choose.

In [Par21] a decision support system was proposed. The author described three variations of an algorithm that uses different combinations of measurements in both objective and decision space. In this thesis, we extend that approach by employing various distance metrics as well as a different cluster analysis. Additionally, we propose an approach to identify alternative paths as well as robust paths.

7.1 Objective Space

In the literature, there are several works on filtering the solution set by using different dominance criteria. Two of the major methodologies are ε-dominance

and *cone*-dominance. Both approaches are more relaxed variants of Pareto-dominance and were described in Section 2.2.2.

For the pathfinding problem, we use these relations to obtain a subset of a large solution set. Cone-dominance is particularly suitable to determine knee-points in a Pareto-front [DZJ03]. Using ε-dominance enables finding an approximation of the Pareto-front, which often has fewer elements than the result solution list of an optimisation technique.

Besides these variants of domination, one can also use cluster analysis to find κ_{obj} sets of similar solutions and determine the respective representative solutions.

7.2 Decision Space

Similar to the objective space, there are measurements in the decision space to find interesting solutions or promising regions during the optimisation [EBN05]. In our approach, we determined κ_{dec} clusters of paths using a data-structure specific metric. Moreover, we determined the optimal number of clusters using the silhouette coefficient, the Dunn index and the Davies-Bouldin index (see Section 2.8.2).

7.2.1 Clustering

To classify each path in a set of paths into a cluster, we used agglomerative clustering with complete linkage.

The goal was to assign a label $l_j^{\mathscr{S}}$ to each path $p \in P$. A label set is $\mathfrak{L}^{\mathscr{S}} = \{l_1^{\mathscr{S}}, \cdots, l_n^{\mathscr{S}}\}$, where $l_i^{\mathscr{S}} \in \{1, \cdots, \kappa\}$. We define a label $l_j^{\mathscr{S}}$ as a set of paths belonging to label j of the labels obtained by a cluster algorithm in space $\mathscr{S} \in \{obj, dec\}$; that is,

$$l_j^{\mathscr{S}} = \left\{ p_i \mid p_i \in P \wedge cl(\mathscr{S}, P, p_i) = l_j^{\mathscr{S}} \right\} \tag{7.1}$$

.

The function $cl(\cdot,\cdot,\cdot)$ assigns a label to a path by analysing the solutions in the respective space, hence $cl : P \to \mathfrak{L}^{\mathscr{S}}$.

7.2.2 Finding Representatives

After we computed the cluster set, we determined a certain representative of each cluster, which is used in the evaluation of the clustering and in the result that is presented to a DM, i.e., interesting solutions. For each cluster, we defined a representative path. We decided to use the medoid of each cluster, which is defined as the data point that has the minimum sum of distances to all other data points in its respective cluster [SHR96]. Mathematically the medoid is defined as:

$$x_{\text{medoid}} = \arg\min_{y \in \mathscr{X}} \sum_{i=1}^{n} d(y, x_i) \tag{7.2}$$

For the distance function d, we again used δ_{DM}. In the following section, we define a function $medoid(P, \delta_{DM})$, which determines the medoid of the given path set P using a path similarity function δ_{DM}.

7.2.3 Obtaining an Adequate κ

To obtain a suitable number of clusters κ, we used the three cluster evaluation metrics presented in Section 2.8.2.

The distance function $d(i,j)$ between data points (cf. Equation (2.19)) was implemented using the discrete Fréchet δ_{dF}, Hausdorff δ_{Hd} and DTW δ_{dtw} distance functions. We needed to compute the distances between data points that were now paths.

Regarding the Davies-Bouldin index, instead of the centroid of cluster, we used the medoid, since a centroid can naturally not be defined on a set of paths. Furthermore, in Equations (2.25) and (2.26) we use different values for q and employ each path distance measurement as a replacement for the Minkowski distance of the medoids. Therefore, we can omit assigning a value to p. The distance metric used in the dispersion measure – or how scattered a single cluster is – should match the distance between clusters. Using a path similarity metric in each of the equations is, therefore, a consistent approach. Furthermore, when computing the Dunn index, for δ we again used the path distance metrics (δ_{DM}) to determine the distance between medoids. However, for Δ, we used the maximum distance of two paths in a cluster. It is computed as $\Delta_i = \max_{x,y \in C_i} d(x,y)$.

7.3 Combining Spaces

We propose incorporating certain metrics from the objective space and others from the decision space using two different approaches. The first involves finding sets of paths with special characteristics, whereas the second is a two-step process resulting in a single set of interesting solutions.

7.3.1 Alternative and Robust Routes

In pathfinding, and especially in route planning on road networks, it can be of interest if there are alternative routes available that result in similar objective values but are expressed as a different set of roads to traverse. Furthermore, one can be interested in other routes that also have similar objectives and are close to each other. We propose two methodologies, based on clustering and set theory, to determine such route sets. It should be noted that we do not define threshold distances of paths in both spaces (objective and decision space) as some form of $\delta_{DM}(p_i,p_j) < \varepsilon_{obj}$ or $\left|\vec{f}(p_i) - \vec{f}(p_j)\right| < \varepsilon_{dec}$ but adjust such distances by choosing a different number of clusters, i.e., κ_{obj} in the objective space and κ_{dec} in the decision space. The median cluster size changes proportionally by increasing or decreasing the space-respective κ.

Robust Routes

To find a robust set of paths or routes, we first define the term '*robust*' with respect to pathfinding. A robust set of routes $P_{robust} \subseteq P$ contains paths that are similar in their objective values while also being similar (i.e., close) to each other in the decision space. Formalised, it is an intersection of clusters. Computing such a set involves a cluster analysis in the two spaces and determining intersections of the two cluster types. After clustering the set of paths, we obtain two label sets that contain the labels for the cluster analysis in

the objective space $\mathfrak{L}^{obj} = \left\{ l_1^{obj}, \cdots, l_{n_{obj}}^{obj} \right\}$, and the label set for the decision space $\mathfrak{L}^{dec} = \left\{ l_1^{dec}, \cdots, l_{n_{dec}}^{dec} \right\}$. After obtaining the two sets, we can identify all intersections between the labels.

Let $\mathscr{L}$ be the cartesian product of $\mathfrak{L}^{obj}$ and $\mathfrak{L}^{dec}$, that is, $\mathscr{L} = \mathfrak{L}^{obj} \times \mathfrak{L}^{dec}$. Each element in $\mathscr{L}$ is therefore a pair of labels, such as $\left(l_1^{obj}, l_2^{dec} \right)$, which are also sets of paths (see Equation (7.1)). We thus define the set of all robust path sets as the set of all pairwise intersections, which is the set of all $\bigcap U_i$, where $U_i \in \mathscr{L}$:

$$\mathscr{P}_{robust} = \left\{ \bigcap U_i \mid U_i \in \mathscr{L} \right\} \tag{7.3}$$

$$\bigcap U_i := \bigcap_{a \in U_i} a = \{ x \mid \forall a \in U_i : x \in a \} \tag{7.4}$$

Finally, an arbitrary robust set of paths is $P_{robust} \in \mathscr{P}_{robust}$.

Alternative Routes

A set of alternative routes contains routes that are similar in the objective space but distant in the decision space. We define such a set as analogous to a robust set of paths. Again, we perform the cluster analysis in both spaces, namely the objective space and the decision space. We then compute the intersections, as we did in the robust path finding, and can find for a path p_i in the intersection set another path in the corresponding objective cluster that is not in the intersection set. This pair of paths is similar in terms of their objective values but distant in the decision space. We can define a set of alternative paths as follows:

For each $U_{l_i^{obj}, l_j^{dec}} = (l_i^{obj}, l_j^{dec}) \in \mathscr{L}$, we determine the intersection set $\bigcap U_{l_i^{obj}, l_j^{dec}}$. The set of pairs of alternative paths is then defined as:

$$\mathscr{P}_{alternative} = \left\{ (p_i, p_j) \mid p_i \in \bigcap U_{l_i^{obj}, l_j^{dec}}, p_j \in l_i^{obj} \wedge p_j \ni \bigcap U_{l_i^{obj}, l_j^{dec}} \right\} \tag{7.5}$$

7.3.2 Obtaining Interesting Solutions

In the first approach to obtain interesting solutions, the methods described above for reducing the number of solutions are combined to identify interesting and unique solutions. We propose to determine an approximation of the non-dominated solution set by using either ε or cone-dominance, which is $P_{DC}^* \subseteq P^*$, where DC is either ε or α, representing the respective dominance criteria (DC). We then apply the cluster analysis in the decision space on P_{DC}^* to obtain a set of labels $\mathfrak{L}^{dec}$, assigning a label to each path $p_i \in P_{DC}^*$.

As a second methodology, we propose using all sets of robust solutions and computing the medoid of each. Therefore, an interesting set of solutions can be defined as:

$$P_{interesting} = \{ p_i \mid p_i = medoid(P_{robust}), P_{robust} \in \mathscr{P}_{robust} \} \tag{7.6}$$

7.4 Decision Points

The term *decision points (DPs)* is used in various contexts. For instance, [LR18] is an article about century-long flood risk management in England. DPs are used

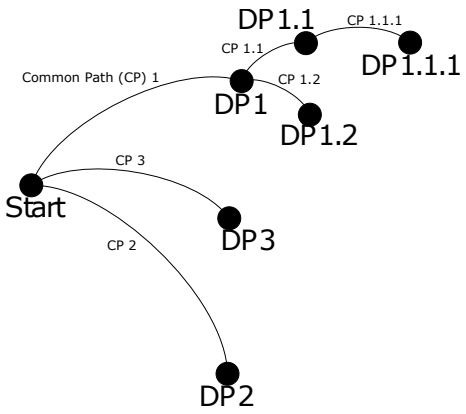

Figure 7.1: Decision Points as a graph representation

as points in time when a specific decision is due, in this case, deciding what measurements should be implemented to lower the flood risk. Such points can be highly dynamic, as the prediction of certain indicators may change. Furthermore, the placements depend on numerous variables, e.g., time to implement a certain measurement or predicted values. In indoor route guidance, DPs are points of action, e.g., change of level or change of directions [DCOVdW+21]. The authors presented a study on the complexity perception of such points when persons are navigating indoor. Numerous DPs in the criminal justice system experience involve some small degree of racial bias. These biases can accumulate over time and negatively impact defendants of colour. The DPs in this domain are, for instance, stopping of a car, search of a suspect or arrest. At each of these points, which form a path in the justice system, biases can occur [Chi16].

Whereas the above examples include fixed DPs, in [OBM] sporadic DPs were addressed. In that study, DPs in lectures were identified, where a different course of action could be taken. The concept of DPs was also used in product development in the pharmaceutical industry [MLFPEAP+11].

Although the specific definitions of DPs in these works differ, they share a commonality: DPs occur on paths. Examples include navigating through flood risk management, where DPs are dynamic in time within a certain range, dependent on other factors and have different result paths; indoor navigation, where DPs are spatially fixed, time-independent and have fixed result path; navigating through the criminal justice system, where DPs are process fixed, have different result paths, and can result in possibly severe outcomes for humans; changing the course of a lecture, where DPs are sporadically occurring and have different result paths; or managing product development, where DPs have different result paths. Hence, the timing (i.e., when an algorithm or a DM should place a DP) is of interest in these scenarios and use cases.

In route planning, that is addressed in this thesis, a DP can be defined as the last common point of sub-sequences of multiple solutions where the next point in each solution is different. With this method, a decision graph can be spanned. Figure 7.1 shows part of such a graph, where each node represents DPs. Note that all other points that define a path have been omitted in the representation and merged into the edges connecting the points (common paths). Furthermore, the result is usually not a tree, as all alternatives can conclude at the same endpoint.

After obtaining a set of non-dominated solutions from an optimisation algorithm, a DM has to choose between several solutions. It can happen that two or more DMs are involved in the process. There are several techniques which can be

applied during such a group decision-making process to evaluate the fairness and several other metrics of a set of solutions [MS99]. However, another case occurs if this process needs to happen while the plan — i.e., the path — is executed or traversed. Here, so-called DPs can be defined or identified on which a new set of solutions is generated and evaluated.

On each DP, the DM has to choose the next sub-alternative route. Naturally, the cardinality of this subset is often much smaller than the complete set of non-dominated solutions. The method reduces the number of paths that are considered at a decision process, as the DM only needs to take the next subset into account. This can improve the performance and speed of a decision where multiple DMs are involved.

Decision points can furthermore be used with other optimisation techniques, such as *rolling horizon evolutionary optimisation* [PSLR13]. With this approach, a sub-route can be generated in a shorter time and evolved as it is traversed. This can be beneficial for long-distance routes with many objectives, where the computational effort is high. Generally, the concept can be applied a priori and a posteriori, i.e., to identify the points either during the optimisation or afterwards. Moreover, an interactive methodology may be possible, e.g., a DM that specifies points where a decision should be made.

In the remaining course of the thesis, the concept of DPs is not pursued in-depth and should be analysed thoroughly in future research. In this chapter, we propose an a posteriori approach to determine DP on a set of routes.

7.5 Evaluation on Large Road Networks

In this section, we evaluate the proposed decision support methodologies. Such an evaluation is not trivial, as the *goodness* of a presented solution set can be highly subjective due to the DM's experience or other factors.

To evaluate our approaches, we use the European Road Network which consists of approximately 6.25×10^8 nodes. After small subnetworks and non-intersection nodes were removed because they would not be used for our routing purpose, the final graph consisted of 1.14×10^8 nodes and 1.46×10^8 edges. It should be noted that an intersection is often represented by several nodes to take different turning constraints into account when using data from OSM. In other chapters, such as Chapter 4, we have simplified the network to one node per intersection. We used the GraphHopper[5] library to employ the already implemented data-handling methodologies for large graphs. In addition, we used single-objective shortest path algorithms in several parts of our methodologies, e.g., to connect random points during the initial solution generation, or to connect points using the crossover and mutation operator. For these parts, we also used the GraphHopper library's *contraction hierarchies* speed-up technique. Finally, due to the generalised definition of the MaOPF, we implemented our algorithms using Java to work with the library.

According to a report by the European Court of Auditors, there are several major routes for trucks transporting goods across Europe. We evaluate one of the most used routes in the European Union, i.e., Madrid to Warsaw [oA20]. The linear distance between these two cities is approximately 2290 km. In Figure 7.2, we show in black the shortest distance (spheric distance) between the cities; the

5. https://www.graphhopper.org

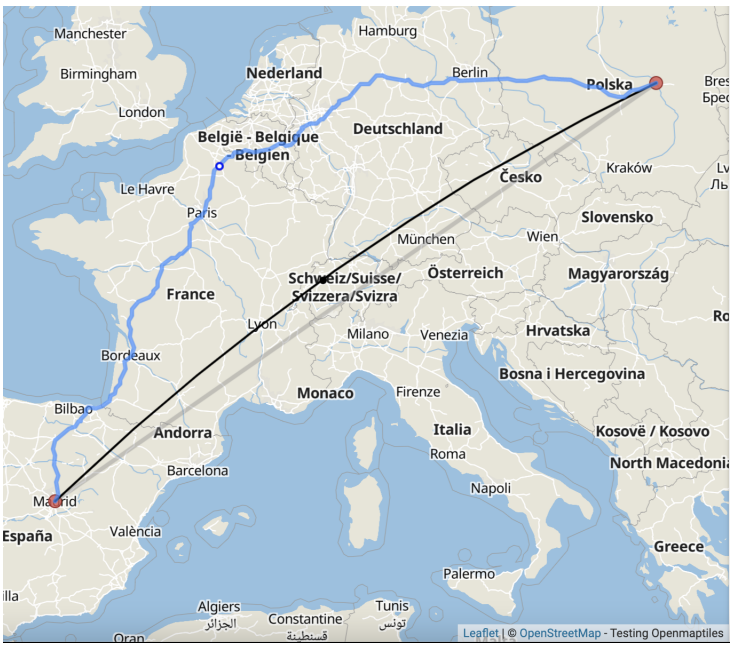

Figure 7.2: Distances from Warsaw, Poland to Madrid, Spain. Linear dist.: 2290 km, *fastest car route (GPS system):* 2858 km

straight line distance is shown in grey. Due to the projection of the map, the grey line looks shorter, but ultimately it is longer when seen on a globe. In blue, the fastest route for car navigation is shown, which is approximately 2858 km long, when using an automotive navigation system.

7.5.1 General experimental settings

We combine here several methodologies that have already been proposed in this thesis. We use a variable-length chromosome representation, where each gene relates to a node in the problem graph. For the initial solution generation, we use RPC. Moreover, to increase the solution set diversity in the decision space, we use the proposed curve ordering technique with contraction points by utilising the Fréchet similarity measurement. Finally, after obtaining the final set of non-dominated solutions, we employ the proposed decision support techniques described in this chapter. This includes computing knee-points using different angles and identifying interesting or alternative routes through the clustering technique.

Other parameters were set with the same settings as in previous experiments. However, population size μ and number of generations were both set to 100 as we assumed a small computational budget. Moreover, to resemble a real-world perspective, we ran the algorithm only once instead of 31 times. With these settings, we consider that our algorithm may be executed on a mobile device in the future.

After all function evaluations (10000) were exhausted, we obtained 69 non-dominated solutions. For this scenario, we did not have information about the true Pareto-front and set. In Figure 7.3 all obtained non-dominated solutions are shown. From a visual perspective, it is already evident that several paths overlap. One can assume that the visible major paths are the most important and interesting routes. Nevertheless, using our methodologies we aimed to identify such routes from the set of non-dominated solutions, as an analysis relying solely on the visual aspects may not be sufficient and is not practicable.

We used the proposed methodologies to filter the solution set to obtain an interesting subset according to different criteria. We employed cone-dominance

Figure 7.3: Non-dominated solutions

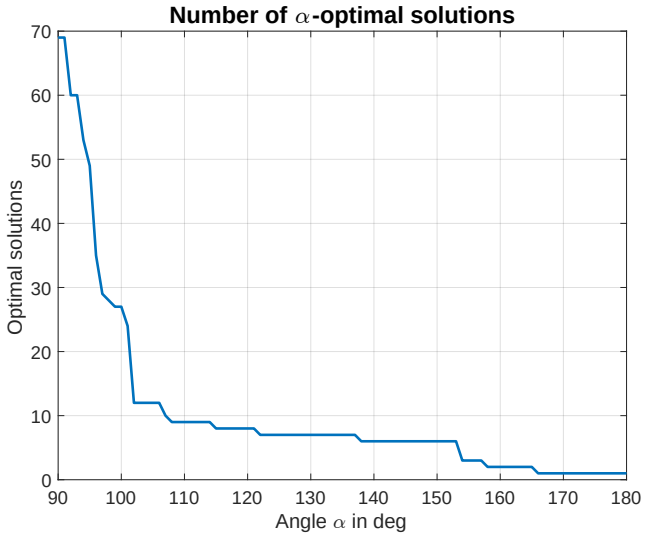

Figure 7.4: Number of non-dominated knee-points over α.

to identify knee-points in the obtained front, and afterwards applied the proposed cluster techniques to identify robust route sets and sets of alternative routes (see Section 7.3.2).

7.5.2 Analysis

Cone-dominance

Figure 7.4 shows the number of non-dominated solutions using different values for the angle α. Figure 7.5 shows the path set for $\alpha = 102°$, as the number of α-non-dominated solutions decreased only marginally after this value. After computing the solutions that were non-dominated using $\alpha = 102°$, we obtained 12 solutions. Assessing the results visually, we concluded that one of the major routes via Lyon was classified as dominated by the others. This approach is, from a computational effort perspective, the one with the least effort, as computing the set requires only matrix operations.

Figure 7.5: Paths for $\alpha = 102$ °.

Representative Identification

One approach to narrow down the set of solutions to a set containing interesting solutions is to cluster the initial set and identify the cluster's medoids. A medoid serves as a representative of a cluster, as the medoid's sum of distances to all other objects inside the cluster is minimal [SHR96].

Using this methodology, a DM can obtain an overview of the distribution of the solutions in each space. The DM can then make an informed decision that can guide further analysis. For instance, in interactive MOO, the DM is required to lead the optimisation in a direction that is most promising or interesting, in their expert opinion. It should be noted that the obtained clusterisation is not reflected in the respective other space and that solutions in a cluster in one space may not be in the same cluster in the other space.

Figure 7.6 shows the obtained medoids following the decision space clustering. It is clearly visible – and was expected – they are well distributed on the map. However, as evident in the lower image of the figure, the distribution in the objective space is suboptimal, not covering a wide range of it. A DM may gain a false impression by analysing only the path's expression on the map.

If we take the clusterisation obtained in the objective space, the medoid computation results in the configuration depicted in Figure 7.7. In this case, the pattern is the opposite, namely, a well distributed set in the objective space, but close solutions on the map of Europe. Therefore, we conclude that a DM must not only take the information of one space into account but should always be presented with information about both spaces.

Robust and alternative routes

As shown in Section 7.3.1, the next step was to perform various cluster analysis techniques to find sets of routes that were either robust or resulted in alternative routes. Since for both approaches the first step of clustering is the same, we present and discuss the results first and then discuss the specific results for each approach.

Figure 7.6: Medoids obtained from decision space clustering.

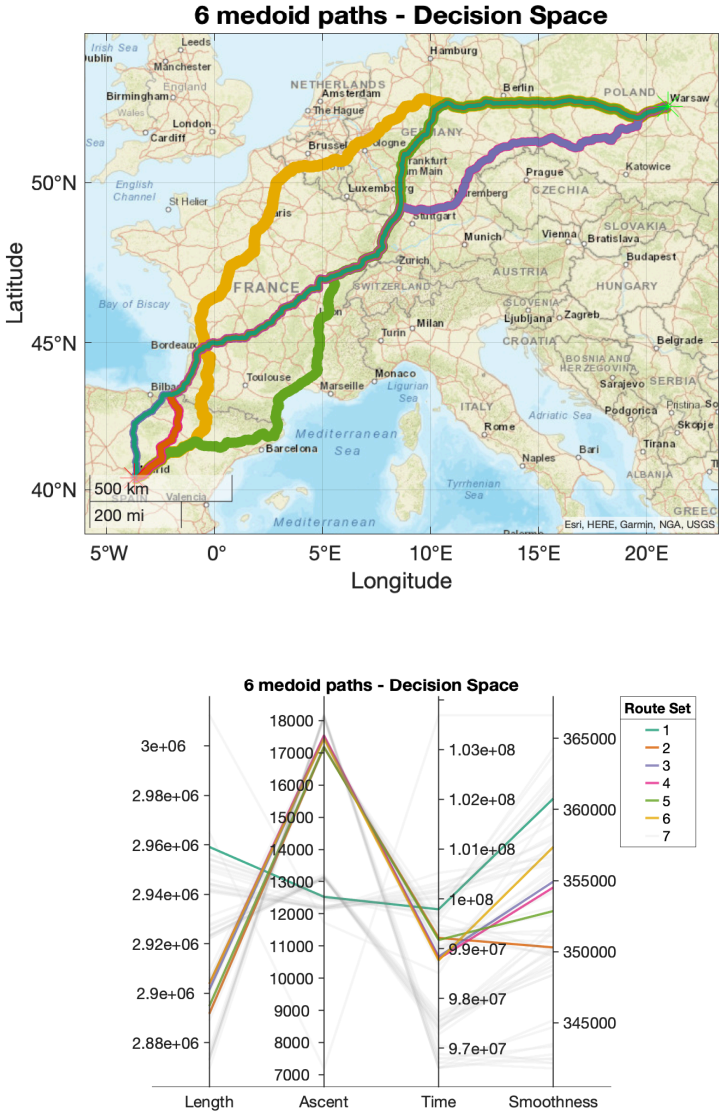

In our analysis, we use *complete linkage*, as this approach tends to result in smaller clusters, whereas *single linkage* tends to result in chaining. To obtain the optimal number of clusters in each space, we use the silhoutte coefficient. For the decision space, we obtained $\kappa_{dec} = 6$ as the optimal number of clusterswhereas we obtained $\kappa_{obj} = 3$ for the objective space. In the later analysis, we discovered that using this number resulted in very large cluster intersection. Therefore, we manually set it to $\kappa_{obj} = 7$, which yielded better results. It should also be noted that during the cluster analysis, we simplified the routes by again employing the RDPA. We set $\varepsilon_{\text{RDPA}}$ to a value for which the routes were still unique. Figure 7.8 illustrates the obtained clusters in the decision space, i.e., the map of Europe. Each cluster is assigned with a colour. In the lower figure, the corresponding objective values are shown. It is evident that the decision space clustering resulted in a fragmented objective space dataset, i.e., the clusterisation could not be transferred to the other space.

When performing the same analysis in the objective space, the results differed. In Figure 7.9, on the upper panel, the paths are shown on the map clustered according to the objective space. The lower image again shows the same paths in the objective space, with the same colour coding.

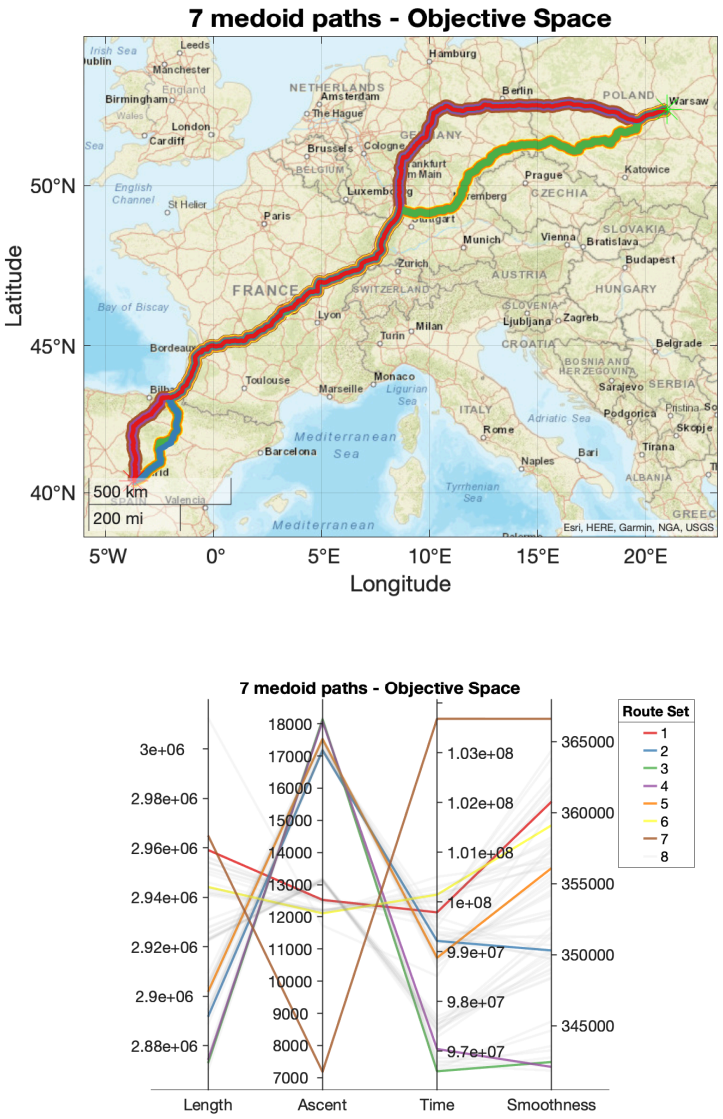

Figure 7.7: Medoids obtained from objective space clustering.

After computing the clusters in both spaces, we applied the proposed techniques for route identification.

Robust Routes To obtain a set of robust paths, we employed the intersection methodology proposed in Section 7.3.1. This resulted in 18 sets of paths with a cardinality of 2 or higher. Other intersections resulting in 1 or zero paths were filtered out, as such sets do not provide evasion routes. In Figure 7.10, three such sets are shown. The lower panel of the figure shows the three clusters in the objective space. Here, the three sets are different in each objective; however, the red and green sets are close in the actual expression as a path on the map. On the map, the difference is barely visible.

The intersection set with the largest cardinality is depicted in Figure 7.11. The paths are largely overlapping when analysed visually. However, as illustrated in the lower panel, the difference is evident in several single spots. For instance, in the area of Vichy, France, the routes do not overlap and result in unique expressions.

As a result, a potential driver may choose one of these clusters. The driver can follow any path of the cluster, knowing that it will result in similar objective

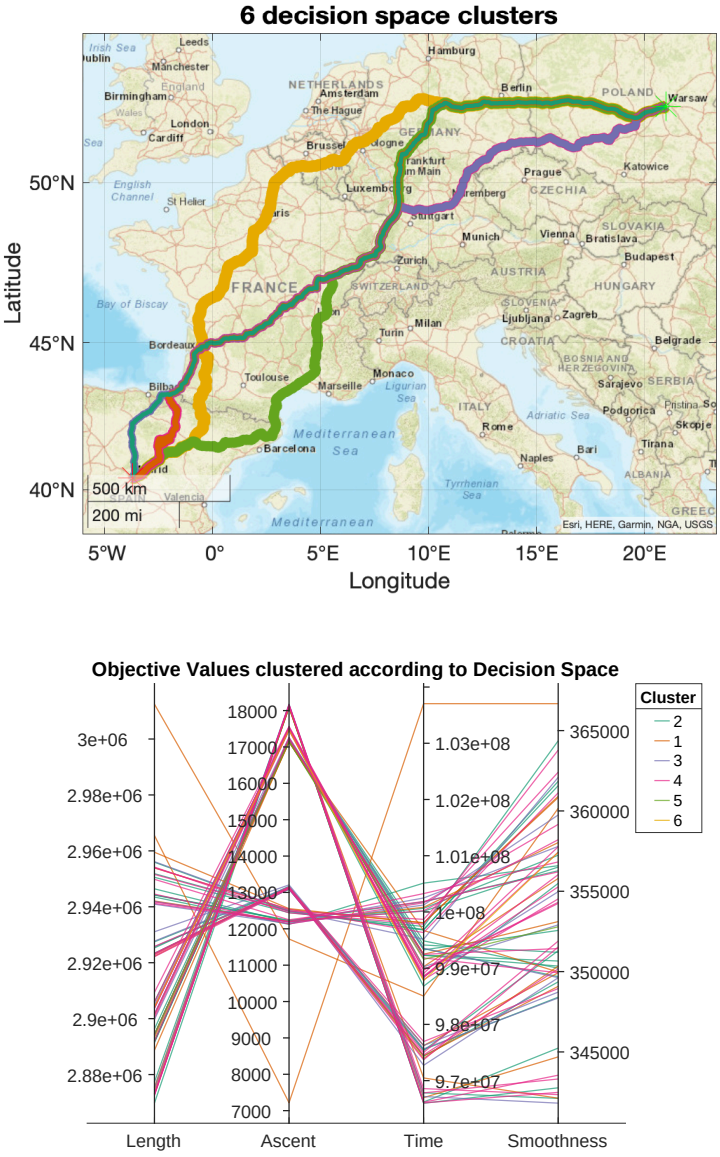

Figure 7.8: Clustered paths according to decision space clustering.

values. Nevertheless, the driver has more freedom in the actual traversal. Using such a set means having the option taking a slightly different route, while not deviating too much from the original route.

Alternative Routes For the alternative route identification, we applied the methodology proposed in Section 7.3.1. However, as this is a generalised approach, we introduced several additional process steps to narrow down the final solution set. After identifying the cluster intersections, we obtained sets of solutions that were contained in a cluster in both spaces. A starting route served as the baseline to identify alternative routes. We applied cone-dominance to the set and identified the solution that remained when using $\alpha = 180°$; this was the starting route. Then, we obtained n routes with the smallest distance according to the objective values in the corresponding objective cluster from which the baseline solution originated. In our case study, we chose $n = 2$, resulting in three routes (baseline+n).

Figure 7.12 shows two examples. Each route is assigned a different colour. The routes have different expressions but similar objective values.

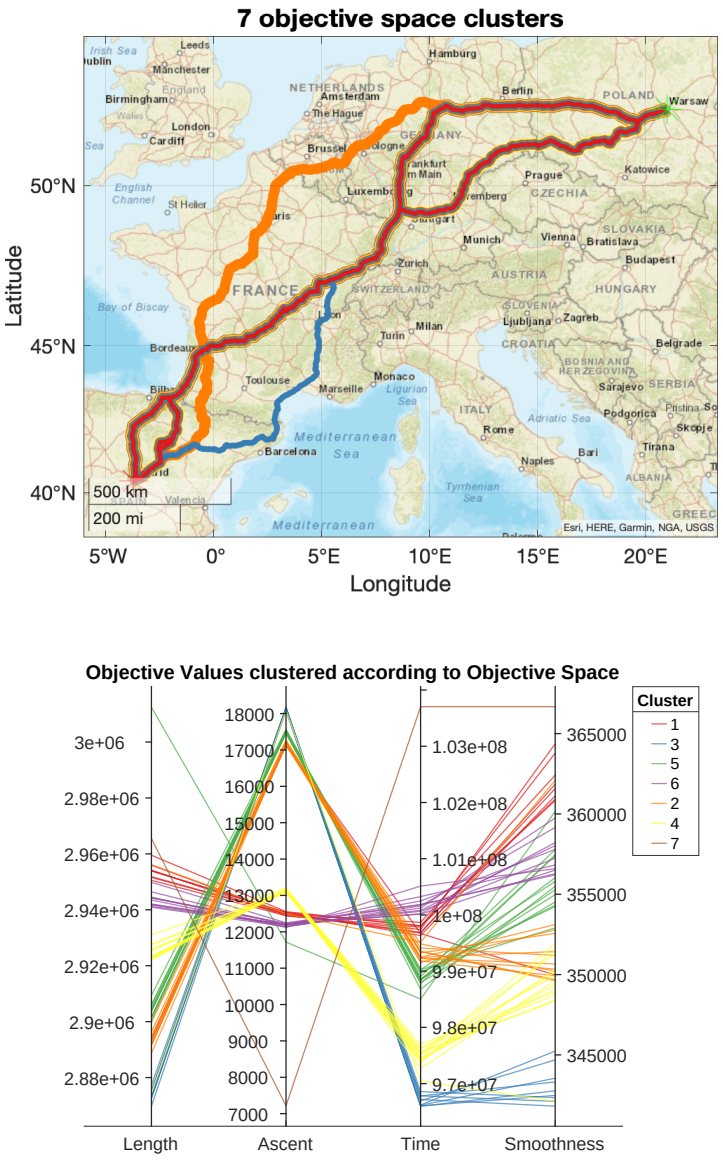

Figure 7.9: Clustered paths according to objective space clustering.

In Figure 7.13, the corresponding objective values are visible in the context of all other solutions. The figure also shows a third set that we do not present in the decision space. Each colour refers to a set of routes. Route set 1 refers to the upper image in Figure 7.12, whereas set 2 refers to the bottom image. Set 3 is a set that is not shown in the decision space, and set 4 refers to all other routes in the solution set. It is evident that each route is close to the others within the set. From a visual analysis it is apparent that several parts of the objective space are not covered by the set, because we chose to display only three sets. However, another problem arises here. It is not trivial which sets should be displayed to a DM. Interactive optimisation can be beneficial for such problems. It should be noted that the colours we used to represent the different paths on the maps (Figure 7.12) are independent of those used in the objective space diagram (Figure 7.13). On the map, the colours are used to distinguish the individual paths.

Sets of alternative routes are an example of *DPs*. It is evident that the respective routes share several points and differ greatly in other areas. The points where routes diverge can be seen as DPs. A driver has to decide which expression, or route, to take. In our case, the alternatives overlap again at a later point. With

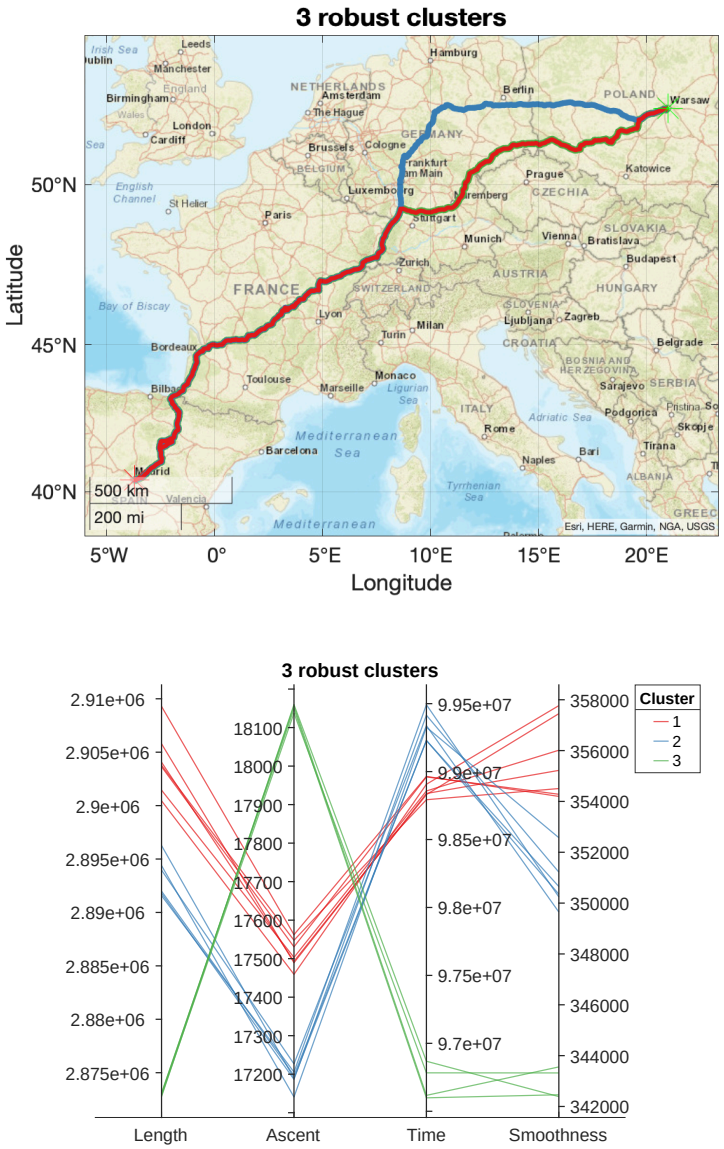

Figure 7.10: Three obtained robust clusters.

expert knowledge, an informed decision can be made when executing a certain route.

7.5.3 Discussion

The proposed approaches of solution set reduction are largely an underestimation of the problem under study. The first reason for this is that the true Pareto-front is unknown as the search space is too large and computing it takes too long. This is the case when trying to reach the global optimal solution using a heuristic approach, as most optimisation problems do. Second, particularly for routes on street networks, there can be a vast number of constraints that, in practice, a human being would consider in their reasoning. It would be of value to incorporate them a priori into the optimisation to narrow down the search space using the available computational budget better. Performing an expert interview with a human participant may give additional insights regarding the problem and would enable empirical evaluation of the underlying assumption of this study.

The proposed methodologies can be combined. For instance, after a robust set of routes is identified, its medoid can be computed and used as a baseline solution.

Figure 7.11: The largest robust cluster and a detail view of differences.

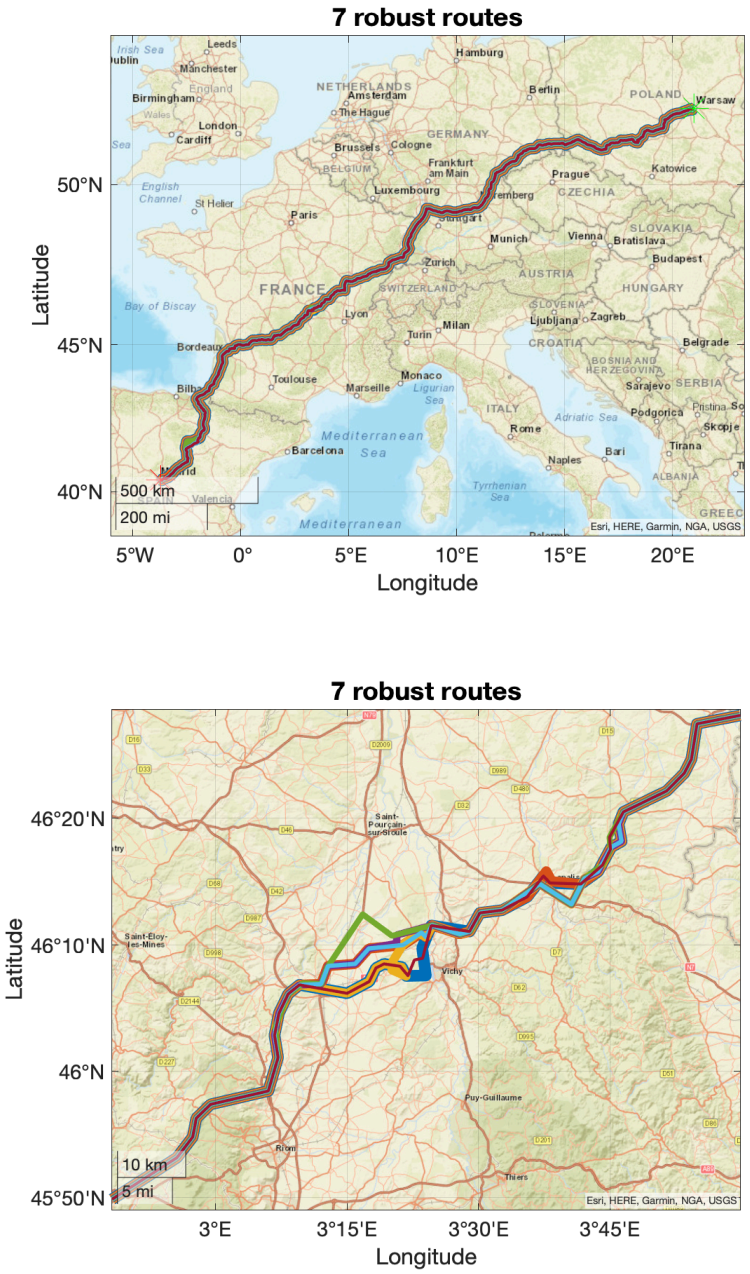

Since the medoid has the least sum of distances to every other solution in the set, it can be considered the route from which all other routes can be reached using the least effort. However, a large similarity between two paths does not necessarily result in a small distance or low time taken to change from one route to the other. Parallel streets can be highly similar; nevertheless, in reality, there may be only a few possibilities to change between the two objects.

7.6 Summary

In this chapter, we have proposed methodologies that can help a DM in selecting a route that accommodates specific requirements, based on the user's preferences. We have explored all of our approaches within the context of both objective space and decision space. This is important, as the solutions to these spaces can provide conflicting information. Our discussed approaches result in

Figure 7.12: Two examples of sets of alternative routes. Each set contains three routes.

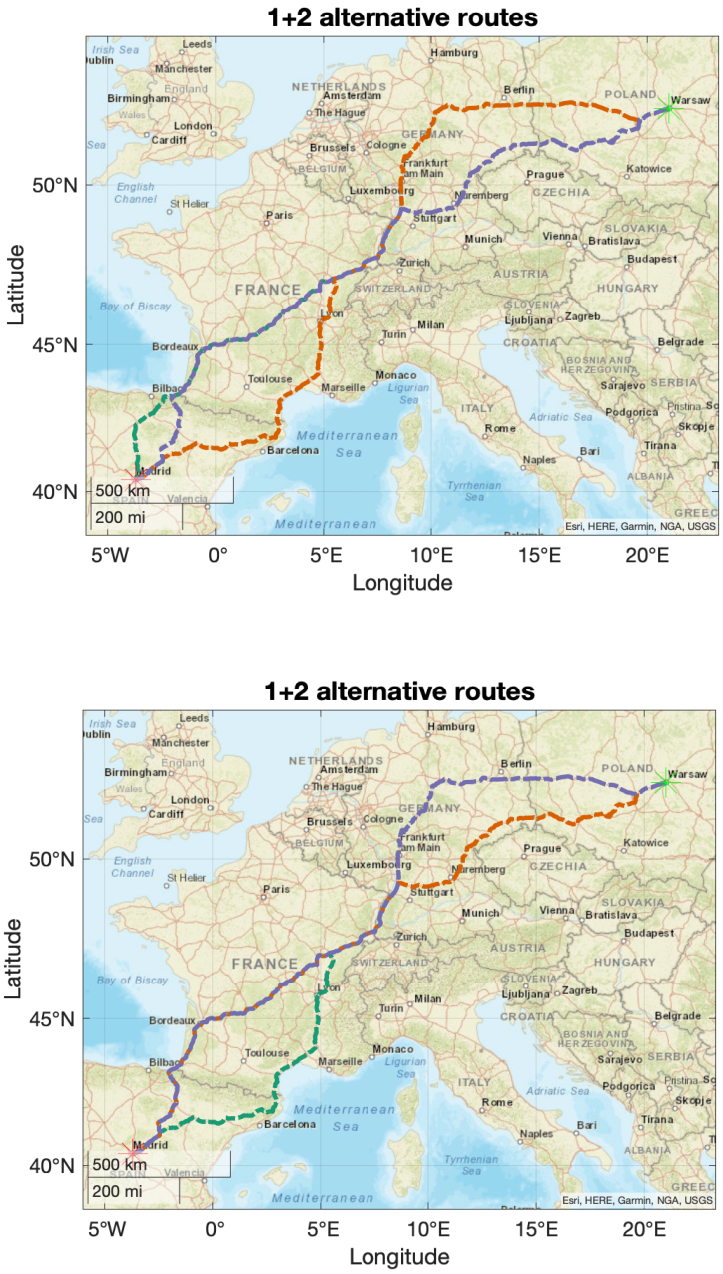

different route suggestions. However, evaluating them is not trivial and must be performed in the future, in an in-depth analysis that considers the actual requirements of real DMs.

Figure 7.13: Found sets in the context of the complete solution set.

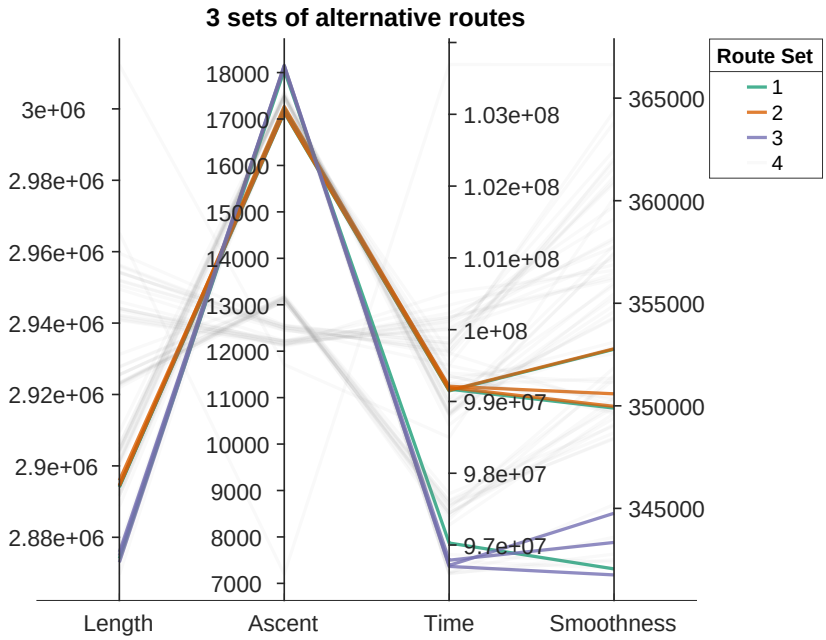

8 Conclusion and Future Work

In this chapter, we conclude this thesis and present a framework that functions as a decision support for arbitrary pathfinding problems. We then give an overview of topics for future research in the field of multi- and many-objective pathfinding.

8.1 Conclusion

In this thesis, we have proposed the graph-based many-objective pathfinding problem, which can be used to model real existing problems. First, we analysed the related work; second, we proposed a benchmark suite that can generate various problem instances. Third, we have illustrated various problem representations that EAs can handle and have analysed their differences in performance, quality and other metrics. In another chapter, we proposed several techniques to diversify the population in the decision and objective spaces, since the many-objective pathfinding problem can be deceptive. Additionally, we have proposed various techniques to support DMs by decreasing the number of presented solutions using methodologies from clustering. In the following sections, we discuss the research questions that were formulated at the start of this study:

RQ 1 Which techniques exist to solve the MaOPF?

- RQ 1.1 Which environmental classes are used and how do they differ?
- RQ 1.2 Which state-of-the-art algorithms are used in the respective environments?
- RQ 1.3 Can single-objective speed-up techniques be used to support a multi-objective approach?

In Chapter 3, we analysed the related work covering several techniques and approaches to various pathfinding problems with a range of environments. We pointed out that exact approaches, due to the NP-hardness of the problem, are usually applied on relatively small environments with few objective functions. However, there are interesting speed-up techniques for single-objective pathfinding problems and their exact solution approaches. For instance, *contraction hierarchies* is a technique for precomputing shortcuts upfront to greatly decrease

the query time. Such approaches can be also used during the meta-heuristic MOO in several phases, as we have shown. In the state of the art, various environments have been proposed which consist of different properties and, sometimes, non-linear constraints. Often, the algorithms were tailored to a specific environment and are not generally applicable in other settings. In the articles we reviewed , other approaches – such as particle swarm optimisation, ant colony optimisation, EAs and q-learning – have been proposed and evaluated.

RQ 2 Is there a significant difference between using problem and solution tailored representations rather than standard encodings?

In Chapter 5, we assessed different encoding schemes for the multi-objective pathfinding problem. We evaluated fixed-length and variable-length representation schemes using our proposed benchmark suite. On smaller problem instances, the fixed-length approach was superior, but its performance deteriorated as the instances became larger. By contrast, the variable-length approach maintained a certain quality level. From this experiment, we concluded that in most cases, a more natural encoding, i.e., variable-length, is suitable for such problems. Considering only fixed-length approaches, we evaluated real-valued and binary encodings. We found that the latter outperformed the former.

The larger the instances, the more problems and challenges occurred in any encoding scheme that could be tackled using techniques from large-scale optimisation. As the true Pareto-front is unknown for such large problems, it is difficult to assess the absolute performance of an algorithm. Although the results seem reasonably sound, they might be far from the global optimum. A way to circumvent this restriction is to compute the true fronts and sets using an exact approach, which would involve a large computational budget.

RQ 3 How should a scalable and variable benchmark test problem be designed to cover a wide variety of pathfinding problems?

RQ 3.1 Which real-world related objectives should be considered in the test problems?

In Chapter 4, we proposed a benchmark suite that enables researchers to create different pathfinding problem environments. Furthermore, we presented objective functions that can be used with such environments. The suite's environments can be populated with different constraining properties, such as obstacles in different variations, neighbourhood relations or elevation profiles. These characteristics can also be found in other related works and resemble real-world pathfinding problems to a certain extent. The properties and settings can also be mapped to pathfinding problems from other domains. Our proposed objective functions are a suggestion. Nevertheless, other objective functions can be used with the same environment.

We also analysed several large maps of the benchmark and found that the optimal values of the *ascent* objective converged towards 0. The reason was that with larger instances more possibilities arise containing almost flat neighbours. While this finding may seem interesting from an optimisation approach, it impacts actual implementations of the benchmark. Such small floating-point values can be an issue, depending on the programming language, and may result in inaccuracies. Comparing different algorithms can be difficult in light of this issue. Solutions are either to accept this inaccuracy or to scale the value to an

integer by multiplication with a factor. Other approaches include specialised techniques to cope with such small numbers.

We have shown how a variable and scalable benchmark can be defined and have assessed the environments as well as the objective functions. Furthermore, we applied them on real-world data.

RQ 4 How can the geometrical properties of a path be assessed?

RQ 4.1 How can differences from other paths be measured?

RQ 5 How can these properties be exploited for the optimisation process?

RQ 6 Can such properties be used to increase the diversity of the resulting solution set?

In one of our studies, we explained that diversification techniques that are applied in the objective space can be detrimental during optimisation. Pathfinding problem often have the characteristic of close solutions in the decision space being far from each other in the objective space, and vice versa. Therefore, emphasising isolated solutions and unexplored objective space areas can lead to a non-diverse set of solutions in the decision space. However, a DM is often interested in such a set. To overcome this issue, in Chapter 6 we proposed utilising path similarity measurements. The geometrical properties of paths are incorporated in the selection process of the EA. Specifically, we measured the similarities (or differences) between paths by computing their respective Fréchet distances. Furthermore, we evaluated alternative measurements, such as the Hausdorff distance or DTW. Each of these possibilities poses specific advantages and disadvantages regarding the accuracy or computational effort. In a first approach, a stochastic measurement of tendency in a set of paths was computed, and the path with the highest value (the most isolated path) was determined as the selection candidate. As this method needed in a large computational budget, we then proposed a technique to determine neighbourhood relations in a path set. We suggest contracting each path to a single representative point and measuring the signed distance to the beeline that connects the common first and last point of each path. Our proposed approaches reduced the computational effort and increased the quality of the solution set. Furthermore, the resulting solution set had an increased diversity, which can be beneficial for a DM's decision.

RQ 7 What performance indicator (PI) can be used to evaluate the algorithm's performance?

In this thesis, in most cases we have employed well-known state-of-the-art performance indicators, such as IGD^+, IGD, IGDX and hypervolume. The IGD^+ was used in most studies, as the computation of the hypervolume results in large computation times when using many objectives. However, we are aware that IGD^+ is only weakly Pareto-compliant. In addition to the standard indicators that are obtained in the objective space, we used IGD's counterpart in the decision space, i.e., IGDX. As the distance function, we utilised the path similarity measurement that was proposed in Chapter 6, specifically the Fréchet distance. However, a major drawback is that the δ_F of two paths can be equal to another pair of paths, although they are different from a visual perspective. Using DTW can solve this issue but can also require a larger computational effort.

RQ 8 How to reduce the number of solutions that are presented to a decision-maker?

In Chapter 7, we proposed several approaches to narrow down a result set of an algorithm to the most interesting solutions that can be presented to a DM. Such techniques are necessary because a many-objective pathfinding problem can result in many non-dominated solutions, which is barely comprehensible for a DM. Again, we employed similarity measurements. We discussed a technique using clustering to determine robust solution sets as well as sets of alternative solutions. To compute such sets, we also incorporated information from the objective space where we had applied clustering techniques. Intersecting the resulting clusters resulted in the respective sets. In addition, we suggested using cone-dominance as an alternative dominance criterion to decrease the cardinality of the solution set. We tested our approaches on real-world data, including determining a set of non-dominated solution paths from Warsaw to Madrid, which is one of the major truck roads in Europe. Four objectives were minimised and only one run was conducted to resemble an optimisation task that may occur in this setting in an actual company. From the result set, we could determine several sets of alternative solutions as well as robust solution sets. Furthermore, the former were an example of decision points, i.e., points where an alternative solution can be chosen. Finally, we represented each subset using the respective medoid that was computed with the proposed path similarity measurement. These representatives can be presented to a DM.

In summary, we generated techniques and approaches to increase the performance of EAs applied to the multi-objective pathfinding problem. These methodologies can be used in other approaches too and are dedicated to a specific aspect of the underlying problem. However, a drawback of this thesis is that it lacks a comparison with existing pathfinding approaches. There were two reasons for this lack. As outlined in Chapter 3, in most cases it was not trivial to reimplement the approaches or recreate the environments used. Furthermore, comparing approaches across programming languages is not trivial. With the proposed benchmark, we created a baseline problem set with well-defined environment characteristics and objective functions. We want to encourage the research community to use it.

Another perspective that was covered only in part is the constraint handling. In reality, several problems are highly constrained and special techniques must be used. In Chapter 5, we implemented a trivial approach of constraint handling by penalising solutions that were outside the desired domain. Although that is a working approach, more sophisticated methodologies are missing from this thesis. In most of our other studies, we decreased the search space by omitting such nodes that are inaccessible. In reality, this information can be hidden or accessed only if the respective node is traversed. In our studies, neglecting such areas can be classified as preprocessing or *offline constraint handling*. Finally, we extracted the feasible search space area with problem knowledge.

8.2 A Guide for Future Pathfinding Problems

In this thesis, different methodologies for arbitrary pathfinding problems have been proposed. However, we have shown that, depending on the problem characteristics, certain techniques often outperform others. Therefore, we propose the following framework as a decision support model for a pathfinding problem.

The framework depends on the size of the problem and its complexity, modality and spatiality as well as the similarity of paths. Analysing a problem regarding these properties leads to suitable approaches, which are proposed in this thesis. It should be noted that the following textual framework is a suggestion based on the empirical results of our studies and further evaluations. For a real-world problem, the algorithmic configuration may differ from the suggested solution, and parameters should be adjusted with care.

Size The problem or environment size has an impact on several algorithmic properties and parameters. For small-scale problems, a fixed-length solution representation can be beneficial, whereas a variable-length method is usually superior when the environment – and therefore also the solution – are large. Furthermore, different path similarity measurements can be used, depending on the size of the environment, which includes their respective computational efforts. In small-scale instances, the Fréchet distance or DTW can give performance gains while maintaining a reasonable computation time. Computing the Hausdorff distance is less complex and can therefore be used with large-scale instances. However, sacrificing quality in the solution may be a trade-off one must accept.

Spatiality If the environment contains spatial information about its entities (e.g., coordinates), the use of a path similarity measurement technique – such as computing isolated solutions in the decision space – is encouraged. If no spatial information is involved, one can also use the proposed similarity measurements, but instead of the Euclidean distance between points, their respective network distance is used. This approach can, however, result in significant performance issues regarding the time needed to obtain the results.

Similarity The similarity factor is a value that reflects the importance of small differences in the actual expression of the path. In Figure 2.6 the different similarity measurements are compared. Using the Fréchet distance is sufficient for most problems. If small differences have a high importance, DTW should be used, whereas the Hausdorff distance can be used if such differences are negligible.

Modality Pathfinding problems can be, depending on the underlying environment, unimodal or multi-modal. The former maps exactly one path to one objective value vector, while the latter allows multiple paths resulting in the same objective values. If a DM is aware of such a property and aims to emphasise those values, decision space diversification should be used. With such a technique, multi-modal solutions can be found.

Complexity Depending on the complexity of an environment together with the complexity of the resulting problem, other techniques have proven beneficial. Although a pathfinding problem can be defined in more than two or three dimensions, using a path similarity measuring technique can be beneficial and would merely add computational effort. The metrics that are used in this thesis are independent of the dimensionality. Solely the distance function that is used to compute distances between single points is impacted.

8.3 Future Work

In the future, several methodologies to tackle the challenges of the many-objective pathfinding benchmark should be developed. In this thesis, we have proposed various starting points for an ongoing research process.

8.3.1 Environmental and Algorithmic Aspects

One of the major tasks in the future is to reduce the environmental impact that results from executing an optimisation task. There are other aspects with respect to problem generation and solution computation, too. We suggest that the energy consumption of an execution should be reduced by finding more sophisticated methodologies to reduce the search space, which in turn would reduce the computational effort.

Environment Generation

In the future, benchmark generators including dynamic obstacles can be developed to better resemble the reality and actual problems. Furthermore, stochastic characteristics can be incorporated, as real-world problems are often not deterministic and highly uncertain. In the related work, variations of such properties can be found and can be implemented with our proposed benchmark suite. In addition, time-dependent networks can be considered to represent timetables of public transports or problems from other domains. In general, real-world problems are often dynamic in several regards, which should be incorporated in the problem generation.

Algorithmic Characteristics

For the algorithmic characteristics, several points should be considered when conducting research on the multi-objective pathfinding problem. In the paragraph above we outlined several aspects of the environment generation. Dynamic problems introduce several challenges in the actual execution of the optimisation methodology. Speed-up techniques, such as contraction hierarchies, are applied on static and deterministic environments and therefore cannot be used on dynamic problems. This introduces drawbacks to our proposed reproduction operators, as they need to determine the shortest path between two points to generate new solutions. For dynamic problems, different techniques must be developed to compute such paths. Furthermore, a different encoding scheme would be beneficial for such environments.

Measuring path similarities assumes some geometrical properties of the respective paths. However, pathfinding problems can also be placed on spatially independent graphs. For such problems, the network distance can be used as a substitute, but this would again result in increased computational effort. In the future, more sophisticated methodologies for such graphs and problems should be evaluated.

Another promising focus point would be to develop sophisticated techniques to find a natural ordering of a set of paths. The inclusion of additional geometrical properties could lead to better determination of neighbourhood relations. The current use of the Fréchet distance has drawbacks, since it considers only the maximum difference.

The concept of *innovisation* relates to extracting knowledge about high-performing solutions from the search process [DS06]. The online innovisation process performs the extraction during the execution of the optimisation to use the knowledge in the following iterations. The use of tailored similarity measurements and diversification techniques in the path search space can be seen as part of this approach, since knowledge about geometric properties is extracted and used. Nonetheless, future research should develop more methodologies using this technique as it is promising in this domain.

With an increasing problem size, the solution paths become proportionally longer, although this is not a necessity as the environment can be large but the desired paths short. Evaluating long and large paths impacts the performance of the optimisation. *Surrogate-assisted optimisation* can be beneficial here, since surrogate paths or representations can be found and used instead. This method has certain disadvantages as the paths are not evaluated as a whole, which can lead to inaccuracies.

8.3.2 Aspects of Real-World Applications

As discussed in Chapter 1, pathfinding problems occur in a variety of different domains and applications. Beyond pathfinding for travel purposes, other use-cases exist where this technique can be used. In the following subsections, we outline a few use-cases which would be interesting fields for applied science in the future, considering the approaches proposed in this thesis.

Spatial Routing Problems

There are numerous spatial routing problems where pathfinding techniques can be beneficial. Other than car routing, 3D pathfinding for air travel using airplanes or other vessels is a promising use-case with conflicting objectives. Furthermore, such problems oppose several constraints that must be considered. Often, these constraining functions strongly decrease the feasible area of the search space, which results in special requirements for an efficient algorithm.

Running Routes

Real-world problems are often highly constrained, which is a challenge for EAs. A running route provides an example. Runners often favour routes of a specific length, which can be modelled as an objective but should also be constrained to result in a path that is in a certain ε range of the desired length. Furthermore, zigzag courses are usually not favoured, and the surface of the track can play a large role for some runners. A certain uniqueness of the route may be required to avoid merely running in circles. Modelling these requirements as objectives is possible, but it can result in many non-dominated solutions. Modelling constraints is often the better solution to emphasise the search on the desired area of the search space. In this thesis, we have not analysed this field. In future research, methodologies can be developed to consider and analyse such constraints. This would also help the community to appreciate how EAs can help in everyday problems.

Medical Applications

Besides pathfinding on actual road networks, other applications can also employ such techniques. One example is medical applications, where a path from the outside of the body to the inside needs to be found. For instance, a cancerous

tumour within liver tissue needs to be treated by ablation. A needle is inserted into the tissue to place the needle's point, or treatment area, at the correct position of the tumour. When surgeons use this technique, they must find a path from the patient's body surface to the tumour.

Manufacturing

There are numerous possibilities to apply pathfinding techniques in the field of manufacturing. In [WBM18], we outlined several applications to use such techniques. A major challenge is to find a suitable representation of spatial and engineering information. For instance, in assembly sequence generation, not only the parts have to be brought into relation but also the free space between them to compute the correct assembly or disassembly sequences. Optimisation in manufacturing has great potential and is also interesting, as the domain's problems usually are more highly constrained than those of scientific benchmark problems. Finally, the reality often consists of edge cases that are mostly not considered.

8.3.3 Decision Support Systems

In Chapter 7, we proposed a concept of using decision points along a path as possible triggers for recomputation or decision-making methodologies. In the future, we hope to see such methodologies evolve, as this would be beneficial to decrease computation times and would emphasise the interactive approach of decision-making for such problems. Interactive decision-making is an approach involving a DM during the optimisation process, which leads the optimisation to an appealing area in the objective space as well as the decision space. Furthermore, *rolling horizon EAs* [PSLR13] are a promising approach for multi-objective pathfinding problems, as they can result in quicker computation times due to the reduced optimisation horizon. However, other challenges arise, especially while optimising paths, since later steps on a chosen path may lead to a marked deterioration of the objective values, which may not be predictable. Furthermore, in Section 7.4, we presented the concept of DPs for pathfinding problems. Moreover, using the proposed algorithmic approaches, the presented use cases of DPs could benefit from it. For instance, identifying a path in the criminal justice system with a minimum racial bias and simultaneously ensuring a trial's speed can help individuals having fairer trials.

Bibliography

[AD11] Faez Ahmed and Kalyanmoy Deb. Multi-objective path planning using spline representation. *2011 IEEE International Conference on Robotics and Biomimetics, ROBIO 2011*, (2011010):1047–1052, 2011. [cited on p. 31, 36, 37, 38, 40 and 41]

[AD13] Faez Ahmed and Kalyanmoy Deb. Multi-objective optimal path planning using elitist non-dominated sorting genetic algorithms. *Soft Computing*, 17(7):1283–1299, 7 2013. [cited on p. 18, 31, 36, 37, 38, 40 and 41]

[AG95] Helmut Alt and Michael Godau. Computing The Fréchet Distance Between Two Polygonal Curves. *International Journal of Computational Geometry & Applications*, 05(01n02):75–91, 3 1995. [cited on p. 23 and 85]

[AKC+13] Maram Alajlan, Anis Koubaa, Imen Chaari, Hachemi Bennaceur, and Adel Ammar. Global path planning for mobile robots in large-scale grid environments using genetic algorithms. In *2013 International Conference on Individual and Collective Behaviors in Robotics (ICBR)*, number 1, pages 1–8. IEEE, 2013. [cited on p. 40]

[AMO93] R K Ahuja, T L Magnanti, and J B Orlin. *Network Flows: Theory, Algorithms, and Applications*. Prentice Hall, 1993. [cited on p. 22 and 43]

[Anb13] R. Anbuselvi. Path Finding Solutions For Grid Based Graph. *Advanced Computing: An International Journal*, 4(2):51–60, 3 2013. [cited on p. 40]

[Ang11] Bobby Anguelov. *Video Game Pathfinding and Improvements to Discrete Search on Grid-based Maps*. PhD thesis, University of Pretoria, 2011. [cited on p. 40]

[AQY09] Aimin Zhou, Qingfu Zhang, and Yaochu Jin. Approximating the Set of Pareto-Optimal Solutions in Both the Decision

and Objective Spaces by an Estimation of Distribution Algorithm. *IEEE Transactions on Evolutionary Computation*, 13(5):1167–1189, 10 2009. [cited on p. 25, 96 and 99]

[BCGR11] Lucas S. Batista, Felipe Campelo, Frederico G. Guimaraes, and Jaime A. Ramirez. A comparison of dominance criteria in many-objective optimization problems. In *2011 IEEE Congress of Evolutionary Computation (CEC)*, number June 2014, pages 2359–2366. IEEE, 6 2011. [cited on p. 18]

[BDDO04] Jürgen Branke, Kalyanmoy Deb, Henning Dierolf, and Matthias Osswald. Finding Knees in Multi-objective Optimization. In *Lecture Notes in Computer Science (including subseries Lecture Notes in Artificial Intelligence and Lecture Notes in Bioinformatics)*, volume 3242, pages 722–731. 2004. [cited on p. 18]

[BM04] John M Boyer and Wendy J Myrvold. On the Cutting Edge: Simplified O(n) Planarity by Edge Addition. *Journal of Graph Algorithms and Applications*, 8(3):241–273, 2004. [cited on p. 12]

[BM16] Karl Bringmann and Wolfgang Mulzer. Approximability of the discrete Fréchet distance. *Journal of Computational Geometry*, 7(2):46–76, 2016. [cited on p. 86]

[Boe17] Geoff Boeing. OSMnx: New methods for acquiring, constructing, analyzing, and visualizing complex street networks. *Computers, Environment and Urban Systems*, 65:126–139, 9 2017. [cited on p. 58]

[Bol79] Béla Bollobás. *Graph Theory*, volume 63 of *Graduate Texts in Mathematics*. Springer New York, New York, NY, 1979. [cited on p. 34]

[BPdlTMRM13] Eva Besada-Portas, Luis de la Torre, Alejandro Moreno, and José L. Risco-Martín. On the performance comparison of multi-objective evolutionary UAV path planners. *Information Sciences*, 238:111–125, 7 2013. [cited on p. 41]

[BS09] Ed Bullmore and Olaf Sporns. Complex brain networks: graph theoretical analysis of structural and functional systems. *Nature Reviews Neuroscience*, 10(4):312, 3 2009. [cited on p. 12]

[BWC20] Lilla Beke, Michal Weiszer, and Jun Chen. A Comparison of Genetic Representations for Multi-objective Shortest Path Problems on Multigraphs. volume 8, pages 35–50. Springer International Publishing, 2020. [cited on p. 41 and 55]

[CBG+20] Theodoros Chondrogiannis, Panagiotis Bouros, Johann Gamper, Ulf Leser, and David B. Blumenthal. Finding k-shortest paths with limited overlap. *The VLDB Journal*, 29(5):1023–1047, 9 2020. [cited on p. 67]

[CCRS04] Carlos A. Coello Coello and Margarita Reyes Sierra. A Study of the Parallelization of a Coevolutionary Multi-objective Evolutionary Algorithm. pages 688–697. 2004. [cited on p. 24]

[Chi16] William Y Chin. Racial cumulative disadvantage: The cumulative effects of racial bias at multiple decision points in the criminal justice system. *Wake Forest JL & Pol'y*, 6:441, 2016. [cited on p. 109]

[CLM+16] Michael B. Cohen, Yin Tat Lee, Gary Miller, Jakub Pachocki, and Aaron Sidford. Geometric median in nearly linear time. In *Proceedings of the forty-eighth annual ACM symposium on Theory of Computing*, pages 9–21, New York, NY, USA, 6 2016. ACM. [cited on p. 91 and 101]

[CNT05] Tsung Sheng Chang, Linda K. Nozick, and Mark A. Turnquist. Multiobjective path finding in stochastic dynamic networks, with application to routing hazardous materials shipments. *Transportation Science*, 39(3):383–399, 2005. [cited on p. 36, 37 and 38]

[CPS11] C. Chitra, Subbaraj Potti, and P. Subbaraj. A novel multiobjective evolutionary algorithm for shortest path routing problem. *International Journal of Communication Networks and Distributed Systems*, 7(3/4):355, 2011. [cited on p. 31]

[CR18] Timothy M. Chan and Zahed Rahmati. An improved approximation algorithm for the discrete Fréchet distance. *Information Processing Letters*, 138:72–74, 10 2018. [cited on p. 86]

[CSF18] Xinye Cai, Haoran Sun, and Zhun Fan. A diversity indicator based on reference vectors for many-objective optimization. *Information Sciences*, 430-431:467–486, 3 2018. [cited on p. 42, 55, 57, 73, 83 and 88]

[CTM07] Oscar Castillo, Leonardo Trujillo, and Patricia Melin. Multiple objective genetic algorithms for path-planning optimization in autonomous mobile robots. *Soft Computing*, 11(3):269–279, 2 2007. [cited on p. 31 and 40]

[CXCG10] Liu Changan, Yan Xiaohu, Liu Chunyang, and Li I Guodong. Dynamic Path Planning for Mobile Robot Based on Improved Genetic Algorithm. *Chinese Journal of Electronics*, 19(2), 2010. [cited on p. 40]

[CZKZ22] Zong-Gan Chen, Zhi-Hui Zhan, Sam Kwong, and Jun Zhang. Evolutionary Computation for Intelligent Transportation in Smart Cities: A Survey [Review Article]. *IEEE Computational Intelligence Magazine*, 17(2):83–102, 5 2022. [cited on p. 4]

[DB79] David L. Davies and Donald W. Bouldin. A Cluster Separation Measure. *IEEE Transactions on Pattern Analysis and Machine Intelligence*, PAMI-1(2):224–227, 4 1979. [cited on p. 29]

[DCOVdW+21] Laure De Cock, Kristien Ooms, Nico Van de Weghe, Nina Vanhaeren, Pieter Pauwels, and Philippe De Maeyer. Identifying what constitutes complexity perception of decision

points during indoor route guidance. *International Journal of Geographical Information Science*, 35(6):1232–1250, June 2021. [cited on p. 109]

[Deb00] Kalyanmoy Deb. An efficient constraint handling method for genetic algorithms. *Computer Methods in Applied Mechanics and Engineering*, 186(2-4):311–338, June 2000. [cited on p. 65]

[Deb11a] K Deb. Multi-objective optimization using evolutionary algorithms. In *Wiley-Interscience series in systems and optimization*, 2011. [cited on p. 16]

[Deb11b] Kalyanmoy Deb. Multi-objective Optimisation Using Evolutionary Algorithms: An Introduction. In *Multi-objective Evolutionary Optimisation for Product Design and Manufacturing*, pages 3–34. Springer London, London, 2011. [cited on p. 19]

[DG11] Kalyanmoy Deb and Shivam Gupta. Understanding knee points in bicriteria problems and their implications as preferred solution principles. *Engineering Optimization*, 43(11):1175–1204, 11 2011. [cited on p. 18]

[DGJ09] C Demetrescu, A Goldberg, and D Johnson. The shortest path problem : ninth DIMACS implementation challenge. 2009. [cited on p. 44]

[Dij59] E W Dijkstra. A note on two problems in connexion with graphs. *Numerische Mathematik*, 1(1):269–271, 1959. [cited on p. 13, 22, 31, 38 and 68]

[DJ14] Kalyanmoy Deb and Himanshu Jain. An Evolutionary Many-Objective Optimization Algorithm Using Reference-Point-Based Nondominated Sorting Approach, Part I: Solving Problems With Box Constraints. *IEEE Transactions on Evolutionary Computation*, 18(4):577–601, 2014. [cited on p. 19, 42, 55, 71, 83, 88 and 105]

[DMS08] Yann Disser, Matthias Müller–Hannemann, and Mathias Schnee. Multi-criteria Shortest Paths in Time-Dependent Train Networks. In *Experimental Algorithms*, volume 5038 LNCS, pages 347–361. Springer Berlin Heidelberg, Berlin, Heidelberg, 2008. [cited on p. 31]

[DP73] David H Douglas and Thomas K Peucker. Algorithms for the Reduction of the Number of Points Required to Represent a Digitized Line or its Caricature. *Cartographica: The International Journal for Geographic Information and Geovisualization*, 10(2):112–122, 10 1973. [cited on p. 69]

[DPAM02] Kalyanmoy Deb, Amrit Pratap, Sameer Agarwal, and T Meyarivan. A fast and elitist multiobjective genetic algorithm: NSGA-II. *IEEE Transactions on Evolutionary Computation*, 6(2):182–197, 2002. [cited on p. 41, 55, 71, 83, 88, 90 and 92]

[DPMH13] Mansoor Davoodi, Fatemeh Panahi, Ali Mohades, and Seyed Naser Hashemi. Multi-objective path planning in

discrete space. *Applied Soft Computing*, 13(1):709–720, 1 2013. [cited on p. 31, 36, 37, 38, 39, 41 and 42]

[DPMH15] Mansoor Davoodi, Fatemeh Panahi, Ali Mohades, and Seyed Naser Hashemi. Clear and smooth path planning. *Applied Soft Computing*, 32:568–579, 7 2015. [cited on p. 33, 36, 37, 38, 39, 42 and 50]

[DS05] Kalyanmoy Deb and Dhish Kumar Saxena. On Finding Pareto-Optimal Solutions Through Dimensionality Reduction for Certain Large-Dimensional Multi-Objective Optimization Problems EMO for Many Objectives. *Kangal report*, 2005011(2005011):3353–3360, 2005. [cited on p. 18]

[DS06] Kalyanmoy Deb and Aravind Srinivasan. Innovization: innovating design principles through optimization. In *Proceedings of the 8th annual conference on Genetic and evolutionary computation - GECCO '06*, number January, page 1629, New York, New York, USA, 2006. ACM Press. [cited on p. 129]

[DSSW09] Daniel Delling, Peter Sanders, Dominik Schultes, and Dorothea Wagner. Engineering Route Planning Algorithms. In Jürgen Lerner, Dorothea Wagner, and Katharina A Zweig, editors, *Algorithmics of large and complex networks*, volume 5515 of *Lecture Notes in Computer Science*, pages 117–139. Springer Berlin Heidelberg, Berlin, Heidelberg, 2009. [cited on p. 31]

[DT05] Kalyanmoy Deb and Santosh Tiwari. Omni-optimizer: A Procedure for Single and Multi-objective Optimization. In *Lecture Notes in Computer Science*, volume 3410, pages 47–61. 2005. [cited on p. 84 and 89]

[DTLZ05] Kalyanmoy Deb, Lothar Thiele, Marco Laumanns, and Eckart Zitzler. Scalable Test Problems for Evolutionary Multiobjective Optimization. In *Evolutionary Multiobjective Optimization: Theoretical Advances and Applications*, pages 105–145. Springer London, London, 2005. [cited on p. 44]

[Dun73] J. C. Dunn. A Fuzzy Relative of the ISODATA Process and Its Use in Detecting Compact Well-Separated Clusters. *Journal of Cybernetics*, 3(3):32–57, 1 1973. [cited on p. 28]

[DZJ03] Kalyanmoy Deb, Pawan Zope, and Abhishek Jain. Distributed Computing of Pareto-Optimal Solutions with Evolutionary Algorithms. In Carlos M Fonseca, Peter J Fleming, Eckart Zitzler, Lothar Thiele, and Kalyanmoy Deb, editors, *Evolutionary Multi-Criterion Optimization*, pages 534–549, Berlin, Heidelberg, 2003. Springer Berlin Heidelberg. [cited on p. 106]

[EAA04] Ahmed Elshamli, Hussein A Abdullah, and Shawki Areibi. Genetic algorithm for dynamic path planning. In *Canadian Conference on Electrical and Computer Engineering 2004 (IEEE Cat. No.04CH37513)*, volume 2, pages 677–680. IEEE, 2004. [cited on p. 41]

[EBN05] Michael Emmerich, Nicola Beume, and Boris Naujoks. An EMO Algorithm Using the Hypervolume Measure as Selection Criterion. In Carlos A Coello Coello, Arturo Hernández Aguirre, and Eckart Zitzler, editors, *Evolutionary Multi-Criterion Optimization*, pages 62–76, Berlin, Heidelberg, 2005. Springer Berlin Heidelberg. [cited on p. 106]

[EC02] Vladimir Estivill-Castro. Why so many clustering algorithms. *ACM SIGKDD Explorations Newsletter*, 4(1):65–75, 2002. [cited on p. 14]

[Eft15] Emre Eftelioglu. Geometric Median. In *Encyclopedia of GIS*, number Haldane 1948, pages 1–4. Springer International Publishing, Cham, 2015. [cited on p. 92]

[EGHP+02] Alon Efrat, Leonidas J. Guibas, Sariel Har-Peled, Joseph S.B. Mitchell, T. M. Murali, Efrat, Guibas, Sariel Har-Peled, Mitchell, and Murali. New Similarity Measures between Polylines with Applications to Morphing and Polygon Sweeping. *Discrete and Computational Geometry*, 28(4):535–569, 11 2002. [cited on p. 23 and 84]

[EM94] Thomas Eiter and Heikki Mannila. Computing discrete Fréchet distance. Technical Report CD-TR 94/64, Christian Doppler Lab. Expert Sys., TU Vienna, Vienna, Austria, 1994. [cited on p. 23, 85 and 86]

[Epp98] David Eppstein. Finding the k Shortest Paths. *SIAM Journal on Computing*, 28(2):652–673, 1 1998. [cited on p. 67]

[FC14] Lavinia Ferariu and Corina Cimpanu. Pareto genetic path planning hybridized with multi-objective Dijkstra's algorithm. In *2014 18th International Conference on System Theory, Control and Computing (ICSTCC)*, pages 341–346. IEEE, 10 2014. [cited on p. 31]

[FCAM19] Jonathan E. Fieldsend, Tinkle Chugh, Richard Allmendinger, and Kaisa Miettinen. A feature rich distance-based many-objective visualisable test problem generator. In *Proceedings of the Genetic and Evolutionary Computation Conference*, pages 541–549, New York, NY, USA, 7 2019. ACM. [cited on p. 44]

[FCEC19] Jesús Guillermo Falcón-Cardona, Michael T. M. Emmerich, and Carlos A. Coello Coello. On the construction of pareto-compliant quality indicators. In *Proceedings of the Genetic and Evolutionary Computation Conference Companion*, number July, pages 2024–2027, New York, NY, USA, 7 2019. ACM. [cited on p. 24]

[FLZ11] Chenglin Fan, Jun Luo, and Binhai Zhu. Fréchet-Distance on Road Networks. pages 61–72. 2011. [cited on p. 84]

[FPLI06] C.M. Fonseca, Luís Paquete, and M. Lopez-Ibanez. An Improved Dimension-Sweep Algorithm for the Hypervolume

Indicator. In *2006 IEEE International Conference on Evolutionary Computation*, pages 1157–1163. IEEE, 2006. [cited on p. 19]

[Fré06] M Maurice Fréchet. Sur quelques points du calcul fonctionnel. *Rendiconti del Circolo Matematico di Palermo (1884-1940)*, 22(1):1–72, 1906. [cited on p. 85]

[Fre77] Linton C Freeman. A Set of Measures of Centrality Based on Betweenness. *Sociometry*, 40(1):35, 1977. [cited on p. 13]

[FS13] Stefan Funke and Sabine Storandt. Polynomial-time Construction of Contraction Hierarchies for Multi-criteria Objectives. In *2013 Proceedings of the Fifteenth Workshop on Algorithm Engineering and Experiments (ALENEX)*, pages 41–54. Society for Industrial and Applied Mathematics, Philadelphia, PA, 1 2013. [cited on p. 31, 36, 37 and 38]

[GBLV15] Alessandro Gasparetto, Paolo Boscariol, Albano Lanzutti, and Renato Vidoni. Path Planning and Trajectory Planning Algorithms: A General Overview. pages 3–27. 2015. [cited on p. 22]

[GBR06] Xavier Gandibleux, Frédéric Beugnies, and Sabine Randriamasy. Martins' algorithm revisited for multi-objective shortest path problems with a MaxMin cost function. *4OR*, 4(1):47–59, 3 2006. [cited on p. 69 and 102]

[GC13] Enric Galceran and Marc Carreras. A survey on coverage path planning for robotics. *Robotics and Autonomous Systems*, 61(12):1258–1276, 12 2013. [cited on p. 5 and 20]

[Gei08] Robert Geisberger. *Contraction Hierarchies: Faster and Simpler Hierarchical Routing in Road Networks*. PhD thesis, Universität Karlsruhe (TH), 2008. [cited on p. 4, 22, 31, 36, 37 and 38]

[GFP20] Andreia P. Guerreiro, Carlos M. Fonseca, and Luís Paquete. The Hypervolume Indicator: Problems and Algorithms. 2020. [cited on p. 25]

[GFPC09] Mario Garza-Fabre, Gregorio Toscano Pulido, and Carlos A. Coello Coello. Ranking Methods for Many-Objective Optimization. In *Lecture Notes in Computer Science (including subseries Lecture Notes in Artificial Intelligence and Lecture Notes in Bioinformatics)*, volume 5845 LNAI, pages 633–645. 2009. [cited on p. 18 and 19]

[GKS10] Robert Geisberger, Moritz Kobitzsch, and Peter Sanders. Route Planning with Flexible Objective Functions. In *2010 Proceedings of the Twelfth Workshop on Algorithm Engineering and Experiments (ALENEX)*, pages 124–137. Society for Industrial and Applied Mathematics, Philadelphia, PA, 1 2010. [cited on p. 31]

[GL06] Mitsuo Gen and Lin Lin. A new approach for shortest path routing problem by random key-based GA. In *Proceedings of the 8th annual conference on Genetic and evolutionary*

computation - GECCO '06, volume 2, page 1411, New York, New York, USA, 2006. ACM Press. [cited on p. 41]

[Gol89] David E Goldberg. *Genetic Algorithms in Search, Optimization and Machine Learning*. Addison-Wesley Longman Publishing Co., Inc., USA, 1st edition, 1989. [cited on p. 16]

[GPN+11] Subhashini Ganapathy, Sasanka Prabhala, S Narayanan, Raymond R Hill, and Jennie J Gallimore. Interactive Model-Based Decision Making for Time-Critical Vehicle Routing. In *Human-in-the-Loop Simulations*, pages 203–220. Springer London, London, 2011. [cited on p. 69]

[GRD97] Mitsuo Gen, Runwei Cheng, and Dingwei Wang. Genetic algorithms for solving shortest path problems. In *Proceedings of 1997 IEEE International Conference on Evolutionary Computation (ICEC '97)*, pages 401–406. IEEE, 1997. [cited on p. 41]

[Gut84] Antonin Guttman. R-trees: a dynamic index structure for spatial searching. *ACM SIGMOD Record*, 14(2):47–57, 6 1984. [cited on p. 55, 56 and 82]

[HA20] Hiba Hliwa and Bassam Atieh. Multi Objective Path Planning in Static Environment using Region of Sight. In *2020 International Youth Conference on Radio Electronics, Electrical and Power Engineering (REEPE)*, pages 1–5. IEEE, 3 2020. [cited on p. 36, 37, 38 and 39]

[HBAO21] Nikolas Hohmann, Mariusz Bujny, Jurgen Adamy, and Markus Olhofer. Hybrid Evolutionary Approach to Multi-objective Path Planning for UAVs. In *2021 IEEE Symposium Series on Computational Intelligence (SSCI)*, pages 1–8. IEEE, 12 2021. [cited on p. 36, 37, 39, 41 and 42]

[HJ98] Michael Pilegaard Hansen and Andrzej Jaszkiewicz. Evaluating the quality of approximations to the non-dominated set. *IMM Technical Report IMM-REP-1998-7*, page 31, 1998. [cited on p. 24]

[HLZ+18] Xiao-Bing Hu, Hang Li, Jun Zhou, Ming-Kong Zhang, and Jian-Qin Liao. Finding all Pareto Optimal Paths for Dynamical Multi-Objective Path optimization Problems. In *2018 IEEE Symposium Series on Computational Intelligence (SSCI)*, pages 965–972. IEEE, 11 2018. [cited on p. 36, 37 and 38]

[HNR68] Peter E Hart, Nils J Nilsson, and Bertram Raphael. A Formal Basis for the Heuristic Determination of Minimum Cost Paths. *IEEE Transactions on Systems Science and Cybernetics*, 4(2):100–107, 1968. [cited on p. 22]

[HPVRFP15] Alejandro Hidalgo-Paniagua, Miguel A. Vega-Rodríguez, Joaquín Ferruz, and Nieves Pavón. MOSFLA-MRPP: Multi-Objective Shuffled Frog-Leaping Algorithm applied to Mobile Robot Path Planning. *Engineering Applications of Artificial Intelligence*, 44:123–136, 2015. [cited on p. 36, 37, 38, 39, 42 and 50]

[HPVRFP17] Alejandro Hidalgo-Paniagua, Miguel A. Vega-Rodríguez, Joaquín Ferruz, and Nieves Pavón. Solving the multi-objective path planning problem in mobile robotics with a firefly-based approach. *Soft Computing*, 21(4):949–964, 2017. [cited on p. 36, 37, 38, 39 and 42]

[HY81] Ching-Lai Hwang and Kwangsun Yoon. *Multiple Attribute Decision Making*, volume 186 of *Lecture Notes in Economics and Mathematical Systems*. Springer Berlin Heidelberg, Berlin, Heidelberg, 1981. [cited on p. 46]

[HZZ+19] Xiao-Bing Hu, Hai-Lin Zhang, Chi Zhang, Ming-Kong Zhang, Hang Li, and Mark S. Leeson. A benchmark test problem toolkit for multi-objective path optimization. *Swarm and Evolutionary Computation*, 44(2):18–30, 2 2019. [cited on p. 44 and 47]

[IHK99] J. Inagaki, M. Haseyama, and H. Kitajima. A genetic algorithm for determining multiple routes and its applications. In *ISCAS'99. Proceedings of the 1999 IEEE International Symposium on Circuits and Systems VLSI (Cat. No.99CH36349)*, volume 6, pages 137–140. IEEE, 1999. [cited on p. 41]

[IKK01] K. Ikeda, H. Kita, and S. Kobayashi. Failure of Pareto-based MOEAs: does non-dominated really mean near to optimal? In *Proceedings of the 2001 Congress on Evolutionary Computation (IEEE Cat. No.01TH8546)*, volume 2, pages 957–962. IEEE, 2001. [cited on p. 18]

[IMN15] Hisao Ishibuchi, Hiroyuki Masuda, and Yusuke Nojima. A Study on Performance Evaluation Ability of a Modified Inverted Generational Distance Indicator. In *Proceedings of the 2015 on Genetic and Evolutionary Computation Conference - GECCO '15*, pages 695–702, New York, New York, USA, 7 2015. ACM Press. [cited on p. 56, 95 and 99]

[IMTN14] Hisao Ishibuchi, Hiroyuki Masuda, Yuki Tanigaki, and Yusuke Nojima. Difficulties in specifying reference points to calculate the inverted generational distance for many-objective optimization problems. In *2014 IEEE Symposium on Computational Intelligence in Multi-Criteria Decision-Making (MCDM)*, pages 170–177. IEEE, 2014. [cited on p. 56]

[IMTN15a] Hisao Ishibuchi, Hiroyuki Masuda, Yuki Tanigaki, and Yusuke Nojima. Modified Distance Calculation in Generational Distance and Inverted Generational Distance. In *Lecture Notes in Computer Science (including subseries Lecture Notes in Artificial Intelligence and Lecture Notes in Bioinformatics)*, volume 9019, pages 110–125. 2015. [cited on p. 24 and 25]

[IMTN15b] Hisao Ishibuchi, Hiroyuki Masuda, Yuki Tanigaki, and Yusuke Nojima. Modified distance calculation in generational distance and inverted generational distance. In António Gaspar-Cunha, Carlos Henggeler Antunes, and Carlos Coello Coello, editors, *Evolutionary Multi-Criterion Optimization*,

pages 110–125, Cham, 2015. Springer International Publishing. [cited on p. 72]

[IPS22] Hisao Ishibuchi, Lie Meng Pang, and Ke Shang. Difficulties in Fair Performance Comparison of Multi-Objective Evolutionary Algorithms. *IEEE Computational Intelligence Magazine*, 17(1):86–101, 2 2022. [cited on p. 23, 24 and 25]

[Jan11] Sylvia J. T. Jansen. The Multi-attribute Utility Method. In *The Measurement and Analysis of Housing Preference and Choice*, pages 101–125. Springer Netherlands, Dordrecht, 2011. [cited on p. 45]

[Jin21] Bo Jin. Multi-Objective A* Algorithm for the Multimodal Multi-Objective Path Planning Optimization. In *2021 IEEE Congress on Evolutionary Computation (CEC)*, pages 1704–1711. IEEE, 6 2021. [cited on p. 21, 36, 37, 38 and 44]

[JKC11] Zhaowang Ji, Yong Seog Kim, and Anthony Chen. Multi-objective α-reliable path finding in stochastic networks with correlated link costs: A simulation-based multi-objective genetic algorithm approach (SMOGA). *Expert Systems with Applications*, 38(3):1515–1528, 3 2011. [cited on p. 41]

[JM21] Mahrokh Javadi and Sanaz Mostaghim. Using Neighborhood-Based Density Measures for Multimodal Multi-objective Optimization. In Hisao Ishibuchi, Qingfu Zhang, Ran Cheng, Ke Li, Hui Li, Handing Wang, and Aimin Zhou, editors, *Evolutionary Multi-Criterion Optimization*, Lecture Notes in Computer Science, pages 335–345, Cham, 2021. Springer International Publishing. [cited on p. 42 and 84]

[JQ10] Hu Jun and Zhu Qingbao. Multi-objective Mobile Robot Path Planning Based on Improved Genetic Algorithm. In *2010 International Conference on Intelligent Computation Technology and Automation*, volume 2, pages 752–756, Changsha, China, 5 2010. IEEE. [cited on p. 31, 36, 37, 38, 39, 41, 42 and 50]

[JRAM20] Mahrokh Javadi, Cristian Ramirez-Atencia, and Sanaz Mostaghim. Combining Manhattan and Crowding distances in Decision Space for Multimodal Multi-objective Optimization problems. In *Springer ECCOMAS book series on Computational Methods in Applied Sciences*, Guimarães, Portugal. In Press, 2020. ACM. [cited on p. 42 and 84]

[JXZ08] Minghui Jiang, Ying Xu, and Binhai Zhu. Protein Structure–Structure Alignment With Discrete Fréchet Distance. *Journal of Bioinformatics and Computational Biology*, 06(01):51–64, 2 2008. [cited on p. 23 and 84]

[JZM19] Mahrokh Javadi, Heiner Zille, and Sanaz Mostaghim. Modified crowding distance and mutation for multimodal multi-objective optimization. In *Proceedings of the Genetic and Evolutionary Computation Conference Companion*, pages 211–212, New York, NY, USA, 7 2019. ACM. [cited on p. 89]

[Kan07] Hitoshi Kanoh. Dynamic route planning for car navigation systems using virus genetic algorithms. *International Journal of Knowledge-based and Intelligent Engineering Systems*, 11(1):65–78, 2 2007. [cited on p. 43]

[KBB+16] Rudolf Kruse, Christian Borgelt, Christian Braune, Sanaz Mostaghim, and Matthias Steinbrecher. *Computational Intelligence*. Texts in Computer Science. Springer London, London, 2016. [cited on p. 15]

[KH08] Hitoshi Kanoh and Kenta Hara. Hybrid genetic algorithm for dynamic multi-objective route planning with predicted traffic in a real-world road network. In *Proceedings of the 10th annual conference on Genetic and evolutionary computation - GECCO '08*, page 657, New York, New York, USA, 2008. ACM Press. [cited on p. 43]

[Kim94] Clark Kimberling. Central Points and Central Lines in the Plane of a Triangle. *Mathematics Magazine*, 67(3):163–187, 6 1994. [cited on p. 92]

[KPK+14] Saso Koceski, Stojanche Panov, Natasa Koceska, Pierluigi Beomonte Zobel, and Francesco Durante. A Novel Quad Harmony Search Algorithm for Grid-Based Path Finding. *International Journal of Advanced Robotic Systems*, 11(9):144, 9 2014. [cited on p. 40]

[KR90] Leonard Kaufmann and Peter J. Rousseeuw. Partitioning Around Medoids (Program PAM). In *Finding Groups in Data*, chapter 2, pages 68–125. John Wiley & Sons, Ltd, 1990. [cited on p. 28]

[KTZ06] Joshua D. Knowles, Lothar Thiele, and Eckart Zitzler. A Tutorial on the Performance Assessment of Stochastic Multiobjective Optimizers. *TIK-Report*, 214, 2006. [cited on p. 56 and 99]

[KWZ84] Pekka Korhonen, Jyrki Wallenius, and Stanley Zionts. Solving the Discrete Multiple Criteria Problem using Convex Cones. *Management Science*, 30(11):1336–1345, 11 1984. [cited on p. 18]

[LBE18] Chaymaa Lamini, Said Benhlima, and Ali Elbekri. Genetic Algorithm Based Approach for Autonomous Mobile Robot Path Planning. *Procedia Computer Science*, 127:180–189, 2018. [cited on p. 55]

[Lew16] R M R Lewis. *A Guide to Graph Colouring*. Springer International Publishing, Cham, 2016. [cited on p. 13]

[LG09] Lin Lin and Mitsuo Gen. Priority-Based Genetic Algorithm for Shortest Path Routing Problem in OSPF. In *Intelligent and Evolutionary Systems*, volume 187, pages 91–103. Springer Berlin Heidelberg, Berlin, Heidelberg, 2009. [cited on p. 66]

[LLHL13] Rongrong Li, Yee Leung, Bo Huang, and Hui Lin. A genetic algorithm for multiobjective dangerous goods route planning. *International Journal of Geographical Information Science*, 27(6):1073–1089, 6 2013. [cited on p. 41]

[Llo82] S. Lloyd. Least squares quantization in PCM. *IEEE Transactions on Information Theory*, 28(2):129–137, 3 1982. [cited on p. 27]

[LPLH12] Xinhua Liu, Gaoliang Peng, Xiumei Liu, and Youfu Hou. Disassembly sequence planning approach for product virtual maintenance based on improved max-min ant system. *International Journal of Advanced Manufacturing Technology*, 2012. [cited on p. 31]

[LR18] Darren Lumbroso and David Ramsbottom. Flood Risk Management in the United Kingdom. In *Resilience*, pages 79–87. January 2018. Journal Abbreviation: Resilience. [cited on p. 108]

[LVEJ16] Adriano Lisboa, Douglas Vieira, Petr Ekel, and Joel Pereira Jr. Multi-objective Dijkstra Algorithm applied to path planning. (June), 2016. [cited on p. 31]

[LZY+06] Qing Li, Wei Zhang, Yixin Yin, Zhiliang Wang, Guangjun Liu, and Zhiliang Wang Guangjun Liu. An Improved Genetic Algorithm of Optimum Path Planning for Mobile Robots. In *Sixth International Conference on Intelligent Systems Design and Applications*, volume 2, pages 637–642. IEEE, 2006. [cited on p. 55]

[Mac67] J Macqueen. Some methods for classification and analysis of multivariate observations. In *In 5-th Berkeley Symposium on Mathematical Statistics and Probability*, pages 281–297, 1967. [cited on p. 27]

[Mar84] Ernesto Queirós Vieira Martins. On a multicriteria shortest path problem. *European Journal of Operational Research*, 16(2):236–245, 5 1984. [cited on p. 39 and 102]

[MDSK07] Shashi Mittal, Kalyanmoy Deb, Shashi Mittal, and Kalyanmoy Deb. Three-dimensional offline path planning for UAVs using multiobjective evolutionary algorithms. In *2007 IEEE Congress on Evolutionary Computation*, pages 3195–3202. IEEE, 2007. [cited on p. 41]

[Mic96] Zbigniew Michalewicz. *Genetic Algorithms + Data Structures = Evolution Programs*. Springer Berlin Heidelberg, Berlin, Heidelberg, 1996. [cited on p. 16]

[Mie08] Kaisa Miettinen. Introduction to Multiobjective Optimization: Noninteractive Approaches. In *SpringerBriefs in Applied Sciences and Technology*, pages 1–26. 2008. [cited on p. 26 and 27]

[Mil56] George A. Miller. The magical number seven, plus or minus two: Some limits on our capacity for processing information. *Psychological Review*, 63(2):81–97, 3 1956. [cited on p. 105]

[MKNS19] Dimitrios Michail, Joris Kinable, Barak Naveh, and John V Sichi. JGraphT – A Java library for graph data structures and algorithms. 4 2019. [cited on p. 99]

[MLFPEAP+11] Morales Mendoza Luis Fernando, Jose Luis Perez Escobedo, Catherine Azzaro-Pantel, Luc Pibouleau, Serge Domenech, and Alberto Aguilar-Lasserre. Selecting the best portfolio alternative from a hybrid multiobjective GA-MCDM approach for New Product Development in the pharmaceutical industry. In *2011 IEEE Symposium on Computational Intelligence in Multicriteria Decision-Making (MDCM)*, pages 159–166. IEEE, 4 2011. [cited on p. 109]

[MM12] E. Machuca and L. Mandow. Multiobjective heuristic search in road maps. *Expert Systems with Applications*, 39(7):6435–6445, 6 2012. [cited on p. 43 and 44]

[MMC05] Efrén Mezura-Montes and Carlos A. Coello Coello. Useful Infeasible Solutions in Engineering Optimization with Evolutionary Algorithms. In *Lecture Notes in Computer Science (including subseries Lecture Notes in Artificial Intelligence and Lecture Notes in Bioinformatics)*, volume 3789 LNAI, pages 652–662. 2005. [cited on p. 75]

[MML+08] A M Mora, J J Merelo, J L J Laredo, P A Castillo, P G Sánchez, J P Sevilla, C Millán, and J Torrecillas. hCHAC-4, an ACO Algorithm for Solving the Four-Criteria Military Path-finding Problem. In *Studies in Computational Intelligence*, volume 129, pages 73–84. 2008. [cited on p. 36, 37 and 38]

[Mou04] A.-I. Mouaddib. Multi-objective decision-theoretic path planning. In *IEEE International Conference on Robotics and Automation, 2004. Proceedings. ICRA '04. 2004*, pages 2814–2819. IEEE, 2004. [cited on p. 36, 37 and 38]

[Mou12] Abdel-illah Mouaddib. Vector-Value Markov Decision Process for multi-objective stochastic path planning. *International Journal of Hybrid Intelligent Systems*, 9(1):45–60, 2012. [cited on p. 36, 37 and 38]

[MP03] ErnestoQ.V. Martins and MartaM.B. Pascoal. A new implementation of Yen's ranking loopless paths algorithm. *Quarterly Journal of the Belgian, French and Italian Operations Research Societies*, 1(2):121–133, 6 2003. [cited on p. 67]

[MS99] Kaisa Miettinen and Pekka Salminen. Decision-aid for discrete multiple criteria decision making problems with imprecise data. *European Journal of Operational Research*, 119(1):50–60, 11 1999. [cited on p. 110]

[MS10] Ellips Masehian and Davoud Sedighizadeh. A multi-objective PSO-based algorithm for robot path planning. In *2010 IEEE International Conference on Industrial Technology*, pages 465–470. IEEE, 2010. [cited on p. 36, 37, 38 and 39]

[MSG08] Ammar W. Mohemmed, Nirod Chandra Sahoo, and Tan Kim Geok. Solving shortest path problem using particle swarm optimization. *Applied Soft Computing*, 8(4):1643–1653, 9 2008. [cited on p. 66]

[MTS98] Masaharu Munetomo, Yoshiaki Takai, and Yoshiharu Sato. A migration scheme for the genetic adaptive routing algorithm. In *SMC'98 Conference Proceedings. 1998 IEEE International Conference on Systems, Man, and Cybernetics (Cat. No.98CH36218)*, volume 3, pages 2774–2779. IEEE, 1998. [cited on p. 41 and 82]

[Mül07] Meinard Müller. Dynamic Time Warping. In *Information Retrieval for Music and Motion*, pages 69–84. Springer Berlin Heidelberg, Berlin, Heidelberg, 2007. [cited on p. 23 and 86]

[Mun00] J R Munkres. *Topology*. Featured Titles for Topology. Prentice Hall, Incorporated, New York, NY, 2000. [cited on p. 84]

[NDV15] Antonio J. Nebro, Juan J. Durillo, and Matthieu Vergne. Redesigning the jMetal Multi-Objective Optimization Framework. In *Proceedings of the Companion Publication of the 2015 on Genetic and Evolutionary Computation Conference - GECCO Companion '15*, pages 1093–1100, New York, New York, USA, 7 2015. ACM Press. [cited on p. 99 and XLIX]

[NN11] Anand Nagar and Tamil Nadu. Strength Pareto Evolutionary Algorithm based Multi-Objective Optimization for Shortest Path Routing Problem in Computer Networks Subbaraj Potti and 2 Chitra Chinnasamy Department of Electronics and Communication Engineering , Theni Kammavar Sangam College. 7(1):17–26, 2011. [cited on p. 31]

[oA20] European Court of Auditors. The EU core road network : shorter travel times but network not yet fully functional. Special report No 09, 2020. Technical report, 2020. [cited on p. 110]

[OBM] Ann O'Shea, Sinead Breen, and Maria Meehan. Decision points in mathematics lectures. 55(6):650–659. [cited on p. 109]

[OMH06] Sathaporn Opasanon and Elise Miller-Hooks. Multicriteria adaptive paths in stochastic, time-varying networks. *European Journal of Operational Research*, 173(1):72–91, 2006. [cited on p. 36, 37 and 38]

[OP16] Tugcem Oral and Faruk Polat. MOD* Lite: An Incremental Path Planning Algorithm Taking Care of Multiple Objectives. *IEEE Transactions on Cybernetics*, 46(1):245–257, 1 2016. [cited on p. 35, 36, 37 and 38]

[ORK14] Bashra K. Oleiwi, Hubert Roth, and Bahaa I. Kazem. Modified Genetic Algorithm based on A* Algorithm of Multi Objective Optimization for Path Planning. *Journal of Automation and Control Engineering*, 2(4):357–362, 2014. [cited on p. 31 and 50]

[Par21] Lukas Partes. *Decision Making for Multi-Objective Pathfinding Problems*. PhD thesis, Otto von Guericke University Magdeburg, 2021. [cited on p. 45 and 105]

[Pat20] Mahesh B. Patil. Improved performance in multi-objective optimization using external archive. *Sādhanā*, 45(1):70, 12 2020. [cited on p. 89]

[PMPDLC15] Francisco-Javier Javier Pulido, Lawrence Mandow, and José-Luis Luis Pérez-De-La-Cruz. Dimensionality reduction in multiobjective shortest path search. *Computers & Operations Research*, 64:60–70, 7 2015. [cited on p. 21, 36, 37, 38 and 40]

[PMS19] Trinadh Pamulapati, Rammohan Mallipeddi, and Ponnuthurai Nagaratnam Suganthan. ISDE+ - An Indicator for Multi and Many-Objective Optimization. *IEEE Transactions on Evolutionary Computation*, 23(2):346–352, 4 2019. [cited on p. 55]

[PSLR13] Diego Perez, Spyridon Samothrakis, Simon Lucas, and Philipp Rohlfshagen. Rolling horizon evolution versus tree search for navigation in single-player real-time games. In *Proceeding of the fifteenth annual conference on Genetic and evolutionary computation conference - GECCO '13*, page 351, New York, New York, USA, 2013. ACM Press. [cited on p. 110 and 130]

[PY00] C.H. Papadimitriou and Mihalis Yannakakis. On the approximability of trade-offs and optimal access of Web sources. In *Proceedings 41st Annual Symposium on Foundations of Computer Science*, pages 86–92. IEEE Comput. Soc, 2000. [cited on p. 18]

[QL16] Zhang Qiongbing and Ding Lixin. A new crossover mechanism for genetic algorithms with variable-length chromosomes for path optimization problems. *Expert Systems with Applications*, 60:183–189, 10 2016. [cited on p. 40]

[QXA13] Hong Qu, Ke Xing, and Takacs Alexander. An improved genetic algorithm with co-evolutionary strategy for global path planning of multiple mobile robots. *Neurocomputing*, 120:509–517, 11 2013. [cited on p. 41]

[QYS21] Jie Qi, Hui Yang, and Haixin Sun. MOD-RRT*: A Sampling-Based Algorithm for Robot Path Planning in Dynamic Environment. *IEEE Transactions on Industrial Electronics*, 68(8):7244–7251, 8 2021. [cited on p. 35, 36, 37, 38 and 39]

[RA15] Jamil Razmak and Belaid Aouni. Decision Support System and Multi-Criteria Decision Aid: A State of the Art and Perspectives. *Journal of Multi-Criteria Decision Analysis*, 22(1-2):101–117, 1 2015. [cited on p. 45]

[RADG17] Matthew L. Ryerkerk, Ronald C. Averill, Kalyanmoy Deb, and Erik D. Goodman. Solving metameric variable-length optimization problems using genetic algorithms. *Genetic*

Programming and Evolvable Machines, 18(2):247–277, June 2017. [cited on p. 66]

[RADG19] Matt Ryerkerk, Ron Averill, Kalyanmoy Deb, and Erik Goodman. A survey of evolutionary algorithms using metameric representations. *Genetic Programming and Evolvable Machines*, 20(4):441–478, December 2019. [cited on p. 66]

[RBSMBA15a] Mojtaba Rajabi-Bahaabadi, Afshin Shariat-Mohaymany, Mohsen Babaei, and Chang Wook Ahn. Multi-objective path finding in stochastic time-dependent road networks using non-dominated sorting genetic algorithm. *Expert Systems with Applications*, 42(12):5056–5064, 2015. [cited on p. 36, 37, 38 and 39]

[RBSMBA15b] Mojtaba Rajabi-Bahaabadi, Afshin Shariat-Mohaymany, Mohsen Babaei, and Chang Wook Ahn. Multi-objective path finding in stochastic time-dependent road networks using non-dominated sorting genetic algorithm. *Expert Systems with Applications*, 42(12):5056–5064, 7 2015. [cited on p. 40]

[RE09] Andrea Raith and Matthias Ehrgott. A comparison of solution strategies for biobjective shortest path problems. *Computers & Operations Research*, 36(4):1299–1331, 4 2009. [cited on p. 21]

[RMC+08] Jeffrey N. Rouder, R. D. Morey, Nelson Cowan, Christopher E. Zwilling, Candice C. Morey, and Michael S. Pratte. An assessment of fixed-capacity models of visual working memory. *Proceedings of the National Academy of Sciences*, 105(16):5975–5979, 4 2008. [cited on p. 105]

[RMHS17] Mohammad Saiedur Rahaman, Yi Mei, Margaret Hamilton, and Flora D. Salim. CAPRA: A contour-based accessible path routing algorithm. *Information Sciences*, 385-386:157–173, 4 2017. [cited on p. 42 and 43]

[RN10] Marko A. Rodriguez and Peter Neubauer. Constructions from dots and lines. *Bulletin of the American Society for Information Science and Technology*, 36(6):35–41, 8 2010. [cited on p. 21]

[Rou87] Peter J. Rousseeuw. Silhouettes: A graphical aid to the interpretation and validation of cluster analysis. *Journal of Computational and Applied Mathematics*, 20(C):53–65, 11 1987. [cited on p. 28]

[RSIS09] Tapabrata Ray, Hemant Kumar Singh, Amitay Isaacs, and Warren Smith. Infeasibility Driven Evolutionary Algorithm for Constrained Optimization. In *Studies in Computational Intelligence*, volume 198, pages 145–165. 2009. [cited on p. 39]

[Saa08] Thomas L. Saaty. Decision making with the analytic hierarchy process. *International Journal of Services Sciences*, 1(1):83, 2008. [cited on p. 46]

[Sab66] Gert Sabidussi. The centrality index of a graph. *Psychometrika*, 31(4):581–603, 1966. [cited on p. 13]

[Shi12] Ofer M. Shir. Niching in Evolutionary Algorithms. In *Handbook of Natural Computing*, volume 1-4, pages 1035–1069. Springer Berlin Heidelberg, Berlin, Heidelberg, 2012. [cited on p. 41 and 83]

[SHR96] Anja Struyf, Mia Hubert, and Peter Rousseeuw. Clustering in an Object-Oriented Environment. *Journal of Statistical Software*, 1(4):1–30, 1996. [cited on p. 106 and 113]

[SK21] Egor Smirnov and Sergei Kudinov. Using a Genetic Algorithm for Planning Interesting Tourist Routes in the City on the Basis of Open Street Map Data. In *2021 IEEE Congress on Evolutionary Computation (CEC)*, pages 264–271. IEEE, 6 2021. [cited on p. 43]

[SKB07] E. Sriraghavendra, Karthik K., and Chiranjib Bhattacharyya. Fréchet Distance Based Approach for Searching Online Handwritten Documents. In *Ninth International Conference on Document Analysis and Recognition (ICDAR 2007)*, volume 1, pages 461–465, Curitiba, Paraná, Brazil, 9 2007. IEEE. [cited on p. 23 and 84]

[SM13] Peter Sanders and Lawrence Mandow. Parallel Label-Setting Multi-objective Shortest Path Search. In *2013 IEEE 27th International Symposium on Parallel and Distributed Processing*, pages 215–224. IEEE, 5 2013. [cited on p. 31]

[SnC19] Antonio Sedeño-noda and Marcos Colebrook. A biobjective Dijkstra algorithm. *European Journal of Operational Research*, 276(1):106–118, 7 2019. [cited on p. 31]

[SPNE09] Ofer M. Shir, Mike Preuss, Boris Naujoks, and Michael Emmerich. Enhancing Decision Space Diversity in Evolutionary Multiobjective Algorithms. In *Lecture Notes in Computer Science (including subseries Lecture Notes in Artificial Intelligence and Lecture Notes in Bioinformatics)*, volume 5467 LNCS, pages 95–109. 2009. [cited on p. 84]

[SSBK21] Jiri Stastny, Vladislav Skorpil, Zoltan Balogh, and Richard Klein. Job Shop Scheduling Problem Optimization by Means of Graph-Based Algorithm. *Applied Sciences*, 11(4):1921, 2 2021. [cited on p. 43]

[SSF+19] Roni Stern, Nathan R Sturtevant, Ariel Felner, Sven Koenig, Hang Ma, Thayne T Walker, Jiaoyang Li, Dor Atzmon, Liron Cohen, T. K. Satish Kumar, Eli Boyarski, Roman Bartak, Roman Bart, Roman Bartak, T K Satish Kumar, Eli Boyarski, and Roman Barták. Multi-Agent Pathfinding: Definitions, Variants, and Benchmarks. (SoCS):151–158, 6 2019. [cited on p. 48]

[Stu12] Nathan R. Sturtevant. Benchmarks for Grid-Based Pathfinding. *IEEE Transactions on Computational Intelligence and AI in Games*, 4(2):144–148, 2012. [cited on p. 40 and 44]

[Suu74] J. W. Suurballe. Disjoint paths in a network. *Networks*, 4(2):125–145, 1974. [cited on p. 67]

[TI20] Ryoji Tanabe and Hisao Ishibuchi. An Analysis of Quality Indicators Using Approximated Optimal Distributions in a 3-D Objective Space. *IEEE Transactions on Evolutionary Computation*, 24(5):853–867, 10 2020. [cited on p. 23]

[TMS17] Bentz Tozer, Thomas Mazzuchi, and Shahram Sarkani. Many-objective stochastic path finding using reinforcement learning. *Expert Systems with Applications*, 72:371–382, 4 2017. [cited on p. 36, 37, 38, 40, 43 and 44]

[Tri00] Evangelos Triantaphyllou. *Multi-criteria Decision Making Methods: A Comparative Study*, volume 44 of *Applied Optimization*. Springer US, Boston, MA, 2000. [cited on p. 46]

[TSKK19] Pang-Ning Tan, Michael Steinbach, Anuj Karpatne, and Vipin Kumar. *Introduction to data mining*. Pearson Education, Harlow, second edi edition, 2019. [cited on p. 27]

[TY12] Adem Tuncer and Mehmet Yildirim. Dynamic path planning of mobile robots with improved genetic algorithm. *Computers and Electrical Engineering*, 38(6):1564–1572, 11 2012. [cited on p. 55]

[UBZ10] Tamara Ulrich, Johannes Bader, and Eckart Zitzler. Integrating decision space diversity into hypervolume-based multiobjective search. In *Proceedings of the 12th annual conference on Genetic and evolutionary computation - GECCO '10*, page 455, New York, New York, USA, 2010. ACM Press. [cited on p. 84]

[Wak02] Kazuyoshi Wakuta. A multi-objective shortest path problem. *Mathematical Methods of Operations Research*, 54(3):445–454, 2002. [cited on p. 36, 37 and 38]

[Wei37] Endre Weiszfeld. Sur le point pour lequel la Somme des distances de n points donnés est minimum. *Tohoku Mathematical Journal, First Series*, 43:355–386, 1937. [cited on p. 91]

[WHBH06a] Lyndon While, Phil Hingston, Luigi Barone, and Simon Huband. A faster algorithm for calculating hypervolume. *IEEE Transactions on Evolutionary Computation*, 10(1):29–38, 2006. [cited on p. 19]

[WHBH06b] Lyndon While, Philip Hingston, Luigi Barone, and Simon Huband. A faster algorithm for calculating hypervolume. *IEEE Transactions on Evolutionary Computation*, 10(1):29–38, 2006. [cited on p. 72]

[Wil10a] E.A.B.S.G. Williamson. *Lists, Decisions and Graphs*. S. Gill Williamson, 2010. [cited on p. 12]

[Wil10b] R J Wilson. *Introduction to Graph Theory*. Longman, 2010. [cited on p. 11]

[WM97] D.H. Wolpert and W.G. Macready. No free lunch theorems for optimization. *IEEE Transactions on Evolutionary Computation*, 1(1):67–82, April 1997. Conference Name: IEEE Transactions on Evolutionary Computation. [cited on p. 43]

[WYMW19] Yishu Wang, Ye Yuan, Yuliang Ma, and Guoren Wang. Time-Dependent Graphs: Definitions, Applications, and Algorithms. *Data Science and Engineering*, 4(4):352–366, 12 2019. [cited on p. 31]

[XS18] Yang Xue and Jian-Qiao Sun. Solving the Path Planning Problem in Mobile Robotics with the Multi-Objective Evolutionary Algorithm. *Applied Sciences*, 8(9):1425, 8 2018. [cited on p. 31, 36, 37, 38, 39 and 42]

[Yap02] Peter Yap. Grid-Based Path-Finding. In *Lecture Notes in Computer Science (including subseries Lecture Notes in Artificial Intelligence and Lecture Notes in Bioinformatics)*, volume 2338, pages 44–55. 2002. [cited on p. 40]

[YBH15] Konstantin Yakovlev, Egor Baskin, and Ivan Hramoin. Grid-Based Angle-Constrained Path Planning. In *Lecture Notes in Computer Science (including subseries Lecture Notes in Artificial Intelligence and Lecture Notes in Bioinformatics)*, volume 9324, pages 208–221. 2015. [cited on p. 40]

[Yen70] Jin Y. Yen. An algorithm for finding shortest routes from all source nodes to a given destination in general networks. *Quarterly of Applied Mathematics*, 27(4):526–530, 1 1970. [cited on p. 67]

[ZCS04] Zhaowang Ji, Anthony Chen, and Kitti Subprasom. Finding multi-objective paths in stochastic networks: a simulation-based genetic algorithm approach. In *Proceedings of the 2004 Congress on Evolutionary Computation (IEEE Cat. No.04TH8753)*, pages 174–180. IEEE, 2004. [cited on p. 36, 37, 38, 39 and 42]

[ZGZ13] Yong Zhang, Dun-wei Wei Gong, and Jian-hua Hua Zhang. Robot path planning in uncertain environment using multi-objective particle swarm optimization. *Neurocomputing*, 103:172–185, 3 2013. [cited on p. 36, 37, 38, 39 and 42]

[ZH21] Sandra Zajac and Sandra Huber. Objectives and methods in multi-objective routing problems: a survey and classification scheme. *European Journal of Operational Research*, 290(1):1–25, 4 2021. [cited on p. 20]

[Zil19] Heiner Zille. *Large-scale multi-objective optimisation: new approaches and a classification of the state-of-the-art*. PhD thesis, Otto-von-Guericke-Universitaet Magdeburg, Fakultaet für Informatik, 2019. [cited on p. 72]

[ZIMN16a] Heiner Zille, Hisao Ishibuchi, Sanaz Mostaghim, and Yusuke Nojima. Mutation operators based on variable grouping for multi-objective large-scale optimization. In *IEEE Symposium*

Series on Computational Intelligence (SSCI), pages 1–8, Dec 2016. [cited on p. 71]

[ZIMN16b] Heiner Zille, Hisao Ishibuchi, Sanaz Mostaghim, and Yusuke Nojima. Weighted optimization framework for large-scale multi-objective optimization. In *ACM Genetic and Evolutionary Computation Conference (GECCO) Companion*, pages 83–84. ACM, 2016. [cited on p. 72]

[ZIMN18] Heiner Zille, Hisao Ishibuchi, Sanaz Mostaghim, and Yusuke Nojima. A framework for large-scale multi-objective optimization based on problem transformation. *IEEE Transactions on Evolutionary Computation*, 22(2):260–275, April 2018. [cited on p. 72]

[ZJWW10] Yudong Zhang, Yan Jun, Geng Wei, and Lenan Wu. Find multi-objective paths in stochastic networks via chaotic immune PSO. *Expert Systems with Applications*, 37(3):1911–1919, 2010. [cited on p. 36, 37, 38, 39 and 41]

[ZM17] Heiner Zille and Sanaz Mostaghim. Comparison study of large-scale optimisation techniques on the LSMOP benchmark functions. In *IEEE Symposium Series on Computational Intelligence (SSCI)*, pages 1–8, November 2017. [cited on p. 72]

[ZM19] Heiner Zille and Sanaz Mostaghim. Linear search mechanism for multi- and many-objective optimisation. In Kalyanmoy Deb, Erik Goodman, Carlos A. Coello Coello, Kathrin Klamroth, Kaisa Miettinen, Sanaz Mostaghim, and Patrick Reed, editors, *Evolutionary Multi-Criterion Optimization*, pages 399–410, Cham, 2019. Springer International Publishing. [cited on p. 72]

[ZT98] Eckart Zitzler and Lothar Thiele. Multiobjective optimization using evolutionary algorithms - A comparative case study. *Lecture Notes in Computer Science (including subseries Lecture Notes in Artificial Intelligence and Lecture Notes in Bioinformatics)*, 1498 LNCS(September):292–301, 1998. [cited on p. 25]

[ZT99] Eckart Zitzler and Lothar Thiele. Multiobjective evolutionary algorithms: a comparative case study and the strength pareto approach. *IEEE Transactions on Evolutionary Computation*, 3(4):257–271, 1999. [cited on p. 72]

[ZXL+15] Zexuan Zhu, Jun Xiao, Jian-Qiang Li, Fangxiao Wang, and Qingfu Zhang. Global path planning of wheeled robots using multi-objective memetic algorithms. *Integrated Computer-Aided Engineering*, 22(4):387–404, 8 2015. [cited on p. 36, 37, 38, 39, 41 and 42]

[ZZN+19] Haitong Zhao, Changsheng Zhang, Jiaxu Ning, Bin Zhang, Peng Sun, and Yunfei Feng. A comparative study of the evolutionary many-objective algorithms. *Progress in Artificial Intelligence*, 8(1):15–43, 4 2019. [cited on p. 18 and 19]

Author's Publications

[CSS+21] Victor Charpenay, Daniel Schraudner, Thomas Seidelmann, Torsten Spieldenner, Jens Weise, Rene Schubotz, Sanaz Mostaghim, and Andreas Harth. MOSAIK: A Formal Model for Self-Organizing Manufacturing Systems. *IEEE Pervasive Computing*, 20(1):9–18, 1 2021.

[SWM21] Thomas Seidelmann, Jens Weise, and Sanaz Mostaghim. Meeting Demands for Mass Customization: A Hybrid Organic Computing Approach. In *2021 IEEE Symposium Series on Computational Intelligence (SSCI)*, pages 1–8, Orlando, Florida, USA, 12 2021. IEEE.

[WBM18] Jens Weise, Steven Benkhardt, and Sanaz Mostaghim. A Survey on Graph-based Systems in Manufacturing Processes. In *2018 IEEE Symposium Series on Computational Intelligence (SSCI)*, pages 112–119. IEEE, 11 2018. [cited on p. 6, 12, 40 and 130]

[WBM19] Jens Weise, Steven Benkhardt, and Sanaz Mostaghim. Graph-based multi-objective generation of customised wiring harnesses. In *Proceedings of the Genetic and Evolutionary Computation Conference Companion*, pages 407–408, New York, NY, USA, 7 2019. ACM. [cited on p. 6]

[WM20] Jens Weise and Sanaz Mostaghim. A many-objective route planning benchmark problem for navigation. In *Proceedings of the 2020 Genetic and Evolutionary Computation Conference Companion*, GECCO '20, pages 183–184, New York, NY, USA, 7 2020. ACM. [cited on p. 81 and 82]

[WM21a] Jens Weise and Sanaz Mostaghim. A Customized Niching Methodology for the Many-Objective Pathfinding Problem. In *2021 IEEE Symposium Series on Computational Intelligence (SSCI)*, pages 1–8, Orlando, Florida, USA, 12 2021. IEEE. [cited on p. 81, 83, 90, 91, 92, 93, 99, 100, 101 and 102]

[WM21b] Jens Weise and Sanaz Mostaghim. Many-Objective Pathfinding Based on Fréchet Similarity Metric. In *11th International*

Conference, EMO 2021, Shenzhen, China, March 28-31, 2021, Proceedings, number 01, pages 375–386. 2021. [cited on p. 23, 40, 42, 81, 84, 85, 88, 89, 92, 93, 94, 95, 99, 100, 101, 102, XCII, XCIII, XCIV, XCV, XCVI, XCVII, XCVIII and XCIX]

[WM22a] Jens Weise and Sanaz Mostaghim. A comparison of distance metrics for the multi-objective pathfinding problem. *Natural Computing*, 8 2022. [cited on p. 81, 84, 86, 87, 88, 89, 96, 97, 98, 102, 103 and 104]

[WM22b] Jens Weise and Sanaz Mostaghim. A Scalable Many-Objective Pathfinding Benchmark Suite. *IEEE Transactions on Evolutionary Computation*, 26(1):188–194, 2 2022. [cited on p. 40, 42, 44, 47, 48, 49, 50, 51, 52, 53, 54, 55, 56, 57, 58, 59, 60, 63, 65, 71, 72, 73, 83, 88, 95, 98, 99, 102, L, LI, LII, LIII and LIV]

[WMZM20] Jens Weise, Sebastian Mai, Heiner Zille, and Sanaz Mostaghim. On the Scalable Multi-Objective Multi-Agent Pathfinding Problem. In *2020 IEEE Congress on Evolutionary Computation (CEC)*, pages 1–8, Glasgow, UK, 7 2020. IEEE. [cited on p. 20]

[WZM21] Jens Weise, Heiner Zille, and Sanaz Mostaghim. A Comparative Study of Different Encodings on the Multi-Objective Pathfinding Problem. In *2021 IEEE Symposium Series on Computational Intelligence (SSCI)*, pages 1–8, Orlando, Florida, USA, 12 2021. IEEE. [cited on p. 63, 64, 65, 71, 72, 73, 74, 75 and 76]

Table of Abbreviations

MaOPF	Many-Objective (Single-Path) Pathfinding Problem	6
DM	decision-maker	3
GBS	graph-based system	12
SPP	shortest path problem	13
DTW	dynamic time warping	23
RPC	random point connection	
KSPF	k-shortest path finding	67
EMO	evolutionary multi-objective optimisation	81
EA	evolutionary algorithm	4
MOO	multi-objective optimisation	
MOP	multi-objective problem	16
PNM	Perimeter Mutation Operator	82
CD	crowding distance	83
RDPA	Ramer-Douglas–Peucker algorithm	69
PI	performance indicator	8
IGD	inverted generational distance	24
IGDX	inverted generational distance X	25
IGD^+	inverted generational distance$^+$	
HV	hypervolume	25
V	Variable chromosome length	
F	Fixed chromosome length	
UAV	unmanned aerial vehicle	32
LRP	location routing problem	20
VRP	vehicle routing problem	20
SPP	shortest path problem	20
LPP	longest path problem	

CPP	coverage path planning	20
MoMAPF	multi-objective multi-agent pathfinding problem	20
MCDM	multi-criteria decision making	26
ISG	initial solution generation	
IQR	interquartile range	
N/A	not applicable	
PF	Pareto-front	17
PS	Pareto-set	17
DP	decision point	8
GA	genetic algorithm	14
OSM	OpenStreetMap	56

List of Tables

List of Figures

List of Symbols

κ	Number of clusters
G	A Graph
V	The graph's set of nodes
E	The graph's set of edges
n	Node in a graph or on a path
ϕ	A function mapping every edge to a ordered pair of nodes
μ	Number of solutions in a population
Ω	Decision Space
m	Number of objectives
$\mathscr{M}$	Objective Space
P	Set of paths
A	A set of agents, or moving entities
p	Path of arbitrary length (general-notation)
$\vec{f}$	Vector of objective functions
$\iota_V(\mathfrak{P})$	A function assigning a set of properties to a set of nodes
$\mathfrak{P}$	Set of Properties
$\iota_E(\mathfrak{P})$	A function assigning a set of properties to a set of edge
n_s	Start node of a pathfinding problem
n_e	End node of a pathfinding problem
I	Performance Indicator
δ_{dF}	Discrete Fréchet distance
δ_{dtw}	Dynamic Time Warping distance
δ_{Hd}	Hausdorff distance
i	Object in a cluster
C	Cluster
ρ	Graph density
G_U	Undirected Graph
G_D	Directed Graph
$\mathbb{P}_c$	Crossover probability
$\mathbb{P}_m$	Mutation probability
δ	Chromosome enlargement factor

deg^+	Outgoing node degree
deg^-	Ingoing node degree
deg	Node degree (undirected graph)
$\mathbb{M}$	An arbitrary space
δ_{DM}	Distance between two curves, $\delta_{DM} \in \{\delta_{dF}, \delta_{Hd}, \delta_{dtw}\}$
δ_F	Fréchet distance

A Benchmark Results

A.1 Benchmark

A.1.1 Data sets and Code

To enable researchers to use the proposed benchmark, we also publish the code to generate different benchmark instances and the obtained true Pareto-fronts and sets. Everything can be downloaded here: https://ci.ovgu.de/Publications/TEVC_WM_2020-p-910.html. We used Java and the jMetal framework in version 6 [NDV15]. However, the code enables researchers to create different grids and export them as a *csv-file* to import it in other software or to use other programming languages. The codes also contain a readme file.

A.1.2 Extended Result Figures of Test Problems

In this section, the results of several test instances are shown. We show the IGD^+ values with respect to the instance type and size. Furthermore, we present the paths, as well as the objective values of the Pareto-optimal solutions for specific instances.

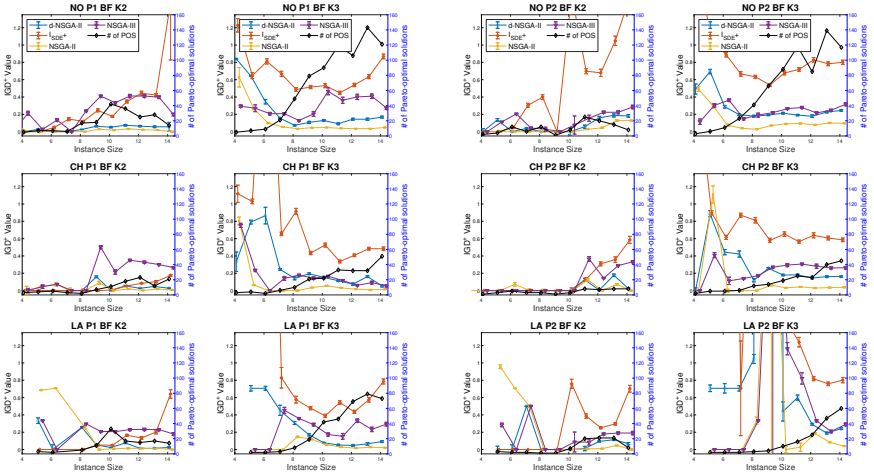

(a) IGD^+ Values for all P1 instances

(b) IGD^+ Values for all P2 instances

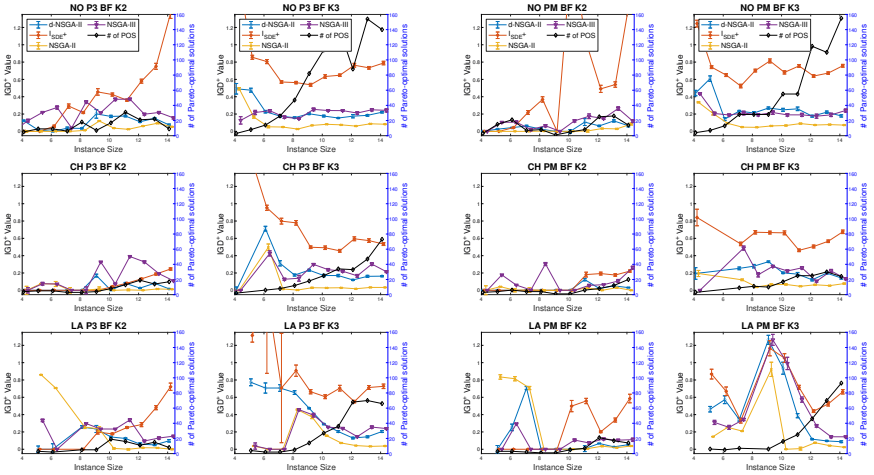

(c) IGD^+ Values for all P3 instances

(d) IGD^+ Values for all PM instances

Figure A.1: The obtained IGD^+ values with respect to the different type, ordered by instance size [WM22b]

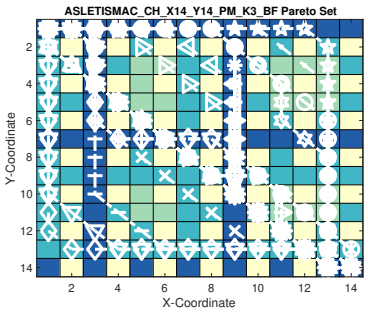

(a) Pareto-set of instance CH_X14_Y14_PM_K3_BF

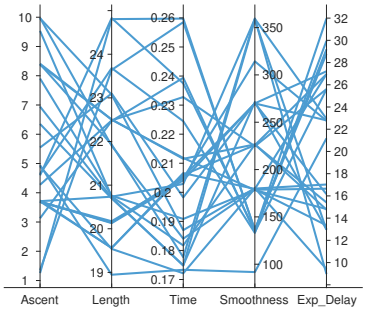

(b) Pareto-Front of instance CH_X14_Y14_PM_K3_BF

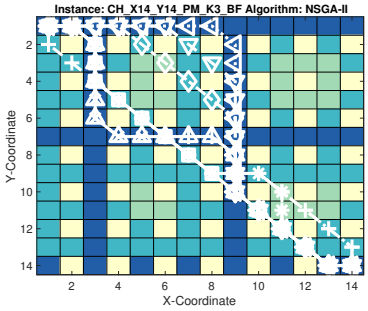

(c) Result set of algorithm NSGA-II

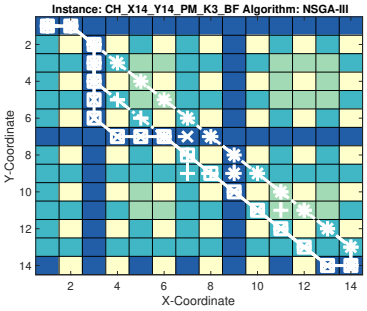

(d) Result set of algorithm NSGA-III

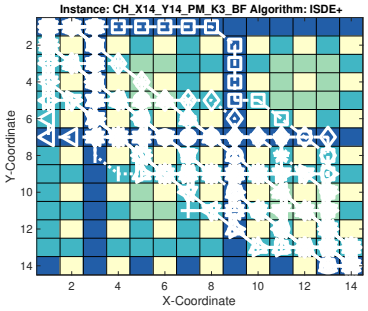

(e) Result set of algorithm $I_{SDE}+$

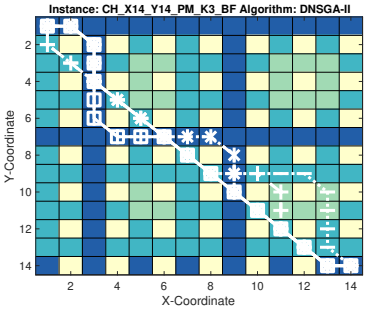

(f) Result set of algorithm D-NSGA-II

Figure A.2: Pareto-set and front of instance CH_X14_Y14_PM_K3_BF and result sets of all algorithm (median run with respect to IGD^+ value) [WM22b]

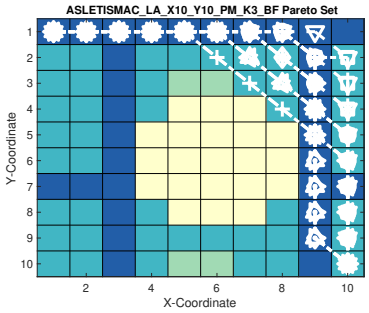

(a) Pareto-set of instance LA_X10_Y10_PM_K3_BF

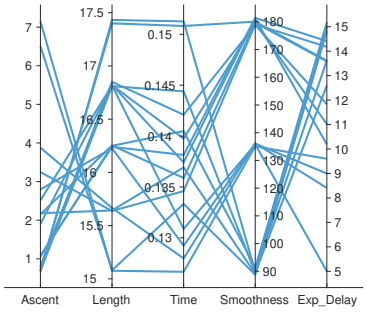

(b) Pareto-Front of instance LA_X10_Y10_PM_K3_BF

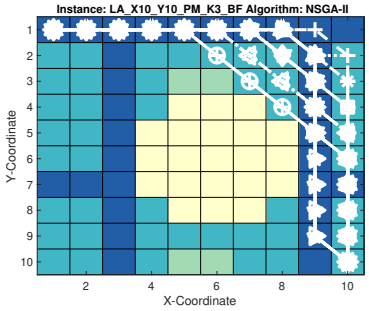

(c) Result set of algorithm NSGA-II

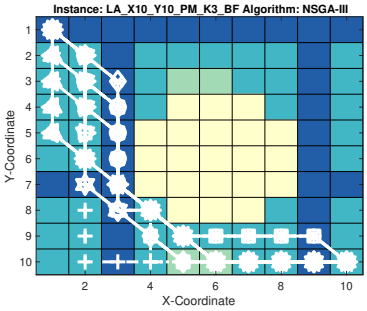

(d) Result set of algorithm NSGA-III

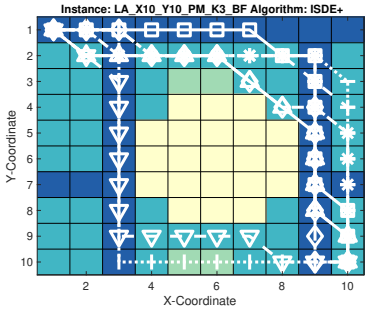

(e) Result set of algorithm $I_{SDE}+$

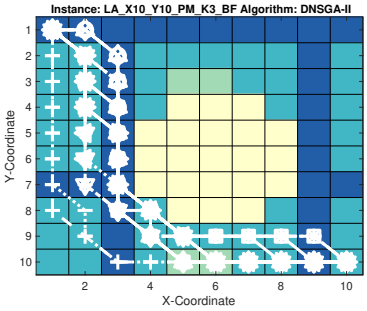

(f) Result set of algorithm D-NSGA-II

Figure A.3: Pareto-set and front of instance LA_X10_Y10_PM_K3_BF and result sets of all algorithm (median run with respect to IGD^+ value) [WM22b]

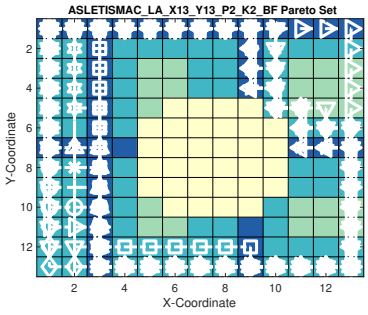

(a) Pareto-set of instance LA_X13_Y13_P2_K2_BF

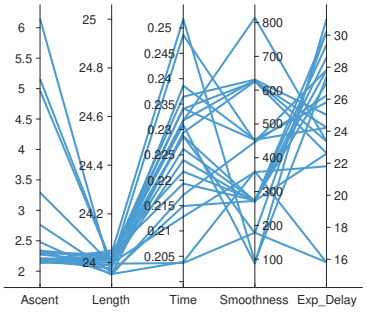

(b) Pareto-Front of instance LA_X13_Y13_P2_K2_BF

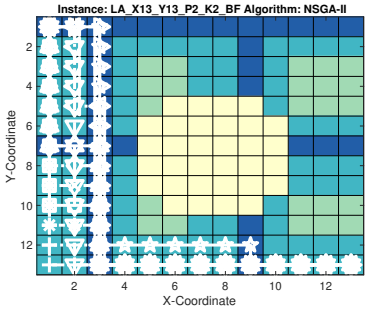

(c) Result set of algorithm NSGA-II

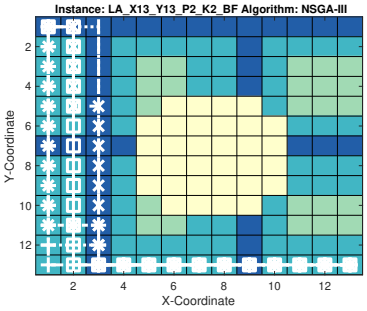

(d) Result set of algorithm NSGA-III

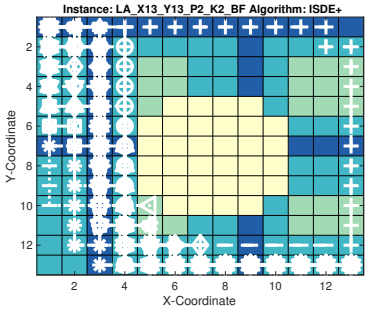

(e) Result set of algorithm $I_{SDE}+$

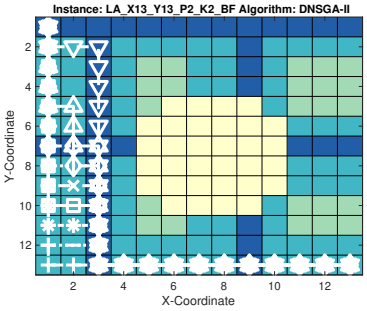

(f) Result set of algorithm D-NSGA-II

Figure A.4: Pareto-set and front of instance LA_X13_Y13_P2_K2_BF and result sets of all algorithm (median run with respect to IGD^+ value) [WM22b]

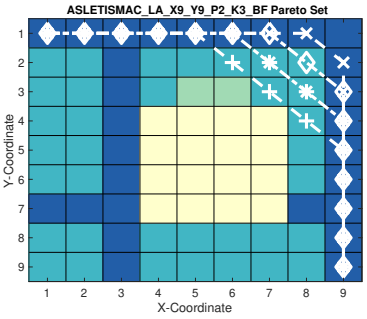

(a) Pareto-set of instance LA_X9_Y9_P2_K3_BF

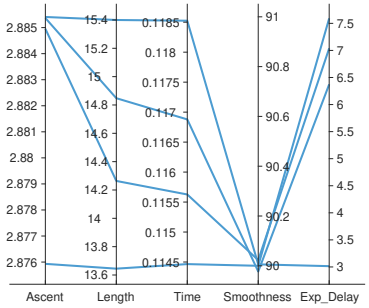

(b) Pareto-Front of instance LA_X9_Y9_P2_K3_BF

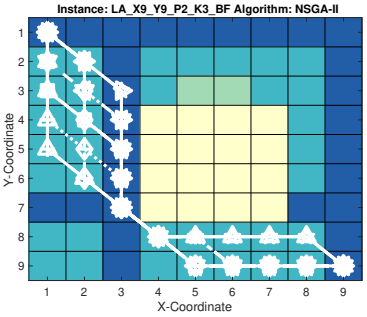

(c) Result set of algorithm NSGA-II

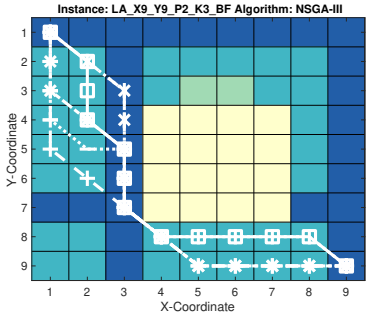

(d) Result set of algorithm NSGA-III

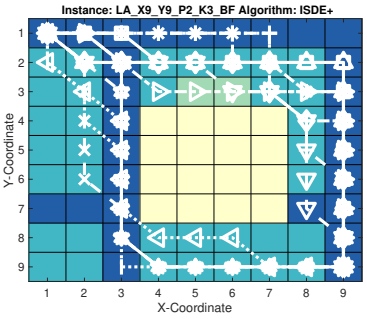

(e) Result set of algorithm $I_{SDE}+$

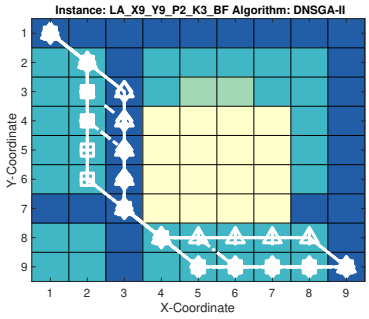

(f) Result set of algorithm D-NSGA-II

Figure A.5: Pareto-set and front of instance LA_X9_Y9_P2_K3_BF and result sets of all algorithm (median run with respect to IGD^+ value) [WM22b]

A.2 Online Appendix

To save trees and the environment, the raw experiment results and values can be found online at: https://ci.ovgu.de/Publications/PhD+Thesis+Jens+Weise+Online+Appendix.html. The QR-Code in Figure A.6 also points to the given URL.

Figure A.6: QR-Code pointing to the online appendix

B Raw Experiment Results

B.1 Details Benchmark Results

B.1.1 IGD$^+$ Values

Instance Name	d-NSGA-II	$I_{SDE}+$	NSGA-II	NSGA-III
CH_X10_Y10_P1_K2_BF	0.0018	0.0083	0	0.22
IQR	0-0.045	0.00077-0.036	0-0	0.12-0.38
CH_X10_Y10_P1_K3_BF	0.15	0.53	0.055	0.17
IQR	0.12-0.2	0.44-0.58	0.028-0.063	0.14-0.2
CH_X10_Y10_P2_K2_BF	0	8.1e-16	0	8.1e-16
IQR	0-0	0-0.24	0-0	2e-16-8.1e-16
CH_X10_Y10_P2_K3_BF	0.18	0.65	0.032	0.29
IQR	0.15-0.23	0.55-0.69	0.027-0.048	0.28-0.41
CH_X10_Y10_P3_K2_BF	0	0.042	0	0.075
IQR	0-1.1e-16	6.3e-05-0.043	0-0	0.075-0.075
CH_X10_Y10_P3_K3_BF	0.17	0.49	0.028	0.24
IQR	0.13-0.24	0.42-0.57	0.017-0.042	0.19-0.29
CH_X10_Y10_PM_K2_BF	0	0	0	0
IQR	0-0	0-0	0-0	0-0
CH_X10_Y10_PM_K3_BF	0.2	0.66	0.068	0.22
IQR	0.18-0.22	0.56-0.73	0.027-0.081	0.19-0.28
CH_X11_Y11_P1_K2_BF	0.054	0.053	0.018	0.35
IQR	0.047-0.067	0.034-0.064	0.013-0.031	0.32-0.39
CH_X11_Y11_P1_K3_BF	0.11	0.34	0.031	0.12
IQR	0.098-0.16	0.29-0.42	0.018-0.033	0.11-0.15
CH_X11_Y11_P2_K2_BF	0.12	0.13	0.12	0.37
IQR	0.022-0.19	0.076-0.19	0.018-0.12	0.2-0.48
CH_X11_Y11_P2_K3_BF	0.18	0.57	0.043	0.31
IQR	0.15-0.22	0.5-0.64	0.029-0.059	0.26-0.32
CH_X11_Y11_P3_K2_BF	0.08	0.082	0.0049	0.39
IQR	0.073-0.11	0.057-0.11	0-0.025	0.37-0.41
CH_X11_Y11_P3_K3_BF	0.17	0.46	0.03	0.22
IQR	0.13-0.21	0.42-0.56	0.027-0.038	0.19-0.3
CH_X11_Y11_PM_K2_BF	0.12	0.18	0.029	0.057
IQR	0.083-0.24	0.091-0.27	0.029-0.029	0.057-0.14
CH_X11_Y11_PM_K3_BF	0.19	0.46	0.046	0.26
IQR	0.17-0.24	0.42-0.52	0.042-0.052	0.22-0.28
CH_X12_Y12_P1_K2_BF	0.026	0.084	0.0016	0.33
IQR	0.02-0.028	0.068-0.11	0-0.0072	0.27-0.35
CH_X12_Y12_P1_K3_BF	0.074	0.41	0.017	0.061
IQR	0.042-0.17	0.35-0.45	0.016-0.03	0.04-0.091
CH_X12_Y12_P2_K2_BF	0.0058	0.31	0	0.14
IQR	0-0.065	0.23-0.42	0-0.0058	0.14-0.15
CH_X12_Y12_P2_K3_BF	0.15	0.64	0.029	0.28
IQR	0.1-0.17	0.52-0.74	0.022-0.039	0.17-0.38
CH_X12_Y12_P3_K2_BF	0.026	0.13	0	0.33

Instance Name	d-NSGA-II	$I_{SDE}+$	NSGA-II	NSGA-III
IQR	0.012-0.037	0.099-0.17	0-0	0.26-0.34
CH_X12_Y12_P3_K3_BF	0.12	0.59	0.018	0.17
IQR	0.089-0.15	0.53-0.67	0.013-0.021	0.13-0.27
CH_X12_Y12_PM_K2_BF	0.021	0.19	0	0.065
IQR	0-0.031	0.13-0.28	0-0	0.065-0.066
CH_X12_Y12_PM_K3_BF	0.12	0.51	0.064	0.11
IQR	0.11-0.17	0.43-0.6	0.062-0.071	0.094-0.13
CH_X13_Y13_P1_K2_BF	0.048	0.1	0.018	0.3
IQR	0.048-0.057	0.077-0.19	0.014-0.047	0.25-0.3
CH_X13_Y13_P1_K3_BF	0.16	0.48	0.009	0.092
IQR	0.12-0.19	0.43-0.56	0.009-0.018	0.083-0.23
CH_X13_Y13_P2_K2_BF	0.18	0.36	0.072	0.29
IQR	0.093-0.19	0.31-0.45	0.016-0.1	0.29-0.29
CH_X13_Y13_P2_K3_BF	0.16	0.61	0.035	0.26
IQR	0.14-0.22	0.48-0.65	0.02-0.043	0.22-0.33
CH_X13_Y13_P3_K2_BF	0.082	0.19	0.016	0.19
IQR	0.061-0.1	0.14-0.21	0.0093-0.029	0.19-0.22
CH_X13_Y13_P3_K3_BF	0.16	0.57	0.033	0.3
IQR	0.13-0.2	0.52-0.65	0.014-0.034	0.27-0.33
CH_X13_Y13_PM_K2_BF	0.052	0.18	0.03	0.11
IQR	0.052-0.091	0.09-0.22	0.0045-0.047	0.11-0.28
CH_X13_Y13_PM_K3_BF	0.2	0.57	0.054	0.22
IQR	0.13-0.22	0.5-0.61	0.045-0.062	0.18-0.32
CH_X14_Y14_P1_K2_BF	0.026	0.18	0.0079	0.27
IQR	0.012-0.039	0.15-0.22	0.0079-0.0079	0.24-0.29
CH_X14_Y14_P1_K3_BF	0.054	0.48	0.015	0.053
IQR	0.031-0.12	0.37-0.54	0.012-0.018	0.035-0.07
CH_X14_Y14_P2_K2_BF	0.024	0.59	0	0.33
IQR	0-0.08	0.43-0.74	0-0	0.33-0.36
CH_X14_Y14_P2_K3_BF	0.16	0.59	0.038	0.26
IQR	0.14-0.2	0.49-0.69	0.027-0.056	0.2-0.31
CH_X14_Y14_P3_K2_BF	0.017	0.25	0.011	0.11
IQR	0.011-0.017	0.21-0.28	0.0069-0.017	0.11-0.11
CH_X14_Y14_P3_K3_BF	0.16	0.53	0.033	0.21
IQR	0.14-0.18	0.47-0.62	0.029-0.04	0.19-0.27
CH_X14_Y14_PM_K2_BF	0.031	0.22	0	0.26
IQR	0.024-0.049	0.17-0.29	0-0	0.12-0.3
CH_X14_Y14_PM_K3_BF	0.14	0.68	0.078	0.13
IQR	0.11-0.21	0.58-0.74	0.07-0.13	0.12-0.16
CH_X3_Y3_P2_K2_BF	0	0	0	0
IQR	0-0	0-0	0-0	0-0
CH_X3_Y3_P2_K3_BF	0	0	0	0
IQR	0-0	0-0	0-0	0-0
CH_X3_Y3_P3_K2_BF	0	0	0	0
IQR	0-0	0-0	0-0	0-0
CH_X3_Y3_P3_K3_BF	0	0	0	0
IQR	0-0	0-0	0-0	0-0
CH_X4_Y4_P1_K2_BF	0	0	0	0
IQR	0-0	0-0	0-0	0-0
CH_X4_Y4_P1_K3_BF	0.33	1.1	0.8	0.75
IQR	0.33-0.8	0.8-1.1	0.45-0.8	0.75-0.75
CH_X4_Y4_P2_K2_BF	0	0	0	0
IQR	0-0	0-0	0-0	0-0
CH_X4_Y4_P2_K3_BF	0	2.4	0	0
IQR	0-0	2.2-2.4	0-0	0-0
CH_X4_Y4_P3_K2_BF	0	0	0	0
IQR	0-0	0-0	0-0	0-0
CH_X4_Y4_P3_K3_BF	0	2	0	0
IQR	0-0	0.71-2.2	0-0	0-0
CH_X4_Y4_PM_K2_BF	0	0	0	0
IQR	0-0	0-0	0-0.54	0-0
CH_X4_Y4_PM_K3_BF	0.19	0.84	0.19	0
IQR	0.19-0.3	0.83-1.2	0-0.19	0-0
CH_X5_Y5_P1_K2_BF	0	0	0.046	0.046
IQR	0-0	0-0	0.046-0.046	0.046-0.28
CH_X5_Y5_P1_K3_BF	0.79	1	0.065	0.24
IQR	0.56-0.79	1-1	0.065-0.065	0.24-0.24
CH_X5_Y5_P2_K2_BF	0	0	0	0
IQR	0-0	0-0	0-0.059	0-0
CH_X5_Y5_P2_K3_BF	0.89	0.9	1.1	0.41
IQR	0.66-0.9	0.88-0.9	0.062-1.2	0.17-0.45
CH_X5_Y5_P3_K2_BF	0	0	0.076	0.076
IQR	0-0	0-0	0.076-0.076	0.076-0.26

Instance Name	d-NSGA-II	$I_{SDE}+$	NSGA-II	NSGA-III
CH_X5_Y5_PM_K2_BF	0	0	0.042	0.18
IQR	0-0	0-0	0.042-0.042	0.18-0.18
CH_X6_Y6_P1_K2_BF	0	0	0.073	0.073
IQR	0-0	0-0	0.073-0.073	0.073-0.073
CH_X6_Y6_P1_K3_BF	0.87	3.8	0	0
IQR	0.87-0.87	3.8-7.5	0-0	0-0
CH_X6_Y6_P2_K2_BF	0	0	0.073	0
IQR	0-0	0-0	0-0.16	0-0
CH_X6_Y6_P2_K3_BF	0.44	0.61	0	0.11
IQR	0.23-0.47	0.52-0.7	0-0.0098	0.0098-0.28
CH_X6_Y6_P3_K2_BF	0	0	0.073	0.073
IQR	0-0	0-0	0-0.34	0.073-0.073
CH_X6_Y6_P3_K3_BF	0.71	0.95	0.5	0.43
IQR	0.5-0.83	0.93-1.2	0.059-0.5	0.099-0.43
CH_X6_Y6_PM_K2_BF	0	0	0	0.06
IQR	0-0	0-0	0-0.081	0.06-0.06
CH_X7_Y7_P1_K2_BF	0	0	4.1e-16	0
IQR	0-0	0-0	4.1e-16-4.1e-16	0-4.1e-16
CH_X7_Y7_P1_K3_BF	0.25	0.66	0	0.14
IQR	0.16-0.25	0.59-0.76	0-0.055	0.055-0.17
CH_X7_Y7_P2_K2_BF	0	0	1.9e-16	1.9e-16
IQR	0-1.9e-16	0-0	1.9e-16-4.1e-16	0-1.9e-16
CH_X7_Y7_P2_K3_BF	0.42	0.87	0	0.14
IQR	0.22-0.62	0.8-0.91	0-0	0.14-0.14
CH_X7_Y7_P3_K2_BF	0	0	4.1e-16	0
IQR	0-0	0-0	1e-16-4.1e-16	0-0
CH_X7_Y7_P3_K3_BF	0.31	0.8	0.015	0.13
IQR	0.26-0.5	0.69-0.86	0.015-0.015	0.13-0.13
CH_X7_Y7_PM_K2_BF	0	0	0.004	0.004
IQR	0-0.11	0-0	0.004-0.004	0.004-0.004
CH_X7_Y7_PM_K3_BF	0.25	0.54	0.12	0.49
IQR	0.23-0.31	0.45-0.56	0.12-0.15	0.28-0.49
CH_X8_Y8_P1_K2_BF	0	0	0	0
IQR	0-0	0-0	0-0	0-0
CH_X8_Y8_P1_K3_BF	0.14	0.92	0	0.18
IQR	0.1-0.17	0.77-0.94	0-0	0.17-0.24
CH_X8_Y8_P2_K2_BF	0	0	4.1e-16	0
IQR	0-0	0-0	0-4.1e-16	0-0
CH_X8_Y8_P2_K3_BF	0.12	0.81	0	0.17
IQR	0.092-0.15	0.66-0.89	0-0	0.14-0.19
CH_X8_Y8_P3_K2_BF	0	0	4.1e-16	4.1e-16
IQR	0-0	0-0	0-4.1e-16	4.1e-16-0.46
CH_X8_Y8_P3_K3_BF	0.18	0.78	0.0029	0.14
IQR	0.16-0.22	0.68-0.88	0.0029-0.0029	0.11-0.17
CH_X8_Y8_PM_K2_BF	0	0	0	0.31
IQR	0-0	0-0	0-0	0.31-0.31
CH_X8_Y8_PM_K3_BF	0.28	0.67	0.038	0.18
IQR	0.23-0.35	0.62-0.75	0.024-0.039	0.14-0.38
CH_X9_Y9_P1_K2_BF	0.16	0	0.089	0.5
IQR	0.089-0.16	0-0.0001	4.8e-17-0.089	0.5-0.5
CH_X9_Y9_P1_K3_BF	0.19	0.43	0.035	0.14
IQR	0.17-0.23	0.36-0.5	0.019-0.044	0.14-0.22
CH_X9_Y9_P2_K2_BF	0	0	0	0
IQR	0-0	0-0	0-0	0-0
CH_X9_Y9_P2_K3_BF	0.26	0.58	0.061	0.27
IQR	0.21-0.29	0.47-0.65	0.032-0.066	0.25-0.3
CH_X9_Y9_P3_K2_BF	0.17	0	0.016	0.33
IQR	0.17-0.31	0-0	0.016-0.19	0.33-0.33
CH_X9_Y9_P3_K3_BF	0.23	0.5	0.03	0.3
IQR	0.19-0.28	0.43-0.56	0.029-0.049	0.25-0.33
CH_X9_Y9_PM_K2_BF	0	0	0	0
IQR	0-0	0-0	0-0	0-0
CH_X9_Y9_PM_K3_BF	0.33	0.67	0.066	0.28
IQR	0.28-0.33	0.61-0.7	0.038-0.12	0.24-0.29
LA_X10_Y10_P1_K2_BF	0.024	0.049	0.0096	0.21
IQR	0.017-0.03	0.034-0.064	0.0096-0.024	0.18-0.25
LA_X10_Y10_P1_K3_BF	0.078	0.39	0.055	0.17
IQR	0.075-0.092	0.31-0.45	0.055-0.059	0.16-0.21
LA_X10_Y10_P2_K2_BF	0	0.76	0	0.087
IQR	0-0	0.42-1	0-0	0.076-0.089
LA_X10_Y10_P2_K3_BF	0.44	1.5	0	1.2
IQR	0.17-1.4	1.3-1.6	0-0	1.1-1.2
LA_X10_Y10_P3_K2_BF	0.14	0.18	0.0099	0.23

Instance Name	d-NSGA-II	$I_{SDE}+$	NSGA-II	NSGA-III
IQR	0.091-0.17	0.13-0.2	0.0031-0.043	0.21-0.25
LA_X10_Y10_P3_K3_BF	0.29	0.61	0.16	0.26
IQR	0.28-0.31	0.51-0.7	0.16-0.16	0.25-0.29
LA_X10_Y10_PM_K2_BF	0	0.5	0	0.11
IQR	0-0	0.44-0.71	0-0	0-0.12
LA_X10_Y10_PM_K3_BF	0.94	1.1	0	0.99
IQR	0.22-0.97	0.89-1.2	0-0	0.28-1
LA_X11_Y11_P1_K2_BF	0.076	0.16	0.015	0.23
IQR	0.064-0.076	0.11-0.18	0.015-0.076	0.23-0.35
LA_X11_Y11_P1_K3_BF	0.053	0.54	0.029	0.15
IQR	0.042-0.068	0.5-0.6	0.029-0.046	0.12-0.44
LA_X11_Y11_P2_K2_BF	0.012	0.39	0.008	0.085
IQR	0.008-0.068	0.26-0.46	0.0026-0.008	0.067-0.12
LA_X11_Y11_P2_K3_BF	0.6	1.2	0.028	0.82
IQR	0.55-0.69	1.1-1.4	0-0.23	0.16-0.91
LA_X11_Y11_P3_K2_BF	0.12	0.25	0	0.34
IQR	0.12-0.15	0.21-0.31	0-0	0.25-0.34
LA_X11_Y11_P3_K3_BF	0.2	0.71	0.072	0.24
IQR	0.14-0.24	0.59-0.84	0.07-0.13	0.23-0.25
LA_X11_Y11_PM_K2_BF	0.0074	0.56	0.0074	0.073
IQR	0.0074-0.19	0.53-0.74	0.0074-0.0074	0.01-0.17
LA_X11_Y11_PM_K3_BF	0.39	0.71	0.0073	0.57
IQR	0.25-0.45	0.65-0.79	5.9e-06-0.0073	0.47-0.69
LA_X12_Y12_P1_K2_BF	0.013	0.13	0.013	0.23
IQR	0.013-0.013	0.078-0.21	0.013-0.013	0.17-0.25
LA_X12_Y12_P1_K3_BF	0.047	0.44	0.016	0.33
IQR	0.036-0.085	0.39-0.49	0.013-0.029	0.26-0.41
LA_X12_Y12_P2_K2_BF	0.094	0.25	0.01	0.18
IQR	0.058-0.13	0.2-0.28	0.00016-0.05	0.12-0.21
LA_X12_Y12_P2_K3_BF	0.29	0.82	0.19	0.33
IQR	0.26-0.32	0.71-0.93	0.17-0.24	0.3-0.36
LA_X12_Y12_P3_K2_BF	0.06	0.28	0.018	0.096
IQR	0.025-0.082	0.21-0.41	0.018-0.018	0.084-0.17
LA_X12_Y12_P3_K3_BF	0.13	0.55	0.043	0.15
IQR	0.12-0.17	0.48-0.6	0.034-0.044	0.13-0.16
LA_X12_Y12_PM_K2_BF	0.067	0.2	0.035	0.12
IQR	0.061-0.073	0.18-0.24	0.011-0.061	0.072-0.13
LA_X12_Y12_PM_K3_BF	0.12	0.44	0.075	0.27
IQR	0.1-0.16	0.37-0.5	0.05-0.087	0.2-0.35
LA_X13_Y13_P1_K2_BF	0.014	0.2	0.014	0.23
IQR	0.014-0.036	0.12-0.32	0.014-0.014	0.17-0.26
LA_X13_Y13_P1_K3_BF	0.066	0.58	0.027	0.23
IQR	0.045-0.094	0.48-0.68	0.021-0.028	0.15-0.41
LA_X13_Y13_P2_K2_BF	0.11	0.3	0.048	0.19
IQR	0.083-0.15	0.26-0.34	0.0034-0.048	0.12-0.23
LA_X13_Y13_P2_K3_BF	0.19	0.76	0.084	0.21
IQR	0.16-0.24	0.7-0.86	0.065-0.087	0.18-0.31
LA_X13_Y13_P3_K2_BF	0.05	0.48	0.016	0.13
IQR	0.038-0.085	0.4-0.53	0.016-0.016	0.12-0.23
LA_X13_Y13_P3_K3_BF	0.14	0.71	0.033	0.26
IQR	0.11-0.19	0.66-0.84	0.026-0.038	0.18-0.3
LA_X13_Y13_PM_K2_BF	0.028	0.34	0.018	0.1
IQR	0.024-0.035	0.28-0.47	0.018-0.018	0.072-0.12
LA_X13_Y13_PM_K3_BF	0.096	0.52	0.042	0.14
IQR	0.071-0.12	0.45-0.65	0.029-0.048	0.13-0.2
LA_X14_Y14_P1_K2_BF	0.024	0.64	0	0.18
IQR	0.014-0.049	0.51-0.95	0-0	0.14-0.22
LA_X14_Y14_P1_K3_BF	0.092	0.79	0.021	0.29
IQR	0.064-0.13	0.63-0.85	0.016-0.031	0.13-0.35
LA_X14_Y14_P2_K2_BF	0.068	0.7	0	0.19
IQR	0.031-0.12	0.53-0.92	0-0.054	0.099-0.24
LA_X14_Y14_P2_K3_BF	0.24	0.8	0.04	0.29
IQR	0.2-0.29	0.71-0.92	0.034-0.049	0.24-0.36
LA_X14_Y14_P3_K2_BF	0.098	0.72	0	0.15
IQR	0.062-0.15	0.6-0.87	0-0.054	0.097-0.19
LA_X14_Y14_P3_K3_BF	0.2	0.73	0.037	0.24
IQR	0.19-0.26	0.62-0.79	0.034-0.044	0.22-0.29
LA_X14_Y14_PM_K2_BF	0.053	0.59	0.038	0.11
IQR	0.045-0.087	0.4-0.82	0.038-0.085	0.069-0.18
LA_X14_Y14_PM_K3_BF	0.087	0.66	0.023	0.14
IQR	0.071-0.14	0.57-0.71	0.021-0.028	0.11-0.19
LA_X5_Y5_P1_K2_BF	0.33	0	0.68	0.33
IQR	0-0.33	0-0	0.68-0.68	0.33-0.33

Instance Name	d-NSGA-II	$I_{SDE}+$	NSGA-II	NSGA-III
LA_X5_Y5_P1_K3_BF	0.71	7.3	0	0
IQR	0.71-0.71	0.71-11	0-0	0-0
LA_X5_Y5_P2_K2_BF	0	0	0.96	0.28
IQR	0-0.28	0-0	0.96-0.96	0.28-0.28
LA_X5_Y5_P2_K3_BF	0.71	7.3	0	0
IQR	0.71-0.71	0.71-11	0-0	0-0
LA_X5_Y5_P3_K2_BF	0	0	0.86	0.33
IQR	0-0.33	0-0	0.86-0.86	0.33-0.33
LA_X5_Y5_P3_K3_BF	0.77	1.3	0.037	0.037
IQR	0.77-0.77	0.73-1.5	0.037-0.037	0.037-0.037
LA_X5_Y5_PM_K2_BF	0	0	0.83	0
IQR	0-0.28	0-0	0.83-0.83	0-0
LA_X5_Y5_PM_K3_BF	0.46	0.87	0.15	0.31
IQR	0.31-0.46	0.53-0.98	0.15-0.15	0.15-0.43
LA_X6_Y6_P1_K2_BF	0	0	0.71	0
IQR	0-0.53	0-0	0.71-0.71	0-0
LA_X6_Y6_P1_K3_BF	0.71	7.3	0	0
IQR	0.71-0.71	0.71-11	0-0	0-0
LA_X6_Y6_P2_K2_BF	0	0	0.71	0
IQR	0-0	0-0	0.71-0.71	0-0
LA_X6_Y6_P2_K3_BF	0.71	11	0	0
IQR	0.71-0.71	0.71-11	0-0	0-0
LA_X6_Y6_P3_K2_BF	0	0	0.71	0
IQR	0-0.71	0-0	0.71-0.71	0-0
LA_X6_Y6_P3_K3_BF	0.71	1.8	0	0
IQR	0-0.71	0.71-11	0-0	0-0
LA_X6_Y6_PM_K2_BF	0.25	0	0.81	0.29
IQR	0.25-0.25	0-0	0.81-0.81	0.29-0.29
LA_X6_Y6_PM_K3_BF	0.57	0.67	0.25	0.25
IQR	0.57-0.9	0.57-0.9	0.25-0.25	0.25-0.25
LA_X7_Y7_P1_K3_BF	0.45	0.83	0	0.45
IQR	0.45-0.83	0.45-1.4	0-0	0.45-0.45
LA_X7_Y7_P2_K2_BF	0.5	0	0.5	0.5
IQR	0.5-0.5	0-0	0.5-0.5	0.5-0.5
LA_X7_Y7_P2_K3_BF	0.71	0.71	0	0
IQR	0.71-0.71	0.71-1.8	0-0	0-0
LA_X7_Y7_P3_K3_BF	0.71	0.71	0	0
IQR	0.71-0.71	0.71-8.3	0-0	0-0
LA_X7_Y7_PM_K2_BF	0.71	0	0.71	0
IQR	0.5-0.71	0-0	0.5-0.71	0-0
LA_X7_Y7_PM_K3_BF	0.34	0.33	0.21	0.34
IQR	0.21-0.34	0.24-0.45	0.21-0.21	0.22-0.34
LA_X8_Y8_P1_K2_BF	0.26	0	0.26	0.3
IQR	0.26-0.26	0-4.9e-09	0.26-0.26	0.3-0.3
LA_X8_Y8_P1_K3_BF	0.31	0.58	0.15	0.36
IQR	0.19-0.36	0.36-0.67	0.15-0.15	0.31-0.36
LA_X8_Y8_P2_K2_BF	0	0	0	0
IQR	0-0	0-0	0-0	0-0
LA_X8_Y8_P2_K3_BF	1	4.5	0.33	0.33
IQR	0.84-1	1.8-4.8	0.33-0.84	0.33-0.33
LA_X8_Y8_P3_K2_BF	0.26	0	0.26	0.3
IQR	0.26-0.26	0-0	0.26-0.26	0.3-0.3
LA_X8_Y8_P3_K3_BF	0.65	0.91	0.46	0.46
IQR	0.46-0.65	0.87-1.4	0.46-0.46	0.46-0.46
LA_X8_Y8_PM_K2_BF	0	0	0	0
IQR	0-0	0-0	0-0	0-0
LA_X9_Y9_P1_K2_BF	0.053	0.053	8.1e-17	0.21
IQR	0.053-0.053	0.023-0.09	8.1e-17-0.053	0.21-0.21
LA_X9_Y9_P1_K3_BF	0.17	0.48	0.12	0.29
IQR	0.16-0.17	0.39-0.54	0.12-0.12	0.19-0.34
LA_X9_Y9_P2_K2_BF	0	0	0	0
IQR	0-0	0-0	0-0	0-0
LA_X9_Y9_P2_K3_BF	2e+02	2.1	4	4
IQR	0.26-2e+02	1.4-3.4	0-4	0-4
LA_X9_Y9_P3_K2_BF	0.23	0.2	0.23	0.23
IQR	0.23-0.23	0.1-0.29	0.23-0.23	0.23-0.23
LA_X9_Y9_P3_K3_BF	0.47	0.66	0.37	0.39
IQR	0.47-0.47	0.57-0.76	0.37-0.37	0.38-0.46
LA_X9_Y9_PM_K2_BF	0	0	0	0
IQR	0-0	0-0	0-0	0-0
LA_X9_Y9_PM_K3_BF	1.3	1.2	0.92	1.3
IQR	1.3-1.3	0.93-1.6	0.0047-0.92	1.1-1.4
NO_X10_Y10_P1_K2_BF	0.051	0.18	0.017	0.33

Instance Name	d-NSGA-II	$I_{SDE}+$	NSGA-II	NSGA-III
IQR	0.035-0.061	0.14-0.2	0.016-0.025	0.3-0.38
NO_X10_Y10_P1_K3_BF	0.13	0.53	0.048	0.47
IQR	0.11-0.17	0.42-0.59	0.043-0.055	0.17-0.64
NO_X10_Y10_P2_K2_BF	1.1e-16	1.6	1.1e-16	0.076
IQR	1.1e-16-1.1e-16	1.3-1.9	1.1e-16-1.1e-16	0.066-0.098
NO_X10_Y10_P2_K3_BF	0.21	0.68	0.09	0.26
IQR	0.19-0.27	0.55-0.74	0.081-0.098	0.23-0.31
NO_X10_Y10_P3_K2_BF	0.17	0.43	0.037	0.37
IQR	0.1-0.2	0.35-0.48	0.034-0.067	0.33-0.39
NO_X10_Y10_P3_K3_BF	0.18	0.63	0.082	0.24
IQR	0.15-0.23	0.54-0.69	0.075-0.095	0.2-0.26
NO_X10_Y10_PM_K2_BF	0	2.1	0	0.12
IQR	0-0	1.4-2.3	0-0	0-0.12
NO_X10_Y10_PM_K3_BF	0.25	0.68	0.068	0.19
IQR	0.18-0.3	0.62-0.77	0.056-0.094	0.18-0.32
NO_X11_Y11_P1_K2_BF	0.074	0.35	0.033	0.41
IQR	0.053-0.12	0.3-0.4	0.025-0.035	0.41-0.5
NO_X11_Y11_P1_K3_BF	0.091	0.45	0.038	0.36
IQR	0.076-0.14	0.4-0.52	0.031-0.046	0.22-0.52
NO_X11_Y11_P2_K2_BF	0.057	0.7	0.027	0.15
IQR	0.031-0.14	0.58-0.8	0.022-0.027	0.085-0.44
NO_X11_Y11_P2_K3_BF	0.19	0.72	0.094	0.28
IQR	0.17-0.21	0.68-0.8	0.079-0.11	0.25-0.33
NO_X11_Y11_P3_K2_BF	0.18	0.36	0.024	0.37
IQR	0.12-0.2	0.3-0.41	0.0097-0.027	0.34-0.39
NO_X11_Y11_P3_K3_BF	0.15	0.65	0.075	0.24
IQR	0.13-0.18	0.61-0.69	0.069-0.081	0.19-0.28
NO_X11_Y11_PM_K2_BF	0.11	1	0.0051	0.17
IQR	0.025-0.43	0.78-1.1	0-0.0051	0.1-0.21
NO_X11_Y11_PM_K3_BF	0.26	0.76	0.09	0.19
IQR	0.2-0.37	0.68-0.84	0.069-0.11	0.17-0.23
NO_X12_Y12_P1_K2_BF	0.063	0.44	0.022	0.41
IQR	0.045-0.065	0.36-0.54	0.022-0.022	0.32-0.41
NO_X12_Y12_P1_K3_BF	0.14	0.54	0.034	0.4
IQR	0.094-0.18	0.47-0.6	0.029-0.04	0.16-0.47
NO_X12_Y12_P2_K2_BF	0.16	0.68	0.044	0.22
IQR	0.14-0.24	0.56-0.88	0.026-0.099	0.19-0.29
NO_X12_Y12_P2_K3_BF	0.18	0.83	0.078	0.22
IQR	0.14-0.29	0.77-0.96	0.068-0.087	0.17-0.23
NO_X12_Y12_P3_K2_BF	0.11	0.58	0.061	0.2
IQR	0.096-0.17	0.44-0.64	0.046-0.067	0.19-0.3
NO_X12_Y12_P3_K3_BF	0.18	0.76	0.061	0.21
IQR	0.16-0.25	0.67-0.81	0.053-0.071	0.15-0.25
NO_X12_Y12_PM_K2_BF	0.063	0.49	0.033	0.15
IQR	0.057-0.12	0.35-0.66	0.026-0.056	0.088-0.2
NO_X12_Y12_PM_K3_BF	0.18	0.64	0.073	0.18
IQR	0.15-0.22	0.55-0.66	0.062-0.081	0.15-0.39
NO_X13_Y13_P1_K2_BF	0.056	0.42	0.017	0.4
IQR	0.044-0.11	0.4-0.5	0.017-0.017	0.34-0.44
NO_X13_Y13_P1_K3_BF	0.14	0.63	0.034	0.41
IQR	0.12-0.19	0.55-0.75	0.029-0.046	0.31-0.45
NO_X13_Y13_P2_K2_BF	0.19	1	0.13	0.22
IQR	0.18-0.2	0.74-1.2	0.081-0.17	0.19-0.27
NO_X13_Y13_P2_K3_BF	0.23	0.78	0.1	0.25
IQR	0.17-0.26	0.66-0.83	0.081-0.11	0.2-0.29
NO_X13_Y13_P3_K2_BF	0.15	0.75	0.094	0.22
IQR	0.12-0.18	0.57-0.93	0.042-0.094	0.19-0.3
NO_X13_Y13_P3_K3_BF	0.18	0.73	0.087	0.25
IQR	0.15-0.24	0.68-0.8	0.079-0.099	0.16-0.29
NO_X13_Y13_PM_K2_BF	0.12	0.54	0.028	0.26
IQR	0.073-0.17	0.45-0.64	0.028-0.071	0.13-0.35
NO_X13_Y13_PM_K3_BF	0.22	0.67	0.078	0.19
IQR	0.17-0.26	0.64-0.74	0.06-0.095	0.17-0.31
NO_X14_Y14_P1_K2_BF	0.056	1.5	0	0.2
IQR	0.033-0.068	1-2.3	0-0.05	0.15-0.26
NO_X14_Y14_P1_K3_BF	0.17	0.87	0.048	0.27
IQR	0.11-0.2	0.74-0.92	0.038-0.06	0.2-0.33
NO_X14_Y14_P2_K2_BF	0.18	1.6	0.13	0.28
IQR	0.14-0.25	1.4-1.8	0.13-0.13	0.17-0.41
NO_X14_Y14_P2_K3_BF	0.24	0.8	0.096	0.32
IQR	0.21-0.26	0.69-0.91	0.087-0.1	0.28-0.34
NO_X14_Y14_P3_K2_BF	0.074	1.4	0.054	0.16
IQR	0.055-0.14	1.1-1.5	0.024-0.054	0.093-0.22

Instance Name	d-NSGA-II	$I_{SDE}+$	NSGA-II	NSGA-III
NO_X14_Y14_P3_K3_BF	0.22	0.79	0.082	0.24
IQR	0.17-0.24	0.72-0.85	0.075-0.092	0.23-0.33
NO_X14_Y14_PM_K2_BF	0.065	1.5	0.085	0.12
IQR	0.042-0.099	1-2	0.038-0.085	0.099-0.15
NO_X14_Y14_PM_K3_BF	0.18	0.76	0.072	0.24
IQR	0.15-0.2	0.68-0.81	0.062-0.095	0.21-0.32
NO_X3_Y3_P1_K2_BF	0	0	0.13	0
IQR	0-0	0-0	0.13-0.13	0-0.47
NO_X3_Y3_P2_K2_BF	0	0	0	0
IQR	0-0	0-0	0-0	0-0
NO_X3_Y3_P3_K2_BF	0	0	0	0
IQR	0-0	0-0	0-0	0-0
NO_X4_Y4_P1_K2_BF	0	0	0	0.21
IQR	0-0	0-0	0-0.03	0.077-0.33
NO_X4_Y4_P1_K3_BF	0.84	1.2	0.63	0.29
IQR	0.84-0.84	0.89-1.8	0.27-0.84	0.29-0.29
NO_X4_Y4_P2_K2_BF	0	0	0	0
IQR	0-0	0-0	0-0	0-0
NO_X4_Y4_P2_K3_BF	0.49	1.9	0.49	0.11
IQR	0.49-0.58	1.6-2.6	0.49-0.49	0.11-0.11
NO_X4_Y4_P3_K2_BF	0.12	0	0	0.12
IQR	0.1-0.13	0-0	0-0	0.12-0.12
NO_X4_Y4_P3_K3_BF	0.49	1.8	0.49	0.13
IQR	0.49-0.49	1.5-2.5	0.49-0.49	0.13-0.4
NO_X4_Y4_PM_K2_BF	0	0	0	0
IQR	0-0	0-0	0-0	0-0
NO_X4_Y4_PM_K3_BF	0.44	1.2	0.34	0.44
IQR	0.42-0.72	1-1.4	0.34-0.34	0.34-0.44
NO_X5_Y5_P1_K2_BF	0.026	0	0	0.026
IQR	0.0073-0.026	0-0	0-0	0.026-0.17
NO_X5_Y5_P1_K3_BF	0.64	0.65	0.26	0.27
IQR	0.6-0.64	0.64-1	0.26-0.27	0.12-0.59
NO_X5_Y5_P2_K2_BF	0.14	0	0	0.11
IQR	0.044-0.21	0-0	0-0	0.11-0.11
NO_X5_Y5_P2_K3_BF	0.69	1.1	0.3	0.3
IQR	0.6-0.8	0.94-1.2	0.29-0.47	0.3-0.34
NO_X5_Y5_P3_K2_BF	0.015	0	0	0.22
IQR	0.015-0.017	0-5.6e-17	0-0	0.22-0.22
NO_X5_Y5_P3_K3_BF	0.48	0.86	0.17	0.22
IQR	0.35-0.5	0.71-0.91	0.17-0.22	0.17-0.35
NO_X5_Y5_PM_K2_BF	0.025	0	0	0.1
IQR	0.014-0.035	0-0.0049	0-0	0.094-0.17
NO_X5_Y5_PM_K3_BF	0.61	0.74	0.21	0.21
IQR	0.57-0.68	0.72-0.83	0.078-0.21	0.17-0.25
NO_X6_Y6_P1_K2_BF	0	0.048	0	0.13
IQR	0-0.029	0.029-0.083	0-0	0.029-0.16
NO_X6_Y6_P1_K3_BF	0.35	0.81	0.097	0.21
IQR	0.28-0.42	0.7-0.95	0.096-0.15	0.16-0.26
NO_X6_Y6_P2_K2_BF	0.00078	0.048	0	0.21
IQR	6.3e-05-0.04	0.017-0.065	0-2.4e-05	0.2-0.21
NO_X6_Y6_P2_K3_BF	0.29	0.89	0.073	0.36
IQR	0.23-0.35	0.79-0.98	0.055-0.12	0.28-0.42
NO_X6_Y6_P3_K2_BF	0	0.06	0	0.28
IQR	0-0	0.016-0.093	0-0	0.22-0.33
NO_X6_Y6_P3_K3_BF	0.23	0.81	0.053	0.24
IQR	0.2-0.29	0.69-0.88	0.042-0.13	0.22-0.37
NO_X6_Y6_PM_K2_BF	0.043	0.043	0	0.11
IQR	0.035-0.053	0.035-0.064	0-0.002	0.08-0.12
NO_X6_Y6_PM_K3_BF	0.14	0.65	0.093	0.19
IQR	0.13-0.25	0.56-0.73	0.071-0.093	0.12-0.23
NO_X7_Y7_P1_K2_BF	9.9e-05	0.15	0	6.8e-05
IQR	7.8e-06-0.056	0.11-0.26	0-0	6.8e-05-0.0001
NO_X7_Y7_P1_K3_BF	0.16	0.67	0.055	0.21
IQR	0.13-0.18	0.53-0.72	0.044-0.072	0.15-0.24
NO_X7_Y7_P2_K2_BF	0.037	0.3	0	0.041
IQR	2e-16-0.039	0.22-0.42	0-0	0.039-0.076
NO_X7_Y7_P2_K3_BF	0.2	0.67	0.039	0.15
IQR	0.15-0.24	0.55-0.77	0.032-0.039	0.11-0.23
NO_X7_Y7_P3_K2_BF	0.037	0.29	0	0.039
IQR	2e-16-0.13	0.17-0.38	0-0	0.039-0.067
NO_X7_Y7_P3_K3_BF	0.18	0.57	0.05	0.16
IQR	0.14-0.21	0.52-0.61	0.05-0.062	0.11-0.27
NO_X7_Y7_PM_K2_BF	0.062	0.22	0	0.021

Instance Name	d-NSGA-II	$I_{SDE}+$	NSGA-II	NSGA-III
IQR	0.021-0.082	0.086-0.29	0-0	0.021-0.034
NO_X7_Y7_PM_K3_BF	0.23	0.52	0.049	0.21
IQR	0.2-0.26	0.47-0.58	0.042-0.061	0.19-0.32
NO_X8_Y8_P1_K2_BF	0.025	0.12	5e-06	0.24
IQR	0.024-0.029	0.068-0.16	0-0.012	0.24-0.31
NO_X8_Y8_P1_K3_BF	0.073	0.49	0.033	0.13
IQR	0.064-0.093	0.4-0.57	0.029-0.047	0.085-0.17
NO_X8_Y8_P2_K2_BF	0.00072	0.4	7.6e-07	0.028
IQR	7.6e-07-0.012	0.27-0.52	1.9e-17-7.6e-07	0.00069-0.065
NO_X8_Y8_P2_K3_BF	0.18	0.63	0.027	0.19
IQR	0.14-0.23	0.54-0.69	0.021-0.039	0.17-0.23
NO_X8_Y8_P3_K2_BF	0.034	0.22	0.011	0.34
IQR	0.031-0.055	0.18-0.28	0-0.011	0.27-0.34
NO_X8_Y8_P3_K3_BF	0.16	0.56	0.026	0.15
IQR	0.14-0.2	0.49-0.6	0.021-0.033	0.12-0.18
NO_X8_Y8_PM_K2_BF	0.025	0.37	0.0033	0.065
IQR	0.0033-0.062	0.26-0.56	0.0033-0.0033	0.038-0.14
NO_X8_Y8_PM_K3_BF	0.21	0.7	0.046	0.19
IQR	0.19-0.34	0.66-0.76	0.043-0.052	0.16-0.22
NO_X9_Y9_P1_K2_BF	0.062	0.25	0.028	0.41
IQR	0.054-0.11	0.17-0.32	6.8e-17-0.028	0.41-0.41
NO_X9_Y9_P1_K3_BF	0.11	0.51	0.045	0.2
IQR	0.073-0.15	0.45-0.59	0.042-0.049	0.12-0.35
NO_X9_Y9_P2_K2_BF	0	0	0	0
IQR	0-0	0-0	0-0	0-0
NO_X9_Y9_P2_K3_BF	0.19	0.54	0.071	0.22
IQR	0.17-0.23	0.48-0.61	0.066-0.077	0.18-0.25
NO_X9_Y9_P3_K2_BF	0.2	0.46	0.12	0.22
IQR	0.13-0.74	0.37-0.66	0.084-0.12	0.22-0.22
NO_X9_Y9_P3_K3_BF	0.2	0.54	0.069	0.25
IQR	0.16-0.25	0.47-0.6	0.064-0.077	0.16-0.28
NO_X9_Y9_PM_K2_BF	0	0	0	0
IQR	0-0	0-0	0-0	0-0
NO_X9_Y9_PM_K3_BF	0.27	0.81	0.063	0.22
IQR	0.22-0.32	0.7-0.88	0.057-0.094	0.19-0.32

Table B.1: Raw values of different instances of the IGD+ indicator. Shown are the median and the IQR values below.

B.1.2 IGD Values

Instance Name	d-NSGA-II	$I_{SDE}+$	NSGA-II	NSGA-III
CH_X10_Y10_P1_K2_BF	0.0077	0.025	0	0.14
IQR	0-0.1	0.011-0.041	0-0	0.13-0.18
CH_X10_Y10_P1_K3_BF	0.1	0.14	0.078	0.12
IQR	0.094-0.11	0.13-0.15	0.041-0.083	0.12-0.13
CH_X10_Y10_P2_K2_BF	0	0.14	0	0.14
IQR	0-0	0-0.2	0-0	0.036-0.17
CH_X10_Y10_P2_K3_BF	0.098	0.17	0.035	0.15
IQR	0.092-0.11	0.15-0.19	0.033-0.068	0.12-0.18
CH_X10_Y10_P3_K2_BF	0	0.043	0	0.16
IQR	0-0.074	0.021-0.065	0-0	0.15-0.16
CH_X10_Y10_P3_K3_BF	0.091	0.13	0.027	0.1
IQR	0.086-0.095	0.11-0.14	0.014-0.039	0.093-0.11
CH_X10_Y10_PM_K2_BF	0	0	0	0
IQR	0-0	0-0	0-0	0-0
CH_X10_Y10_PM_K3_BF	0.13	0.18	0.058	0.14
IQR	0.11-0.13	0.16-0.2	0.033-0.074	0.12-0.15
CH_X11_Y11_P1_K2_BF	0.069	0.036	0.035	0.12
IQR	0.045-0.072	0.03-0.042	0.032-0.055	0.12-0.14
CH_X11_Y11_P1_K3_BF	0.078	0.078	0.069	0.087
IQR	0.076-0.08	0.073-0.087	0.068-0.069	0.083-0.094
CH_X11_Y11_P2_K2_BF	0.087	0.093	0.1	0.19
IQR	0.08-0.11	0.077-0.11	0.028-0.1	0.18-0.23
CH_X11_Y11_P2_K3_BF	0.078	0.13	0.043	0.1
IQR	0.069-0.082	0.12-0.14	0.041-0.047	0.095-0.12
CH_X11_Y11_P3_K2_BF	0.064	0.058	0.014	0.16
IQR	0.053-0.077	0.046-0.071	0-0.031	0.14-0.18
CH_X11_Y11_P3_K3_BF	0.063	0.092	0.028	0.077
IQR	0.06-0.067	0.086-0.11	0.025-0.032	0.07-0.083

Instance Name	d-NSGA-II	$I_{SDE}+$	NSGA-II	NSGA-III
CH_X11_Y11_PM_K2_BF	0.13	0.15	0.093	0.16
IQR	0.11-0.16	0.11-0.23	0.093-0.093	0.16-0.19
CH_X11_Y11_PM_K3_BF	0.069	0.11	0.034	0.093
IQR	0.063-0.084	0.098-0.12	0.032-0.037	0.082-0.11
CH_X12_Y12_P1_K2_BF	0.045	0.04	0.0016	0.11
IQR	0.032-0.055	0.035-0.043	0-0.033	0.11-0.12
CH_X12_Y12_P1_K3_BF	0.063	0.093	0.053	0.077
IQR	0.061-0.069	0.085-0.099	0.052-0.054	0.07-0.085
CH_X12_Y12_P2_K2_BF	0.077	0.18	0	0.13
IQR	0-0.086	0.15-0.21	0-0.086	0.13-0.16
CH_X12_Y12_P2_K3_BF	0.071	0.15	0.037	0.12
IQR	0.067-0.082	0.13-0.17	0.032-0.043	0.086-0.16
CH_X12_Y12_P3_K2_BF	0.033	0.057	0	0.11
IQR	0.021-0.046	0.055-0.064	0-0	0.11-0.12
CH_X12_Y12_P3_K3_BF	0.067	0.12	0.032	0.079
IQR	0.061-0.074	0.11-0.13	0.032-0.035	0.077-0.083
CH_X12_Y12_PM_K2_BF	0.04	0.12	0	0.12
IQR	0-0.081	0.094-0.14	0-0	0.12-0.12
CH_X12_Y12_PM_K3_BF	0.093	0.12	0.075	0.092
IQR	0.078-0.094	0.11-0.13	0.071-0.078	0.088-0.095
CH_X13_Y13_P1_K2_BF	0.11	0.095	0.086	0.17
IQR	0.099-0.12	0.082-0.1	0.073-0.1	0.16-0.17
CH_X13_Y13_P1_K3_BF	0.067	0.1	0.047	0.08
IQR	0.063-0.071	0.099-0.11	0.046-0.047	0.074-0.088
CH_X13_Y13_P2_K2_BF	0.12	0.2	0.06	0.18
IQR	0.077-0.14	0.17-0.22	0.02-0.12	0.18-0.18
CH_X13_Y13_P2_K3_BF	0.051	0.1	0.025	0.071
IQR	0.048-0.054	0.09-0.11	0.022-0.027	0.066-0.077
CH_X13_Y13_P3_K2_BF	0.074	0.086	0.047	0.1
IQR	0.07-0.082	0.074-0.091	0.023-0.052	0.1-0.15
CH_X13_Y13_P3_K3_BF	0.049	0.094	0.028	0.069
IQR	0.045-0.056	0.09-0.1	0.022-0.028	0.065-0.076
CH_X13_Y13_PM_K2_BF	0.08	0.093	0.04	0.19
IQR	0.057-0.083	0.076-0.1	0.023-0.051	0.13-0.19
CH_X13_Y13_PM_K3_BF	0.069	0.11	0.047	0.09
IQR	0.064-0.071	0.1-0.12	0.037-0.051	0.082-0.1
CH_X14_Y14_P1_K2_BF	0.056	0.066	0.051	0.11
IQR	0.054-0.06	0.059-0.072	0.051-0.051	0.11-0.12
CH_X14_Y14_P1_K3_BF	0.043	0.081	0.034	0.057
IQR	0.041-0.05	0.071-0.09	0.033-0.034	0.054-0.071
CH_X14_Y14_P2_K2_BF	0.046	0.26	0	0.21
IQR	0-0.08	0.21-0.3	0-0	0.21-0.22
CH_X14_Y14_P2_K3_BF	0.048	0.093	0.02	0.069
IQR	0.045-0.052	0.086-0.11	0.018-0.023	0.06-0.072
CH_X14_Y14_P3_K2_BF	0.06	0.091	0.041	0.1
IQR	0.033-0.061	0.085-0.1	0.024-0.06	0.099-0.1
CH_X14_Y14_P3_K3_BF	0.04	0.075	0.02	0.051
IQR	0.036-0.042	0.065-0.079	0.019-0.023	0.045-0.058
CH_X14_Y14_PM_K2_BF	0.036	0.077	0	0.11
IQR	0.032-0.041	0.069-0.082	0-0	0.097-0.12
CH_X14_Y14_PM_K3_BF	0.11	0.15	0.11	0.12
IQR	0.1-0.12	0.14-0.16	0.098-0.12	0.11-0.13
CH_X3_Y3_P2_K2_BF	0	0	0	0
IQR	0-0	0-0	0-0	0-0
CH_X3_Y3_P2_K3_BF	0	0	0	0
IQR	0-0	0-0	0-0	0-0
CH_X3_Y3_P3_K2_BF	0	0	0	0
IQR	0-0	0-0	0-0	0-0
CH_X3_Y3_P3_K3_BF	0	0	0	0
IQR	0-0	0-0	0-0	0-0
CH_X4_Y4_P1_K2_BF	0	0	0	0
IQR	0-0	0-0	0-0	0-0
CH_X4_Y4_P1_K3_BF	0.47	0.69	0.76	0.63
IQR	0.47-0.76	0.58-0.73	0.51-0.76	0.63-0.63
CH_X4_Y4_P2_K2_BF	0	0	0	0
IQR	0-0	0-0	0-0	0-0
CH_X4_Y4_P2_K3_BF	0	1.7	0	0
IQR	0-0	1.6-1.7	0-0	0-0
CH_X4_Y4_P3_K2_BF	0	0	0	0
IQR	0-0	0-0	0-0	0-0
CH_X4_Y4_P3_K3_BF	0	1.5	0	0
IQR	0-0	1-1.6	0-0	0-0
CH_X4_Y4_PM_K2_BF	0	0	0	0

Instance Name	d-NSGA-II	$I_{SDE}+$	NSGA-II	NSGA-III
IQR	0-0	0-0	0-0.7	0-0
CH_X4_Y4_PM_K3_BF	0.51	0.61	0.51	0
IQR	0.51-0.51	0.61-0.73	0-0.51	0-0
CH_X5_Y5_P1_K2_BF	0	0	0.37	0.37
IQR	0-0	0-0	0.37-0.37	0.37-0.37
CH_X5_Y5_P1_K3_BF	0.54	0.64	0.3	0.45
IQR	0.51-0.54	0.64-0.64	0.3-0.3	0.45-0.45
CH_X5_Y5_P2_K2_BF	0	0	0	0
IQR	0-0	0-0	0-0.19	0-0
CH_X5_Y5_P2_K3_BF	0.47	0.47	0.59	0.32
IQR	0.39-0.48	0.46-0.47	0.08-0.73	0.13-0.46
CH_X5_Y5_P3_K2_BF	0	0	0.39	0.39
IQR	0-0	0-0	0.39-0.39	0.39-0.39
CH_X5_Y5_PM_K2_BF	0	0	0.24	0.3
IQR	0-0	0-0	0.24-0.24	0.3-0.3
CH_X6_Y6_P1_K2_BF	0	0	0.21	0.21
IQR	0-0	0-0	0.21-0.21	0.21-0.21
CH_X6_Y6_P1_K3_BF	1.1	2.8	0	0
IQR	1.1-1.1	2.8-5.3	0-0	0-0
CH_X6_Y6_P2_K2_BF	0	0	0.078	0
IQR	0-0	0-0	0-0.17	0-0
CH_X6_Y6_P2_K3_BF	0.35	0.43	0	0.19
IQR	0.26-0.41	0.39-0.44	0-0.082	0.082-0.24
CH_X6_Y6_P3_K2_BF	0	0	0.18	0.18
IQR	0-0	0-0	0-0.29	0.18-0.18
CH_X6_Y6_P3_K3_BF	0.43	0.5	0.31	0.36
IQR	0.38-0.49	0.46-0.54	0.22-0.31	0.22-0.36
CH_X6_Y6_PM_K2_BF	0	0	0	0.079
IQR	0-0	0-0	0-0.13	0.079-0.079
CH_X7_Y7_P1_K2_BF	0	0	0.33	0
IQR	0-0	0-0	0.33-0.33	0-0.33
CH_X7_Y7_P1_K3_BF	0.22	0.37	0	0.17
IQR	0.2-0.25	0.33-0.39	0-0.057	0.15-0.19
CH_X7_Y7_P2_K2_BF	0	0	4.5e-16	4.5e-16
IQR	0-4.5e-16	0-0	4.5e-16-4.5e-16	0-4.5e-16
CH_X7_Y7_P2_K3_BF	0.27	0.43	0	0.14
IQR	0.2-0.35	0.38-0.44	0-0	0.14-0.17
CH_X7_Y7_P3_K2_BF	0	0	0.16	0
IQR	0-0	0-0	0.041-0.16	0-0
CH_X7_Y7_P3_K3_BF	0.23	0.34	0.12	0.18
IQR	0.22-0.28	0.31-0.36	0.12-0.12	0.18-0.19
CH_X7_Y7_PM_K2_BF	0	0	0.29	0.27
IQR	0-0.11	0-0	0.29-0.29	0.27-0.27
CH_X7_Y7_PM_K3_BF	0.18	0.23	0.099	0.26
IQR	0.15-0.18	0.21-0.27	0.099-0.12	0.18-0.28
CH_X8_Y8_P1_K2_BF	0	0	0	0
IQR	0-0	0-0	0-0	0-0
CH_X8_Y8_P1_K3_BF	0.11	0.34	0	0.13
IQR	0.096-0.13	0.3-0.39	0-0	0.13-0.15
CH_X8_Y8_P2_K2_BF	0	0	0.33	0
IQR	0-0	0-0	0-0.33	0-0
CH_X8_Y8_P2_K3_BF	0.092	0.26	0	0.11
IQR	0.079-0.11	0.22-0.29	0-0	0.1-0.13
CH_X8_Y8_P3_K2_BF	0	0	0.44	0.44
IQR	0-0	0-0	0-0.44	0.44-0.46
CH_X8_Y8_P3_K3_BF	0.12	0.25	0.072	0.12
IQR	0.11-0.13	0.23-0.28	0.072-0.072	0.11-0.13
CH_X8_Y8_PM_K2_BF	0	0	0	0.39
IQR	0-0	0-0	0-0	0.33-0.39
CH_X8_Y8_PM_K3_BF	0.16	0.24	0.074	0.18
IQR	0.14-0.19	0.22-0.25	0.059-0.14	0.17-0.22
CH_X9_Y9_P1_K2_BF	0.18	0	0.15	0.28
IQR	0.17-0.18	0-0.0001	0.00049-0.17	0.28-0.28
CH_X9_Y9_P1_K3_BF	0.095	0.12	0.039	0.11
IQR	0.088-0.1	0.11-0.13	0.032-0.046	0.11-0.12
CH_X9_Y9_P2_K2_BF	0	0	0	0
IQR	0-0	0-0	0-0	0-0
CH_X9_Y9_P2_K3_BF	0.14	0.2	0.075	0.17
IQR	0.13-0.17	0.18-0.21	0.066-0.081	0.14-0.21
CH_X9_Y9_P3_K2_BF	0.17	0	0.24	0.47
IQR	0.17-0.32	0-0	0.24-0.27	0.38-0.47
CH_X9_Y9_P3_K3_BF	0.11	0.14	0.044	0.13
IQR	0.1-0.12	0.13-0.16	0.042-0.051	0.12-0.14

Instance Name	d-NSGA-II	$I_{SDE}+$	NSGA-II	NSGA-III
CH_X9_Y9_PM_K2_BF	0	0	0	0
IQR	0-0	0-0	0-0	0-0
CH_X9_Y9_PM_K3_BF	0.2	0.25	0.089	0.19
IQR	0.19-0.23	0.23-0.25	0.077-0.11	0.19-0.23
LA_X10_Y10_P1_K2_BF	0.04	0.028	0.019	0.072
IQR	0.031-0.041	0.026-0.03	0.019-0.038	0.068-0.076
LA_X10_Y10_P1_K3_BF	0.068	0.074	0.063	0.081
IQR	0.068-0.071	0.067-0.079	0.063-0.064	0.079-0.089
LA_X10_Y10_P2_K2_BF	0	0.34	0	0.11
IQR	0-0	0.27-0.39	0-0	0.076-0.11
LA_X10_Y10_P2_K3_BF	0.2	0.5	0	0.43
IQR	0.12-0.47	0.44-0.54	0-0	0.41-0.43
LA_X10_Y10_P3_K2_BF	0.059	0.057	0.021	0.11
IQR	0.054-0.078	0.051-0.063	0.01-0.033	0.097-0.12
LA_X10_Y10_P3_K3_BF	0.11	0.13	0.076	0.11
IQR	0.093-0.11	0.12-0.15	0.076-0.076	0.1-0.12
LA_X10_Y10_PM_K2_BF	0	0.37	0	0.11
IQR	0-0	0.3-0.51	0-0	0-0.12
LA_X10_Y10_PM_K3_BF	0.25	0.28	0	0.29
IQR	0.1-0.26	0.26-0.32	0-0	0.11-0.29
LA_X11_Y11_P1_K2_BF	0.12	0.077	0.039	0.15
IQR	0.055-0.12	0.073-0.082	0.039-0.12	0.14-0.16
LA_X11_Y11_P1_K3_BF	0.064	0.092	0.06	0.087
IQR	0.063-0.066	0.084-0.097	0.059-0.06	0.08-0.095
LA_X11_Y11_P2_K2_BF	0.053	0.11	0.053	0.1
IQR	0.05-0.056	0.09-0.12	0.033-0.053	0.099-0.11
LA_X11_Y11_P2_K3_BF	0.19	0.33	0.073	0.26
IQR	0.17-0.23	0.29-0.36	0-0.097	0.18-0.28
LA_X11_Y11_P3_K2_BF	0.099	0.093	0	0.18
IQR	0.065-0.1	0.084-0.1	0-0	0.12-0.19
LA_X11_Y11_P3_K3_BF	0.085	0.13	0.06	0.1
IQR	0.073-0.1	0.12-0.15	0.06-0.084	0.1-0.11
LA_X11_Y11_PM_K2_BF	0.098	0.25	0.098	0.14
IQR	0.098-0.18	0.24-0.29	0.098-0.098	0.098-0.14
LA_X11_Y11_PM_K3_BF	0.094	0.16	0.027	0.14
IQR	0.073-0.11	0.14-0.17	0.022-0.034	0.13-0.16
LA_X12_Y12_P1_K2_BF	0.077	0.09	0.075	0.12
IQR	0.076-0.079	0.08-0.11	0.075-0.075	0.11-0.13
LA_X12_Y12_P1_K3_BF	0.038	0.062	0.031	0.061
IQR	0.037-0.039	0.057-0.065	0.03-0.035	0.052-0.072
LA_X12_Y12_P2_K2_BF	0.076	0.073	0.016	0.095
IQR	0.071-0.091	0.071-0.078	0.005-0.073	0.079-0.1
LA_X12_Y12_P2_K3_BF	0.088	0.17	0.06	0.1
IQR	0.079-0.098	0.15-0.19	0.057-0.087	0.098-0.11
LA_X12_Y12_P3_K2_BF	0.074	0.12	0.056	0.14
IQR	0.065-0.093	0.11-0.15	0.056-0.056	0.11-0.16
LA_X12_Y12_P3_K3_BF	0.033	0.073	0.022	0.042
IQR	0.031-0.038	0.067-0.079	0.016-0.024	0.038-0.046
LA_X12_Y12_PM_K2_BF	0.056	0.081	0.044	0.07
IQR	0.056-0.059	0.074-0.088	0.013-0.056	0.063-0.087
LA_X12_Y12_PM_K3_BF	0.049	0.076	0.037	0.067
IQR	0.048-0.052	0.072-0.084	0.026-0.046	0.06-0.075
LA_X13_Y13_P1_K2_BF	0.071	0.1	0.066	0.11
IQR	0.068-0.075	0.097-0.12	0.066-0.066	0.1-0.12
LA_X13_Y13_P1_K3_BF	0.03	0.071	0.023	0.049
IQR	0.028-0.032	0.064-0.08	0.018-0.023	0.042-0.06
LA_X13_Y13_P2_K2_BF	0.073	0.081	0.068	0.094
IQR	0.067-0.079	0.076-0.092	0.012-0.068	0.077-0.11
LA_X13_Y13_P2_K3_BF	0.053	0.12	0.037	0.071
IQR	0.05-0.058	0.11-0.13	0.031-0.038	0.056-0.082
LA_X13_Y13_P3_K2_BF	0.057	0.15	0.039	0.095
IQR	0.051-0.067	0.13-0.16	0.039-0.039	0.079-0.13
LA_X13_Y13_P3_K3_BF	0.037	0.093	0.021	0.063
IQR	0.035-0.042	0.086-0.1	0.017-0.025	0.047-0.068
LA_X13_Y13_PM_K2_BF	0.04	0.12	0.031	0.073
IQR	0.036-0.055	0.11-0.14	0.031-0.031	0.068-0.081
LA_X13_Y13_PM_K3_BF	0.043	0.077	0.035	0.054
IQR	0.041-0.045	0.07-0.085	0.032-0.036	0.051-0.063
LA_X14_Y14_P1_K2_BF	0.033	0.2	0	0.11
IQR	0.024-0.045	0.16-0.26	0-0	0.071-0.13
LA_X14_Y14_P1_K3_BF	0.037	0.1	0.026	0.052
IQR	0.035-0.04	0.083-0.11	0.025-0.026	0.048-0.057
LA_X14_Y14_P2_K2_BF	0.063	0.27	0	0.14

Instance Name	d-NSGA-II	$I_{SDE}+$	NSGA-II	NSGA-III
IQR	0.051-0.084	0.24-0.34	0-0.054	0.11-0.15
LA_X14_Y14_P2_K3_BF	0.049	0.11	0.022	0.084
IQR	0.044-0.055	0.1-0.13	0.02-0.025	0.06-0.099
LA_X14_Y14_P3_K2_BF	0.075	0.29	0	0.12
IQR	0.062-0.097	0.24-0.31	0-0.054	0.091-0.16
LA_X14_Y14_P3_K3_BF	0.044	0.099	0.022	0.078
IQR	0.041-0.049	0.094-0.11	0.02-0.024	0.063-0.085
LA_X14_Y14_PM_K2_BF	0.051	0.2	0.038	0.074
IQR	0.043-0.062	0.16-0.24	0.038-0.061	0.064-0.11
LA_X14_Y14_PM_K3_BF	0.031	0.074	0.023	0.04
IQR	0.03-0.034	0.069-0.079	0.023-0.024	0.038-0.044
LA_X5_Y5_P1_K2_BF	0.55	0	0.71	0.55
IQR	0-0.55	0-0	0.71-0.71	0.55-0.55
LA_X5_Y5_P1_K3_BF	0.87	5.2	0	0
IQR	0.87-0.87	0.87-8.1	0-0	0-0
LA_X5_Y5_P2_K2_BF	0	0	0.79	0.44
IQR	0-0.44	0-0	0.79-0.79	0.44-0.44
LA_X5_Y5_P2_K3_BF	0.87	5.2	0	0
IQR	0.87-0.87	0.87-8.1	0-0	0-0
LA_X5_Y5_P3_K2_BF	0	0	0.73	0.47
IQR	0-0.47	0-0	0.73-0.73	0.47-0.47
LA_X5_Y5_P3_K3_BF	0.66	0.77	0.55	0.55
IQR	0.63-0.66	0.47-0.83	0.55-0.55	0.55-0.55
LA_X5_Y5_PM_K2_BF	0	0	0.72	0
IQR	0-0.42	0-0	0.72-0.72	0-0
LA_X5_Y5_PM_K3_BF	0.46	0.46	0.3	0.3
IQR	0.35-0.48	0.36-0.48	0.3-0.3	0.3-0.3
LA_X6_Y6_P1_K2_BF	0	0	1	0
IQR	0-0.75	0-0	1-1	0-0
LA_X6_Y6_P1_K3_BF	0.87	5.2	0	0
IQR	0.87-0.87	0.87-8.1	0-0	0-0
LA_X6_Y6_P2_K2_BF	0	0	1	0
IQR	0-0	0-0	1-1	0-0
LA_X6_Y6_P2_K3_BF	0.87	8.1	0	0
IQR	0.87-0.87	0.87-8.1	0-0	0-0
LA_X6_Y6_P3_K2_BF	0	0	1	0
IQR	0-1	0-0	1-1	0-0
LA_X6_Y6_P3_K3_BF	0.87	1.3	0	0
IQR	0-0.87	0.87-8.1	0-0	0-0
LA_X6_Y6_PM_K2_BF	0.39	0	0.82	0.39
IQR	0.39-0.39	0-0	0.82-0.82	0.39-0.39
LA_X6_Y6_PM_K3_BF	0.45	0.39	0.35	0.35
IQR	0.4-0.54	0.38-0.49	0.35-0.35	0.35-0.35
LA_X7_Y7_P1_K3_BF	0.45	0.59	0	0.45
IQR	0.45-0.59	0.45-0.86	0-0	0.45-0.45
LA_X7_Y7_P2_K2_BF	0.71	0	0.71	0.71
IQR	0.71-0.71	0-0	0.71-0.71	0.71-0.71
LA_X7_Y7_P2_K3_BF	0.87	0.87	0	0
IQR	0.87-0.87	0.87-1.3	0-0	0-0
LA_X7_Y7_P3_K3_BF	0.87	0.87	0	0
IQR	0.87-0.87	0.87-5.9	0-0	0-0
LA_X7_Y7_PM_K2_BF	0.87	0	0.87	0
IQR	0.87-0.87	0-0	0.87-0.87	0-0
LA_X7_Y7_PM_K3_BF	0.21	0.21	0.2	0.21
IQR	0.2-0.29	0.18-0.25	0.2-0.2	0.21-0.24
LA_X8_Y8_P1_K2_BF	0.33	0	0.33	0.34
IQR	0.33-0.33	0-0.04	0.33-0.33	0.34-0.34
LA_X8_Y8_P1_K3_BF	0.28	0.25	0.28	0.28
IQR	0.28-0.29	0.21-0.3	0.28-0.28	0.28-0.29
LA_X8_Y8_P2_K2_BF	0	0	0	0
IQR	0-0	0-0	0-0	0-0
LA_X8_Y8_P2_K3_BF	0.9	2.7	0.49	0.49
IQR	0.89-0.9	1.2-2.8	0.49-0.89	0.49-0.49
LA_X8_Y8_P3_K2_BF	0.26	0	0.26	0.39
IQR	0.26-0.26	0-0	0.26-0.26	0.39-0.39
LA_X8_Y8_P3_K3_BF	0.52	0.56	0.49	0.49
IQR	0.49-0.52	0.52-0.67	0.49-0.49	0.49-0.49
LA_X8_Y8_PM_K2_BF	0	0	0	0
IQR	0-0	0-0	0-0	0-0
LA_X9_Y9_P1_K2_BF	0.11	0.06	7.2e-06	0.16
IQR	0.11-0.11	0.029-0.083	7.2e-06-0.11	0.16-0.16
LA_X9_Y9_P1_K3_BF	0.12	0.14	0.11	0.14
IQR	0.12-0.13	0.13-0.15	0.11-0.11	0.14-0.15

Instance Name	d-NSGA-II	$I_{SDE}+$	NSGA-II	NSGA-III
LA_X9_Y9_P2_K2_BF	0	0	0	0
IQR	0-0	0-0	0-0	0-0
LA_X9_Y9_P2_K3_BF	1e+02	1.1	2.1	2.1
IQR	0.27-1e+02	0.75-1.7	0-2.1	0-2.1
LA_X9_Y9_P3_K2_BF	0.28	0.13	0.28	0.29
IQR	0.28-0.28	0.1-0.2	0.28-0.28	0.28-0.31
LA_X9_Y9_P3_K3_BF	0.18	0.2	0.17	0.18
IQR	0.18-0.18	0.19-0.22	0.17-0.17	0.17-0.19
LA_X9_Y9_PM_K2_BF	0	0	0	0
IQR	0-0	0-0	0-0	0-0
LA_X9_Y9_PM_K3_BF	0.6	0.53	0.48	0.6
IQR	0.6-0.61	0.43-0.66	0.32-0.48	0.51-0.62
NO_X10_Y10_P1_K2_BF	0.037	0.045	0.029	0.084
IQR	0.033-0.04	0.043-0.047	0.028-0.03	0.075-0.087
NO_X10_Y10_P1_K3_BF	0.037	0.061	0.032	0.063
IQR	0.036-0.039	0.054-0.068	0.031-0.032	0.044-0.078
NO_X10_Y10_P2_K2_BF	0.087	0.58	0.087	0.13
IQR	0.087-0.087	0.47-0.68	0.087-0.087	0.11-0.13
NO_X10_Y10_P2_K3_BF	0.036	0.075	0.025	0.05
IQR	0.035-0.042	0.064-0.083	0.022-0.026	0.046-0.056
NO_X10_Y10_P3_K2_BF	0.09	0.12	0.036	0.14
IQR	0.077-0.11	0.11-0.14	0.031-0.051	0.13-0.15
NO_X10_Y10_P3_K3_BF	0.031	0.063	0.02	0.039
IQR	0.03-0.033	0.058-0.068	0.019-0.022	0.036-0.04
NO_X10_Y10_PM_K2_BF	0	0.94	0	0.12
IQR	0-0	0.64-1	0-0	0-0.12
NO_X10_Y10_PM_K3_BF	0.056	0.096	0.026	0.065
IQR	0.049-0.064	0.091-0.11	0.023-0.032	0.062-0.07
NO_X11_Y11_P1_K2_BF	0.052	0.076	0.046	0.11
IQR	0.049-0.059	0.071-0.082	0.044-0.046	0.1-0.11
NO_X11_Y11_P1_K3_BF	0.025	0.047	0.02	0.045
IQR	0.024-0.028	0.044-0.052	0.02-0.021	0.037-0.057
NO_X11_Y11_P2_K2_BF	0.036	0.15	0.03	0.095
IQR	0.031-0.053	0.13-0.17	0.029-0.03	0.077-0.13
NO_X11_Y11_P2_K3_BF	0.033	0.07	0.022	0.044
IQR	0.031-0.034	0.066-0.077	0.018-0.024	0.04-0.05
NO_X11_Y11_P3_K2_BF	0.051	0.076	0.023	0.12
IQR	0.047-0.057	0.068-0.081	0.02-0.025	0.089-0.13
NO_X11_Y11_P3_K3_BF	0.026	0.057	0.02	0.034
IQR	0.025-0.027	0.054-0.059	0.02-0.021	0.031-0.036
NO_X11_Y11_PM_K2_BF	0.11	0.37	0.063	0.14
IQR	0.071-0.19	0.3-0.41	0-0.063	0.12-0.17
NO_X11_Y11_PM_K3_BF	0.06	0.11	0.03	0.068
IQR	0.055-0.066	0.1-0.12	0.025-0.051	0.059-0.074
NO_X12_Y12_P1_K2_BF	0.066	0.11	0.05	0.12
IQR	0.057-0.078	0.097-0.12	0.049-0.05	0.1-0.13
NO_X12_Y12_P1_K3_BF	0.035	0.06	0.029	0.057
IQR	0.033-0.037	0.055-0.067	0.028-0.029	0.045-0.061
NO_X12_Y12_P2_K2_BF	0.081	0.16	0.066	0.11
IQR	0.075-0.1	0.15-0.2	0.056-0.067	0.093-0.12
NO_X12_Y12_P2_K3_BF	0.037	0.093	0.024	0.041
IQR	0.034-0.04	0.087-0.11	0.023-0.025	0.038-0.047
NO_X12_Y12_P3_K2_BF	0.071	0.13	0.048	0.12
IQR	0.066-0.078	0.12-0.15	0.042-0.052	0.12-0.13
NO_X12_Y12_P3_K3_BF	0.037	0.085	0.028	0.042
IQR	0.035-0.04	0.077-0.089	0.026-0.029	0.039-0.046
NO_X12_Y12_PM_K2_BF	0.059	0.12	0.034	0.075
IQR	0.054-0.063	0.11-0.15	0.031-0.047	0.068-0.075
NO_X12_Y12_PM_K3_BF	0.027	0.061	0.02	0.045
IQR	0.025-0.033	0.055-0.063	0.019-0.021	0.04-0.048
NO_X13_Y13_P1_K2_BF	0.057	0.099	0.045	0.11
IQR	0.051-0.064	0.092-0.11	0.045-0.045	0.1-0.12
NO_X13_Y13_P1_K3_BF	0.029	0.06	0.023	0.048
IQR	0.028-0.032	0.054-0.067	0.023-0.023	0.04-0.05
NO_X13_Y13_P2_K2_BF	0.099	0.28	0.072	0.12
IQR	0.098-0.11	0.21-0.32	0.067-0.083	0.1-0.14
NO_X13_Y13_P2_K3_BF	0.027	0.068	0.018	0.034
IQR	0.025-0.029	0.059-0.073	0.017-0.018	0.031-0.037
NO_X13_Y13_P3_K2_BF	0.062	0.17	0.053	0.11
IQR	0.057-0.072	0.14-0.2	0.046-0.053	0.085-0.11
NO_X13_Y13_P3_K3_BF	0.026	0.061	0.02	0.032
IQR	0.024-0.028	0.058-0.066	0.019-0.02	0.03-0.038
NO_X13_Y13_PM_K2_BF	0.057	0.13	0.027	0.11

Instance Name	d-NSGA-II	$I_{SDE}+$	NSGA-II	NSGA-III
IQR	0.054-0.088	0.12-0.14	0.026-0.042	0.095-0.12
NO_X13_Y13_PM_K3_BF	0.036	0.068	0.023	0.05
IQR	0.031-0.043	0.065-0.074	0.022-0.024	0.043-0.055
NO_X14_Y14_P1_K2_BF	0.045	0.41	0	0.11
IQR	0.033-0.051	0.31-0.61	0-0.044	0.086-0.14
NO_X14_Y14_P1_K3_BF	0.033	0.083	0.025	0.042
IQR	0.031-0.036	0.073-0.088	0.025-0.026	0.04-0.045
NO_X14_Y14_P2_K2_BF	0.13	0.56	0.098	0.2
IQR	0.1-0.17	0.51-0.64	0.098-0.098	0.17-0.23
NO_X14_Y14_P2_K3_BF	0.031	0.077	0.019	0.043
IQR	0.029-0.036	0.069-0.087	0.018-0.02	0.04-0.051
NO_X14_Y14_P3_K2_BF	0.083	0.46	0.076	0.12
IQR	0.076-0.09	0.38-0.5	0.059-0.076	0.1-0.14
NO_X14_Y14_P3_K3_BF	0.029	0.07	0.021	0.038
IQR	0.028-0.032	0.063-0.073	0.021-0.023	0.035-0.042
NO_X14_Y14_PM_K2_BF	0.056	0.42	0.061	0.075
IQR	0.052-0.065	0.3-0.55	0.038-0.061	0.071-0.092
NO_X14_Y14_PM_K3_BF	0.025	0.064	0.017	0.039
IQR	0.022-0.029	0.058-0.066	0.016-0.018	0.034-0.042
NO_X3_Y3_P1_K2_BF	0	0	0.36	0
IQR	0-0	0-0	0.36-0.36	0-0.58
NO_X3_Y3_P2_K2_BF	0	0	0	0
IQR	0-0	0-0	0-0	0-0
NO_X3_Y3_P3_K2_BF	0	0	0	0
IQR	0-0	0-0	0-0	0-0
NO_X4_Y4_P1_K2_BF	0	0	0	0.31
IQR	0-0	0-0	0-0.066	0.22-0.31
NO_X4_Y4_P1_K3_BF	0.54	0.57	0.42	0.35
IQR	0.54-0.54	0.5-0.86	0.35-0.54	0.35-0.35
NO_X4_Y4_P2_K2_BF	0	0	0	0
IQR	0-0	0-0	0-0	0-0
NO_X4_Y4_P2_K3_BF	0.67	1.1	0.67	0.24
IQR	0.67-0.7	0.97-1.5	0.67-0.67	0.24-0.24
NO_X4_Y4_P3_K2_BF	0.28	0	0	0.28
IQR	0.22-0.32	0-0	0-0	0.28-0.28
NO_X4_Y4_P3_K3_BF	0.65	1.1	0.65	0.24
IQR	0.65-0.65	0.88-1.5	0.65-0.65	0.24-0.54
NO_X4_Y4_PM_K2_BF	0	0	0	0
IQR	0-0	0-0	0-0	0-0
NO_X4_Y4_PM_K3_BF	0.44	0.67	0.39	0.39
IQR	0.41-0.48	0.56-0.76	0.39-0.39	0.36-0.41
NO_X5_Y5_P1_K2_BF	0.17	0	0	0.17
IQR	0.053-0.17	0-0	0-0	0.17-0.21
NO_X5_Y5_P1_K3_BF	0.33	0.37	0.24	0.29
IQR	0.33-0.33	0.34-0.43	0.24-0.24	0.26-0.33
NO_X5_Y5_P2_K2_BF	0.14	0	0	0.27
IQR	0.14-0.31	0-0	0-0	0.27-0.27
NO_X5_Y5_P2_K3_BF	0.41	0.47	0.29	0.27
IQR	0.39-0.44	0.45-0.53	0.24-0.29	0.27-0.29
NO_X5_Y5_P3_K2_BF	0.13	0	0	0.19
IQR	0.12-0.13	0-0.015	0-0	0.19-0.19
NO_X5_Y5_P3_K3_BF	0.27	0.33	0.18	0.21
IQR	0.24-0.28	0.3-0.35	0.18-0.24	0.18-0.24
NO_X5_Y5_PM_K2_BF	0.039	0	0	0.076
IQR	0.032-0.044	0-0.016	0-0	0.07-0.088
NO_X5_Y5_PM_K3_BF	0.29	0.31	0.14	0.2
IQR	0.26-0.32	0.31-0.34	0.11-0.16	0.18-0.22
NO_X6_Y6_P1_K2_BF	0	0.062	0	0.13
IQR	0-0.034	0.051-0.071	0-0	0.038-0.16
NO_X6_Y6_P1_K3_BF	0.22	0.32	0.18	0.21
IQR	0.21-0.25	0.3-0.36	0.17-0.19	0.19-0.22
NO_X6_Y6_P2_K2_BF	0.041	0.062	0	0.18
IQR	0.029-0.047	0.05-0.068	0-0.018	0.16-0.18
NO_X6_Y6_P2_K3_BF	0.15	0.28	0.063	0.18
IQR	0.13-0.16	0.25-0.3	0.054-0.1	0.15-0.23
NO_X6_Y6_P3_K2_BF	0	0.072	0	0.15
IQR	0-0	0.059-0.089	0-0	0.12-0.23
NO_X6_Y6_P3_K3_BF	0.12	0.23	0.05	0.14
IQR	0.11-0.13	0.21-0.25	0.041-0.083	0.13-0.18
NO_X6_Y6_PM_K2_BF	0.038	0.031	0	0.061
IQR	0.034-0.044	0.025-0.036	0-0.008	0.056-0.069
NO_X6_Y6_PM_K3_BF	0.12	0.19	0.081	0.14
IQR	0.1-0.14	0.17-0.21	0.069-0.081	0.12-0.14

Instance Name	d-NSGA-II	$I_{SDE}+$	NSGA-II	NSGA-III
NO_X7_Y7_P1_K2_BF	0.17	0.18	0	0.18
IQR	0.079-0.18	0.15-0.22	0-0	0.18-0.18
NO_X7_Y7_P1_K3_BF	0.092	0.17	0.076	0.099
IQR	0.091-0.095	0.14-0.18	0.076-0.081	0.092-0.11
NO_X7_Y7_P2_K2_BF	0.054	0.19	0	0.095
IQR	2.2e-16-0.078	0.17-0.23	0-0	0.087-0.14
NO_X7_Y7_P2_K3_BF	0.076	0.15	0.052	0.083
IQR	0.073-0.083	0.13-0.17	0.049-0.052	0.078-0.089
NO_X7_Y7_P3_K2_BF	0.099	0.18	0	0.13
IQR	0.082-0.11	0.16-0.22	0-0	0.11-0.13
NO_X7_Y7_P3_K3_BF	0.07	0.12	0.054	0.078
IQR	0.065-0.077	0.11-0.13	0.054-0.056	0.066-0.084
NO_X7_Y7_PM_K2_BF	0.092	0.17	0	0.092
IQR	0.072-0.099	0.12-0.18	0-0	0.092-0.1
NO_X7_Y7_PM_K3_BF	0.079	0.11	0.036	0.085
IQR	0.065-0.083	0.1-0.12	0.033-0.038	0.072-0.11
NO_X8_Y8_P1_K2_BF	0.065	0.069	0.0064	0.13
IQR	0.064-0.068	0.064-0.08	0-0.06	0.13-0.14
NO_X8_Y8_P1_K3_BF	0.039	0.08	0.032	0.049
IQR	0.037-0.041	0.069-0.087	0.032-0.035	0.046-0.056
NO_X8_Y8_P2_K2_BF	0.067	0.15	0.037	0.09
IQR	0.063-0.074	0.13-0.18	0.017-0.063	0.079-0.097
NO_X8_Y8_P2_K3_BF	0.051	0.1	0.025	0.061
IQR	0.047-0.055	0.099-0.11	0.024-0.029	0.056-0.07
NO_X8_Y8_P3_K2_BF	0.033	0.077	0.011	0.17
IQR	0.03-0.045	0.07-0.085	0-0.011	0.14-0.17
NO_X8_Y8_P3_K3_BF	0.046	0.088	0.03	0.053
IQR	0.044-0.049	0.082-0.093	0.029-0.031	0.051-0.057
NO_X8_Y8_PM_K2_BF	0.1	0.21	0.056	0.14
IQR	0.09-0.14	0.17-0.24	0.056-0.09	0.13-0.17
NO_X8_Y8_PM_K3_BF	0.076	0.14	0.045	0.087
IQR	0.068-0.088	0.13-0.15	0.035-0.059	0.08-0.091
NO_X9_Y9_P1_K2_BF	0.074	0.089	0.062	0.15
IQR	0.067-0.091	0.084-0.11	0.00019-0.062	0.15-0.15
NO_X9_Y9_P1_K3_BF	0.031	0.063	0.026	0.045
IQR	0.029-0.035	0.057-0.071	0.026-0.026	0.039-0.061
NO_X9_Y9_P2_K2_BF	0	0	0	0
IQR	0-0	0-0	0-0	0-0
NO_X9_Y9_P2_K3_BF	0.043	0.075	0.027	0.054
IQR	0.039-0.05	0.068-0.082	0.025-0.028	0.049-0.061
NO_X9_Y9_P3_K2_BF	0.18	0.25	0.095	0.24
IQR	0.12-0.35	0.23-0.29	0.084-0.095	0.22-0.24
NO_X9_Y9_P3_K3_BF	0.037	0.065	0.023	0.044
IQR	0.031-0.041	0.057-0.07	0.022-0.023	0.038-0.048
NO_X9_Y9_PM_K2_BF	0	0	0	0
IQR	0-0	0-0	0-0	0-0
NO_X9_Y9_PM_K3_BF	0.086	0.16	0.045	0.086
IQR	0.078-0.1	0.14-0.17	0.04-0.049	0.079-0.1

Table B.2: Raw values of different instances of the IGD indicator. Shown are the median and the IQR values below.

B.2 Initial Solution Generation

	ISG-RANDOM	ISG-YENSK
CH_X10_Y10_P1_K2_BF	0 (0-0.001205)	0 (0-0.001205)
CH_X10_Y10_P1_K2_BT	0.02398 (0.007642-0.04216)	0.005254 (2.007e-08-0.02317)
CH_X10_Y10_P1_K3_BF	0.2365 (0.217-0.2886)	0.2052 (0.07055-0.2141)
CH_X10_Y10_P1_K3_BT	0.9672 (0.6862-1.22)	0.1224 (0.05398-0.1331)
CH_X10_Y10_P2_K2_BF	0.1667 (0-0.1844)	0.6125 (0.08777-0.6125)
CH_X10_Y10_P2_K2_BT	8.142e-16 (0-0.1667)	0.4537 (0.4537-0.4987)
CH_X10_Y10_P2_K3_BF	0.2636 (0.222-0.3353)	0.07955 (0.05946-0.09121)
CH_X10_Y10_P2_K3_BT	0.9284 (0.7736-1.136)	0.09753 (0.06687-0.3103)
CH_X10_Y10_P3_K2_BF	0.04173 (1.563e-05-0.04303)	0 (0-0.002127)
CH_X10_Y10_P3_K2_BT	0.04167 (6.253e-05-0.04308)	0.04316 (6.253e-05-0.06078)
CH_X10_Y10_P3_K3_BF	0.4841 (0.286-0.5504)	0.0832 (0.06963-0.0933)
CH_X10_Y10_P3_K3_BT	0.7758 (0.6505-0.9489)	0.2077 (0.2015-0.2279)

	ISG-RANDOM	ISG-YENSK
CH_X10_Y10_PM_K2_BF	0 (0-0)	0 (0-0)
CH_X10_Y10_PM_K2_BT	0 (0-0)	0 (0-0)
CH_X10_Y10_PM_K3_BF	0.5142 (0.475-0.5738)	0.23 (0.2082-0.2355)
CH_X10_Y10_PM_K3_BT	0.9521 (0.8042-1.141)	0.08734 (0.07161-0.103)
CH_X15_Y15_P1_K2_BF	0.01986 (0.00848-0.03283)	0.03455 (0.01772-0.05628)
CH_X15_Y15_P1_K2_BT	0.3297 (0.2177-0.4111)	0.03709 (0.02993-0.06931)
CH_X15_Y15_P1_K3_BF	0.2553 (0.2161-0.2955)	0.07747 (0.07445-0.08508)
CH_X15_Y15_P1_K3_BT	1.357 (1.157-1.814)	0.09264 (0.05957-0.6214)
CH_X15_Y15_P2_K2_BF	0 (0-0)	0 (0-0)
CH_X15_Y15_P2_K2_BT	0 (0-0)	0 (0-0)
CH_X15_Y15_P2_K3_BF	0.4398 (0.3631-0.5373)	0.1094 (0.09178-0.13)
CH_X15_Y15_P2_K3_BT	1.894 (1.74-2.029)	0.1123 (0.08825-0.1225)
CH_X15_Y15_P3_K2_BF	0.2095 (0.07146-0.3463)	0.459 (0.2455-0.5362)
CH_X15_Y15_P3_K2_BT	0.5368 (0.3718-0.8918)	0.5074 (0.4759-0.5723)
CH_X15_Y15_P3_K3_BF	0.315 (0.2778-0.3715)	0.09752 (0.09319-0.1122)
CH_X15_Y15_P3_K3_BT	1.637 (1.455-1.899)	0.2807 (0.2582-0.3031)
CH_X15_Y15_PM_K2_BF	0 (0-0)	0 (0-0)
CH_X15_Y15_PM_K2_BT	0 (0-0)	0 (0-0)
CH_X15_Y15_PM_K3_BF	0.4179 (0.3725-0.477)	0.4162 (0.1543-0.4262)
CH_X15_Y15_PM_K3_BT	1.849 (1.527-2.073)	0.1366 (0.1271-0.1442)
CH_X20_Y20_P1_K2_BF	0.3815 (0.3126-0.4393)	0.0142 (0.01115-0.02457)
CH_X20_Y20_P1_K2_BT	0.5497 (0.4917-0.698)	0.02015 (0.01504-0.03449)
CH_X20_Y20_P1_K3_BF	0.3719 (0.2799-0.4365)	0.03312 (0.03008-0.03803)
CH_X20_Y20_P1_K3_BT	2.383 (2.136-2.722)	0.03336 (0.02968-0.04227)
CH_X20_Y20_P2_K2_BF	0.808 (0.6993-0.9018)	0.1972 (0.1692-0.2453)
CH_X20_Y20_P2_K2_BT	0.9224 (0.6834-1.083)	0.3318 (0.266-0.4978)
CH_X20_Y20_P2_K3_BF	0.6808 (0.6134-0.759)	0.4296 (0.3038-0.6389)
CH_X20_Y20_P2_K3_BT	2.461 (2.165-2.824)	0.7109 (0.4392-0.7127)
CH_X20_Y20_P3_K2_BF	0.5656 (0.4979-0.6308)	0.09579 (0.07553-0.1274)
CH_X20_Y20_P3_K2_BT	0.7006 (0.6217-0.8468)	0.1724 (0.1095-0.21)
CH_X20_Y20_P3_K3_BF	0.5907 (0.5251-0.6467)	0.44 (0.2466-0.4713)
CH_X20_Y20_P3_K3_BT	2.639 (2.342-2.906)	0.3131 (0.312-0.3151)
CH_X20_Y20_PM_K2_BF	1.007 (0.8392-1.103)	0.1671 (0.1224-0.2496)
CH_X20_Y20_PM_K2_BT	1.253 (1.077-1.531)	0.2592 (0.09795-0.2907)
CH_X20_Y20_PM_K3_BF	0.5045 (0.3821-0.5738)	0.1257 (0.1207-0.1424)
CH_X20_Y20_PM_K3_BT	1.777 (1.55-2.12)	0.1577 (0.1543-0.1635)
CH_X30_Y30_P1_K2_BF	0.6221 (0.5607-0.7032)	0.0428 (0.03337-0.05673)
CH_X30_Y30_P1_K2_BT	0.9146 (0.7935-1.144)	0.05427 (0.03742-0.1175)
CH_X30_Y30_P1_K3_BF	0.5411 (0.4933-0.5915)	0.02313 (0.02301-0.02455)
CH_X30_Y30_P1_K3_BT	2.801 (2.346-3.081)	0.02145 (0.02065-0.02922)
CH_X30_Y30_P2_K2_BF	2.452 (2.35-2.694)	0.4521 (0.4128-0.511)
CH_X30_Y30_P2_K2_BT	3.593 (3.418-3.828)	0.447 (0.4128-0.5141)
CH_X30_Y30_P2_K3_BF	1.021 (0.9133-1.051)	1.098 (0.44-1.098)
CH_X30_Y30_P2_K3_BT	3.378 (3.083-3.753)	0.4659 (0.4652-0.4793)
CH_X30_Y30_P3_K2_BF	0.769 (0.6155-0.8528)	0.1459 (0.1133-0.1585)
CH_X30_Y30_P3_K2_BT	1.195 (1.054-1.326)	0.3135 (0.2682-0.3387)
CH_X30_Y30_P3_K3_BF	0.7731 (0.7215-0.8598)	0.4028 (0.4018-0.4083)
CH_X30_Y30_P3_K3_BT	3.252 (3.038-3.492)	0.3983 (0.3977-0.4054)
CH_X30_Y30_PM_K2_BF	2.618 (2.367-2.798)	0.4266 (0.3943-0.4473)
CH_X30_Y30_PM_K2_BT	3.817 (3.12-4.179)	0.4266 (0.3788-0.4429)
CH_X30_Y30_PM_K3_BF	0.9592 (0.8971-1.011)	0.3943 (0.3925-0.4368)
CH_X30_Y30_PM_K3_BT	2.458 (2.321-2.677)	0.3089 (0.3079-0.3134)
CH_X5_Y5_P1_K2_BF	0 (0-0)	0 (0-0)
CH_X5_Y5_P1_K2_BT	0.09952 (0.09952-0.09952)	0 (0-0)
CH_X5_Y5_P1_K3_BF	0 (0-0)	0 (0-0)
CH_X5_Y5_P1_K3_BT	0 (0-0)	0.06452 (0-0.1707)
CH_X5_Y5_P2_K2_BF	0 (0-0)	0.3088 (0-0.3088)
CH_X5_Y5_P2_K2_BT	0 (0-0)	0 (0-0)
CH_X5_Y5_P2_K3_BF	0 (0-0)	0 (0-0)
CH_X5_Y5_P2_K3_BT	0.01377 (0.004552-0.05992)	0.07343 (0.03687-0.09074)
CH_X5_Y5_P3_K2_BF	0 (0-0)	0 (0-0)
CH_X5_Y5_P3_K2_BT	0 (0-0)	0 (0-0)
CH_X5_Y5_P3_K3_BF	0 (0-0)	0 (0-0)
CH_X5_Y5_P3_K3_BT	0.06049 (0-0.321)	0.7297 (0.7297-0.7297)
CH_X5_Y5_PM_K2_BF	0.2322 (0.2322-0.2322)	0 (0-0)
CH_X5_Y5_PM_K2_BT	0 (0-0)	0 (0-0)
CH_X5_Y5_PM_K3_BF	0 (0-0)	0 (0-0)
CH_X5_Y5_PM_K3_BT	0.02154 (0.001291-0.02283)	0.1291 (0.03336-0.2199)
LA_X10_Y10_P1_K2_BF	0.0576 (0.04877-0.06664)	0.02296 (0.01939-0.02517)
LA_X10_Y10_P1_K2_BT	0.2248 (0.1593-0.2989)	0.01303 (0.008897-0.02213)
LA_X10_Y10_P1_K3_BF	0.1379 (0.1265-0.1711)	0.0379 (0.0293-0.05081)
LA_X10_Y10_P1_K3_BT	1.495 (1.258-1.717)	0.04194 (0.02756-0.05821)
LA_X10_Y10_P2_K2_BF	0.664 (0.6066-0.9295)	0.07563 (0.01457-0.1538)

	ISG-RANDOM	ISG-YENSK
LA_X10_Y10_P2_K2_BT	1.441 (0.926-1.797)	0.1667 (0.1667-0.3333)
LA_X10_Y10_P2_K3_BF	1.107 (0.8364-1.389)	0.1434 (0.06561-0.2426)
LA_X10_Y10_P2_K3_BT	3.928 (3.48-4.891)	0.09388 (0.05086-0.2052)
LA_X10_Y10_P3_K2_BF	0.1504 (0.1363-0.1942)	0.1606 (0.1292-0.1841)
LA_X10_Y10_P3_K2_BT	0.3767 (0.2864-0.4267)	0.1425 (0.1039-0.2012)
LA_X10_Y10_P3_K3_BF	0.4062 (0.3711-0.4406)	0.06307 (0.05453-0.0973)
LA_X10_Y10_P3_K3_BT	1.546 (1.192-1.888)	0.06128 (0.05579-0.06587)
LA_X10_Y10_PM_K2_BF	0.7089 (0.4916-1.209)	0.509 (0.494-0.5574)
LA_X10_Y10_PM_K2_BT	1.065 (0.8253-1.216)	0.04235 (0.01635-0.06308)
LA_X10_Y10_PM_K3_BF	0.9667 (0.8226-1.02)	0.2815 (0.2584-0.3548)
LA_X10_Y10_PM_K3_BT	2.134 (1.68-2.45)	0.1623 (0.1496-0.1752)
LA_X15_Y15_P1_K2_BF	0.2993 (0.2644-0.3561)	0.07021 (0.02956-0.1039)
LA_X15_Y15_P1_K2_BT	1.16 (1.038-1.342)	0.02451 (0.02021-0.02941)
LA_X15_Y15_P1_K3_BF	0.4939 (0.4286-0.5459)	0.07797 (0.03709-0.1627)
LA_X15_Y15_P1_K3_BT	3.261 (2.841-3.637)	0.1135 (0.1135-0.1183)
LA_X15_Y15_P2_K2_BF	0 (0-0)	0 (0-0)
LA_X15_Y15_P2_K2_BT	0 (0-0)	0 (0-0)
LA_X15_Y15_P2_K3_BF	1.279 (1.034-1.39)	0.374 (0.2869-0.4993)
LA_X15_Y15_P2_K3_BT	4.963 (4.16-5.442)	0.4237 (0.3883-0.5647)
LA_X15_Y15_P3_K2_BF	0.4699 (0.4142-0.5461)	0.6441 (0.5451-0.7635)
LA_X15_Y15_P3_K2_BT	1.795 (1.474-2.156)	0.8611 (0.6792-0.9132)
LA_X15_Y15_P3_K3_BF	0.7087 (0.6643-0.8015)	0.9174 (0.9174-1.059)
LA_X15_Y15_P3_K3_BT	2.849 (2.625-3.049)	0.3186 (0.2897-0.3342)
LA_X15_Y15_PM_K2_BF	0 (0-0)	0 (0-0)
LA_X15_Y15_PM_K2_BT	0 (0-0)	0 (0-0)
LA_X15_Y15_PM_K3_BF	0.6442 (0.5644-0.7331)	0.6691 (0.6683-0.6827)
LA_X15_Y15_PM_K3_BT	3.567 (3.178-3.816)	0.1714 (0.1667-0.1776)
LA_X20_Y20_P1_K2_BF	1.471 (0.932-1.965)	0.4903 (0.4683-0.5503)
LA_X20_Y20_P1_K2_BT	6.553 (5.346-8.766)	0.5556 (0.4816-0.6188)
LA_X20_Y20_P1_K3_BF	0.7637 (0.606-0.844)	0.02904 (0.02766-0.03846)
LA_X20_Y20_P1_K3_BT	5.371 (4.68-5.818)	0.02901 (0.02708-0.03952)
LA_X20_Y20_P2_K2_BF	1.276 (0.9601-1.635)	0.5316 (0.5039-0.5637)
LA_X20_Y20_P2_K2_BT	4.904 (4.3-5.305)	0.5564 (0.5097-0.6029)
LA_X20_Y20_P2_K3_BF	0.9352 (0.8591-1.029)	0.4851 (0.4832-0.5981)
LA_X20_Y20_P2_K3_BT	5.542 (4.718-6.112)	0.5887 (0.5881-0.5917)
LA_X20_Y20_P3_K2_BF	1.408 (1.077-1.55)	0.515 (0.4823-0.537)
LA_X20_Y20_P3_K2_BT	5.118 (4.447-5.481)	0.6485 (0.536-0.7524)
LA_X20_Y20_P3_K3_BF	0.8049 (0.6837-0.8924)	0.2749 (0.2707-0.2842)
LA_X20_Y20_P3_K3_BT	5.164 (4.794-5.672)	0.1241 (0.1232-0.1376)
LA_X20_Y20_PM_K2_BF	1.888 (1.609-2.41)	0.454 (0.4526-0.5289)
LA_X20_Y20_PM_K2_BT	4.419 (3.639-5.044)	0.4625 (0.2309-0.4659)
LA_X20_Y20_PM_K3_BF	0.8867 (0.7545-0.9238)	0.3331 (0.3167-0.4533)
LA_X20_Y20_PM_K3_BT	4.689 (4.336-5.04)	0.3198 (0.2625-0.3878)
LA_X30_Y30_P1_K2_BF	0.6923 (0.6181-0.7383)	0.01234 (0.01189-0.02688)
LA_X30_Y30_P1_K2_BT	6.187 (5.107-6.725)	0.02616 (0.01185-0.02661)
LA_X30_Y30_P1_K3_BF	0.8273 (0.7146-0.8895)	0.2172 (0.2114-0.2241)
LA_X30_Y30_P1_K3_BT	5.637 (5.008-6.086)	0.6951 (0.6949-0.6956)
LA_X30_Y30_P2_K2_BF	2.784 (2.447-2.929)	0.8071 (0.7835-0.8071)
LA_X30_Y30_P2_K2_BT	7.949 (7.413-8.583)	0.7689 (0.7688-0.7835)
LA_X30_Y30_P2_K3_BF	1.139 (1.068-1.191)	0.1716 (0.1716-0.1731)
LA_X30_Y30_P2_K3_BT	5.502 (4.991-5.938)	0.1205 (0.1202-0.1654)
LA_X30_Y30_P3_K2_BF	0.9054 (0.7776-1.011)	0.7605 (0.6346-0.7669)
LA_X30_Y30_P3_K2_BT	5.944 (5.368-6.874)	0.4532 (0.4362-0.4681)
LA_X30_Y30_P3_K3_BF	0.9423 (0.8453-1.01)	0.1738 (0.1728-0.1752)
LA_X30_Y30_P3_K3_BT	5.494 (5.152-5.919)	0.2265 (0.2034-0.2277)
LA_X30_Y30_PM_K2_BF	8.735 (6.701-11.31)	0.6948 (0.6948-0.7401)
LA_X30_Y30_PM_K2_BT	10.99 (10.3-12.28)	0.602 (0.5965-0.6682)
LA_X30_Y30_PM_K3_BF	1.399 (1.287-1.467)	0.3609 (0.3589-0.3667)
LA_X30_Y30_PM_K3_BT	7.705 (7.162-8.017)	0.5628 (0.5625-0.5723)
LA_X5_Y5_P1_K2_BF	0.1943 (0-0.1943)	0 (0-0)
LA_X5_Y5_P1_K2_BT	0.2967 (0.2967-0.2967)	0 (0-0)
LA_X5_Y5_P1_K3_BF	0 (0-0)	0 (0-0)
LA_X5_Y5_P1_K3_BT	0.02101 (0-0.3333)	0.08333 (0-0.4192)
LA_X5_Y5_P2_K2_BF	0 (0-0)	0 (0-0)
LA_X5_Y5_P2_K2_BT	0 (0-0)	0 (0-0)
LA_X5_Y5_P2_K3_BF	0 (0-0)	0 (0-0)
LA_X5_Y5_P2_K3_BT	0.02101 (0-0.3333)	0 (0-0.2176)
LA_X5_Y5_P3_K2_BF	0.329 (0-0.329)	0 (0-0)
LA_X5_Y5_P3_K2_BT	0 (0-0)	0 (0-0)
LA_X5_Y5_P3_K3_BF	0.004272 (0-0.004272)	0 (0-0)
LA_X5_Y5_P3_K3_BT	0 (0-0.12)	0.1249 (0.1249-0.1262)
LA_X5_Y5_PM_K2_BF	0 (0-0.4297)	0 (0-0)
LA_X5_Y5_PM_K2_BT	0 (0-0)	0 (0-0)

	ISG-RANDOM	ISG-YENSK
LA_X5_Y5_PM_K3_BF	0 (0-0)	0 (0-0)
LA_X5_Y5_PM_K3_BT	0.05357 (0.03297-0.08686)	0.07195 (0.005787-0.1031)
NO_X10_Y10_P1_K2_BF	0.2038 (0.1552-0.2348)	0.04728 (0.04145-0.1042)
NO_X10_Y10_P1_K2_BT	0.3939 (0.3041-0.4707)	0.04649 (0.04162-0.1076)
NO_X10_Y10_P1_K3_BF	0.2535 (0.2238-0.2871)	0.03354 (0.02848-0.04609)
NO_X10_Y10_P1_K3_BT	1.104 (0.7431-1.28)	0.1967 (0.1831-0.2421)
NO_X10_Y10_P2_K2_BF	1.027 (0.5287-1.193)	0.2787 (0.2298-0.3453)
NO_X10_Y10_P2_K2_BT	2.163 (1.653-2.382)	0.7404 (0.6486-0.7736)
NO_X10_Y10_P2_K3_BF	0.4362 (0.3878-0.4753)	0.2529 (0.2481-0.2778)
NO_X10_Y10_P2_K3_BT	0.9972 (0.8973-1.206)	0.2583 (0.2502-0.2667)
NO_X10_Y10_P3_K2_BF	0.2855 (0.2016-0.3264)	0.497 (0.4908-0.5108)
NO_X10_Y10_P3_K2_BT	0.6191 (0.509-0.7272)	0.4815 (0.4683-0.5029)
NO_X10_Y10_P3_K3_BF	0.3638 (0.3164-0.4058)	0.2275 (0.2199-0.2393)
NO_X10_Y10_P3_K3_BT	0.8891 (0.7246-0.9787)	0.4154 (0.4087-0.4428)
NO_X10_Y10_PM_K2_BF	0.6884 (0.4916-1.058)	0.6191 (0.4568-0.7842)
NO_X10_Y10_PM_K2_BT	1.901 (1.343-2.383)	0.4365 (0.2695-0.4855)
NO_X10_Y10_PM_K3_BF	0.496 (0.4205-0.5447)	0.1909 (0.1079-0.2063)
NO_X10_Y10_PM_K3_BT	1.085 (0.9712-1.273)	0.1052 (0.09889-0.1132)
NO_X15_Y15_P1_K2_BF	0.4795 (0.4035-0.5704)	0.0247 (0.01852-0.06795)
NO_X15_Y15_P1_K2_BT	1.345 (1.064-1.511)	0.0247 (0.0247-0.06588)
NO_X15_Y15_P1_K3_BF	0.5384 (0.4142-0.6317)	0.03899 (0.03543-0.04398)
NO_X15_Y15_P1_K3_BT	2.13 (1.897-2.36)	0.1092 (0.03616-0.1219)
NO_X15_Y15_P2_K2_BF	0 (0-0)	0 (0-0)
NO_X15_Y15_P2_K2_BT	0 (0-0)	0 (0-0)
NO_X15_Y15_P2_K3_BF	0.6088 (0.5128-0.6738)	0.3068 (0.2959-0.3329)
NO_X15_Y15_P2_K3_BT	2.634 (2.378-3)	0.335 (0.3232-0.3547)
NO_X15_Y15_P3_K2_BF	0.6743 (0.5643-0.8147)	0.6458 (0.6458-1.092)
NO_X15_Y15_P3_K2_BT	2.517 (2.143-2.962)	0.9564 (0.8466-1.18)
NO_X15_Y15_P3_K3_BF	0.6091 (0.5447-0.6605)	0.2914 (0.2835-0.3127)
NO_X15_Y15_P3_K3_BT	1.841 (1.55-2.027)	0.2844 (0.2805-0.2985)
NO_X15_Y15_PM_K2_BF	0 (0-0)	0 (0-0)
NO_X15_Y15_PM_K2_BT	0 (0-0)	0 (0-0)
NO_X15_Y15_PM_K3_BF	0.952 (0.9051-1.008)	0.1188 (0.1008-0.1263)
NO_X15_Y15_PM_K3_BT	2.216 (1.895-2.431)	0.7348 (0.09514-0.7455)
NO_X20_Y20_P1_K2_BF	3.136 (2.236-5.691)	0.7412 (0.7412-0.782)
NO_X20_Y20_P1_K2_BT	11.11 (8.852-21.47)	0.6796 (0.6796-0.7104)
NO_X20_Y20_P1_K3_BF	0.7187 (0.6362-0.8496)	0.128 (0.1214-0.1336)
NO_X20_Y20_P1_K3_BT	3.417 (2.942-3.85)	0.1323 (0.1239-0.1368)
NO_X20_Y20_P2_K2_BF	1.899 (1.594-2.223)	0.6318 (0.6318-0.6573)
NO_X20_Y20_P2_K2_BT	3.109 (2.787-3.527)	0.8837 (0.8837-0.9003)
NO_X20_Y20_P2_K3_BF	0.8733 (0.8189-0.9199)	0.4567 (0.4484-0.4885)
NO_X20_Y20_P2_K3_BT	2.915 (2.548-3.061)	0.5057 (0.474-0.758)
NO_X20_Y20_P3_K2_BF	1.943 (1.599-2.234)	0.609 (0.609-0.6361)
NO_X20_Y20_P3_K2_BT	5.718 (5.343-5.984)	0.609 (0.609-0.6271)
NO_X20_Y20_P3_K3_BF	0.691 (0.6144-0.7977)	0.3801 (0.3727-0.4075)
NO_X20_Y20_P3_K3_BT	2.704 (2.476-3.149)	0.3526 (0.35-0.3987)
NO_X20_Y20_PM_K2_BF	2.736 (1.662-3.492)	0.5349 (0.4418-0.5349)
NO_X20_Y20_PM_K2_BT	5.246 (4.212-5.697)	0.9347 (0.9137-0.9383)
NO_X20_Y20_PM_K3_BF	0.7697 (0.6803-0.8226)	0.1462 (0.1414-0.1515)
NO_X20_Y20_PM_K3_BT	2.88 (2.584-3.11)	0.1508 (0.1466-0.1657)
NO_X30_Y30_P1_K2_BF	0.8965 (0.7933-0.9642)	0.01183 (0.005815-0.01296)
NO_X30_Y30_P1_K2_BT	4.504 (3.731-4.856)	0.01236 (0.01225-0.01285)
NO_X30_Y30_P1_K3_BF	0.6528 (0.5942-0.7111)	0.08196 (0.05557-0.08381)
NO_X30_Y30_P1_K3_BT	3.104 (2.77-3.327)	0.03115 (0.03043-0.08168)
NO_X30_Y30_P2_K2_BF	3.416 (3.054-3.762)	0.7635 (0.7164-0.7927)
NO_X30_Y30_P2_K2_BT	8.483 (8.008-9.004)	0.8091 (0.7754-0.8577)
NO_X30_Y30_P2_K3_BF	0.954 (0.9142-1.011)	0.6079 (0.5969-0.6128)
NO_X30_Y30_P2_K3_BT	3.544 (3.347-3.752)	0.6254 (0.6244-0.6382)
NO_X30_Y30_P3_K2_BF	1.385 (1.171-1.52)	0.5007 (0.3262-0.5157)
NO_X30_Y30_P3_K2_BT	5.27 (4.456-6.181)	0.7173 (0.6145-0.7194)
NO_X30_Y30_P3_K3_BF	1.006 (0.9387-1.04)	0.5246 (0.5167-0.545)
NO_X30_Y30_P3_K3_BT	3.543 (3.269-3.741)	0.8048 (0.5326-0.8058)
NO_X30_Y30_PM_K2_BF	12.72 (9.122-17.07)	0.9871 (0.6948-1.912)
NO_X30_Y30_PM_K2_BT	12.65 (11.1-16.18)	0.8616 (0.8616-8.062)
NO_X30_Y30_PM_K3_BF	0.9392 (0.8887-0.9873)	0.222 (0.2204-0.2237)
NO_X30_Y30_PM_K3_BT	3.656 (3.363-3.922)	0.2297 (0.2273-0.2314)

Table B.3: Raw values of different instances of the IGD+ indicator. Median (lower quartile - upper quartile).

	ISG-RANDOM	ISG-YENSK
CH_X10_Y10_P1_K2_BF	0.3278 (0.1358-1.016)	0.5455 (0.02273-2.265)
CH_X10_Y10_P1_K2_BT	0.2033 (0.1575-0.3081)	0.2227 (0.1286-0.5567)
CH_X10_Y10_P1_K3_BF	0.3116 (0.2621-0.3993)	0.2033 (0.1874-0.225)
CH_X10_Y10_P1_K3_BT	0.3451 (0.2981-7.071)	0.2085 (0.1944-0.2206)
CH_X10_Y10_P2_K2_BF	0.5477 (0.3333-0.7454)	0 (0-0)
CH_X10_Y10_P2_K2_BT	0 (0-0.6667)	0.6667 (0-4.082)
CH_X10_Y10_P2_K3_BF	7.071 (0.2834-7.81)	0.1969 (0.1842-0.217)
CH_X10_Y10_P2_K3_BT	3.592 (0.3683-3.592)	0.2 (0.1871-0.2277)
CH_X10_Y10_P3_K2_BF	0.5735 (0.3234-0.5735)	0 (0-0.125)
CH_X10_Y10_P3_K2_BT	0.25 (0.1768-0.2995)	0.25 (0.125-0.3417)
CH_X10_Y10_P3_K3_BF	1.202 (1.079-1.563)	0.1876 (0.18-0.2069)
CH_X10_Y10_P3_K3_BT	0.278 (0.2632-0.3065)	0.1951 (0.1825-0.204)
CH_X10_Y10_PM_K2_BF	0 (0-0.401)	1.162 (1.162-1.162)
CH_X10_Y10_PM_K2_BT	0.868 (0.868-0.868)	0 (0-2.132)
CH_X10_Y10_PM_K3_BF	0.3057 (0.2851-0.3857)	0.1765 (0.1689-0.2038)
CH_X10_Y10_PM_K3_BT	0.3608 (0.3287-0.5106)	0.2038 (0.1898-0.2154)
CH_X15_Y15_P1_K2_BF	0.2857 (0.2227-0.5207)	2.673 (2.132-2.673)
CH_X15_Y15_P1_K2_BT	0.269 (0.269-0.6316)	0.4151 (0.3498-0.4542)
CH_X15_Y15_P1_K3_BF	0.203 (0.1952-0.2155)	0.319 (0.3111-0.3331)
CH_X15_Y15_P1_K3_BT	0.2733 (0.2453-0.3213)	0.2997 (0.2878-0.309)
CH_X15_Y15_P2_K2_BF	1.091 (0-1.512)	0 (0-2)
CH_X15_Y15_P2_K2_BT	2 (2-2)	0.5758 (0.5643-0.7755)
CH_X15_Y15_P2_K3_BF	4.123 (2.236-4.472)	0.2759 (0.2688-0.2821)
CH_X15_Y15_P2_K3_BT	0.3665 (0.3281-0.4091)	0.288 (0.282-0.2921)
CH_X15_Y15_P3_K2_BF	0.7713 (0.6263-1.118)	1 (0.8649-1.061)
CH_X15_Y15_P3_K2_BT	1.042 (0.9749-1.212)	1.155 (1.018-1.197)
CH_X15_Y15_P3_K3_BF	0.236 (0.2208-0.2547)	0.2656 (0.259-0.2718)
CH_X15_Y15_P3_K3_BT	0.3336 (0.3102-0.3784)	0.2617 (0.2579-0.2683)
CH_X15_Y15_PM_K2_BF	3.282 (2-3.282)	0.5185 (0.5185-0.9866)
CH_X15_Y15_PM_K2_BT	1.416 (1.414-2)	0 (0-2)
CH_X15_Y15_PM_K3_BF	0.23 (0.2186-0.2361)	0.3462 (0.2962-0.3602)
CH_X15_Y15_PM_K3_BT	0.3187 (0.2946-0.356)	0.2906 (0.2521-0.3338)
CH_X20_Y20_P1_K2_BF	0.6132 (0.5186-2.402)	0.3001 (0.2753-0.3406)
CH_X20_Y20_P1_K2_BT	0.6426 (0.564-1.129)	0.5336 (0.3964-0.5575)
CH_X20_Y20_P1_K3_BF	0.285 (0.245-0.2879)	0.3486 (0.3398-0.3502)
CH_X20_Y20_P1_K3_BT	1.004 (0.7906-1.223)	0.3607 (0.3536-0.3632)
CH_X20_Y20_P2_K2_BF	0.7589 (0.6585-0.8476)	0.329 (0.2871-0.3426)
CH_X20_Y20_P2_K2_BT	0.7882 (0.6093-3.656)	0.6261 (0.5986-1.163)
CH_X20_Y20_P2_K3_BF	1.611 (1.559-1.862)	0.3166 (0.3101-0.327)
CH_X20_Y20_P2_K3_BT	0.4975 (0.4975-5)	0.3632 (0.3515-0.3656)
CH_X20_Y20_P3_K2_BF	0.8119 (0.3064-2.949)	0.4118 (0.3847-10.61)
CH_X20_Y20_P3_K2_BT	0.604 (0.3225-0.7296)	1.491 (1.294-7.071)
CH_X20_Y20_P3_K3_BF	0.2301 (0.214-1.243)	3.536 (0.3031-3.536)
CH_X20_Y20_P3_K3_BT	0.5293 (0.5293-0.5295)	0.3133 (0.3072-2.749)
CH_X20_Y20_PM_K2_BF	0.2799 (0.2435-0.6858)	2.626 (2.626-2.626)
CH_X20_Y20_PM_K2_BT	0.5455 (0.3413-6.325)	0.4832 (0.4141-0.75)
CH_X20_Y20_PM_K3_BF	3.162 (0.3627-3.162)	0.461 (0.4325-0.4611)
CH_X20_Y20_PM_K3_BT	0.2498 (0.2126-0.906)	0.4306 (0.4079-0.435)
CH_X30_Y30_P1_K2_BF	0.6798 (0.5838-0.7167)	2.887 (2.887-2.887)
CH_X30_Y30_P1_K2_BT	1.114 (0.8607-21.21)	0.6202 (0.6202-3.015)
CH_X30_Y30_P1_K3_BF	0.5939 (0.5939-3.086)	1.388 (0.2604-11.2)
CH_X30_Y30_P1_K3_BT	0.1269 (0.1212-0.1312)	0.2595 (0.2571-0.2595)
CH_X30_Y30_P2_K2_BF	3.086 (1.848-3.086)	0.06135 (0.0603-0.06925)
CH_X30_Y30_P2_K2_BT	1.016 (0.7787-1.387)	3.536 (3.536-8.944)
CH_X30_Y30_P2_K3_BF	0.7184 (0.3019-0.7908)	10 (0.3065-10)
CH_X30_Y30_P2_K3_BT	3.43 (2.914-8.357)	2.265 (2.265-2.265)
CH_X30_Y30_P3_K2_BF	0.585 (0.5052-0.6238)	0.2534 (0.2424-0.2701)
CH_X30_Y30_P3_K2_BT	0.4145 (0.3764-0.4991)	1.598 (1.598-1.598)
CH_X30_Y30_P3_K3_BF	0.1798 (0.1728-0.1904)	0.2724 (0.2724-0.2749)
CH_X30_Y30_P3_K3_BT	1.225 (1.225-4.082)	0.258 (0.258-0.2596)
CH_X30_Y30_PM_K2_BF	0.1424 (0.1181-0.2001)	21.21 (1.65-21.21)
CH_X30_Y30_PM_K2_BT	5.657 (2.846-10)	0.8607 (0.8607-2.012)
CH_X30_Y30_PM_K3_BF	0.2483 (0.239-0.2703)	0.1489 (0.1478-0.3491)
CH_X30_Y30_PM_K3_BT	0.2654 (0.2067-3.313)	3.015 (3.015-17.68)
CH_X5_Y5_P1_K2_BF	5.303 (0-5.303)	0 (0-0)
CH_X5_Y5_P1_K2_BT	0 (0-0)	0 (0-0)
CH_X5_Y5_P1_K3_BF	0 (0-0)	0 (0-0)
CH_X5_Y5_P1_K3_BT	0 (0-0)	0.25 (0-0.25)
CH_X5_Y5_P2_K2_BF	0 (0-0)	0 (0-0)
CH_X5_Y5_P2_K2_BT	4.243 (0-4.243)	0 (0-0)
CH_X5_Y5_P2_K3_BF	0 (0-0)	0 (0-0)
CH_X5_Y5_P2_K3_BT	0.202 (0.1429-0.2474)	0.202 (0.202-0.2857)
CH_X5_Y5_P3_K2_BF	0 (0-0)	0 (0-0)

	ISG-RANDOM	ISG-YENSK
CH_X5_Y5_P3_K2_BT	0 (0-0)	0 (0-0)
CH_X5_Y5_P3_K3_BF	0 (0-0)	0 (0-0)
CH_X5_Y5_P3_K3_BT	0 (0-0.2184)	0.2357 (0.1667-2.828)
CH_X5_Y5_PM_K2_BF	14.14 (14.14-14.14)	0 (0-0)
CH_X5_Y5_PM_K2_BT	1.768 (0-1.768)	0 (0-0)
CH_X5_Y5_PM_K3_BF	0 (0-9.806)	0 (0-0)
CH_X5_Y5_PM_K3_BT	0.1571 (0.1111-0.1925)	0.3333 (0.2485-1.622)
LA_X10_Y10_P1_K2_BF	0.1603 (0.1575-0.1632)	0.5033 (0.4866-0.5098)
LA_X10_Y10_P1_K2_BT	1 (0.3769-1)	0.1556 (0.1507-4.082)
LA_X10_Y10_P1_K3_BF	0.1717 (0.1619-0.1805)	0.1304 (0.1282-0.1368)
LA_X10_Y10_P1_K3_BT	0.2155 (0.1805-0.2266)	0.1296 (0.1277-0.1329)
LA_X10_Y10_P2_K2_BF	0.3499 (0.3499-0.378)	1.456 (0.5626-1.483)
LA_X10_Y10_P2_K2_BT	0.378 (0.3499-0.378)	7.071 (7.071-7.071)
LA_X10_Y10_P2_K3_BF	1.098 (1.098-1.098)	0.2236 (0.2-0.2449)
LA_X10_Y10_P2_K3_BT	0.3606 (0.3317-0.4663)	0.2449 (0.2236-3.592)
LA_X10_Y10_P3_K2_BF	0.217 (0.217-0.2294)	0.2632 (0.2121-0.2735)
LA_X10_Y10_P3_K2_BT	0.2236 (0.2236-0.2487)	0.1732 (0.1658-0.1803)
LA_X10_Y10_P3_K3_BF	0.404 (0.3776-0.433)	0.1434 (0.1335-0.1516)
LA_X10_Y10_P3_K3_BT	0.2334 (0.2064-0.2635)	0.1348 (0.1315-0.1403)
LA_X10_Y10_PM_K2_BF	0.4472 (0.4-0.4472)	0.2 (0.2-0.2828)
LA_X10_Y10_PM_K2_BT	0.3536 (0.3536-0.3536)	0.25 (0.2249-0.25)
LA_X10_Y10_PM_K3_BF	0.2652 (0.25-4.023)	3.162 (0.2253-3.162)
LA_X10_Y10_PM_K3_BT	0.2259 (0.2141-0.3004)	0.1895 (0.1845-5)
LA_X15_Y15_P1_K2_BF	0.3122 (0.2113-0.3605)	0.182 (0.181-0.201)
LA_X15_Y15_P1_K2_BT	1.094 (1.091-1.581)	0.2015 (0.1997-0.3011)
LA_X15_Y15_P1_K3_BF	0.09938 (0.08945-0.108)	0.1228 (0.1174-0.1236)
LA_X15_Y15_P1_K3_BT	0.1377 (0.1308-0.1946)	0.1869 (0.1178-0.4161)
LA_X15_Y15_P2_K2_BF	7.071 (2-7.071)	2.99 (1.104-8.165)
LA_X15_Y15_P2_K2_BT	2 (2-3.122)	0 (0-1)
LA_X15_Y15_P2_K3_BF	0.2211 (0.2049-0.2408)	1.091 (1.091-1.091)
LA_X15_Y15_P2_K3_BT	0.3105 (0.2878-0.347)	3.162 (3.162-3.162)
LA_X15_Y15_P3_K2_BF	0.2884 (0.2245-0.3033)	1.054 (1.054-1.055)
LA_X15_Y15_P3_K2_BT	0.5983 (0.5429-0.6455)	0.762 (0.4195-2.719)
LA_X15_Y15_P3_K3_BF	0.1229 (0.1172-0.1287)	7.071 (0.1645-7.071)
LA_X15_Y15_P3_K3_BT	0.184 (0.173-0.3442)	0.1686 (0.1616-0.176)
LA_X15_Y15_PM_K2_BF	1.414 (1-2)	1 (0-1)
LA_X15_Y15_PM_K2_BT	7.071 (2-7.071)	0 (0-0.75)
LA_X15_Y15_PM_K3_BF	0.1219 (0.1179-0.1275)	0.1415 (0.1409-0.1447)
LA_X15_Y15_PM_K3_BT	0.1647 (0.1563-0.1705)	0.1316 (0.1168-0.1335)
LA_X20_Y20_P1_K2_BF	0.4518 (0.3665-0.5364)	0.3265 (0.323-0.3392)
LA_X20_Y20_P1_K2_BT	0.7015 (0.4885-5)	12.65 (0.3299-13)
LA_X20_Y20_P1_K3_BF	0.1754 (0.1575-0.3582)	0.2232 (0.2231-0.2232)
LA_X20_Y20_P1_K3_BT	1.782 (1.782-2.204)	0.223 (0.2229-10.61)
LA_X20_Y20_P2_K2_BF	1.014 (0.5557-2.626)	0.3946 (0.3857-0.4105)
LA_X20_Y20_P2_K2_BT	0.3877 (0.3252-0.6538)	7.071 (0.3902-7.071)
LA_X20_Y20_P2_K3_BF	1.644 (0.1797-1.644)	3.43 (0.5548-3.43)
LA_X20_Y20_P2_K3_BT	0.6131 (0.6131-1.796)	0.3344 (0.3341-0.3395)
LA_X20_Y20_P3_K2_BF	0.5449 (0.4507-0.625)	0.9851 (0.982-0.9851)
LA_X20_Y20_P3_K2_BT	0.18 (0.1797-0.5961)	2.425 (2.425-2.828)
LA_X20_Y20_P3_K3_BF	0.2032 (0.1758-0.3651)	0.2428 (0.2422-0.5935)
LA_X20_Y20_P3_K3_BT	0.258 (0.2254-0.7979)	1.404 (0.2319-1.438)
LA_X20_Y20_PM_K2_BF	0.8512 (0.6537-1.731)	1.07 (1.069-1.763)
LA_X20_Y20_PM_K2_BT	0.395 (0.3151-5)	0.5909 (0.5909-0.5913)
LA_X20_Y20_PM_K3_BF	0.209 (0.1824-1)	0.9613 (0.9312-0.9791)
LA_X20_Y20_PM_K3_BT	0.7538 (0.7538-6.325)	0.3478 (0.3476-0.3521)
LA_X30_Y30_P1_K2_BF	0.3065 (0.2803-0.3479)	6.325 (4.364-6.325)
LA_X30_Y30_P1_K2_BT	1.037 (0.303-6.489)	0.4654 (0.4488-0.4716)
LA_X30_Y30_P1_K3_BF	21.21 (2.828-21.21)	0.141 (0.1399-0.1426)
LA_X30_Y30_P1_K3_BT	0.07277 (0.06577-0.1027)	6.489 (0.3281-13.36)
LA_X30_Y30_P2_K2_BF	3.536 (2.998-3.536)	3.536 (3.536-11.79)
LA_X30_Y30_P2_K2_BT	0.5989 (0.5726-0.8775)	0.2229 (0.2223-0.2229)
LA_X30_Y30_P2_K3_BF	2.132 (2.132-2.132)	0.1012 (0.101-3.086)
LA_X30_Y30_P2_K3_BT	0.8319 (0.1274-0.8319)	0.1113 (0.1109-2.343)
LA_X30_Y30_P3_K2_BF	0.3922 (0.3616-0.43)	1.213 (1.213-10)
LA_X30_Y30_P3_K2_BT	0.3435 (0.3057-0.3994)	0.1931 (0.07809-0.1999)
LA_X30_Y30_P3_K3_BF	0.07428 (0.06971-0.07905)	0.2699 (0.2542-0.2707)
LA_X30_Y30_P3_K3_BT	0.07431 (0.07287-0.08447)	10.69 (4.364-10.69)
LA_X30_Y30_PM_K2_BF	2.265 (2.265-2.981)	5.154 (3.606-5.154)
LA_X30_Y30_PM_K2_BT	4.851 (0.6084-21.21)	0.2223 (0.2223-0.2229)
LA_X30_Y30_PM_K3_BF	2.887 (2.887-2.887)	0.1734 (0.167-0.1736)
LA_X30_Y30_PM_K3_BT	1.555 (0.1375-1.555)	21.21 (21.21-21.21)
LA_X5_Y5_P1_K2_BF	0 (0-0)	0 (0-0)
LA_X5_Y5_P1_K2_BT	0 (0-1.308)	0 (0-0)

	ISG-RANDOM	ISG-YENSK
LA_X5_Y5_P1_K3_BF	0 (0-2.673)	0 (0-0)
LA_X5_Y5_P1_K3_BT	0.3333 (0-0.3333)	0.3333 (0-0.3333)
LA_X5_Y5_P2_K2_BF	0 (0-0)	0 (0-0)
LA_X5_Y5_P2_K2_BT	0.9303 (0-0.9303)	0 (0-0)
LA_X5_Y5_P2_K3_BF	0 (0-0)	0 (0-0)
LA_X5_Y5_P2_K3_BT	0.3333 (0-0.3333)	0.4472 (0.08333-0.8246)
LA_X5_Y5_P3_K2_BF	0 (0-0)	0 (0-0)
LA_X5_Y5_P3_K2_BT	0 (0-0)	0 (0-0)
LA_X5_Y5_P3_K3_BF	0 (0-0)	0 (0-0)
LA_X5_Y5_P3_K3_BT	0 (0-0.2)	0.2 (0.2-0.2)
LA_X5_Y5_PM_K2_BF	0 (0-0)	0 (0-0)
LA_X5_Y5_PM_K2_BT	0 (0-0)	1.715 (0-1.715)
LA_X5_Y5_PM_K3_BF	0 (0-0)	0 (0-0)
LA_X5_Y5_PM_K3_BT	0.1429 (0.1429-0.202)	0.202 (0.1429-0.2474)
NO_X10_Y10_P1_K2_BF	0.1615 (0.1579-0.1662)	0.3499 (0.3442-0.4139)
NO_X10_Y10_P1_K2_BT	0.1875 (0.1813-0.2099)	0.3012 (0.2845-0.31)
NO_X10_Y10_P1_K3_BF	0.1257 (0.1167-0.1391)	0.1681 (0.1674-0.1712)
NO_X10_Y10_P1_K3_BT	0.448 (0.3661-0.6026)	0.1678 (0.1663-0.1694)
NO_X10_Y10_P2_K2_BF	0.433 (0.3801-0.496)	0.7806 (0.375-0.7906)
NO_X10_Y10_P2_K2_BT	0.5222 (0.4192-0.5874)	0.7806 (0.3801-0.7979)
NO_X10_Y10_P2_K3_BF	0.1159 (0.1109-0.1228)	0.157 (0.1558-0.1767)
NO_X10_Y10_P2_K3_BT	0.1628 (0.1457-0.1763)	0.1569 (0.1537-0.1581)
NO_X10_Y10_P3_K2_BF	3.78 (0.4027-3.78)	1.459 (0.5764-1.486)
NO_X10_Y10_P3_K2_BT	0.4201 (0.3674-0.4853)	1.696 (1.696-1.696)
NO_X10_Y10_P3_K3_BF	0.1105 (0.1026-0.1157)	0.1319 (0.1271-0.1338)
NO_X10_Y10_P3_K3_BT	0.1488 (0.1363-0.1575)	0.1325 (0.1312-0.1387)
NO_X10_Y10_PM_K2_BF	0.4 (0.4-0.4472)	0.4 (0.3464-0.4472)
NO_X10_Y10_PM_K2_BT	0.3536 (0.3536-0.3696)	0.3307 (0.3123-0.3307)
NO_X10_Y10_PM_K3_BF	0.151 (0.1435-0.1696)	0.2869 (0.2857-0.2891)
NO_X10_Y10_PM_K3_BT	0.1969 (0.1752-0.2541)	0.309 (0.3078-0.3112)
NO_X15_Y15_P1_K2_BF	0.2407 (0.2072-0.268)	0.2619 (0.2388-0.2632)
NO_X15_Y15_P1_K2_BT	0.2946 (0.2796-0.3573)	0.2632 (0.2619-0.3435)
NO_X15_Y15_P1_K3_BF	0.1071 (0.09885-0.1183)	0.2023 (0.2022-0.2064)
NO_X15_Y15_P1_K3_BT	0.1403 (0.1333-0.15)	0.2022 (0.2021-0.205)
NO_X15_Y15_P2_K2_BF	2.236 (2-3)	0 (0-1)
NO_X15_Y15_P2_K2_BT	2.828 (2-4.182)	0 (0-1)
NO_X15_Y15_P2_K3_BF	0.1487 (0.1419-0.1557)	0.2621 (0.2589-1.825)
NO_X15_Y15_P2_K3_BT	0.2126 (0.1968-0.2407)	0.2622 (0.2496-0.2631)
NO_X15_Y15_P3_K2_BF	0.4303 (0.4049-0.4544)	2.549 (1.571-2.549)
NO_X15_Y15_P3_K2_BT	0.5427 (0.4762-0.6123)	0.798 (0.798-0.8544)
NO_X15_Y15_P3_K3_BF	0.1412 (0.1362-0.1494)	0.2293 (0.2285-0.6066)
NO_X15_Y15_P3_K3_BT	0.2133 (0.2027-0.2519)	0.2312 (0.2244-0.2316)
NO_X15_Y15_PM_K2_BF	2.673 (1.414-2.957)	1.622 (1.622-2.192)
NO_X15_Y15_PM_K2_BT	2 (2-2.68)	0.7486 (0-1)
NO_X15_Y15_PM_K3_BF	0.09672 (0.0897-0.1271)	2.466 (2.466-2.466)
NO_X15_Y15_PM_K3_BT	0.1472 (0.1292-0.1727)	0.1814 (0.1647-1.523)
NO_X20_Y20_P1_K2_BF	0.646 (0.5695-0.6845)	4.714 (0.3956-6.168)
NO_X20_Y20_P1_K2_BT	1.543 (1.543-1.543)	0.3927 (0.3927-0.3956)
NO_X20_Y20_P1_K3_BF	0.2544 (0.116-0.2544)	0.9005 (0.9003-0.9005)
NO_X20_Y20_P1_K3_BT	0.1444 (0.1324-0.9715)	0.5274 (0.2118-0.5294)
NO_X20_Y20_P2_K2_BF	2.958 (2.5-5)	2.949 (0.9326-2.949)
NO_X20_Y20_P2_K2_BT	0.8972 (0.2629-1.155)	1.321 (0.7376-1.321)
NO_X20_Y20_P2_K3_BF	0.3679 (0.3679-0.3679)	0.1896 (0.1879-0.1926)
NO_X20_Y20_P2_K3_BT	0.2334 (0.2041-0.2334)	0.1929 (0.1913-0.1989)
NO_X20_Y20_P3_K2_BF	0.8484 (0.7026-0.8629)	0.4593 (0.4593-0.4635)
NO_X20_Y20_P3_K2_BT	0.8467 (0.7673-0.8496)	0.4593 (0.4593-0.4625)
NO_X20_Y20_P3_K3_BF	0.104 (0.09949-0.1092)	0.544 (0.5436-0.5442)
NO_X20_Y20_P3_K3_BT	0.1487 (0.1374-0.1667)	0.1851 (0.1848-0.189)
NO_X20_Y20_PM_K2_BF	2.108 (2.108-2.182)	2.406 (2.153-2.406)
NO_X20_Y20_PM_K2_BT	0.2791 (0.2273-0.324)	0.5913 (0.3273-3.899)
NO_X20_Y20_PM_K3_BF	0.2255 (0.2039-0.2366)	0.3714 (0.3675-0.3753)
NO_X20_Y20_PM_K3_BT	7.071 (2.297-7.071)	0.347 (0.3452-0.3517)
NO_X30_Y30_P1_K2_BF	2.265 (0.5808-2.265)	5.198 (3.738-15.81)
NO_X30_Y30_P1_K2_BT	0.7161 (0.129-6.489)	0.4228 (0.2283-2.998)
NO_X30_Y30_P1_K3_BF	1.812 (1.812-13.36)	16.33 (0.1034-16.33)
NO_X30_Y30_P1_K3_BT	0.05844 (0.05496-0.4394)	0.1324 (0.1033-0.1411)
NO_X30_Y30_P2_K2_BF	1.535 (0.898-6.489)	0.3008 (0.297-0.7789)
NO_X30_Y30_P2_K2_BT	2.887 (0.1083-2.887)	3.294 (3.262-3.552)
NO_X30_Y30_P2_K3_BF	2.914 (2.914-2.914)	0.1431 (0.1373-0.1929)
NO_X30_Y30_P2_K3_BT	0.3351 (0.08763-0.4231)	3.78 (3.78-3.78)
NO_X30_Y30_P3_K2_BF	7.071 (0.5012-7.071)	0.3814 (0.3339-1.027)
NO_X30_Y30_P3_K2_BT	1.215 (0.5929-21.21)	1.195 (1.178-21.21)
NO_X30_Y30_P3_K3_BF	0.08263 (0.07908-0.08581)	2.626 (0.1311-2.626)

	ISG-RANDOM	ISG-YENSK
NO_X30_Y30_P3_K3_BT	0.1085 (0.09394-0.1151)	1.129 (0.379-1.129)
NO_X30_Y30_PM_K2_BF	1.474 (1.237-1.747)	0.2106 (0.1754-0.3123)
NO_X30_Y30_PM_K2_BT	2.661 (1.156-21.21)	2.914 (0.6998-10)
NO_X30_Y30_PM_K3_BF	1.029 (0.1119-1.029)	0.1467 (0.1416-0.1469)
NO_X30_Y30_PM_K3_BT	0.2107 (0.1841-0.314)	0.1741 (0.1729-1.115)

Table B.4: Raw values of different instances of the IGDX indicator. Median (lower quartile - upper quartile).

B.3 Distance Matrices Approaches

B.3.1 IGD$^+$ Values

Instance Name	NSGA-II	NSGA-II-FD	NSGA-II-FDAO	NSGA-II-FDWOA
CH_X10_Y10_P1_K2_BF	0	0	0	0
IQR	0-0	0-0	0-0	0-0
CH_X10_Y10_P1_K3_BF	0.063	0.044	0.049	0.044
IQR	0.05-0.064	0.029-0.062	0.021-0.061	0.028-0.062
CH_X10_Y10_P2_K2_BF	0	0	0	0
IQR	0-0	0-0	0-0	0-0
CH_X10_Y10_P2_K3_BF	0.032	0.0062	0.0062	0.024
IQR	0.022-0.05	9e-18-0.024	3.6e-17-0.03	0.02-0.032
CH_X10_Y10_P3_K2_BF	0	0	0	0
IQR	0-0	0-0	0-0	0-0
CH_X10_Y10_P3_K3_BF	0.018	0.0075	0.0089	0.01
IQR	0.015-0.038	0-0.01	4.1e-05-0.023	3.3e-05-0.017
CH_X10_Y10_PM_K2_BF	0	0	0	0
IQR	0-0	0-0	0-0	0-0
CH_X10_Y10_PM_K3_BF	0.04	0.051	0.062	0.068
IQR	0.023-0.077	0.019-0.072	0.021-0.075	0.012-0.077
CH_X11_Y11_P1_K2_BF	0.017	0.021	0	0.0036
IQR	0.013-0.032	0.00089-0.023	0-0.024	0-0.021
CH_X11_Y11_P1_K3_BF	0.03	0.024	0.024	0.02
IQR	0.016-0.033	0.015-0.031	0.015-0.031	0.015-0.031
CH_X11_Y11_P2_K2_BF	0.12	0.008	0	0.016
IQR	0.016-0.12	0-0.016	0-0.016	0-0.016
CH_X11_Y11_P2_K3_BF	0.048	0.026	0.019	0.036
IQR	0.043-0.059	0.0081-0.031	0.0056-0.03	0.023-0.044
CH_X11_Y11_P3_K2_BF	0	0	0	0
IQR	0-0.025	0-0	0-0	0-0
CH_X11_Y11_P3_K3_BF	0.033	0.012	0.021	0.019
IQR	0.027-0.051	0.0032-0.023	0.0041-0.028	0.0096-0.024
CH_X11_Y11_PM_K2_BF	0.029	0	0	0
IQR	0.029-0.029	0-0	0-0	0-0
CH_X11_Y11_PM_K3_BF	0.046	0.037	0.032	0.042
IQR	0.042-0.051	0.0058-0.046	0.0089-0.054	0.029-0.046
CH_X12_Y12_P1_K2_BF	0	0	0	0
IQR	0-0.0016	0-0.0072	0-0	0-0.0072
CH_X12_Y12_P1_K3_BF	0.016	0.016	0.016	0.016
IQR	0.015-0.027	0.015-0.026	0.015-0.027	0.015-0.021
CH_X12_Y12_P2_K2_BF	0	0	0.0058	0
IQR	0-0.0058	0-0.0058	0-0.0058	0-0.0058
CH_X12_Y12_P2_K3_BF	0.029	0.016	0.012	0.016
IQR	0.019-0.033	0.0085-0.028	0.0085-0.022	0.0085-0.029
CH_X12_Y12_P3_K2_BF	0	0	0	0
IQR	0-0	0-0	0-0	0-0
CH_X12_Y12_P3_K3_BF	0.018	0.0087	0.0087	0.011
IQR	0.013-0.023	0.0058-0.012	0.0058-0.014	0.0073-0.016
CH_X12_Y12_PM_K2_BF	0	0	0	0
IQR	0-0	0-0	0-0	0-0
CH_X12_Y12_PM_K3_BF	0.063	0.063	0.063	0.063
IQR	0.062-0.071	0.0056-0.078	0.038-0.069	0.021-0.077
CH_X13_Y13_P1_K2_BF	0.014	0.03	0.03	0.0045
IQR	0.0045-0.044	0.0045-0.03	0.0011-0.03	5.6e-17-0.03
CH_X13_Y13_P1_K3_BF	0.018	0.009	0.009	0.009
IQR	0.009-0.018	0.009-0.018	0.009-0.018	0.009-0.009

Instance Name	NSGA-II	NSGA-II-FD	NSGA-II-FDAO	NSGA-II-FDWOA
CH_X13_Y13_P2_K2_BF	0.093	0.016	0.016	0.016
IQR	0.02-0.16	0.011-0.079	0-0.1	0.0029-0.071
CH_X13_Y13_P2_K3_BF	0.033	0.021	0.014	0.033
IQR	0.024-0.055	0.005-0.04	0.0015-0.042	0.013-0.068
CH_X13_Y13_P3_K2_BF	0.022	0	0	4e-17
IQR	0.013-0.029	0-0.0091	0-0.0091	0-0.0091
CH_X13_Y13_P3_K3_BF	0.034	0.024	0.021	0.034
IQR	0.02-0.035	0.0093-0.033	0.01-0.034	0.011-0.034
CH_X13_Y13_PM_K2_BF	0.03	0.03	0.0045	0.012
IQR	0.0045-0.047	5.6e-17-0.03	5.6e-17-0.03	5.6e-17-0.03
CH_X13_Y13_PM_K3_BF	0.058	0.046	0.047	0.054
IQR	0.041-0.072	0.034-0.059	0.036-0.059	0.043-0.063
CH_X14_Y14_P1_K2_BF	0.0079	0.0079	0.0079	0.0079
IQR	0-0.0079	0.0079-0.0079	0.0079-0.0079	0.0079-0.032
CH_X14_Y14_P1_K3_BF	0.015	0.012	0.012	0.015
IQR	0.011-0.02	0.01-0.017	0.0097-0.017	0.012-0.017
CH_X14_Y14_P2_K2_BF	0	0	0	0
IQR	0-0	0-0	0-0	0-0
CH_X14_Y14_P2_K3_BF	0.042	0.033	0.026	0.031
IQR	0.031-0.057	0.024-0.041	0.019-0.033	0.026-0.046
CH_X14_Y14_P3_K2_BF	0.011	0.017	0.011	0.011
IQR	0.011-0.017	0.011-0.017	0-0.017	0.0069-0.017
CH_X14_Y14_P3_K3_BF	0.036	0.025	0.031	0.029
IQR	0.031-0.045	0.021-0.037	0.021-0.042	0.023-0.038
CH_X14_Y14_PM_K2_BF	0	0	0	0
IQR	0-0.025	0-0	0-0	0-0.017
CH_X14_Y14_PM_K3_BF	0.076	0.074	0.08	0.074
IQR	0.074-0.12	0.055-0.084	0.074-0.1	0.071-0.12
CH_X4_Y4_P1_K2_BF	0	0	0	0
IQR	0-0	0-0	0-0	0-0
CH_X4_Y4_P1_K3_BF	0.8	0.33	0.33	0.8
IQR	0.8-0.8	0.33-0.33	0.33-0.33	0.44-0.8
CH_X4_Y4_P2_K2_BF	0	0	0	0
IQR	0-0	0-0	0-0	0-0
CH_X4_Y4_P2_K3_BF	0	0	0	0
IQR	0-0	0-0	0-0	0-0
CH_X4_Y4_P3_K2_BF	0	0	0	0
IQR	0-4.7e-16	0-0	0-0	0-0
CH_X4_Y4_P3_K3_BF	0	0	0	0
IQR	0-0	0-0	0-0	0-0
CH_X4_Y4_PM_K2_BF	0.21	0	0	0
IQR	0-0.66	0-0	0-0	0-0
CH_X4_Y4_PM_K3_BF	0.19	0	0	0
IQR	0-0.44	0-0	0-0	0-0.19
CH_X5_Y5_P1_K2_BF	0.046	0	0	0
IQR	0.046-0.046	0-0	0-0	0-0
CH_X5_Y5_P1_K3_BF	0.065	0	0	0.065
IQR	0.065-0.065	0-0.065	0-0.048	0.065-0.065
CH_X5_Y5_P2_K2_BF	0.059	0	0	0
IQR	0-0.059	0-0	0-0	0-0
CH_X5_Y5_P2_K3_BF	0.17	0	0	0.062
IQR	0.062-0.79	0-0	0-0	0.052-0.17
CH_X5_Y5_P3_K2_BF	0.076	0	0	0
IQR	0.076-0.076	0-0	0-0	0-0
CH_X5_Y5_P3_K3_BF	1.2	0.11	0	0.11
IQR	0.62-1.4	0-0.11	0-0.11	0.11-0.38
CH_X5_Y5_PM_K2_BF	0.042	0	0	0
IQR	0.042-0.042	0-0	0-0	0-0
CH_X5_Y5_PM_K3_BF	0.062	0	0	0.062
IQR	0.062-0.47	0-0	0-0	0-0.062
CH_X6_Y6_P1_K2_BF	0.073	0	0	0
IQR	0.018-0.25	0-0	0-0	0-0
CH_X6_Y6_P1_K3_BF	0	0	0	0
IQR	0-0	0-0	0-0	0-0
CH_X6_Y6_P2_K2_BF	0.073	0	0	0
IQR	0.073-0.28	0-0	0-0	0-0
CH_X6_Y6_P2_K3_BF	0	0	0	0.0098
IQR	0-0.17	0-0.0098	0-0	0-0.0098
CH_X6_Y6_P3_K2_BF	0.073	0	0	0
IQR	0.073-0.27	0-0	0-0	0-0
CH_X6_Y6_P3_K3_BF	0.5	0	0	0.059
IQR	0.059-0.5	0-0	0-0	0.03-0.059
CH_X6_Y6_PM_K2_BF	0.06	0	0	0

Instance Name	NSGA-II	NSGA-II-FD	NSGA-II-FDAO	NSGA-II-FDWOA
IQR	0-0.22	0-0	0-0	0-0
CH_X6_Y6_PM_K3_BF	0.16	0	0	0.16
IQR	0.16-0.71	0-0	0-0	0.16-0.16
CH_X7_Y7_P1_K2_BF	4.1e-16	0	0	0
IQR	4.1e-16-0.33	0-0	0-0	0-0
CH_X7_Y7_P1_K3_BF	0	0	0	0
IQR	0-0	0-0	0-0.055	0-0.055
CH_X7_Y7_P2_K2_BF	1.9e-16	0	0	0
IQR	1.9e-16-4.1e-16	0-0	0-0	0-0
CH_X7_Y7_P2_K3_BF	0	0	0	0
IQR	0-0	0-0	0-0	0-0
CH_X7_Y7_P3_K2_BF	4.1e-16	0	0	0
IQR	4.1e-16-0.12	0-0	0-0	0-0
CH_X7_Y7_P3_K3_BF	0.015	0.015	0	0.015
IQR	0.015-0.015	0-0.046	0-0.015	0.015-0.029
CH_X7_Y7_PM_K2_BF	0.004	0	0	0
IQR	0.004-0.004	0-0	0-0	0-0
CH_X7_Y7_PM_K3_BF	0.12	0	0	0.047
IQR	0.12-0.13	0-0.047	0-0.044	0.047-0.047
CH_X8_Y8_P1_K2_BF	0	0	0	0
IQR	0-0	0-0	0-0	0-0
CH_X8_Y8_P1_K3_BF	0	0	0	0
IQR	0-0	0-0	0-0	0-0
CH_X8_Y8_P2_K2_BF	0	0	0	0
IQR	0-4.1e-16	0-0	0-0	0-0
CH_X8_Y8_P2_K3_BF	0	0	0	0
IQR	0-0	0-0	0-0	0-0
CH_X8_Y8_P3_K2_BF	4.1e-16	0	0	0
IQR	0-4.1e-16	0-0	0-0	0-0
CH_X8_Y8_P3_K3_BF	0.0029	0	0	0.0029
IQR	0.0029-0.0029	0-0.0029	0-0	0.0029-0.0029
CH_X8_Y8_PM_K2_BF	0	0	0	0
IQR	0-0	0-0	0-0	0-0
CH_X8_Y8_PM_K3_BF	0.024	0.015	0.015	0.024
IQR	0.018-0.039	0.015-0.016	0.0037-0.016	0.015-0.038
CH_X9_Y9_P1_K2_BF	0.089	0	0	0
IQR	0.053-0.089	0-0	0-0	0-0
CH_X9_Y9_P1_K3_BF	0.035	0.019	0.0083	0.019
IQR	0.019-0.035	0.0074-0.019	0.0074-0.019	0.019-0.019
CH_X9_Y9_P2_K2_BF	0	0	0	0
IQR	0-0	0-0	0-0	0-0
CH_X9_Y9_P2_K3_BF	0.05	0.018	0.0049	0.018
IQR	0.029-0.066	0-0.018	0-0.018	0.018-0.045
CH_X9_Y9_P3_K2_BF	0.016	0	0	0
IQR	0.016-0.19	0-0	0-0	0-0
CH_X9_Y9_P3_K3_BF	0.03	0.014	9.2e-05	0.029
IQR	0.029-0.049	0-0.03	0-0.016	0.016-0.03
CH_X9_Y9_PM_K2_BF	0	0	0	0
IQR	0-0	0-0	0-0	0-0
CH_X9_Y9_PM_K3_BF	0.061	0.034	0.043	0.061
IQR	0.049-0.12	0.024-0.059	0.023-0.053	0.034-0.11
LA_X10_Y10_P1_K2_BF	0.024	0.0054	0	0.024
IQR	0.0096-0.024	0.0013-0.0062	0-0.0062	0.0096-0.024
LA_X10_Y10_P1_K3_BF	0.055	0.055	0.055	0.055
IQR	0.055-0.055	0.055-0.056	0.049-0.055	0.055-0.055
LA_X10_Y10_P2_K2_BF	0	0	0	0
IQR	0-0	0-0	0-0	0-0
LA_X10_Y10_P2_K3_BF	0	0	0	0
IQR	0-0	0-1.1	0-0	0-1.1
LA_X10_Y10_P3_K2_BF	0.025	0.041	0.0015	0.1
IQR	0.0099-0.14	0.017-0.062	0-0.0074	0.033-0.15
LA_X10_Y10_P3_K3_BF	0.16	0.19	0.061	0.21
IQR	0.16-0.21	0.13-0.21	0.024-0.2	0.2-0.21
LA_X10_Y10_PM_K2_BF	0	0	0	0
IQR	0-0	0-0	0-0	0-0
LA_X10_Y10_PM_K3_BF	0	0	0	0
IQR	0-0	0-0.39	0-0	0-0.94
LA_X11_Y11_P1_K2_BF	0.015	0	0	0
IQR	0.015-0.076	0-0.015	0-0.011	0-0.015
LA_X11_Y11_P1_K3_BF	0.029	0.029	0.029	0.029
IQR	0.029-0.047	0.029-0.036	0.029-0.036	0.029-0.059
LA_X11_Y11_P2_K2_BF	0.008	0.0026	0.0036	0.0026
IQR	0.0026-0.008	0-0.0036	3.4e-06-0.0036	0.0026-0.008

Instance Name	NSGA-II	NSGA-II-FD	NSGA-II-FDAO	NSGA-II-FDWOA
LA_X11_Y11_P2_K3_BF	0.028	0.53	0.028	0.53
IQR	0-0.55	0.079-0.53	0-0.51	0-0.67
LA_X11_Y11_P3_K2_BF	0	0	0	0
IQR	0-0	0-0.052	0-0	0-0
LA_X11_Y11_P3_K3_BF	0.071	0.07	0.07	0.089
IQR	0.07-0.1	0.07-0.1	0.07-0.071	0.07-0.14
LA_X11_Y11_PM_K2_BF	0.0074	0	0	0.0074
IQR	0.0074-0.0074	0-0.0074	0-0.0074	0-0.0074
LA_X11_Y11_PM_K3_BF	5.9e-06	0.0073	5.9e-06	0.0073
IQR	5.9e-06-0.0073	5.9e-06-0.36	5.9e-06-0.0073	5.9e-06-0.37
LA_X12_Y12_P1_K2_BF	0.013	0.013	0.013	0.013
IQR	0.013-0.013	0.013-0.013	0-0.013	0.013-0.013
LA_X12_Y12_P1_K3_BF	0.013	0.0097	0.0097	0.013
IQR	0.012-0.029	0.0097-0.029	0.0097-0.029	0.0097-0.029
LA_X12_Y12_P2_K2_BF	0.015	0	0	0.02
IQR	0.0034-0.05	0-0.027	0-0	0.015-0.05
LA_X12_Y12_P2_K3_BF	0.19	0.17	0.17	0.17
IQR	0.17-0.24	0.17-0.24	0.14-0.24	0.17-0.24
LA_X12_Y12_P3_K2_BF	0.018	0.018	0.018	0.018
IQR	0.018-0.018	0-0.018	0-0.018	0.018-0.018
LA_X12_Y12_P3_K3_BF	0.036	0.028	0.042	0.03
IQR	0.033-0.043	0.027-0.042	0.027-0.042	0.028-0.042
LA_X12_Y12_PM_K2_BF	0.061	0.013	0.0067	0.035
IQR	0.035-0.061	0.0067-0.054	0-0.035	0.018-0.061
LA_X12_Y12_PM_K3_BF	0.071	0.078	0.062	0.062
IQR	0.062-0.08	0.059-0.087	0.025-0.085	0.062-0.087
LA_X13_Y13_P1_K2_BF	0.014	0.014	0.014	0.014
IQR	0.014-0.014	0.014-0.014	0.014-0.014	0.014-0.014
LA_X13_Y13_P1_K3_BF	0.018	0.024	0.026	0.0094
IQR	0.011-0.028	0.0056-0.026	0.0077-0.028	0.0065-0.028
LA_X13_Y13_P2_K2_BF	0.048	0.048	0.048	0.048
IQR	0.0021-0.048	0-0.048	0.036-0.048	0.012-0.048
LA_X13_Y13_P2_K3_BF	0.07	0.084	0.057	0.059
IQR	0.06-0.087	0.057-0.084	0.053-0.084	0.055-0.084
LA_X13_Y13_P3_K2_BF	0.016	0.016	0.016	0.016
IQR	0.016-0.016	0.016-0.016	0.016-0.016	0.016-0.016
LA_X13_Y13_P3_K3_BF	0.033	0.019	0.017	0.022
IQR	0.025-0.04	0.014-0.032	0.013-0.032	0.017-0.031
LA_X13_Y13_PM_K2_BF	0.018	0	0	0.018
IQR	0.018-0.018	0-0.018	0-0.018	0-0.018
LA_X13_Y13_PM_K3_BF	0.048	0.035	0.042	0.04
IQR	0.027-0.049	0.022-0.048	0.024-0.048	0.024-0.048
LA_X14_Y14_P1_K2_BF	0	0	0	0
IQR	0-0	0-0.05	0-0.05	0-0.05
LA_X14_Y14_P1_K3_BF	0.022	0.017	0.017	0.017
IQR	0.017-0.029	0.015-0.02	0.012-0.02	0.015-0.022
LA_X14_Y14_P2_K2_BF	0	0	0.054	0
IQR	0-0	0-0.054	0-0.054	0-0.054
LA_X14_Y14_P2_K3_BF	0.041	0.023	0.03	0.03
IQR	0.032-0.049	0.02-0.031	0.022-0.033	0.024-0.036
LA_X14_Y14_P3_K2_BF	0	0	0	0
IQR	0-0.054	0-0.054	0-0	0-0.054
LA_X14_Y14_P3_K3_BF	0.039	0.031	0.029	0.031
IQR	0.034-0.049	0.026-0.036	0.025-0.033	0.027-0.035
LA_X14_Y14_PM_K2_BF	0.038	0.038	0	0.038
IQR	0.038-0.085	0.032-0.085	0-0.038	0.032-0.038
LA_X14_Y14_PM_K3_BF	0.026	0.018	0.017	0.02
IQR	0.02-0.032	0.016-0.023	0.014-0.018	0.017-0.026
LA_X5_Y5_P1_K2_BF	0.68	0	0	0
IQR	0.68-0.68	0-0	0-0	0-0
LA_X5_Y5_P1_K3_BF	0	0	0	0
IQR	0-0	0-0	0-0	0-0
LA_X5_Y5_P2_K2_BF	0.96	0	0	0
IQR	0.96-0.96	0-0	0-0	0-0
LA_X5_Y5_P2_K3_BF	0	0	0	0
IQR	0-0	0-0	0-0	0-0
LA_X5_Y5_P3_K2_BF	0.86	0	0	0
IQR	0.86-0.86	0-0	0-0	0-0
LA_X5_Y5_P3_K3_BF	0.037	0.037	0.016	0.037
IQR	0.037-0.037	0.037-0.037	0.0028-0.037	0.037-0.037
LA_X5_Y5_PM_K2_BF	0.83	0	0	0
IQR	0.83-0.83	0-0	0-0	0-0
LA_X5_Y5_PM_K3_BF	0.15	0.15	0.0069	0.15

Instance Name	NSGA-II	NSGA-II-FD	NSGA-II-FDAO	NSGA-II-FDWOA
IQR	0.15-0.15	0.14-0.15	0-0.13	0.15-0.15
LA_X6_Y6_P1_K2_BF	0.71	0	0	0
IQR	0.71-0.71	0-0	0-0	0-0
LA_X6_Y6_P1_K3_BF	0	0	0	0
IQR	0-0	0-0	0-0	0-0
LA_X6_Y6_P2_K2_BF	0.71	0	0	0
IQR	0.71-0.71	0-0	0-0	0-0
LA_X6_Y6_P2_K3_BF	0	0	0	0
IQR	0-0	0-0	0-0	0-0
LA_X6_Y6_P3_K2_BF	0.71	0	0	0
IQR	0.71-0.71	0-0	0-0	0-0
LA_X6_Y6_P3_K3_BF	0	0	0	0
IQR	0-0	0-0	0-0	0-0
LA_X6_Y6_PM_K2_BF	0.81	0	0	0
IQR	0.81-0.81	0-0	0-0	0-0
LA_X6_Y6_PM_K3_BF	0.25	0.25	0.1	0.25
IQR	0.25-0.25	0.25-0.25	0.067-0.25	0.25-0.25
LA_X7_Y7_P1_K2_BF	0.5	0.5	0	0.5
IQR	0.12-0.5	0.5-0.5	0-0	0.5-0.71
LA_X7_Y7_P1_K3_BF	0	0	0	0
IQR	0-0	0-0	0-0	0-0
LA_X7_Y7_P2_K2_BF	0.5	0.5	0	0.5
IQR	0.5-0.5	0.5-0.5	0-0.5	0.5-0.5
LA_X7_Y7_P2_K3_BF	0	0	0	0
IQR	0-0	0-0	0-0	0-0
LA_X7_Y7_P3_K2_BF	0.5	0.5	0	0.5
IQR	0.5-0.71	0.5-0.71	0-0	0.5-0.71
LA_X7_Y7_P3_K3_BF	0	0	0	0
IQR	0-0	0-0	0-0	0-0
LA_X7_Y7_PM_K2_BF	0.71	0.5	0	0.71
IQR	0.5-0.71	0.5-0.71	0-0.71	0.55-0.71
LA_X7_Y7_PM_K3_BF	0.21	0.21	0.032	0.21
IQR	0.21-0.21	0.12-0.21	0.0089-0.21	0.21-0.21
LA_X8_Y8_P1_K2_BF	0.26	0	0	0
IQR	0.06-0.26	0-0	0-0	0-0.26
LA_X8_Y8_P1_K3_BF	0.15	0.15	0.15	0.15
IQR	0.15-0.15	0.15-0.15	0.053-0.15	0.15-0.15
LA_X8_Y8_P2_K2_BF	0	0	0	0
IQR	0-0	0-0	0-0	0-0
LA_X8_Y8_P2_K3_BF	0.33	0.33	0.33	0.33
IQR	0.33-0.33	0.33-0.47	0.33-0.33	0.33-0.33
LA_X8_Y8_P3_K2_BF	0.26	0	0	0
IQR	0-0.26	0-0	0-0	0-0.26
LA_X8_Y8_P3_K3_BF	0.46	0.46	0.37	0.46
IQR	0.39-0.46	0.4-0.46	0.3-0.46	0.37-0.46
LA_X8_Y8_PM_K2_BF	0	0	0	0
IQR	0-0	0-0	0-0	0-0
LA_X8_Y8_PM_K3_BF	0.12	0.12	0.12	0.12
IQR	0.12-0.55	0.12-0.12	0.056-0.12	0.12-0.55
LA_X9_Y9_P1_K2_BF	8.1e-17	8.1e-17	8.1e-17	8.1e-17
IQR	8.1e-17-0.053	8.1e-17-8.1e-17	0-8.1e-17	8.1e-17-8.1e-17
LA_X9_Y9_P1_K3_BF	0.12	0.12	0.1	0.12
IQR	0.12-0.12	0.12-0.12	0.045-0.12	0.12-0.12
LA_X9_Y9_P2_K2_BF	0	0	0	0
IQR	0-0	0-0	0-0	0-0
LA_X9_Y9_P2_K3_BF	0	4	0	4
IQR	0-4	0.21-4	0-1.2	4-4
LA_X9_Y9_P3_K2_BF	0.23	0.23	0	0.23
IQR	0.23-0.23	0.23-0.23	0-0.23	0.23-0.66
LA_X9_Y9_P3_K3_BF	0.37	0.37	0.2	0.37
IQR	0.37-0.37	0.35-0.37	0.12-0.36	0.37-0.37
LA_X9_Y9_PM_K2_BF	0	0	0	0
IQR	0-0	0-0	0-0	0-0
LA_X9_Y9_PM_K3_BF	0.92	0.92	0.21	0.92
IQR	0.0047-0.92	0.36-0.92	0.0047-0.92	0.92-0.92
NO_X10_Y10_P1_K2_BF	0.019	0.0088	0.0088	0.016
IQR	0.016-0.025	0.0082-0.0088	0.0082-0.0093	0.016-0.016
NO_X10_Y10_P1_K3_BF	0.054	0.029	0.031	0.034
IQR	0.047-0.056	0.025-0.034	0.029-0.038	0.03-0.04
NO_X10_Y10_P2_K2_BF	1.1e-16	1.1e-16	1.1e-16	1.1e-16
IQR	1.1e-16-1.1e-16	1.1e-16-1.1e-16	1.1e-16-1.1e-16	1.1e-16-1.1e-16
NO_X10_Y10_P2_K3_BF	0.084	0.039	0.046	0.073
IQR	0.076-0.094	0.031-0.06	0.041-0.057	0.067-0.085

Instance Name	NSGA-II	NSGA-II-FD	NSGA-II-FDAO	NSGA-II-FDWOA
NO_X10_Y10_P3_K2_BF	0.037	0.025	0.0035	0.037
IQR	0.034-0.067	0.0035-0.067	0.0035-0.018	0.037-0.067
NO_X10_Y10_P3_K3_BF	0.081	0.048	0.05	0.069
IQR	0.075-0.088	0.04-0.05	0.044-0.055	0.061-0.074
NO_X10_Y10_PM_K2_BF	0	0	0	0
IQR	0-0	0-0	0-0	0-0
NO_X10_Y10_PM_K3_BF	0.06	0.046	0.051	0.054
IQR	0.055-0.1	0.031-0.079	0.036-0.084	0.048-0.081
NO_X11_Y11_P1_K2_BF	0.031	0.031	0.03	0.03
IQR	0.029-0.034	0.027-0.034	0.025-0.033	0.026-0.033
NO_X11_Y11_P1_K3_BF	0.034	0.025	0.022	0.028
IQR	0.028-0.044	0.019-0.03	0.02-0.024	0.024-0.032
NO_X11_Y11_P2_K2_BF	0.027	0.025	0.025	0.027
IQR	0.022-0.027	0.025-0.026	0.02-0.025	0.027-0.027
NO_X11_Y11_P2_K3_BF	0.086	0.063	0.051	0.098
IQR	0.074-0.11	0.036-0.087	0.041-0.069	0.074-0.11
NO_X11_Y11_P3_K2_BF	0.012	0.024	0.023	0.024
IQR	0.0097-0.029	0.0081-0.026	0.012-0.024	0.011-0.027
NO_X11_Y11_P3_K3_BF	0.08	0.052	0.058	0.065
IQR	0.072-0.092	0.049-0.058	0.051-0.066	0.06-0.07
NO_X11_Y11_PM_K2_BF	0.0051	0	0	0.0051
IQR	0-0.0051	0-0.0051	0-0.0051	0-0.0051
NO_X11_Y11_PM_K3_BF	0.089	0.083	0.072	0.077
IQR	0.061-0.099	0.05-0.096	0.052-0.1	0.06-0.087
NO_X12_Y12_P1_K2_BF	0.022	0.022	0.022	0.022
IQR	0.022-0.06	0.021-0.056	0.02-0.049	0.02-0.042
NO_X12_Y12_P1_K3_BF	0.034	0.025	0.024	0.033
IQR	0.026-0.037	0.021-0.032	0.02-0.031	0.026-0.038
NO_X12_Y12_P2_K2_BF	0.045	0.065	0.038	0.065
IQR	0.026-0.065	0.039-0.12	0.02-0.065	0.045-0.12
NO_X12_Y12_P2_K3_BF	0.08	0.062	0.065	0.069
IQR	0.062-0.089	0.051-0.076	0.052-0.078	0.063-0.08
NO_X12_Y12_P3_K2_BF	0.067	0.061	0.058	0.061
IQR	0.043-0.067	0.029-0.067	0.051-0.067	0.042-0.067
NO_X12_Y12_P3_K3_BF	0.062	0.052	0.053	0.057
IQR	0.056-0.073	0.044-0.065	0.043-0.068	0.048-0.069
NO_X12_Y12_PM_K2_BF	0.034	0.032	0.033	0.035
IQR	0.03-0.056	0.028-0.056	0.028-0.056	0.028-0.056
NO_X12_Y12_PM_K3_BF	0.074	0.056	0.051	0.055
IQR	0.061-0.08	0.049-0.063	0.044-0.058	0.048-0.064
NO_X13_Y13_P1_K2_BF	0.017	0.017	0.017	0.017
IQR	0.017-0.047	0.017-0.045	0.017-0.05	0.017-0.047
NO_X13_Y13_P1_K3_BF	0.032	0.025	0.026	0.035
IQR	0.027-0.043	0.021-0.033	0.024-0.03	0.029-0.039
NO_X13_Y13_P2_K2_BF	0.13	0.13	0.091	0.16
IQR	0.069-0.17	0.074-0.17	0.067-0.16	0.074-0.18
NO_X13_Y13_P2_K3_BF	0.11	0.075	0.073	0.087
IQR	0.086-0.11	0.065-0.089	0.052-0.092	0.077-0.099
NO_X13_Y13_P3_K2_BF	0.083	0.068	0.068	0.068
IQR	0.046-0.094	0.041-0.094	0.044-0.094	0.039-0.083
NO_X13_Y13_P3_K3_BF	0.084	0.062	0.07	0.072
IQR	0.076-0.091	0.049-0.075	0.057-0.078	0.061-0.085
NO_X13_Y13_PM_K2_BF	0.028	0.028	0.026	0.028
IQR	0.028-0.054	0.022-0.063	0.019-0.055	0.026-0.063
NO_X13_Y13_PM_K3_BF	0.074	0.068	0.061	0.068
IQR	0.063-0.093	0.056-0.093	0.055-0.072	0.06-0.084
NO_X14_Y14_P1_K2_BF	0	0	0.05	0
IQR	0-0.05	0-0.05	0-0.05	0-0.05
NO_X14_Y14_P1_K3_BF	0.049	0.032	0.029	0.04
IQR	0.041-0.067	0.026-0.042	0.022-0.035	0.029-0.045
NO_X14_Y14_P2_K2_BF	0.13	0.13	0.13	0.13
IQR	0.13-0.13	0.13-0.13	0.13-0.13	0.13-0.13
NO_X14_Y14_P2_K3_BF	0.099	0.071	0.073	0.083
IQR	0.089-0.11	0.066-0.079	0.067-0.079	0.075-0.093
NO_X14_Y14_P3_K2_BF	0.054	0.054	0.024	0.024
IQR	0.024-0.054	0.024-0.054	0.024-0.054	0.024-0.054
NO_X14_Y14_P3_K3_BF	0.093	0.062	0.067	0.073
IQR	0.08-0.1	0.055-0.069	0.061-0.072	0.065-0.081
NO_X14_Y14_PM_K2_BF	0.038	0.038	0.047	0.085
IQR	0.038-0.085	0.0076-0.085	0.031-0.085	0.038-0.085
NO_X14_Y14_PM_K3_BF	0.074	0.05	0.055	0.067
IQR	0.064-0.093	0.046-0.058	0.045-0.059	0.059-0.072
NO_X4_Y4_P1_K2_BF	0	0	0	0

Instance Name	NSGA-II	NSGA-II-FD	NSGA-II-FDAO	NSGA-II-FDWOA
IQR	0-0.04	0-0	0-0	0-0
NO_X4_Y4_P1_K3_BF	0.63	0.27	0.076	0.27
IQR	0.27-0.77	0.067-0.27	0-0.22	0.27-0.27
NO_X4_Y4_P2_K2_BF	0	0	0	0
IQR	0-0	0-0	0-0	0-0
NO_X4_Y4_P2_K3_BF	0.49	0	0	0.49
IQR	0.49-0.49	0-0	0-0.21	0.14-0.49
NO_X4_Y4_P3_K2_BF	0	0	0	0
IQR	0-0.018	0-0	0-0	0-0
NO_X4_Y4_P3_K3_BF	0.49	0	0	0.49
IQR	0.49-0.49	0-0.21	0-0	0.21-0.49
NO_X4_Y4_PM_K2_BF	0	0	0	0
IQR	0-0	0-0	0-0	0-0
NO_X4_Y4_PM_K3_BF	0.34	0.083	0.1	0.34
IQR	0.33-0.34	0-0.34	0-0.34	0.33-0.34
NO_X5_Y5_P1_K2_BF	0	0	0	0
IQR	0-0	0-0	0-0	0-0
NO_X5_Y5_P1_K3_BF	0.26	0.11	0.1	0.11
IQR	0.26-0.27	0.1-0.25	0.1-0.11	0.1-0.27
NO_X5_Y5_P2_K2_BF	0	0	0	0
IQR	0-0	0-0	0-0	0-0
NO_X5_Y5_P2_K3_BF	0.3	0.2	0.11	0.3
IQR	0.3-0.53	0.11-0.3	0.049-0.2	0.3-0.35
NO_X5_Y5_P3_K2_BF	0	0	0	0
IQR	0-0	0-0	0-0	0-0
NO_X5_Y5_P3_K3_BF	0.17	0.17	0.093	0.17
IQR	0.17-0.22	0.058-0.17	0.036-0.14	0.17-0.22
NO_X5_Y5_PM_K2_BF	0	0	0	0
IQR	0-0	0-0	0-0	0-0
NO_X5_Y5_PM_K3_BF	0.21	0.078	0.036	0.18
IQR	0.078-0.21	0.036-0.11	0-0.11	0.036-0.21
NO_X6_Y6_P1_K2_BF	0	0	0	0
IQR	0-0	0-0	0-0	0-0
NO_X6_Y6_P1_K3_BF	0.097	0.095	0.084	0.097
IQR	0.095-0.097	0.058-0.11	0.031-0.097	0.095-0.15
NO_X6_Y6_P2_K2_BF	0	0	0	0
IQR	0-0	0-3.2e-05	0-2.4e-05	0-3.2e-05
NO_X6_Y6_P2_K3_BF	0.083	0.055	0.055	0.11
IQR	0.028-0.12	0.023-0.08	0-0.065	0.0047-0.17
NO_X6_Y6_P3_K2_BF	0	0	0	0
IQR	0-0	0-0	0-0	0-0
NO_X6_Y6_P3_K3_BF	0.053	0.043	0.0035	0.043
IQR	0.043-0.082	0-0.043	0-0.043	0.034-0.053
NO_X6_Y6_PM_K2_BF	0	0	0	0
IQR	0-0	0-0	0-0	0-0
NO_X6_Y6_PM_K3_BF	0.093	0.041	0.03	0.056
IQR	0.082-0.093	0.013-0.056	0.011-0.056	0.013-0.082
NO_X7_Y7_P1_K2_BF	0	0	0	0
IQR	0-0	0-0	0-0	0-0
NO_X7_Y7_P1_K3_BF	0.044	0.044	0.044	0.044
IQR	0.04-0.068	0.039-0.056	0.044-0.044	0.041-0.069
NO_X7_Y7_P2_K2_BF	0	0	0	0
IQR	0-0	0-0	0-0	0-0
NO_X7_Y7_P2_K3_BF	0.039	0.035	0.035	0.039
IQR	0.039-0.039	0.019-0.039	0.025-0.039	0.028-0.04
NO_X7_Y7_P3_K2_BF	0	0	0	0
IQR	0-0	0-0	0-0	0-0
NO_X7_Y7_P3_K3_BF	0.05	0.04	0.041	0.05
IQR	0.047-0.05	0.028-0.05	0.034-0.065	0.036-0.05
NO_X7_Y7_PM_K2_BF	0	0	0	0
IQR	0-0	0-0	0-0	0-0
NO_X7_Y7_PM_K3_BF	0.061	0.028	0.017	0.042
IQR	0.053-0.067	0.015-0.035	0.012-0.027	0.034-0.053
NO_X8_Y8_P1_K2_BF	0	0	0	0
IQR	0-0.0088	0-0	0-0	0-0
NO_X8_Y8_P1_K3_BF	0.031	0.028	0.025	0.026
IQR	0.027-0.047	0.025-0.047	0.022-0.041	0.025-0.047
NO_X8_Y8_P2_K2_BF	7.6e-07	7.6e-07	7.6e-07	7.6e-07
IQR	7.6e-07-7.6e-07	1.9e-17-7.6e-07	7.6e-07-7.6e-07	1.9e-17-7.6e-07
NO_X8_Y8_P2_K3_BF	0.029	0.017	0.022	0.02
IQR	0.024-0.036	0.017-0.021	0.016-0.025	0.017-0.029
NO_X8_Y8_P3_K2_BF	0.011	0	0	0
IQR	0-0.011	0-0	0-0	0-0

Instance Name	NSGA-II	NSGA-II-FD	NSGA-II-FDAO	NSGA-II-FDWOA
NO_X8_Y8_P3_K3_BF	0.025	0.022	0.018	0.023
IQR	0.022-0.031	0.018-0.046	0.016-0.021	0.02-0.029
NO_X8_Y8_PM_K2_BF	0.0033	0.0033	0.0033	0.0033
IQR	0.00084-0.0033	0.00084-0.0033	0.0033-0.0033	0.00084-0.0033
NO_X8_Y8_PM_K3_BF	0.046	0.038	0.038	0.042
IQR	0.044-0.051	0.026-0.042	0.023-0.046	0.028-0.052
NO_X9_Y9_P1_K2_BF	6.8e-17	6.8e-17	6.8e-17	6.8e-17
IQR	1.9e-17-0.021	6.8e-17-6.8e-17	1.9e-17-6.8e-17	6.8e-17-6.8e-17
NO_X9_Y9_P1_K3_BF	0.046	0.028	0.025	0.035
IQR	0.04-0.049	0.024-0.033	0.018-0.031	0.032-0.04
NO_X9_Y9_P2_K2_BF	0	0	0	0
IQR	0-0	0-0	0-0	0-0
NO_X9_Y9_P2_K3_BF	0.073	0.03	0.034	0.05
IQR	0.062-0.089	0.021-0.041	0.028-0.041	0.041-0.059
NO_X9_Y9_P3_K2_BF	0.12	0.12	0.036	0.12
IQR	0.084-0.12	0.048-0.12	0.036-0.084	0.12-0.12
NO_X9_Y9_P3_K3_BF	0.075	0.033	0.028	0.052
IQR	0.063-0.089	0.018-0.044	0.021-0.042	0.049-0.06
NO_X9_Y9_PM_K2_BF	0	0	0	0
IQR	0-0	0-0	0-0	0-0
NO_X9_Y9_PM_K3_BF	0.066	0.048	0.052	0.041
IQR	0.053-0.084	0.028-0.055	0.038-0.061	0.03-0.06

Table B.5: Raw values of different instances of the IGD^+indicator. Shown are the median and the IQR values below.

B.3.2 IGD Values

Instance Name	NSGA-II	NSGA-II-FD	NSGA-II-FDAO	NSGA-II-FDWOA
CH_X10_Y10_P1_K2_BF	0	0	0	0
IQR	0-0	0-0	0-0	0-0
CH_X10_Y10_P1_K3_BF	0.083	0.077	0.077	0.077
IQR	0.042-0.083	0.033-0.081	0.033-0.079	0.031-0.081
CH_X10_Y10_P2_K2_BF	0	0	0	0
IQR	0-0	0-0	0-0	0-0
CH_X10_Y10_P2_K3_BF	0.033	0.012	0.012	0.033
IQR	0.019-0.069	0.0026-0.066	0.011-0.059	0.022-0.066
CH_X10_Y10_P3_K2_BF	0	0	0	0
IQR	0-0	0-0	0-0	0-0
CH_X10_Y10_P3_K3_BF	0.019	0.011	0.012	0.011
IQR	0.014-0.029	0-0.012	0.0088-0.023	0.0061-0.017
CH_X10_Y10_PM_K2_BF	0	0	0	0
IQR	0-0	0-0	0-0	0-0
CH_X10_Y10_PM_K3_BF	0.057	0.057	0.057	0.058
IQR	0.027-0.071	0.027-0.074	0.03-0.071	0.023-0.073
CH_X11_Y11_P1_K2_BF	0.036	0.057	0	0.013
IQR	0.032-0.064	0.0032-0.058	0-0.058	0-0.057
CH_X11_Y11_P1_K3_BF	0.069	0.068	0.068	0.069
IQR	0.037-0.069	0.059-0.069	0.026-0.069	0.068-0.069
CH_X11_Y11_P2_K2_BF	0.1	0.018	0	0.018
IQR	0.018-0.1	0-0.018	0-0.018	0-0.018
CH_X11_Y11_P2_K3_BF	0.044	0.039	0.035	0.04
IQR	0.043-0.047	0.035-0.04	0.022-0.041	0.034-0.043
CH_X11_Y11_P3_K2_BF	0	0	0	0
IQR	0-0.032	0-0	0-0	0-0
CH_X11_Y11_P3_K3_BF	0.03	0.019	0.02	0.019
IQR	0.025-0.034	0.013-0.024	0.014-0.022	0.015-0.023
CH_X11_Y11_PM_K2_BF	0.093	0	0	0
IQR	0.093-0.093	0-0	0-0	0-0
CH_X11_Y11_PM_K3_BF	0.034	0.03	0.029	0.033
IQR	0.032-0.035	0.026-0.034	0.026-0.038	0.029-0.035
CH_X12_Y12_P1_K2_BF	0	0	0	0
IQR	0-0.0016	0-0.039	0-0	0-0.039
CH_X12_Y12_P1_K3_BF	0.052	0.052	0.052	0.052
IQR	0.036-0.054	0.032-0.053	0.05-0.054	0.052-0.053
CH_X12_Y12_P2_K2_BF	0	0	0.035	0
IQR	0-0.086	0-0.035	0-0.086	0-0.086
CH_X12_Y12_P2_K3_BF	0.038	0.028	0.026	0.031
IQR	0.032-0.04	0.025-0.033	0.025-0.031	0.025-0.037
CH_X12_Y12_P3_K2_BF	0	0	0	0

Instance Name	NSGA-II	NSGA-II-FD	NSGA-II-FDAO	NSGA-II-FDWOA
IQR	0-0	0-0	0-0	0-0
CH_X12_Y12_P3_K3_BF	0.033	0.019	0.022	0.028
IQR	0.031-0.038	0.016-0.024	0.017-0.028	0.019-0.03
CH_X12_Y12_PM_K2_BF	0	0	0	0
IQR	0-0	0-0	0-0	0-0
CH_X12_Y12_PM_K3_BF	0.079	0.072	0.071	0.075
IQR	0.071-0.079	0.025-0.076	0.03-0.076	0.03-0.078
CH_X13_Y13_P1_K2_BF	0.073	0.065	0.065	0.045
IQR	0.045-0.1	0.027-0.069	0.021-0.069	0.021-0.065
CH_X13_Y13_P1_K3_BF	0.047	0.046	0.047	0.046
IQR	0.046-0.047	0.046-0.047	0.046-0.047	0.046-0.046
CH_X13_Y13_P2_K2_BF	0.077	0.02	0.02	0.02
IQR	0.028-0.12	0.02-0.09	0-0.14	0.0049-0.06
CH_X13_Y13_P2_K3_BF	0.025	0.02	0.016	0.022
IQR	0.023-0.03	0.0097-0.026	0.01-0.025	0.017-0.028
CH_X13_Y13_P3_K2_BF	0.045	0	0	0.013
IQR	0.026-0.051	0-0.013	0-0.013	0-0.022
CH_X13_Y13_P3_K3_BF	0.028	0.025	0.024	0.027
IQR	0.026-0.03	0.019-0.027	0.021-0.028	0.025-0.028
CH_X13_Y13_PM_K2_BF	0.039	0.034	0.031	0.034
IQR	0.023-0.052	0.01-0.04	0.0067-0.034	0.019-0.04
CH_X13_Y13_PM_K3_BF	0.048	0.045	0.044	0.046
IQR	0.036-0.053	0.034-0.051	0.033-0.05	0.036-0.051
CH_X14_Y14_P1_K2_BF	0.051	0.051	0.051	0.051
IQR	0-0.051	0.051-0.051	0.051-0.051	0.032-0.057
CH_X14_Y14_P1_K3_BF	0.033	0.033	0.033	0.033
IQR	0.024-0.034	0.032-0.034	0.016-0.034	0.033-0.034
CH_X14_Y14_P2_K2_BF	0	0	0	0
IQR	0-0	0-0	0-0	0-0
CH_X14_Y14_P2_K3_BF	0.022	0.017	0.015	0.018
IQR	0.018-0.028	0.014-0.022	0.012-0.018	0.016-0.026
CH_X14_Y14_P3_K2_BF	0.041	0.051	0.041	0.041
IQR	0.041-0.06	0.041-0.06	0-0.06	0.024-0.06
CH_X14_Y14_P3_K3_BF	0.02	0.017	0.018	0.019
IQR	0.02-0.024	0.015-0.018	0.016-0.021	0.018-0.022
CH_X14_Y14_PM_K2_BF	0	0	0	0
IQR	0-0.021	0-0	0-0	0-0.021
CH_X14_Y14_PM_K3_BF	0.11	0.11	0.11	0.11
IQR	0.1-0.11	0.093-0.11	0.11-0.11	0.099-0.12
CH_X4_Y4_P1_K2_BF	0	0	0	0
IQR	0-0	0-0	0-0	0-0
CH_X4_Y4_P1_K3_BF	0.76	0.47	0.47	0.63
IQR	0.69-0.76	0.47-0.47	0.47-0.47	0.51-0.76
CH_X4_Y4_P2_K2_BF	0	0	0	0
IQR	0-0	0-0	0-0	0-0
CH_X4_Y4_P2_K3_BF	0	0	0	0
IQR	0-0	0-0	0-0	0-0
CH_X4_Y4_P3_K2_BF	0	0	0	0
IQR	0-0.26	0-0	0-0	0-0
CH_X4_Y4_P3_K3_BF	0	0	0	0
IQR	0-0	0-0	0-0	0-0
CH_X4_Y4_PM_K2_BF	0.4	0	0	0
IQR	0-0.66	0-0	0-0	0-0
CH_X4_Y4_PM_K3_BF	0.51	0	0	0
IQR	0-0.54	0-0	0-0	0-0.51
CH_X5_Y5_P1_K2_BF	0.37	0	0	0
IQR	0.37-0.37	0-0	0-0	0-0
CH_X5_Y5_P1_K3_BF	0.3	0	0	0.3
IQR	0.3-0.3	0-0.3	0-0.23	0.3-0.3
CH_X5_Y5_P2_K2_BF	0.19	0	0	0
IQR	0-0.19	0-0	0-0	0-0
CH_X5_Y5_P2_K3_BF	0.13	0	0	0.08
IQR	0.08-0.45	0-0	0-0	0.08-0.13
CH_X5_Y5_P3_K2_BF	0.39	0	0	0
IQR	0.39-0.39	0-0	0-0	0-0
CH_X5_Y5_P3_K3_BF	0.57	0.13	0	0.13
IQR	0.4-0.72	0-0.13	0-0.13	0.13-0.27
CH_X5_Y5_PM_K2_BF	0.24	0	0	0
IQR	0.24-0.24	0-0	0-0	0-0
CH_X5_Y5_PM_K3_BF	0.095	0	0	0.095
IQR	0.095-0.33	0-0	0-0	0-0.095
CH_X6_Y6_P1_K2_BF	0.21	0	0	0
IQR	0.048-0.28	0-0	0-0	0-0

Instance Name	NSGA-II	NSGA-II-FD	NSGA-II-FDAO	NSGA-II-FDWOA
CH_X6_Y6_P1_K3_BF	0	0	0	0
IQR	0-0	0-0	0-0	0-0
CH_X6_Y6_P2_K2_BF	0.078	0	0	0
IQR	0.078-0.23	0-0	0-0	0-0
CH_X6_Y6_P2_K3_BF	0	0	0	0.082
IQR	0-0.19	0-0.082	0-0	0-0.082
CH_X6_Y6_P3_K2_BF	0.18	0	0	0
IQR	0.18-0.26	0-0	0-0	0-0
CH_X6_Y6_P3_K3_BF	0.31	0	0	0.2
IQR	0.22-0.31	0-0	0-0	0.086-0.22
CH_X6_Y6_PM_K2_BF	0.095	0	0	0
IQR	0-0.2	0-0	0-0	0-0
CH_X6_Y6_PM_K3_BF	0.29	0	0	0.29
IQR	0.29-0.43	0-0	0-0	0.29-0.29
CH_X7_Y7_P1_K2_BF	0.33	0	0	0
IQR	0.33-0.33	0-0	0-0	0-0
CH_X7_Y7_P1_K3_BF	0	0	0	0
IQR	0-0	0-0	0-0.057	0-0.057
CH_X7_Y7_P2_K2_BF	4.5e-16	0	0	0
IQR	4.5e-16-4.5e-16	0-0	0-0	0-0
CH_X7_Y7_P2_K3_BF	0	0	0	0
IQR	0-0	0-0	0-0	0-0
CH_X7_Y7_P3_K2_BF	0.16	0	0	0
IQR	0.16-0.16	0-0	0-0	0-0
CH_X7_Y7_P3_K3_BF	0.12	0.047	0	0.12
IQR	0.12-0.12	0-0.12	0-0.11	0.12-0.13
CH_X7_Y7_PM_K2_BF	0.29	0	0	0
IQR	0.26-0.29	0-0	0-0	0-0
CH_X7_Y7_PM_K3_BF	0.099	0	0	0.059
IQR	0.099-0.11	0-0.059	0-0.053	0.059-0.059
CH_X8_Y8_P1_K2_BF	0	0	0	0
IQR	0-0	0-0	0-0	0-0
CH_X8_Y8_P1_K3_BF	0	0	0	0
IQR	0-0	0-0	0-0	0-0
CH_X8_Y8_P2_K2_BF	0	0	0	0
IQR	0-0.33	0-0	0-0	0-0
CH_X8_Y8_P2_K3_BF	0	0	0	0
IQR	0-0	0-0	0-0	0-0
CH_X8_Y8_P3_K2_BF	0.44	0	0	0
IQR	0-0.44	0-0	0-0	0-0
CH_X8_Y8_P3_K3_BF	0.072	0	0	0.072
IQR	0.072-0.072	0-0.059	0-0	0.072-0.072
CH_X8_Y8_PM_K2_BF	0	0	0	0
IQR	0-0	0-0	0-0	0-0
CH_X8_Y8_PM_K3_BF	0.074	0.044	0.044	0.069
IQR	0.053-0.14	0.031-0.074	0.011-0.074	0.026-0.12
CH_X9_Y9_P1_K2_BF	0.17	0	0	0
IQR	0.077-0.17	0-0	0-0	0-0
CH_X9_Y9_P1_K3_BF	0.039	0.032	0.026	0.032
IQR	0.032-0.045	0.019-0.032	0.019-0.032	0.032-0.032
CH_X9_Y9_P2_K2_BF	0	0	0	0
IQR	0-0	0-0	0-0	0-0
CH_X9_Y9_P2_K3_BF	0.067	0.037	0.032	0.06
IQR	0.05-0.083	0-0.06	0-0.06	0.051-0.067
CH_X9_Y9_P3_K2_BF	0.24	0	0	0
IQR	0.24-0.27	0-0	0-0	0-0
CH_X9_Y9_P3_K3_BF	0.044	0.023	0.023	0.038
IQR	0.042-0.052	0-0.042	0-0.038	0.023-0.044
CH_X9_Y9_PM_K2_BF	0	0	0	0
IQR	0-0	0-0	0-0	0-0
CH_X9_Y9_PM_K3_BF	0.09	0.078	0.075	0.11
IQR	0.071-0.12	0.044-0.097	0.047-0.089	0.078-0.12
LA_X10_Y10_P1_K2_BF	0.038	0.0054	0	0.038
IQR	0.019-0.038	0.0013-0.0062	0-0.0062	0.019-0.038
LA_X10_Y10_P1_K3_BF	0.064	0.063	0.062	0.063
IQR	0.063-0.064	0.063-0.063	0.04-0.063	0.063-0.063
LA_X10_Y10_P2_K2_BF	0	0	0	0
IQR	0-0	0-0	0-0	0-0
LA_X10_Y10_P2_K3_BF	0	0	0	0
IQR	0-0	0-0.41	0-0	0-0.42
LA_X10_Y10_P3_K2_BF	0.025	0.032	0.0093	0.046
IQR	0.017-0.067	0.018-0.053	0-0.018	0.038-0.07
LA_X10_Y10_P3_K3_BF	0.076	0.078	0.038	0.089

Instance Name	NSGA-II	NSGA-II-FD	NSGA-II-FDAO	NSGA-II-FDWOA
IQR	0.076-0.1	0.062-0.089	0.027-0.084	0.084-0.11
LA_X10_Y10_PM_K2_BF	0	0	0	0
IQR	0-0	0-0	0-0	0-0
LA_X10_Y10_PM_K3_BF	0	0	0	0
IQR	0-0	0-0.14	0-0	0-0.25
LA_X11_Y11_P1_K2_BF	0.039	0	0	0
IQR	0.039-0.12	0-0.039	0-0.024	0-0.039
LA_X11_Y11_P1_K3_BF	0.06	0.059	0.059	0.059
IQR	0.059-0.061	0.059-0.059	0.059-0.059	0.059-0.067
LA_X11_Y11_P2_K2_BF	0.053	0.031	0.036	0.033
IQR	0.033-0.053	0-0.036	0.005-0.036	0.033-0.053
LA_X11_Y11_P2_K3_BF	0.054	0.18	0.054	0.18
IQR	0-0.18	0.078-0.18	0-0.18	0-0.22
LA_X11_Y11_P3_K2_BF	0	0	0	0
IQR	0-0	0-0.042	0-0	0-0
LA_X11_Y11_P3_K3_BF	0.06	0.06	0.06	0.06
IQR	0.06-0.066	0.054-0.06	0.06-0.06	0.06-0.091
LA_X11_Y11_PM_K2_BF	0.098	0	0	0.098
IQR	0.098-0.098	0-0.098	0-0.098	0-0.098
LA_X11_Y11_PM_K3_BF	0.022	0.026	0.022	0.034
IQR	0.022-0.034	0.022-0.087	0.022-0.031	0.022-0.089
LA_X12_Y12_P1_K2_BF	0.075	0.075	0.075	0.075
IQR	0.075-0.075	0.075-0.075	0-0.075	0.075-0.075
LA_X12_Y12_P1_K3_BF	0.03	0.03	0.03	0.03
IQR	0.03-0.035	0.03-0.035	0.03-0.035	0.03-0.035
LA_X12_Y12_P2_K2_BF	0.018	0	0	0.02
IQR	0.0066-0.067	0-0.059	0-0	0.015-0.073
LA_X12_Y12_P2_K3_BF	0.062	0.057	0.057	0.057
IQR	0.057-0.087	0.057-0.086	0.05-0.086	0.057-0.084
LA_X12_Y12_P3_K2_BF	0.056	0.056	0.056	0.056
IQR	0.056-0.056	0-0.056	0-0.056	0.056-0.056
LA_X12_Y12_P3_K3_BF	0.017	0.015	0.02	0.016
IQR	0.016-0.024	0.015-0.023	0.015-0.023	0.015-0.021
LA_X12_Y12_PM_K2_BF	0.056	0.022	0.012	0.044
IQR	0.044-0.056	0.012-0.05	0-0.042	0.027-0.056
LA_X12_Y12_PM_K3_BF	0.038	0.038	0.037	0.037
IQR	0.03-0.04	0.026-0.046	0.017-0.04	0.037-0.046
LA_X13_Y13_P1_K2_BF	0.066	0.066	0.066	0.066
IQR	0.066-0.066	0.066-0.066	0.066-0.066	0.066-0.066
LA_X13_Y13_P1_K3_BF	0.018	0.022	0.022	0.016
IQR	0.017-0.023	0.015-0.022	0.015-0.023	0.016-0.023
LA_X13_Y13_P2_K2_BF	0.068	0.066	0.067	0.068
IQR	0.012-0.068	0-0.068	0.061-0.068	0.017-0.068
LA_X13_Y13_P2_K3_BF	0.036	0.035	0.029	0.03
IQR	0.031-0.038	0.029-0.037	0.028-0.037	0.029-0.037
LA_X13_Y13_P3_K2_BF	0.039	0.039	0.039	0.039
IQR	0.039-0.039	0.039-0.039	0.039-0.039	0.039-0.039
LA_X13_Y13_P3_K3_BF	0.021	0.016	0.015	0.016
IQR	0.018-0.025	0.015-0.023	0.014-0.023	0.015-0.023
LA_X13_Y13_PM_K2_BF	0.031	0	0	0.031
IQR	0.031-0.031	0-0.031	0-0.031	0-0.031
LA_X13_Y13_PM_K3_BF	0.035	0.034	0.033	0.033
IQR	0.032-0.036	0.031-0.036	0.031-0.036	0.032-0.036
LA_X14_Y14_P1_K2_BF	0	0	0	0
IQR	0-0	0-0.044	0-0.044	0-0.044
LA_X14_Y14_P1_K3_BF	0.026	0.024	0.024	0.025
IQR	0.025-0.026	0.023-0.025	0.023-0.025	0.024-0.025
LA_X14_Y14_P2_K2_BF	0	0	0.054	0
IQR	0-0	0-0.054	0-0.054	0-0.054
LA_X14_Y14_P2_K3_BF	0.024	0.014	0.021	0.017
IQR	0.02-0.026	0.012-0.023	0.013-0.024	0.015-0.023
LA_X14_Y14_P3_K2_BF	0	0	0	0
IQR	0-0.054	0-0.054	0-0	0-0.054
LA_X14_Y14_P3_K3_BF	0.022	0.017	0.018	0.018
IQR	0.02-0.023	0.016-0.021	0.016-0.021	0.017-0.021
LA_X14_Y14_PM_K2_BF	0.038	0.052	0	0.038
IQR	0.038-0.061	0.038-0.061	0-0.038	0.038-0.038
LA_X14_Y14_PM_K3_BF	0.023	0.022	0.021	0.022
IQR	0.023-0.024	0.02-0.022	0.021-0.022	0.022-0.023
LA_X5_Y5_P1_K2_BF	0.71	0	0	0
IQR	0.71-0.71	0-0	0-0	0-0
LA_X5_Y5_P1_K3_BF	0	0	0	0
IQR	0-0	0-0	0-0	0-0

Instance Name	NSGA-II	NSGA-II-FD	NSGA-II-FDAO	NSGA-II-FDWOA
LA_X5_Y5_P2_K2_BF	0.79	0	0	0
IQR	0.79-0.79	0-0	0-0	0-0
LA_X5_Y5_P2_K3_BF	0	0	0	0
IQR	0-0	0-0	0-0	0-0
LA_X5_Y5_P3_K2_BF	0.73	0	0	0
IQR	0.73-0.73	0-0	0-0	0-0
LA_X5_Y5_P3_K3_BF	0.55	0.55	0.25	0.55
IQR	0.55-0.55	0.5-0.55	0.063-0.54	0.55-0.55
LA_X5_Y5_PM_K2_BF	0.72	0	0	0
IQR	0.72-0.72	0-0	0-0	0-0
LA_X5_Y5_PM_K3_BF	0.3	0.3	0.17	0.3
IQR	0.3-0.3	0.24-0.3	0-0.17	0.3-0.3
LA_X6_Y6_P1_K2_BF	1	0	0	0
IQR	1-1	0-0	0-0	0-0
LA_X6_Y6_P1_K3_BF	0	0	0	0
IQR	0-0	0-0	0-0	0-0
LA_X6_Y6_P2_K2_BF	1	0	0	0
IQR	1-1	0-0	0-0	0-0
LA_X6_Y6_P2_K3_BF	0	0	0	0
IQR	0-0	0-0	0-0	0-0
LA_X6_Y6_P3_K2_BF	1	0	0	0
IQR	1-1	0-0	0-0	0-0
LA_X6_Y6_P3_K3_BF	0	0	0	0
IQR	0-0	0-0	0-0	0-0
LA_X6_Y6_PM_K2_BF	0.82	0	0	0
IQR	0.82-0.82	0-0	0-0	0-0
LA_X6_Y6_PM_K3_BF	0.35	0.35	0.21	0.35
IQR	0.35-0.35	0.35-0.35	0.21-0.35	0.35-0.35
LA_X7_Y7_P1_K2_BF	0.87	0.87	0	0.87
IQR	0.22-0.87	0.87-0.87	0-0	0.87-0.87
LA_X7_Y7_P1_K3_BF	0	0	0	0
IQR	0-0	0-0	0-0	0-0
LA_X7_Y7_P2_K2_BF	0.71	0.71	0	0.71
IQR	0.71-0.71	0.71-0.71	0-0.71	0.71-0.71
LA_X7_Y7_P2_K3_BF	0	0	0	0
IQR	0-0	0-0	0-0	0-0
LA_X7_Y7_P3_K2_BF	0.87	0.87	0	0.87
IQR	0.87-0.87	0.87-0.87	0-0	0.87-0.87
LA_X7_Y7_P3_K3_BF	0	0	0	0
IQR	0-0	0-0	0-0	0-0
LA_X7_Y7_PM_K2_BF	0.87	0.87	0	0.87
IQR	0.87-0.87	0.87-0.87	0-0.87	0.87-0.87
LA_X7_Y7_PM_K3_BF	0.2	0.2	0.14	0.2
IQR	0.2-0.2	0.16-0.2	0.085-0.19	0.2-0.2
LA_X8_Y8_P1_K2_BF	0.33	0	0	0
IQR	0.06-0.33	0-0	0-0	0-0.33
LA_X8_Y8_P1_K3_BF	0.28	0.28	0.26	0.28
IQR	0.28-0.28	0.26-0.28	0.14-0.28	0.28-0.28
LA_X8_Y8_P2_K2_BF	0	0	0	0
IQR	0-0	0-0	0-0	0-0
LA_X8_Y8_P2_K3_BF	0.49	0.49	0.49	0.49
IQR	0.49-0.49	0.49-0.65	0.49-0.49	0.49-0.49
LA_X8_Y8_P3_K2_BF	0.26	0	0	0
IQR	0-0.26	0-0	0-0	0-0.26
LA_X8_Y8_P3_K3_BF	0.49	0.49	0.38	0.49
IQR	0.41-0.49	0.38-0.49	0.33-0.49	0.38-0.49
LA_X8_Y8_PM_K2_BF	0	0	0	0
IQR	0-0	0-0	0-0	0-0
LA_X8_Y8_PM_K3_BF	0.26	0.26	0.22	0.26
IQR	0.26-0.44	0.26-0.26	0.14-0.26	0.26-0.44
LA_X9_Y9_P1_K2_BF	7.2e-06	7.2e-06	7.2e-06	7.2e-06
IQR	7.2e-06-0.11	7.2e-06-7.2e-06	0-7.2e-06	7.2e-06-7.2e-06
LA_X9_Y9_P1_K3_BF	0.11	0.11	0.079	0.11
IQR	0.11-0.11	0.09-0.11	0.05-0.11	0.11-0.11
LA_X9_Y9_P2_K2_BF	0	0	0	0
IQR	0-0	0-0	0-0	0-0
LA_X9_Y9_P2_K3_BF	0	2.1	0	2.1
IQR	0-2.1	0.12-2.1	0-0.67	2.1-2.1
LA_X9_Y9_P3_K2_BF	0.28	0.28	0	0.28
IQR	0.28-0.28	0.27-0.28	0-0.27	0.28-0.59
LA_X9_Y9_P3_K3_BF	0.17	0.16	0.099	0.17
IQR	0.17-0.17	0.14-0.17	0.082-0.17	0.16-0.17
LA_X9_Y9_PM_K2_BF	0	0	0	0

Instance Name	NSGA-II	NSGA-II-FD	NSGA-II-FDAO	NSGA-II-FDWOA
IQR	0-0	0-0	0-0	0-0
LA_X9_Y9_PM_K3_BF	0.48	0.48	0.32	0.48
IQR	0.32-0.48	0.36-0.48	0.22-0.48	0.48-0.48
NO_X10_Y10_P1_K2_BF	0.029	0.017	0.017	0.029
IQR	0.029-0.03	0.006-0.017	0.0066-0.017	0.02-0.029
NO_X10_Y10_P1_K3_BF	0.032	0.03	0.03	0.031
IQR	0.031-0.032	0.03-0.03	0.03-0.031	0.031-0.031
NO_X10_Y10_P2_K2_BF	0.087	0.087	0.087	0.087
IQR	0.087-0.087	0.087-0.087	0.087-0.087	0.087-0.087
NO_X10_Y10_P2_K3_BF	0.023	0.019	0.019	0.023
IQR	0.021-0.025	0.016-0.022	0.017-0.021	0.022-0.024
NO_X10_Y10_P3_K2_BF	0.036	0.025	0.019	0.037
IQR	0.033-0.051	0.019-0.049	0.019-0.023	0.036-0.051
NO_X10_Y10_P3_K3_BF	0.022	0.017	0.017	0.021
IQR	0.019-0.023	0.013-0.019	0.013-0.019	0.018-0.022
NO_X10_Y10_PM_K2_BF	0	0	0	0
IQR	0-0	0-0	0-0	0-0
NO_X10_Y10_PM_K3_BF	0.026	0.023	0.023	0.024
IQR	0.023-0.03	0.02-0.027	0.02-0.041	0.021-0.03
NO_X11_Y11_P1_K2_BF	0.045	0.045	0.044	0.045
IQR	0.045-0.046	0.04-0.046	0.034-0.045	0.043-0.046
NO_X11_Y11_P1_K3_BF	0.02	0.019	0.019	0.019
IQR	0.02-0.02	0.018-0.019	0.019-0.019	0.019-0.02
NO_X11_Y11_P2_K2_BF	0.03	0.023	0.023	0.03
IQR	0.029-0.03	0.023-0.029	0.021-0.026	0.03-0.03
NO_X11_Y11_P2_K3_BF	0.021	0.02	0.018	0.024
IQR	0.018-0.025	0.014-0.024	0.014-0.023	0.019-0.026
NO_X11_Y11_P3_K2_BF	0.02	0.019	0.02	0.023
IQR	0.02-0.026	0.015-0.023	0.018-0.023	0.019-0.025
NO_X11_Y11_P3_K3_BF	0.02	0.017	0.019	0.02
IQR	0.019-0.021	0.016-0.019	0.018-0.019	0.019-0.02
NO_X11_Y11_PM_K2_BF	0.063	0	0	0.063
IQR	0-0.063	0-0.063	0-0.063	0-0.063
NO_X11_Y11_PM_K3_BF	0.031	0.029	0.027	0.035
IQR	0.027-0.051	0.023-0.045	0.023-0.043	0.024-0.051
NO_X12_Y12_P1_K2_BF	0.05	0.05	0.05	0.05
IQR	0.05-0.055	0.049-0.057	0.049-0.055	0.049-0.054
NO_X12_Y12_P1_K3_BF	0.029	0.028	0.028	0.028
IQR	0.028-0.029	0.027-0.028	0.028-0.028	0.028-0.029
NO_X12_Y12_P2_K2_BF	0.062	0.066	0.04	0.066
IQR	0.028-0.072	0.054-0.066	0.022-0.057	0.061-0.072
NO_X12_Y12_P2_K3_BF	0.025	0.023	0.022	0.024
IQR	0.024-0.025	0.02-0.025	0.019-0.024	0.022-0.025
NO_X12_Y12_P3_K2_BF	0.045	0.046	0.045	0.044
IQR	0.04-0.048	0.04-0.049	0.042-0.049	0.037-0.051
NO_X12_Y12_P3_K3_BF	0.028	0.027	0.026	0.027
IQR	0.027-0.029	0.025-0.028	0.025-0.028	0.027-0.028
NO_X12_Y12_PM_K2_BF	0.034	0.032	0.039	0.036
IQR	0.029-0.047	0.028-0.045	0.026-0.045	0.028-0.045
NO_X12_Y12_PM_K3_BF	0.021	0.018	0.017	0.019
IQR	0.019-0.022	0.017-0.02	0.015-0.019	0.017-0.02
NO_X13_Y13_P1_K2_BF	0.045	0.045	0.045	0.045
IQR	0.045-0.049	0.045-0.049	0.043-0.049	0.045-0.049
NO_X13_Y13_P1_K3_BF	0.023	0.022	0.022	0.022
IQR	0.022-0.023	0.021-0.022	0.021-0.022	0.022-0.023
NO_X13_Y13_P2_K2_BF	0.076	0.073	0.071	0.083
IQR	0.066-0.083	0.065-0.083	0.061-0.083	0.071-0.091
NO_X13_Y13_P2_K3_BF	0.018	0.016	0.016	0.017
IQR	0.017-0.019	0.015-0.017	0.013-0.017	0.015-0.018
NO_X13_Y13_P3_K2_BF	0.053	0.05	0.051	0.05
IQR	0.045-0.055	0.043-0.053	0.041-0.054	0.042-0.054
NO_X13_Y13_P3_K3_BF	0.02	0.018	0.018	0.019
IQR	0.019-0.02	0.017-0.018	0.017-0.019	0.018-0.02
NO_X13_Y13_PM_K2_BF	0.026	0.026	0.026	0.026
IQR	0.026-0.035	0.024-0.042	0.021-0.036	0.025-0.041
NO_X13_Y13_PM_K3_BF	0.023	0.022	0.022	0.023
IQR	0.022-0.025	0.02-0.023	0.021-0.023	0.021-0.024
NO_X14_Y14_P1_K2_BF	0	0	0.044	0
IQR	0-0.044	0-0.044	0-0.044	0-0.044
NO_X14_Y14_P1_K3_BF	0.025	0.024	0.024	0.025
IQR	0.025-0.026	0.024-0.025	0.024-0.024	0.024-0.025
NO_X14_Y14_P2_K2_BF	0.098	0.098	0.098	0.098
IQR	0.098-0.098	0.098-0.098	0.098-0.098	0.098-0.098

Instance Name	NSGA-II	NSGA-II-FD	NSGA-II-FDAO	NSGA-II-FDWOA
NO_X14_Y14_P2_K3_BF	0.019	0.016	0.016	0.018
IQR	0.018-0.021	0.015-0.017	0.015-0.017	0.017-0.019
NO_X14_Y14_P3_K2_BF	0.076	0.076	0.059	0.059
IQR	0.059-0.076	0.059-0.076	0.059-0.074	0.059-0.076
NO_X14_Y14_P3_K3_BF	0.021	0.019	0.019	0.02
IQR	0.02-0.022	0.018-0.02	0.018-0.02	0.019-0.022
NO_X14_Y14_PM_K2_BF	0.052	0.048	0.052	0.061
IQR	0.038-0.061	0.0094-0.061	0.038-0.061	0.038-0.061
NO_X14_Y14_PM_K3_BF	0.017	0.015	0.015	0.016
IQR	0.016-0.018	0.014-0.015	0.014-0.016	0.015-0.016
NO_X4_Y4_P1_K2_BF	0	0	0	0
IQR	0-0.088	0-0	0-0	0-0
NO_X4_Y4_P1_K3_BF	0.42	0.35	0.1	0.42
IQR	0.42-0.52	0.1-0.42	0-0.27	0.35-0.42
NO_X4_Y4_P2_K2_BF	0	0	0	0
IQR	0-0	0-0	0-0	0-0
NO_X4_Y4_P2_K3_BF	0.67	0	0	0.67
IQR	0.67-0.67	0-0	0-0.24	0.24-0.67
NO_X4_Y4_P3_K2_BF	0	0	0	0
IQR	0-0.1	0-0	0-0	0-0
NO_X4_Y4_P3_K3_BF	0.65	0	0	0.65
IQR	0.65-0.65	0-0.24	0-0	0.24-0.65
NO_X4_Y4_PM_K2_BF	0	0	0	0
IQR	0-0	0-0	0-0	0-0
NO_X4_Y4_PM_K3_BF	0.39	0.13	0.13	0.39
IQR	0.34-0.39	0-0.37	0-0.39	0.33-0.39
NO_X5_Y5_P1_K2_BF	0	0	0	0
IQR	0-0	0-0	0-0	0-0
NO_X5_Y5_P1_K3_BF	0.24	0.2	0.2	0.21
IQR	0.24-0.24	0.2-0.22	0.18-0.2	0.2-0.24
NO_X5_Y5_P2_K2_BF	0	0	0	0
IQR	0-0	0-0	0-0	0-0
NO_X5_Y5_P2_K3_BF	0.29	0.19	0.17	0.27
IQR	0.25-0.35	0.17-0.26	0.12-0.21	0.23-0.29
NO_X5_Y5_P3_K2_BF	0	0	0	0
IQR	0-0	0-0	0-0	0-0
NO_X5_Y5_P3_K3_BF	0.18	0.14	0.11	0.18
IQR	0.18-0.18	0.093-0.18	0.084-0.16	0.18-0.18
NO_X5_Y5_PM_K2_BF	0	0	0	0
IQR	0-0	0-0	0-0	0-0
NO_X5_Y5_PM_K3_BF	0.14	0.091	0.036	0.14
IQR	0.14-0.18	0.036-0.11	0-0.11	0.081-0.16
NO_X6_Y6_P1_K2_BF	0	0	0	0
IQR	0-0	0-0	0-0	0-0
NO_X6_Y6_P1_K3_BF	0.18	0.17	0.11	0.18
IQR	0.17-0.18	0.11-0.18	0.11-0.17	0.17-0.19
NO_X6_Y6_P2_K2_BF	0	0	0	0
IQR	0-0	0-0.024	0-0.018	0-0.024
NO_X6_Y6_P2_K3_BF	0.072	0.06	0.06	0.086
IQR	0.029-0.097	0.026-0.076	0-0.063	0.0047-0.12
NO_X6_Y6_P3_K2_BF	0	0	0	0
IQR	0-0	0-0	0-0	0-0
NO_X6_Y6_P3_K3_BF	0.05	0.046	0.038	0.046
IQR	0.046-0.067	0-0.046	0-0.046	0.038-0.05
NO_X6_Y6_PM_K2_BF	0	0	0	0
IQR	0-0	0-0	0-0	0-0
NO_X6_Y6_PM_K3_BF	0.081	0.047	0.047	0.049
IQR	0.07-0.081	0.02-0.052	0.013-0.047	0.02-0.07
NO_X7_Y7_P1_K2_BF	0	0	0	0
IQR	0-0	0-0	0-0	0-0
NO_X7_Y7_P1_K3_BF	0.076	0.076	0.076	0.076
IQR	0.074-0.079	0.046-0.076	0.074-0.076	0.074-0.078
NO_X7_Y7_P2_K2_BF	0	0	0	0
IQR	0-0	0-0	0-0	0-0
NO_X7_Y7_P2_K3_BF	0.052	0.037	0.036	0.052
IQR	0.051-0.052	0.035-0.052	0.03-0.05	0.049-0.052
NO_X7_Y7_P3_K2_BF	0	0	0	0
IQR	0-0	0-0	0-0	0-0
NO_X7_Y7_P3_K3_BF	0.054	0.048	0.05	0.054
IQR	0.053-0.054	0.045-0.052	0.043-0.053	0.053-0.054
NO_X7_Y7_PM_K2_BF	0	0	0	0
IQR	0-0	0-0	0-0	0-0
NO_X7_Y7_PM_K3_BF	0.039	0.022	0.024	0.033

Instance Name	NSGA-II	NSGA-II-FD	NSGA-II-FDAO	NSGA-II-FDWOA
IQR	0.035-0.039	0.02-0.029	0.018-0.027	0.031-0.036
NO_X8_Y8_P1_K2_BF	0	0	0	0
IQR	0-0.045	0-0	0-0	0-0
NO_X8_Y8_P1_K3_BF	0.032	0.031	0.031	0.031
IQR	0.031-0.034	0.031-0.035	0.03-0.032	0.031-0.034
NO_X8_Y8_P2_K2_BF	0.063	0.061	0.037	0.063
IQR	0.037-0.063	0.017-0.063	0.028-0.062	0.017-0.063
NO_X8_Y8_P2_K3_BF	0.027	0.023	0.023	0.024
IQR	0.025-0.029	0.02-0.024	0.02-0.025	0.023-0.026
NO_X8_Y8_P3_K2_BF	0.011	0	0	0
IQR	0-0.011	0-0	0-0	0-0
NO_X8_Y8_P3_K3_BF	0.03	0.029	0.027	0.03
IQR	0.029-0.03	0.026-0.031	0.026-0.029	0.029-0.03
NO_X8_Y8_PM_K2_BF	0.071	0.09	0.056	0.09
IQR	0.056-0.09	0.071-0.09	0.056-0.09	0.071-0.09
NO_X8_Y8_PM_K3_BF	0.04	0.032	0.032	0.041
IQR	0.034-0.057	0.026-0.037	0.026-0.037	0.036-0.056
NO_X9_Y9_P1_K2_BF	0.00019	0.00019	0.00019	0.00019
IQR	0.00019-0.046	0.00019-0.00019	4.4e-06-0.00019	0.00019-0.00019
NO_X9_Y9_P1_K3_BF	0.026	0.024	0.015	0.025
IQR	0.026-0.027	0.012-0.025	0.011-0.025	0.025-0.026
NO_X9_Y9_P2_K2_BF	0	0	0	0
IQR	0-0	0-0	0-0	0-0
NO_X9_Y9_P2_K3_BF	0.026	0.018	0.017	0.024
IQR	0.024-0.029	0.016-0.021	0.016-0.022	0.02-0.026
NO_X9_Y9_P3_K2_BF	0.095	0.095	0.045	0.095
IQR	0.084-0.095	0.055-0.095	0.045-0.084	0.095-0.095
NO_X9_Y9_P3_K3_BF	0.023	0.014	0.014	0.022
IQR	0.022-0.024	0.011-0.019	0.012-0.016	0.02-0.022
NO_X9_Y9_PM_K2_BF	0	0	0	0
IQR	0-0	0-0	0-0	0-0
NO_X9_Y9_PM_K3_BF	0.044	0.037	0.038	0.037
IQR	0.04-0.05	0.031-0.042	0.035-0.045	0.034-0.046

Table B.6: Raw values of different instances of the IGD indicator. Shown are the median and the IQR values below.

B.4 Curve Ordering Results

B.4.1 IGD$^+$ Values

Instance Name	[WM21b]	Centroid	Geo. Med.
CH_X10_Y10_P1_K2_BF	0.31	0.079	0
IQR	0.19-0.47	0.063-0.27	0-0.045
CH_X10_Y10_P1_K3_BF	0.65	0.44	0.075
IQR	0.48-0.79	0.32-0.54	0.062-0.16
CH_X10_Y10_P2_K2_BF	0.48	0.42	0.43
IQR	0.32-0.66	0.42-0.93	0.42-0.43
CH_X10_Y10_P2_K3_BF	0.61	0.31	0.31
IQR	0.5-0.71	0.31-0.42	0.048-0.43
CH_X10_Y10_P3_K2_BF	0.25	0.067	0.071
IQR	0.12-0.31	0.00042-0.098	0.00012-0.071
CH_X10_Y10_P3_K3_BF	0.63	0.29	0.42
IQR	0.5-0.74	0.2-0.43	0.19-0.55
CH_X10_Y10_PM_K2_BF	0	0	0
IQR	0-0	0-0	0-0
CH_X10_Y10_PM_K3_BF	0.54	0.17	0.17
IQR	0.4-0.73	0.083-0.33	0.092-0.39
CH_X11_Y11_P1_K2_BF	0.59	0.094	0.021
IQR	0.34-0.72	0.085-0.19	0.0036-0.044
CH_X11_Y11_P1_K3_BF	0.32	0.27	0.035
IQR	0.19-0.52	0.12-0.48	0.016-0.12
CH_X11_Y11_P2_K2_BF	0.59	0.31	0.18
IQR	0.47-0.79	0.25-0.32	0.15-0.31
CH_X11_Y11_P2_K3_BF	0.73	0.24	0.54
IQR	0.57-1	0.068-0.39	0.45-0.72

Instance Name	[WM21b]	Centroid	Geo. Med.
CH_X11_Y11_P3_K2_BF	0.59	0.11	0.09
IQR	0.48-0.66	0.093-0.15	0.01-0.093
CH_X11_Y11_P3_K3_BF	0.69	0.39	0.51
IQR	0.54-0.81	0.34-0.66	0.28-0.67
CH_X11_Y11_PM_K2_BF	0.57	0.17	0.34
IQR	0.44-0.76	0-0.33	0.3-0.36
CH_X11_Y11_PM_K3_BF	0.52	0.33	0.22
IQR	0.45-0.61	0.27-0.55	0.17-0.3
CH_X12_Y12_P1_K2_BF	0.36	0.073	0.015
IQR	0.28-0.54	0.066-0.12	0.015-0.13
CH_X12_Y12_P1_K3_BF	0.5	0.25	0.21
IQR	0.31-0.78	0.13-0.33	0.098-0.29
CH_X12_Y12_P2_K2_BF	0.34	0.052	0.14
IQR	0.29-0.45	0.052-0.29	0.14-0.15
CH_X12_Y12_P2_K3_BF	0.52	0.13	0.31
IQR	0.42-0.63	0.088-0.34	0.3-0.48
CH_X12_Y12_P3_K2_BF	0.42	0.16	0.098
IQR	0.37-0.5	0.067-0.2	0.082-0.16
CH_X12_Y12_P3_K3_BF	0.46	0.25	0.4
IQR	0.35-0.64	0.14-0.37	0.17-0.56
CH_X12_Y12_PM_K2_BF	0.43	0.23	0.38
IQR	0.37-0.53	0.21-0.29	0.35-0.38
CH_X12_Y12_PM_K3_BF	0.64	0.3	0.19
IQR	0.42-0.82	0.2-0.38	0.17-0.21
CH_X13_Y13_P1_K2_BF	0.32	0.054	0.037
IQR	0.26-0.82	0.036-0.065	0.032-0.044
CH_X13_Y13_P1_K3_BF	0.47	0.022	0.13
IQR	0.32-0.56	0.01-0.076	0.12-0.18
CH_X13_Y13_P2_K2_BF	0.52	0.37	0.49
IQR	0.44-0.62	0.31-0.45	0.27-0.55
CH_X13_Y13_P2_K3_BF	0.76	0.25	0.47
IQR	0.58-0.88	0.18-0.33	0.27-0.63
CH_X13_Y13_P3_K2_BF	0.56	0.25	0.26
IQR	0.46-0.7	0.11-0.3	0.18-0.35
CH_X13_Y13_P3_K3_BF	0.55	0.26	0.6
IQR	0.39-0.81	0.17-0.39	0.35-0.74
CH_X13_Y13_PM_K2_BF	0.4	0.1	0.059
IQR	0.35-0.58	0.056-0.23	0.017-0.2
CH_X13_Y13_PM_K3_BF	0.65	0.33	0.18
IQR	0.5-0.82	0.095-0.5	0.13-0.26
CH_X14_Y14_P1_K2_BF	0.19	0.1	0.0066
IQR	0.14-0.33	0.076-0.14	0.0015-0.019
CH_X14_Y14_P1_K3_BF	0.65	0.11	0.14
IQR	0.36-0.88	0.016-0.47	0.12-0.18
CH_X14_Y14_P2_K2_BF	0.43	0.23	0.16
IQR	0.43-0.46	0.058-0.23	0-0.26
CH_X14_Y14_P2_K3_BF	0.62	0.26	0.26
IQR	0.39-0.72	0.12-0.3	0.15-0.3
CH_X14_Y14_P3_K2_BF	0.22	0.061	0.32
IQR	0.13-0.69	0.061-0.29	0.12-0.39
CH_X14_Y14_P3_K3_BF	0.72	0.38	0.35
IQR	0.48-0.86	0.18-0.48	0.18-0.45
CH_X14_Y14_PM_K2_BF	0.53	0.13	0.025
IQR	0.41-0.92	0.05-0.29	0-0.26
CH_X14_Y14_PM_K3_BF	0.64	0.42	0.1
IQR	0.43-0.79	0.4-0.43	0.089-0.24
CH_X5_Y5_P1_K2_BF	0.42	0.89	1.1
IQR	0.36-0.71	0.85-1	0.91-1.1
CH_X5_Y5_P1_K3_BF	0.61	0.87	0.86
IQR	0.61-0.69	0.75-0.97	0.59-0.97
CH_X5_Y5_P2_K2_BF	0.54	0.43	0.79
IQR	0.42-0.64	0.43-0.5	0.61-0.91
CH_X5_Y5_P2_K3_BF	0.81	1.2	1
IQR	0.81-1.1	1-1.5	1-1.2
CH_X5_Y5_P3_K2_BF	0.46	1.2	1
IQR	0.32-1	0.8-1.3	0.95-1.3
CH_X5_Y5_P3_K3_BF	0.43	0.35	0.31
IQR	0.39-0.44	0.29-0.42	0.2-0.41
CH_X5_Y5_PM_K2_BF	0.41	0.64	0.64
IQR	0.41-0.52	0.53-0.66	0.64-0.71
CH_X5_Y5_PM_K3_BF	0.48	1.1	0.15
IQR	0.4-0.49	1-1.2	0-0.24
CH_X6_Y6_P1_K2_BF	0.3	0.99	0.94

Instance Name	[WM21b]	Centroid	Geo. Med.
IQR	0.21-0.31	0.95-1.2	0.83-1.6
CH_X6_Y6_P1_K3_BF	0.71	0.87	0.72
IQR	0.57-0.74	0.66-1.2	0.64-0.87
CH_X6_Y6_P2_K2_BF	0.3	0.56	0.65
IQR	0.29-0.31	0.52-0.69	0.58-0.71
CH_X6_Y6_P2_K3_BF	0.72	1.3	1.3
IQR	0.6-0.94	0.87-1.3	0.85-1.3
CH_X6_Y6_P3_K2_BF	0.34	0.92	0.99
IQR	0.23-0.48	0.86-0.96	0.77-0.99
CH_X6_Y6_P3_K3_BF	0.87	0.96	0.96
IQR	0.82-0.93	0.96-0.99	0.85-0.98
CH_X6_Y6_PM_K2_BF	0.26	0.57	0.5
IQR	0.26-0.33	0.41-0.59	0.35-0.62
CH_X6_Y6_PM_K3_BF	0.43	0.6	0.6
IQR	0.42-0.52	0.52-0.73	0.56-0.67
CH_X7_Y7_P1_K2_BF	0.84	0.96	1.1
IQR	0.61-0.87	0.91-1.1	0.96-1.1
CH_X7_Y7_P1_K3_BF	0.62	0.87	0.6
IQR	0.49-0.91	0.65-0.93	0.54-0.76
CH_X7_Y7_P2_K2_BF	0.73	0.73	0.84
IQR	0.73-0.81	0.73-0.82	0.76-0.86
CH_X7_Y7_P2_K3_BF	0.6	0.92	0.67
IQR	0.43-0.72	0.62-1.3	0.54-1.2
CH_X7_Y7_P3_K2_BF	0.74	0.8	0.64
IQR	0.57-0.91	0.8-1	0.64-0.76
CH_X7_Y7_P3_K3_BF	0.71	0.93	0.91
IQR	0.31-0.91	0.75-0.93	0.75-1.1
CH_X7_Y7_PM_K2_BF	0.66	0.75	0.8
IQR	0.47-0.76	0.71-0.77	0.74-0.86
CH_X7_Y7_PM_K3_BF	0.85	1.1	0.77
IQR	0.71-1.1	0.89-1.2	0.71-1.2
CH_X8_Y8_P1_K2_BF	0	0.63	0
IQR	0-0.63	0.59-0.88	0-0.71
CH_X8_Y8_P1_K3_BF	0.78	0.66	0.64
IQR	0.57-0.88	0.48-0.95	0.46-0.93
CH_X8_Y8_P2_K2_BF	0.75	0.71	0.71
IQR	0.64-0.86	0.43-1.4	0.5-1
CH_X8_Y8_P2_K3_BF	0.78	1.2	1.3
IQR	0.48-1.1	0.84-1.8	1-1.7
CH_X8_Y8_P3_K2_BF	0.65	0.91	0.94
IQR	0.49-0.84	0.45-1.1	0.43-1.1
CH_X8_Y8_P3_K3_BF	0.68	0.83	0.8
IQR	0.67-0.91	0.69-0.9	0.76-0.95
CH_X8_Y8_PM_K2_BF	0.8	0.54	0.91
IQR	0.77-0.83	0.47-0.65	0.75-0.92
CH_X8_Y8_PM_K3_BF	0.65	0.54	0.55
IQR	0.38-1	0.48-0.9	0.53-0.78
CH_X9_Y9_P1_K2_BF	0.43	0.26	0.53
IQR	0.43-0.5	0.09-0.31	0.38-0.92
CH_X9_Y9_P1_K3_BF	0.81	0.43	0.89
IQR	0.63-1	0.23-0.96	0.72-1.1
CH_X9_Y9_P2_K2_BF	0	0	0
IQR	0-0	0-0	0-0
CH_X9_Y9_P2_K3_BF	0.64	0.71	0.72
IQR	0.51-0.82	0.64-1	0.65-1
CH_X9_Y9_P3_K2_BF	0.35	0.7	0.73
IQR	0.29-0.39	0.46-0.75	0.73-0.74
CH_X9_Y9_P3_K3_BF	0.66	0.58	0.65
IQR	0.54-0.78	0.54-0.74	0.54-0.79
CH_X9_Y9_PM_K2_BF	0	0	0
IQR	0-0	0-0	0-0
CH_X9_Y9_PM_K3_BF	0.7	0.85	0.68
IQR	0.52-1	0.66-1	0.65-0.9
LA_X10_Y10_P1_K2_BF	0.32	0.18	0.18
IQR	0.27-0.46	0.14-0.24	0.1-0.23
LA_X10_Y10_P1_K3_BF	0.43	0.18	0.1
IQR	0.31-0.52	0.12-0.34	0.067-0.31
LA_X10_Y10_P2_K2_BF	0.33	0.31	0.33
IQR	0.33-0.47	0.26-0.45	0.33-0.33
LA_X10_Y10_P2_K3_BF	1	0.86	0
IQR	0.55-1.3	0.09-1.1	0-1.1
LA_X10_Y10_P3_K2_BF	0.18	0.4	0.2
IQR	0.15-0.43	0.35-0.44	0.19-0.27

Instance Name	[WM21b]	Centroid	Geo. Med.
LA_X10_Y10_P3_K3_BF	0.45	0.4	0.21
IQR	0.35-0.59	0.32-0.5	0.19-0.28
LA_X10_Y10_PM_K2_BF	0.39	0.35	0.39
IQR	0.35-0.98	0.33-0.45	0.064-0.39
LA_X10_Y10_PM_K3_BF	1.1	0.93	0.19
IQR	0.68-1.2	0.16-1	0-0.27
LA_X11_Y11_P1_K2_BF	0.57	0.11	0.076
IQR	0.29-0.74	0.077-0.11	0.015-0.22
LA_X11_Y11_P1_K3_BF	0.37	0.27	0.029
IQR	0.17-0.54	0.1-0.34	0.021-0.036
LA_X11_Y11_P2_K2_BF	0.37	0.12	0.053
IQR	0.21-0.54	0.09-0.37	0.047-0.27
LA_X11_Y11_P2_K3_BF	1	0.79	0.57
IQR	0.72-1.2	0.29-0.96	0.26-0.62
LA_X11_Y11_P3_K2_BF	0.47	0.33	0.16
IQR	0.38-0.55	0.31-0.39	0.082-0.18
LA_X11_Y11_P3_K3_BF	0.58	0.53	0.17
IQR	0.43-0.78	0.4-0.58	0.17-0.29
LA_X11_Y11_PM_K2_BF	0.55	0.072	0
IQR	0.34-0.68	0.072-0.15	0-0.11
LA_X11_Y11_PM_K3_BF	0.68	0.1	0.32
IQR	0.62-0.8	0.0073-0.49	0.0073-0.41
LA_X12_Y12_P1_K2_BF	0.16	0.11	0.028
IQR	0.019-0.54	0.065-0.15	0.0091-0.083
LA_X12_Y12_P1_K3_BF	0.39	0.17	0.1
IQR	0.27-0.61	0.14-0.25	0.029-0.41
LA_X12_Y12_P2_K2_BF	0.25	0.17	0.13
IQR	0.15-0.45	0.078-0.2	0.082-0.24
LA_X12_Y12_P2_K3_BF	1.1	0.79	0.53
IQR	0.76-1.4	0.72-0.88	0.18-0.56
LA_X12_Y12_P3_K2_BF	0.24	0.018	0.09
IQR	0.12-0.49	9.3e-17-0.13	0.018-0.18
LA_X12_Y12_P3_K3_BF	0.61	0.53	0.24
IQR	0.49-0.8	0.27-0.61	0.1-0.39
LA_X12_Y12_PM_K2_BF	0.61	0.45	0.49
IQR	0.54-0.71	0.43-0.48	0.39-0.53
LA_X12_Y12_PM_K3_BF	0.5	0.38	0.22
IQR	0.35-0.63	0.31-0.47	0.087-0.33
LA_X13_Y13_P1_K2_BF	0.14	0.12	0.014
IQR	0.085-0.23	0.052-0.16	0.014-0.022
LA_X13_Y13_P1_K3_BF	0.46	0.3	0.068
IQR	0.39-0.64	0.26-0.36	0.026-0.081
LA_X13_Y13_P2_K2_BF	0.31	0.083	0.066
IQR	0.22-0.52	0.068-0.13	0.048-0.2
LA_X13_Y13_P2_K3_BF	0.64	0.48	0.31
IQR	0.52-0.87	0.38-0.53	0.23-0.33
LA_X13_Y13_P3_K2_BF	0.29	0.1	0.082
IQR	0.16-0.37	0.083-0.19	0.016-0.095
LA_X13_Y13_P3_K3_BF	0.56	0.38	0.12
IQR	0.49-0.69	0.25-0.42	0.1-0.13
LA_X13_Y13_PM_K2_BF	0.5	0.17	0.12
IQR	0.36-0.62	0.14-0.26	0.092-0.12
LA_X13_Y13_PM_K3_BF	0.46	0.21	0.24
IQR	0.3-0.55	0.16-0.28	0.05-0.47
LA_X14_Y14_P1_K2_BF	0.69	0.29	0.33
IQR	0.39-0.81	0.072-0.35	0.17-0.35
LA_X14_Y14_P1_K3_BF	0.44	0.32	0.019
IQR	0.33-0.64	0.22-0.54	0.014-0.024
LA_X14_Y14_P2_K2_BF	0.48	0	0.054
IQR	0.29-0.67	0-0.18	0-0.054
LA_X14_Y14_P2_K3_BF	0.66	0.41	0.29
IQR	0.54-0.79	0.37-0.51	0.2-0.33
LA_X14_Y14_P3_K2_BF	0.73	0.22	0.22
IQR	0.49-1.1	0.21-0.23	0.093-0.23
LA_X14_Y14_P3_K3_BF	0.65	0.24	0.1
IQR	0.55-0.89	0.2-0.33	0.073-0.27
LA_X14_Y14_PM_K2_BF	0.71	0.53	0.49
IQR	0.47-0.81	0.47-0.9	0.29-0.49
LA_X14_Y14_PM_K3_BF	0.95	0.16	0.6
IQR	0.69-1.1	0.1-0.39	0.44-0.6
LA_X5_Y5_P1_K2_BF	0.33	0.91	0.91
IQR	0.32-0.43	0.8-0.91	0.83-0.91
LA_X5_Y5_P1_K3_BF	0.23	0	0.46

Instance Name	[WM21b]	Centroid	Geo. Med.
IQR	0.23-0.46	0-0.71	0.23-0.57
LA_X5_Y5_P2_K2_BF	0.4	0.6	0.62
IQR	0.28-0.63	0.48-0.6	0.6-0.75
LA_X5_Y5_P2_K3_BF	0.32	0.61	0.61
IQR	0.28-0.51	0.52-0.84	0.32-0.84
LA_X5_Y5_P3_K2_BF	0.54	0.66	0.76
IQR	0.35-0.6	0.65-0.85	0.66-0.76
LA_X5_Y5_P3_K3_BF	0.33	0.72	1
IQR	0.27-0.53	0.68-0.76	0.92-1.1
LA_X5_Y5_PM_K2_BF	0.51	0.56	0.57
IQR	0.37-0.57	0.45-0.56	0.55-0.62
LA_X5_Y5_PM_K3_BF	0.71	0.96	0.96
IQR	0.45-0.82	0.93-0.97	0.96-0.97
LA_X6_Y6_P1_K2_BF	0.39	0.39	0.59
IQR	0-0.54	0.24-0.54	0.39-1.3
LA_X6_Y6_P1_K3_BF	0.29	0.71	0.47
IQR	0.065-0.71	0.31-0.9	0.24-1.7
LA_X6_Y6_P2_K2_BF	0.53	0.59	0.66
IQR	0.48-0.73	0.48-0.95	0.52-0.81
LA_X6_Y6_P2_K3_BF	0.58	0.62	0.21
IQR	0.21-0.59	0.58-0.95	0.21-0.61
LA_X6_Y6_P3_K2_BF	0.59	0.74	0.68
IQR	0.53-0.71	0.51-0.85	0.35-0.77
LA_X6_Y6_P3_K3_BF	0.29	0.71	0.7
IQR	0.26-0.36	0.52-34	0.29-1.6
LA_X6_Y6_PM_K2_BF	0.29	0.92	0.72
IQR	0.29-0.29	0.83-0.92	0.67-0.72
LA_X6_Y6_PM_K3_BF	0.49	1.2	0.8
IQR	0.4-0.85	1.1-1.8	0.67-1.9
LA_X7_Y7_P1_K2_BF	0.48	0.8	0.8
IQR	0.074-0.54	0.71-0.85	0.69-0.83
LA_X7_Y7_P1_K3_BF	0.054	0.97	1.9
IQR	0.032-0.92	0.8-1.1	0.017-3.8e+05
LA_X7_Y7_P2_K2_BF	0.49	0.46	0.49
IQR	0.43-0.52	0.41-0.63	0.42-0.59
LA_X7_Y7_P2_K3_BF	0.31	0.89	0.5
IQR	0-0.56	0.46-0.89	0.31-13
LA_X7_Y7_P3_K2_BF	0.33	0.84	0.71
IQR	0.33-0.47	0.84-0.94	0.71-0.86
LA_X7_Y7_P3_K3_BF	0.32	0.32	0.51
IQR	0-0.67	0.32-0.81	0.32-0.6
LA_X7_Y7_PM_K2_BF	0.41	0.45	0.45
IQR	0.29-0.49	0.29-0.57	0.41-0.45
LA_X7_Y7_PM_K3_BF	0.87	1.1	0.68
IQR	0.57-0.9	0.78-1.4	0.35-1.1
LA_X8_Y8_P1_K2_BF	0.21	0.8	0.8
IQR	0.041-0.3	0.55-0.83	0.27-0.8
LA_X8_Y8_P1_K3_BF	0.68	0.76	0.88
IQR	0.11-0.87	0.68-1.1	0.76-1.3
LA_X8_Y8_P2_K2_BF	0	0	0
IQR	0-0	0-0	0-0
LA_X8_Y8_P2_K3_BF	0.65	4.6	4.5
IQR	0.51-1.1	1.1-8.2	1.1-8.3
LA_X8_Y8_P3_K2_BF	0.41	0.62	0.64
IQR	0.0039-0.49	0.62-0.88	0.5-0.88
LA_X8_Y8_P3_K3_BF	0.63	1.9	1.8
IQR	0.37-1.1	1.2-2	1.2-2.5
LA_X8_Y8_PM_K2_BF	0	0	0
IQR	0-0	0-0	0-0
LA_X8_Y8_PM_K3_BF	0.72	1.3	1
IQR	0.44-1.1	0.91-1.8	0.57-2
LA_X9_Y9_P1_K2_BF	0.35	0.91	0.92
IQR	0.17-0.54	0.6-1.2	0.91-1.3
LA_X9_Y9_P1_K3_BF	1	1.1	1.1
IQR	0.55-1.5	0.89-1.6	0.81-1.2
LA_X9_Y9_P2_K2_BF	0	0	0
IQR	0-0	0-0	0-0
LA_X9_Y9_P2_K3_BF	2.3	1.7	1.5e+02
IQR	1.4-25	1-23	1.6-2e+02
LA_X9_Y9_P3_K2_BF	0.48	0.67	0.8
IQR	0.35-0.72	0.42-1.2	0.74-1
LA_X9_Y9_P3_K3_BF	0.99	1.1	1.2
IQR	0.76-1.2	0.8-1.4	0.87-1.4

Instance Name	[WM21b]	Centroid	Geo. Med.
LA_X9_Y9_PM_K2_BF	0	0	0
IQR	0-0	0-0	0-0
LA_X9_Y9_PM_K3_BF	1.5	1.9	2.2
IQR	1.1-2.3	1.6-3.5	1.6-3.6
NO_X10_Y10_P1_K2_BF	0.23	0.32	0.12
IQR	0.15-0.42	0.21-0.61	0.082-0.18
NO_X10_Y10_P1_K3_BF	0.52	0.29	0.099
IQR	0.39-0.8	0.12-0.51	0.084-0.17
NO_X10_Y10_P2_K2_BF	0.55	0.19	0.24
IQR	0.36-0.8	1.1e-16-0.3	1.1e-16-0.41
NO_X10_Y10_P2_K3_BF	0.84	0.6	0.55
IQR	0.7-0.92	0.53-0.67	0.34-0.82
NO_X10_Y10_P3_K2_BF	0.32	0.14	0.22
IQR	0.25-0.39	0.11-0.25	0.19-0.27
NO_X10_Y10_P3_K3_BF	0.53	0.68	0.69
IQR	0.4-0.76	0.57-0.73	0.57-0.75
NO_X10_Y10_PM_K2_BF	0.59	0.43	0.33
IQR	0.2-0.68	0.43-0.47	0-0.53
NO_X10_Y10_PM_K3_BF	0.67	0.45	0.4
IQR	0.51-1.1	0.31-0.59	0.37-0.45
NO_X11_Y11_P1_K2_BF	0.47	0.21	0.062
IQR	0.24-0.59	0.1-0.33	0.042-0.071
NO_X11_Y11_P1_K3_BF	0.52	0.59	0.2
IQR	0.37-0.67	0.49-0.94	0.085-0.37
NO_X11_Y11_P2_K2_BF	0.33	0.12	0.028
IQR	0.21-0.54	0.084-0.19	0.027-0.084
NO_X11_Y11_P2_K3_BF	0.64	0.68	0.36
IQR	0.53-0.79	0.4-0.88	0.24-0.65
NO_X11_Y11_P3_K2_BF	0.41	0.19	0.28
IQR	0.31-0.52	0.13-0.23	0.11-0.34
NO_X11_Y11_P3_K3_BF	0.82	0.68	0.47
IQR	0.7-0.9	0.54-0.8	0.39-0.54
NO_X11_Y11_PM_K2_BF	0.65	0.24	0.18
IQR	0.5-0.74	0.1-0.24	0.0051-0.22
NO_X11_Y11_PM_K3_BF	0.73	0.24	0.52
IQR	0.59-1	0.14-0.48	0.3-0.59
NO_X12_Y12_P1_K2_BF	0.61	0.15	0.17
IQR	0.27-0.84	0.061-0.21	0.11-0.42
NO_X12_Y12_P1_K3_BF	0.5	0.43	0.25
IQR	0.31-0.83	0.21-0.52	0.091-0.33
NO_X12_Y12_P2_K2_BF	0.42	0.2	0.2
IQR	0.32-0.5	0.19-0.68	0.12-0.68
NO_X12_Y12_P2_K3_BF	0.99	0.62	0.6
IQR	0.69-1.1	0.48-0.68	0.43-0.69
NO_X12_Y12_P3_K2_BF	0.42	0.35	0.38
IQR	0.23-0.65	0.19-0.47	0.2-0.53
NO_X12_Y12_P3_K3_BF	0.67	0.49	0.52
IQR	0.54-0.79	0.23-0.68	0.41-0.62
NO_X12_Y12_PM_K2_BF	0.45	0.23	0.4
IQR	0.34-0.53	0.15-0.27	0.19-0.53
NO_X12_Y12_PM_K3_BF	0.52	0.36	0.44
IQR	0.39-0.83	0.17-0.54	0.4-0.56
NO_X13_Y13_P1_K2_BF	0.29	0.14	0.043
IQR	0.17-0.83	0.093-0.19	0.041-0.046
NO_X13_Y13_P1_K3_BF	0.39	0.42	0.17
IQR	0.26-0.52	0.22-0.51	0.072-0.3
NO_X13_Y13_P2_K2_BF	0.43	0.22	0.15
IQR	0.31-0.53	0.17-0.29	0.13-0.25
NO_X13_Y13_P2_K3_BF	0.76	0.52	0.52
IQR	0.43-0.88	0.26-0.6	0.31-0.64
NO_X13_Y13_P3_K2_BF	0.35	0.13	0.25
IQR	0.29-0.44	0.084-0.17	0.15-0.41
NO_X13_Y13_P3_K3_BF	0.76	0.59	0.57
IQR	0.59-0.85	0.53-0.67	0.44-0.61
NO_X13_Y13_PM_K2_BF	0.35	0.16	0.1
IQR	0.25-0.49	0.11-0.25	0.076-0.14
NO_X13_Y13_PM_K3_BF	0.68	0.39	0.45
IQR	0.53-0.94	0.29-0.62	0.41-0.53
NO_X14_Y14_P1_K2_BF	0.51	0.25	0.24
IQR	0.34-0.68	0.21-0.34	0.18-0.27
NO_X14_Y14_P1_K3_BF	0.56	0.62	0.17
IQR	0.44-1.2	0.48-0.78	0.12-0.19
NO_X14_Y14_P2_K2_BF	0.83	0.48	1

Instance Name	[WM21b]	Centroid	Geo. Med.
IQR	0.49-1.4	0.46-0.98	0.13-1.2
NO_X14_Y14_P2_K3_BF	0.71	0.34	0.36
IQR	0.52-0.8	0.31-0.52	0.3-0.44
NO_X14_Y14_P3_K2_BF	0.67	0.23	0.22
IQR	0.44-0.7	0.098-0.37	0.054-0.26
NO_X14_Y14_P3_K3_BF	0.69	0.61	0.56
IQR	0.51-0.91	0.32-0.7	0.46-0.6
NO_X14_Y14_PM_K2_BF	0.71	0.58	0.77
IQR	0.63-0.9	0.52-0.65	0.56-1
NO_X14_Y14_PM_K3_BF	0.76	0.66	0.43
IQR	0.55-0.97	0.56-0.71	0.3-0.57
NO_X5_Y5_P1_K2_BF	0.56	1	1
IQR	0.36-1	0.88-1.1	0.95-1
NO_X5_Y5_P1_K3_BF	0.96	1.1	1
IQR	0.81-1.1	1-1.7	0.16-1.1
NO_X5_Y5_P2_K2_BF	0.37	0.56	0.61
IQR	0.36-0.52	0.56-0.67	0.56-0.67
NO_X5_Y5_P2_K3_BF	1	1.6	1.3
IQR	0.81-1.2	1.2-2.3	0.84-1.7
NO_X5_Y5_P3_K2_BF	0.29	0.39	1
IQR	0.19-0.4	0.28-1.1	0.85-1.2
NO_X5_Y5_P3_K3_BF	1.1	1.1	0.96
IQR	0.61-1.1	1.1-1.2	0.9-1.2
NO_X5_Y5_PM_K2_BF	0.45	0.31	0.59
IQR	0.32-0.46	0.31-0.43	0.4-0.59
NO_X5_Y5_PM_K3_BF	0.52	1.1	1.1
IQR	0.49-0.92	0.45-1.1	1-1.1
NO_X6_Y6_P1_K2_BF	0.32	0.36	0.46
IQR	0.31-0.46	0.26-0.52	0.34-0.58
NO_X6_Y6_P1_K3_BF	0.96	0.98	0.78
IQR	0.78-1.2	0.68-5.6	0.65-6.9
NO_X6_Y6_P2_K2_BF	0.24	0.38	0.29
IQR	0.23-0.26	0.28-0.63	0.18-0.4
NO_X6_Y6_P2_K3_BF	0.86	1.5	0.9
IQR	0.82-1.2	0.79-2.3	0.64-1.6
NO_X6_Y6_P3_K2_BF	0.46	0.34	0.3
IQR	0.34-0.51	0.25-0.55	0.23-0.46
NO_X6_Y6_P3_K3_BF	0.81	1	1.2
IQR	0.51-1.1	0.9-1.5	0.54-1.6
NO_X6_Y6_PM_K2_BF	0.42	0.59	0.5
IQR	0.41-0.66	0.53-0.68	0.4-0.52
NO_X6_Y6_PM_K3_BF	0.82	1	1.2
IQR	0.48-0.9	0.79-1.3	0.56-1.4
NO_X7_Y7_P1_K2_BF	0.5	1	0.98
IQR	0.39-0.86	0.98-1	0.98-1.1
NO_X7_Y7_P1_K3_BF	1.1	13	2.7
IQR	0.95-1.5	0.84-82	0.96-82
NO_X7_Y7_P2_K2_BF	0.85	0.47	0.47
IQR	0.7-0.86	0.47-1.2	0.47-0.65
NO_X7_Y7_P2_K3_BF	1.2	2	1.4
IQR	0.95-1.3	1.4-2.2	1.2-2.1
NO_X7_Y7_P3_K2_BF	0.71	0.8	0.56
IQR	0.65-0.71	0.66-0.88	0.56-0.81
NO_X7_Y7_P3_K3_BF	0.6	0.8	0.92
IQR	0.49-0.68	0.68-0.95	0.68-1.1
NO_X7_Y7_PM_K2_BF	0.47	0.47	0.47
IQR	0.47-0.47	0.39-0.5	0.47-0.47
NO_X7_Y7_PM_K3_BF	0.8	0.91	0.74
IQR	0.62-1.1	0.76-1.2	0.52-0.9
NO_X8_Y8_P1_K2_BF	0.51	0.62	0.88
IQR	0.41-0.63	0.26-0.77	0.56-0.98
NO_X8_Y8_P1_K3_BF	0.76	0.82	0.85
IQR	0.47-0.93	0.62-1.1	0.61-1.1
NO_X8_Y8_P2_K2_BF	0.79	0.51	0.8
IQR	0.59-0.87	0.25-0.52	0.58-0.99
NO_X8_Y8_P2_K3_BF	1.1	1.2	1.2
IQR	0.88-1.4	1-1.5	0.92-1.3
NO_X8_Y8_P3_K2_BF	0.37	0.32	0.45
IQR	0.24-0.62	0.26-0.37	0.26-0.56
NO_X8_Y8_P3_K3_BF	0.64	0.9	0.78
IQR	0.58-0.8	0.73-1.1	0.63-1.1
NO_X8_Y8_PM_K2_BF	0.68	0.61	0.61
IQR	0.48-0.79	0.48-0.76	0.49-0.75

Instance Name	[WM21b]	Centroid	Geo. Med.
NO_X8_Y8_PM_K3_BF	0.87	1.1	0.88
IQR	0.75-1.1	0.88-1.3	0.78-1.1
NO_X9_Y9_P1_K2_BF	0.62	0.74	0.87
IQR	0.43-0.7	0.39-1.1	0.6-1.1
NO_X9_Y9_P1_K3_BF	1.1	1.2	0.96
IQR	0.9-1.4	1.1-1.5	0.7-1.1
NO_X9_Y9_P2_K2_BF	0	0	0
IQR	0-0	0-0	0-0
NO_X9_Y9_P2_K3_BF	0.84	0.73	0.75
IQR	0.63-0.9	0.53-0.85	0.62-0.94
NO_X9_Y9_P3_K2_BF	0.63	0.8	0.75
IQR	0.46-0.8	0.67-1.3	0.74-1.3
NO_X9_Y9_P3_K3_BF	0.67	0.79	0.77
IQR	0.56-0.87	0.6-1	0.59-0.99
NO_X9_Y9_PM_K2_BF	0	0	0
IQR	0-0	0-0	0-0
NO_X9_Y9_PM_K3_BF	0.95	1	0.9
IQR	0.83-1.1	0.87-1.2	0.78-1

Table B.7: Raw values of different instances of the IGD+ indicator. Shown are the median and the IQR values below.

B.5 Distance Measurement Comparison

B.5.1 IGD^+ Values - Median Approach

Instance Name	DTW-MED	FD-MED	HD-MED
CH_X10_Y10_P1_K3_BT	1.2	1.5	1.1
IQR	0.93-2	0.82-2.2	0.76-1.8
CH_X10_Y10_P2_K3_BT	1	1.5	1
IQR	0.73-1.6	0.95-1.9	0.61-1.3
CH_X10_Y10_P3_K3_BT	1.1	1	0.68
IQR	0.8-1.5	0.73-1.2	0.55-1
CH_X10_Y10_PM_K3_BT	1.3	1.2	0.74
IQR	0.92-1.9	0.54-1.7	0.48-1.2
CH_X15_Y15_P1_K3_BT	1.5	1.5	1.2
IQR	1.1-1.9	1.2-1.9	0.8-1.8
CH_X15_Y15_P2_K3_BT	1.6	1.8	1.5
IQR	1.3-2	1.4-2.3	1.1-2
CH_X15_Y15_P3_K3_BT	1.5	1.7	1.6
IQR	1.2-1.9	1.4-2.2	1.2-2.1
CH_X15_Y15_PM_K3_BT	2.1	1.9	1.4
IQR	1.5-2.6	1.4-2.4	1.1-1.9
CH_X20_Y20_P1_K3_BT	2.1	2	2.3
IQR	1.6-2.9	1.4-2.6	1.4-3
CH_X20_Y20_P2_K3_BT	2.4	2.5	2.5
IQR	2.1-2.9	2-3.2	1.8-3.3
CH_X20_Y20_P3_K3_BT	2.8	2.1	2.3
IQR	2.1-3.2	1.6-2.5	1.8-2.8
CH_X20_Y20_PM_K3_BT	2.1	1.7	1.8
IQR	1.6-2.4	1.2-2.4	1.3-2.3
CH_X24_Y24_P1_K3_BT	2	1.8	1.9
IQR	1.3-3.1	1.4-2	1.3-2.4
CH_X24_Y24_P2_K3_BT	3.3	3	3.1
IQR	2.7-4.2	2.7-4	2.3-3.6
CH_X24_Y24_P3_K3_BT	2.5	2.2	2.2
IQR	2-2.9	1.9-2.6	1.8-2.5
CH_X24_Y24_PM_K3_BT	2.3	2.7	2.3
IQR	1.8-2.9	2.1-3.4	1.8-2.8
CH_X26_Y26_P1_K3_BT	2.5	2.3	2.4
IQR	2-2.9	1.6-3.1	1.4-2.9
CH_X26_Y26_P2_K3_BT	3	3.3	3.1
IQR	2.5-3.4	2.6-3.8	2.5-3.7
CH_X26_Y26_P3_K3_BT	3.1	2.6	2.8
IQR	2.6-3.4	2.1-3.4	2.3-3.4
CH_X26_Y26_PM_K3_BT	2.3	2.4	1.9

Instance Name	DTW-MED	FD-MED	HD-MED
IQR	1.8-2.8	1.9-2.8	1.5-2.4
CH_X28_Y28_P1_K3_BT	2.3	2.2	2.7
IQR	1.7-3	1.9-2.7	2.2-3.4
CH_X28_Y28_P2_K3_BT	3.3	3.2	2.7
IQR	2.6-3.9	2.5-3.7	2.2-3.2
CH_X28_Y28_P3_K3_BT	2.8	2.6	2.8
IQR	2.2-3.4	2.1-3.1	2.5-3.1
CH_X28_Y28_PM_K3_BT	2	1.5	1.9
IQR	1.7-2.4	1-2.6	1.6-2.3
CH_X30_Y30_P1_K3_BT	2.5	2.2	2.3
IQR	1.9-3.5	1.9-2.8	1.7-2.7
CH_X30_Y30_P2_K3_BT	3.3	3.5	3
IQR	2.9-3.8	2.7-3.9	2.5-3.4
CH_X30_Y30_P3_K3_BT	2.6	2.7	2.7
IQR	2.2-3	2.3-2.9	2.3-3.1
CH_X30_Y30_PM_K3_BT	2.3	1.8	2
IQR	1.9-2.9	1.5-2.5	1.6-2.5
LA_X10_Y10_P1_K3_BT	1.4	1.2	1.1
IQR	0.93-1.8	0.88-1.6	0.84-1.6
LA_X10_Y10_P2_K3_BT	3.9	2.8	3.3
IQR	2.4-5.2	1.9-4	2.3-4.4
LA_X10_Y10_P3_K3_BT	1.1	0.91	1
IQR	0.78-1.6	0.73-1.4	0.7-1.2
LA_X10_Y10_PM_K3_BT	2.7	2.5	1.9
IQR	2.2-3.3	2-2.9	1.3-2.7
LA_X15_Y15_P1_K3_BT	2.4	2.2	2.3
IQR	2-3.2	1.8-3	2-2.9
LA_X15_Y15_P2_K3_BT	4.5	4	3.6
IQR	3.5-5.5	3-5	2.7-4.2
LA_X15_Y15_P3_K3_BT	2.5	2.1	1.9
IQR	2-2.9	1.8-2.8	1.6-2.5
LA_X15_Y15_PM_K3_BT	3.8	3.7	2.7
IQR	3.3-5	2.9-4.7	1.9-3.6
LA_X20_Y20_P1_K3_BT	4.5	4.6	4.6
IQR	3.9-5.6	4.1-5.1	4.4-5.5
LA_X20_Y20_P2_K3_BT	4.8	4.7	4.8
IQR	4-5.7	4.2-5.5	3.7-5.4
LA_X20_Y20_P3_K3_BT	4.3	3.7	4
IQR	3.8-5.4	3.3-4.2	3.5-4.9
LA_X20_Y20_PM_K3_BT	5.1	4.9	4.6
IQR	4.4-5.8	4.3-5.5	3.6-5.2
LA_X24_Y24_P1_K3_BT	3.7	3.3	3.3
IQR	3.1-4.8	2.8-4.3	2.9-4.1
LA_X24_Y24_P2_K3_BT	4.3	4.6	3.9
IQR	3.4-4.7	3.6-5.1	3.5-4.5
LA_X24_Y24_P3_K3_BT	2.9	2.9	2.8
IQR	2.6-3.5	2.4-3.4	2.1-3.2
LA_X24_Y24_PM_K3_BT	7.2	7	6.8
IQR	6.4-7.8	6.3-7.8	5.8-7.6
LA_X26_Y26_P1_K3_BT	4.4	4.5	4
IQR	3.9-5.2	3.8-5.2	3-5.1
LA_X26_Y26_P2_K3_BT	4.6	4.7	4.2
IQR	3.7-5.9	4.3-5.3	3.7-4.9
LA_X26_Y26_P3_K3_BT	3.8	4.1	3.9
IQR	3.5-4.2	3.3-4.5	2.9-4.7
LA_X26_Y26_PM_K3_BT	4.7	5.3	5
IQR	3.8-5.9	4.8-6	4.4-5.5
LA_X28_Y28_P1_K3_BT	4.7	4.3	4.3
IQR	4.1-5	3.9-5.2	3.7-4.9
LA_X28_Y28_P2_K3_BT	7.5	7.3	7.8
IQR	6.4-9.2	6.6-8.9	6.8-8.7
LA_X28_Y28_P3_K3_BT	3.1	3	3.3
IQR	2.6-3.6	2.4-3.5	2.6-3.5
LA_X28_Y28_PM_K3_BT	6.5	6.4	6.2
IQR	5.6-7.8	5.5-6.9	5.5-7.2
LA_X30_Y30_P1_K3_BT	5	5.3	4.4
IQR	4.1-5.6	4.2-5.8	3.8-4.9
LA_X30_Y30_P2_K3_BT	5.2	4.6	4.7
IQR	4.6-5.7	4.1-5.4	4.1-5.1
LA_X30_Y30_P3_K3_BT	4.6	4.4	4.5
IQR	4.2-5.2	3.9-5.3	4-5.2
LA_X30_Y30_PM_K3_BT	8.1	8.1	7.9
IQR	7.4-9	6.9-9.3	6.7-9

C

Instance Name	DTW-MED	FD-MED	HD-MED
NO_X10_Y10_P1_K3_BT	1.1	0.83	0.93
IQR	0.74-1.4	0.61-1.6	0.55-1.8
NO_X10_Y10_P2_K3_BT	1.1	1.3	1.1
IQR	0.9-1.8	0.84-1.6	0.86-1.4
NO_X10_Y10_P3_K3_BT	0.93	0.91	0.88
IQR	0.81-1.1	0.66-1.2	0.66-1.1
NO_X10_Y10_PM_K3_BT	1.2	1.3	1
IQR	0.89-1.8	0.79-1.8	0.74-1.4
NO_X15_Y15_P1_K3_BT	1.9	1.7	1.4
IQR	1.1-2.4	1.3-2.4	1.1-2
NO_X15_Y15_P2_K3_BT	2.6	2.8	2.2
IQR	1.8-3.1	2.2-3.1	1.7-2.5
NO_X15_Y15_P3_K3_BT	1.8	2	1.6
IQR	1.3-2.2	1.5-2.3	1.1-2.1
NO_X15_Y15_PM_K3_BT	2.3	1.8	1.8
IQR	1.6-2.8	1.4-2.8	1.3-2.4
NO_X20_Y20_P1_K3_BT	3	2.8	2.7
IQR	2.4-3.8	2.1-3.3	2.2-3.4
NO_X20_Y20_P2_K3_BT	2.8	2.6	2.8
IQR	2.4-3.1	2.2-3.2	2.2-3
NO_X20_Y20_P3_K3_BT	2.6	2.5	2.6
IQR	1.9-3.5	2.1-3	2.2-3.1
NO_X20_Y20_PM_K3_BT	2.8	2.8	2.5
IQR	2.1-3.5	1.9-3.3	2-3
NO_X24_Y24_P1_K3_BT	2.4	2.2	2.4
IQR	2-2.9	1.8-2.9	1.9-3.4
NO_X24_Y24_P2_K3_BT	3.3	3.4	3
IQR	2.8-3.8	2.9-4	2.4-3.4
NO_X24_Y24_P3_K3_BT	2.3	2.3	2.3
IQR	2-2.9	1.9-2.7	1.8-2.8
NO_X24_Y24_PM_K3_BT	3.1	2.8	2.7
IQR	2.2-4.3	2.3-3.4	2.3-3.8
NO_X26_Y26_P1_K3_BT	3	3	3
IQR	2.2-4.3	2.3-3.6	2.3-3.8
NO_X26_Y26_P2_K3_BT	3.3	3.3	3.3
IQR	2.5-3.7	2.9-3.7	2.9-3.6
NO_X26_Y26_P3_K3_BT	3.3	3.4	3.4
IQR	2.6-3.6	3-3.9	3-3.9
NO_X26_Y26_PM_K3_BT	2.3	2.9	2.7
IQR	2-3.4	2.3-3.6	2.1-3
NO_X28_Y28_P1_K3_BT	3.2	3.2	2.6
IQR	2.5-3.6	2.7-3.8	2.2-3.2
NO_X28_Y28_P2_K3_BT	3.6	3.6	3.8
IQR	3.2-4.3	3.3-4.2	3.3-4.4
NO_X28_Y28_P3_K3_BT	3.2	3.2	2.8
IQR	2.7-3.6	2.6-3.6	2.3-3.3
NO_X28_Y28_PM_K3_BT	2.8	3.1	2.4
IQR	2.4-3.8	2.7-3.8	1.9-3.5
NO_X30_Y30_P1_K3_BT	2.8	2.5	2.6
IQR	2.1-3.2	2.1-2.9	2.1-3
NO_X30_Y30_P2_K3_BT	3.6	3.1	3.5
IQR	2.6-4	2.9-3.7	2.8-3.8
NO_X30_Y30_P3_K3_BT	3.2	3.1	3
IQR	2.7-3.7	2.7-3.6	2.5-3.5
NO_X30_Y30_PM_K3_BT	3.7	3.6	3.7
IQR	2.9-4.4	3.1-4.5	2.8-4.7

Table B.8: Raw values of different instances of the IGD+ indicator. Shown are the median and the IQR values below.

B.5.2 IGDX Values - Median Approach

Instance Name	DTW-MED	FD-MED	HD-MED
CH_X10_Y10_P1_K3_BT	0.55	0.34	0.64
IQR	0.48-0.65	0.24-0.45	0.52-0.81
CH_X10_Y10_P2_K3_BT	0.62	0.76	0.72
IQR	0.61-0.78	0.62-0.93	0.68-0.87
CH_X10_Y10_P3_K3_BT	0.53	0.48	0.53
IQR	0.41-0.61	0.42-0.56	0.46-0.73

Instance Name	DTW-MED	FD-MED	HD-MED
CH_X10_Y10_PM_K3_BT	0.68	1.1	0.58
IQR	0.54-1.1	0.57-1.1	0.55-0.69
CH_X15_Y15_P1_K3_BT	1.1	1.1	0.46
IQR	0.54-1.1	0.48-1.1	0.43-0.5
CH_X15_Y15_P2_K3_BT	0.7	0.74	0.73
IQR	0.47-0.7	0.68-1	0.73-0.74
CH_X15_Y15_P3_K3_BT	0.52	0.48	0.47
IQR	0.48-0.59	0.44-0.5	0.32-0.54
CH_X15_Y15_PM_K3_BT	0.72	0.58	0.57
IQR	0.55-0.74	0.49-0.79	0.51-0.8
CH_X20_Y20_P1_K3_BT	0.43	0.37	0.27
IQR	0.27-0.54	0.27-0.49	0.27-0.27
CH_X20_Y20_P2_K3_BT	0.48	0.61	0.45
IQR	0.39-0.67	0.39-1.1	0.38-0.54
CH_X20_Y20_P3_K3_BT	0.42	0.35	0.52
IQR	0.39-0.49	0.17-0.41	0.51-0.54
CH_X20_Y20_PM_K3_BT	0.26	0.26	1
IQR	0.24-0.3	0.24-0.34	0.23-1.1
CH_X24_Y24_P1_K3_BT	0.42	0.64	0.27
IQR	0.24-0.88	0.24-0.88	0.24-0.3
CH_X24_Y24_P2_K3_BT	4.5	1.3	0.36
IQR	2.1-4.5	0.44-4.1	0.31-0.55
CH_X24_Y24_P3_K3_BT	0.4	0.83	2.1
IQR	0.33-0.69	0.41-0.93	0.18-2.1
CH_X24_Y24_PM_K3_BT	1.9	0.39	0.4
IQR	0.34-1.9	0.27-0.49	0.29-0.48
CH_X26_Y26_P1_K3_BT	0.24	0.23	0.36
IQR	0.15-0.37	0.15-0.28	0.31-0.44
CH_X26_Y26_P2_K3_BT	0.36	0.32	1.9
IQR	0.33-0.39	0.3-0.4	0.29-1.9
CH_X26_Y26_P3_K3_BT	0.24	0.24	0.22
IQR	0.17-0.39	0.16-0.3	0.18-0.3
CH_X26_Y26_PM_K3_BT	0.38	0.34	0.45
IQR	0.26-0.46	0.28-0.46	0.4-0.55
CH_X28_Y28_P1_K3_BT	0.32	0.28	2.7
IQR	0.24-0.35	0.24-0.34	0.38-2.7
CH_X28_Y28_P2_K3_BT	0.48	0.4	0.39
IQR	0.33-0.62	0.31-0.51	0.32-0.5
CH_X28_Y28_P3_K3_BT	0.32	0.32	0.35
IQR	0.29-0.43	0.27-0.45	0.32-0.45
CH_X28_Y28_PM_K3_BT	0.42	0.38	0.35
IQR	0.31-0.5	0.27-0.43	0.31-0.43
CH_X30_Y30_P1_K3_BT	0.72	0.66	0.16
IQR	0.22-2.7	0.2-2.7	0.15-0.22
CH_X30_Y30_P2_K3_BT	0.26	0.31	1.8
IQR	0.18-0.4	0.18-0.37	0.26-6.3
CH_X30_Y30_P3_K3_BT	0.32	0.3	0.34
IQR	0.27-0.42	0.26-0.37	0.32-0.42
CH_X30_Y30_PM_K3_BT	0.34	0.29	0.39
IQR	0.23-0.4	0.21-0.37	0.35-0.49
LA_X10_Y10_P1_K3_BT	0.48	0.51	0.56
IQR	0.48-0.48	0.3-0.54	0.52-0.77
LA_X10_Y10_P2_K3_BT	0.64	0.49	2.1
IQR	0.37-0.64	0.36-0.77	0.49-2.1
LA_X10_Y10_P3_K3_BT	0.59	0.72	1
IQR	0.39-0.64	0.65-0.88	0.85-1
LA_X10_Y10_PM_K3_BT	0.69	0.57	0.63
IQR	0.61-0.93	0.26-0.7	0.63-0.64
LA_X15_Y15_P1_K3_BT	0.24	0.39	0.53
IQR	0.21-0.39	0.21-0.53	0.21-0.57
LA_X15_Y15_P2_K3_BT	0.99	0.94	0.58
IQR	0.77-1.2	0.87-1.1	0.58-0.89
LA_X15_Y15_P3_K3_BT	0.43	0.42	0.57
IQR	0.39-0.78	0.39-0.68	0.49-0.78
LA_X15_Y15_PM_K3_BT	2.2	0.72	0.4
IQR	0.43-2.2	0.58-0.72	0.32-0.51
LA_X20_Y20_P1_K3_BT	0.5	0.5	0.27
IQR	0.23-0.51	0.24-0.51	0.19-0.67
LA_X20_Y20_P2_K3_BT	0.6	0.5	0.39
IQR	0.43-0.72	0.31-0.8	0.37-1
LA_X20_Y20_P3_K3_BT	0.34	0.29	0.38
IQR	0.27-1	0.24-0.42	0.38-0.41
LA_X20_Y20_PM_K3_BT	0.9	1.5	0.39

Instance Name	DTW-MED	FD-MED	HD-MED
IQR	0.34-1.5	0.27-1.5	0.26-1.1
LA_X24_Y24_P1_K3_BT	0.32	0.31	0.5
IQR	0.2-0.5	0.11-0.49	0.38-0.68
LA_X24_Y24_P2_K3_BT	0.51	0.37	0.29
IQR	0.27-0.74	0.18-0.56	0.18-0.41
LA_X24_Y24_P3_K3_BT	0.42	0.42	0.23
IQR	0.23-0.57	0.21-0.44	0.21-0.44
LA_X24_Y24_PM_K3_BT	1.3	0.81	0.32
IQR	1.3-4.5	0.26-1.3	0.28-0.46
LA_X26_Y26_P1_K3_BT	0.35	0.3	0.35
IQR	0.28-2.3	0.25-0.37	0.31-0.41
LA_X26_Y26_P2_K3_BT	4.7	4.7	0.55
IQR	0.41-4.7	2.1-4.7	0.27-1.3
LA_X26_Y26_P3_K3_BT	0.24	0.26	0.71
IQR	0.21-0.43	0.23-0.47	0.24-1.1
LA_X26_Y26_PM_K3_BT	0.54	0.49	0.51
IQR	0.32-1.1	0.19-1.1	0.38-2.1
LA_X28_Y28_P1_K3_BT	0.16	0.13	0.45
IQR	0.1-0.46	0.09-0.2	0.36-0.76
LA_X28_Y28_P2_K3_BT	0.48	0.47	0.47
IQR	0.39-0.92	0.41-0.56	0.4-0.52
LA_X28_Y28_P3_K3_BT	0.31	0.3	0.35
IQR	0.28-0.52	0.26-0.48	0.18-4.1
LA_X28_Y28_PM_K3_BT	0.55	0.43	2.7
IQR	0.37-0.69	0.2-0.68	0.61-2.7
LA_X30_Y30_P1_K3_BT	3.2	3.2	0.34
IQR	1.6-4.2	1.6-4	0.22-0.52
LA_X30_Y30_P2_K3_BT	0.18	0.21	0.33
IQR	0.17-0.4	0.15-0.44	0.28-3
LA_X30_Y30_P3_K3_BT	1.8	1.8	3.6
IQR	0.18-5.2	0.17-5.2	3.6-4.9
LA_X30_Y30_PM_K3_BT	0.5	0.47	0.51
IQR	0.4-0.68	0.38-0.64	0.35-0.58
NO_X10_Y10_P1_K3_BT	0.3	0.81	0.27
IQR	0.24-0.81	0.66-0.81	0.25-0.31
NO_X10_Y10_P2_K3_BT	0.64	0.64	0.46
IQR	0.49-1.2	0.46-0.64	0.34-0.46
NO_X10_Y10_P3_K3_BT	0.31	0.8	0.81
IQR	0.24-0.65	0.68-0.8	0.43-0.81
NO_X10_Y10_PM_K3_BT	1.4	0.4	1
IQR	1.4-1.4	0.34-0.58	1-1.4
NO_X15_Y15_P1_K3_BT	0.21	0.22	1.3
IQR	0.2-0.41	0.2-0.41	0.24-1.3
NO_X15_Y15_P2_K3_BT	0.51	0.5	1.5
IQR	0.5-0.52	0.38-0.51	1.5-1.6
NO_X15_Y15_P3_K3_BT	0.44	0.7	0.69
IQR	0.35-0.73	0.33-0.7	0.37-0.69
NO_X15_Y15_PM_K3_BT	1.3	1.3	0.23
IQR	0.27-1.3	0.29-1.3	0.22-0.27
NO_X20_Y20_P1_K3_BT	0.26	0.21	0.57
IQR	0.19-0.34	0.19-0.25	0.32-0.58
NO_X20_Y20_P2_K3_BT	0.33	0.29	0.31
IQR	0.22-0.42	0.2-0.45	0.24-0.39
NO_X20_Y20_P3_K3_BT	0.87	0.88	1.1
IQR	0.31-1.1	0.27-1.2	1-1.3
NO_X20_Y20_PM_K3_BT	0.38	0.31	2.1
IQR	0.24-0.67	0.22-0.37	0.77-3
NO_X24_Y24_P1_K3_BT	0.32	0.27	0.39
IQR	0.25-0.35	0.15-0.35	0.33-0.47
NO_X24_Y24_P2_K3_BT	0.33	1.8	0.36
IQR	0.18-4.1	1.6-4.1	0.18-0.85
NO_X24_Y24_P3_K3_BT	0.19	0.18	0.19
IQR	0.15-0.21	0.16-0.21	0.18-0.22
NO_X24_Y24_PM_K3_BT	0.3	0.28	0.37
IQR	0.18-0.34	0.15-0.38	0.33-0.42
NO_X26_Y26_P1_K3_BT	0.18	0.18	0.39
IQR	0.16-0.27	0.16-0.2	0.13-1.3
NO_X26_Y26_P2_K3_BT	0.31	0.24	0.33
IQR	0.21-0.46	0.17-0.44	0.22-0.44
NO_X26_Y26_P3_K3_BT	0.38	0.27	0.15
IQR	0.25-1.1	0.22-0.95	0.11-0.18
NO_X26_Y26_PM_K3_BT	0.35	0.4	0.7
IQR	0.23-0.49	0.3-0.51	0.38-1.9

Instance Name	DTW-MED	FD-MED	HD-MED
NO_X28_Y28_P1_K3_BT	0.86	0.86	2.3
IQR	0.86-2.3	0.86-2.3	0.18-5.3
NO_X28_Y28_P2_K3_BT	2.2	2.2	0.74
IQR	0.22-2.2	0.24-2.2	0.43-1.9
NO_X28_Y28_P3_K3_BT	0.31	0.29	1.3
IQR	0.25-0.42	0.23-0.34	0.29-2.7
NO_X28_Y28_PM_K3_BT	0.17	0.18	0.16
IQR	0.15-0.31	0.15-0.33	0.16-0.2
NO_X30_Y30_P1_K3_BT	0.22	0.22	2.6
IQR	0.2-0.4	0.12-0.26	0.92-5.9
NO_X30_Y30_P2_K3_BT	0.32	0.36	0.21
IQR	0.26-3	0.26-3	0.14-0.32
NO_X30_Y30_P3_K3_BT	0.2	0.19	0.4
IQR	0.18-0.26	0.17-0.21	0.22-0.43
NO_X30_Y30_PM_K3_BT	3.6	3.6	3.6
IQR	3.6-4.9	1.1-4.9	0.63-3.6

Table B.9: Raw values of different instances of the IGDX indicator. Shown are the median and the IQR values below.

B.5.3 IGD^+ Values - Minimum Approach

Instance Name	DTW-MIN	FD-MIN	HD-MIN
CH_X10_Y10_P1_K3_BT	3	1.8	1.4
IQR	2-4	0.81-2.7	0.66-2.9
CH_X10_Y10_P2_K3_BT	0.99	1.5	0.97
IQR	0.64-1.5	0.83-2	0.74-1.9
CH_X10_Y10_P3_K3_BT	1.3	1.4	0.97
IQR	0.94-2.4	0.89-1.8	0.68-1.4
CH_X10_Y10_PM_K3_BT	1.8	1	1.1
IQR	1.2-2.9	0.63-1.7	0.66-1.7
CH_X15_Y15_P1_K3_BT	3.3	2.4	1.9
IQR	2.4-3.7	1.8-3.2	1.3-2.8
CH_X15_Y15_P2_K3_BT	2.5	1.9	2
IQR	1.8-3.1	1.6-2.6	1.5-2.7
CH_X15_Y15_P3_K3_BT	2.3	1.8	1.6
IQR	1.6-2.9	1.4-2.2	1.1-1.8
CH_X15_Y15_PM_K3_BT	2.3	1.9	1.9
IQR	1.7-3.2	1.5-2.8	1.2-2.9
CH_X20_Y20_P1_K3_BT	3.6	3.7	3
IQR	2-4.9	2.9-4	2.1-4
CH_X20_Y20_P2_K3_BT	2.7	2.4	2.7
IQR	1.9-3.4	1.6-3.4	2.1-3.5
CH_X20_Y20_P3_K3_BT	3	3	2.5
IQR	2.5-4.2	1.9-3.5	1.9-3.2
CH_X20_Y20_PM_K3_BT	1.8	1.8	2.1
IQR	0.89-2.7	1.2-2.4	1.5-2.8
CH_X24_Y24_P1_K3_BT	2.9	3.2	2.9
IQR	2-3.9	2.7-4	1.6-3.6
CH_X24_Y24_P2_K3_BT	4	3.6	3.2
IQR	3-4.7	2.6-4.6	2.3-4.8
CH_X24_Y24_P3_K3_BT	2.3	2.7	2
IQR	1.8-3.4	1.7-3.4	1.5-2.6
CH_X24_Y24_PM_K3_BT	3	3.2	2.1
IQR	2-4.2	2-4	1.5-2.8
CH_X26_Y26_P1_K3_BT	4	3.4	3.3
IQR	2.5-5	2-4.9	2.3-4.3
CH_X26_Y26_P2_K3_BT	3.8	4	3.5
IQR	2.8-4.7	3-4.8	3-4
CH_X26_Y26_P3_K3_BT	3.5	3.1	3.1
IQR	2.8-4.1	1.9-4.1	2.6-3.8
CH_X26_Y26_PM_K3_BT	2.3	1.9	2.8
IQR	1.8-3	1.6-2.9	1.8-3.2
CH_X28_Y28_P1_K3_BT	4	4.4	3.2
IQR	3.1-4.6	3.1-5.4	2.6-3.7
CH_X28_Y28_P2_K3_BT	3.6	3.2	3.6
IQR	3-4.3	2.6-4.2	2.6-4.1
CH_X28_Y28_P3_K3_BT	2.8	3.2	3.1
IQR	2.4-3.7	2.3-4.2	2.4-3.6

Instance Name	DTW-MIN	FD-MIN	HD-MIN
CH_X28_Y28_PM_K3_BT	2.2	2.1	1.9
IQR	1.4-3	1.4-2.7	1.2-2.4
CH_X30_Y30_P1_K3_BT	3.6	3.4	2.4
IQR	2.5-4.6	2.1-4.3	1.6-3.6
CH_X30_Y30_P2_K3_BT	4	3.6	3.2
IQR	3.5-4.6	2.9-5	2.4-4
CH_X30_Y30_P3_K3_BT	3.2	3.2	2.5
IQR	2.9-4.2	2.3-3.8	2-3.1
CH_X30_Y30_PM_K3_BT	2.3	2.2	2
IQR	1.7-3	1.6-3.1	1.2-2.6
LA_X10_Y10_P1_K3_BT	2.7	1.6	1.4
IQR	1.4-3.5	1-3.1	0.9-1.9
LA_X10_Y10_P2_K3_BT	4	3.3	3.1
IQR	2.6-5.2	2.7-4.7	2.1-4.5
LA_X10_Y10_P3_K3_BT	1.3	1.2	0.78
IQR	0.84-1.7	0.93-1.6	0.63-1.3
LA_X10_Y10_PM_K3_BT	3.5	2.9	2
IQR	2.5-4.7	1.8-4.1	1.3-2.8
LA_X15_Y15_P1_K3_BT	3.9	3.7	2.6
IQR	3.2-4.8	2.1-4.7	2-4
LA_X15_Y15_P2_K3_BT	4.8	4.7	4.6
IQR	3.9-6.8	4.1-6.8	4-5.9
LA_X15_Y15_P3_K3_BT	2.4	2.3	2.9
IQR	2-3	1.9-3	1.8-3.4
LA_X15_Y15_PM_K3_BT	5.2	4.1	4.5
IQR	4.2-6.3	3.4-5.1	3.6-5.4
LA_X20_Y20_P1_K3_BT	6.6	5.8	6.4
IQR	5.3-8	4.7-7.7	5-7.1
LA_X20_Y20_P2_K3_BT	5.6	5.4	4.8
IQR	4.8-6.1	4.1-6.3	3.7-5.6
LA_X20_Y20_P3_K3_BT	5.3	4.7	4.4
IQR	4.5-6.6	3.8-5.9	3.2-5.4
LA_X20_Y20_PM_K3_BT	6.1	5.8	5.2
IQR	4.9-7.3	4.6-6.8	4.5-6.2
LA_X24_Y24_P1_K3_BT	5.8	5.4	4.6
IQR	4.7-6.7	4.3-6.3	3.6-5.4
LA_X24_Y24_P2_K3_BT	4.7	4.5	4.2
IQR	3.7-5.9	3.6-5.8	3.6-5.1
LA_X24_Y24_P3_K3_BT	3.6	3.3	3.1
IQR	2.7-4.3	2.8-3.5	2.6-4
LA_X24_Y24_PM_K3_BT	9.3	8.4	7.7
IQR	7.9-10	7.3-9.5	6.4-9.3
LA_X26_Y26_P1_K3_BT	6.8	6	5.6
IQR	5.8-8.3	5.2-7.3	4.1-6.7
LA_X26_Y26_P2_K3_BT	5.8	5.5	4.8
IQR	4.7-6.7	4.7-6.5	4.1-5.2
LA_X26_Y26_P3_K3_BT	4.5	4.6	4.5
IQR	3.5-5.7	3.2-5.3	3.7-5.4
LA_X26_Y26_PM_K3_BT	5.5	5.8	5.2
IQR	4.5-6.8	5-6.5	4.7-6.5
LA_X28_Y28_P1_K3_BT	5.9	5.8	5.4
IQR	5-7.7	4.1-7.7	4.2-6.5
LA_X28_Y28_P2_K3_BT	9	8	8.5
IQR	7.4-10	7.4-9.6	7.3-9.2
LA_X28_Y28_P3_K3_BT	3.6	3.5	3.5
IQR	3.1-4.5	2.8-4.2	2.6-4.2
LA_X28_Y28_PM_K3_BT	7.9	7.4	7.2
IQR	6.2-8.8	6.6-8.9	6.1-8.1
LA_X30_Y30_P1_K3_BT	6.5	6.8	5
IQR	5.5-7.8	5.7-8.6	4.1-6.8
LA_X30_Y30_P2_K3_BT	6.1	5.3	5
IQR	4.5-6.7	4.6-5.9	4.3-6.1
LA_X30_Y30_P3_K3_BT	4.8	5.6	4.6
IQR	4.2-6.8	4.4-6.2	4.2-5.6
LA_X30_Y30_PM_K3_BT	10	9.4	7.6
IQR	8-11	7.6-11	6.9-8.9
NO_X10_Y10_P1_K3_BT	2.3	1.3	1.1
IQR	1.1-3	0.81-2.1	0.8-2.1
NO_X10_Y10_P2_K3_BT	1.8	1.2	1.2
IQR	1.1-2.6	0.96-2.1	0.84-2.4
NO_X10_Y10_P3_K3_BT	1.3	1.5	0.94
IQR	0.95-1.9	0.87-1.9	0.81-1.3
NO_X10_Y10_PM_K3_BT	1.4	1.2	1.3

Instance Name	DTW-MIN	FD-MIN	HD-MIN
IQR	1.2-1.9	0.84-2.3	0.8-2.4
NO_X15_Y15_P1_K3_BT	4	3.1	2.2
IQR	2.6-4.3	2-3.9	1.7-3.4
NO_X15_Y15_P2_K3_BT	2.5	3.1	2.7
IQR	2-3.7	2.4-4.6	2.1-3.1
NO_X15_Y15_P3_K3_BT	2	1.8	1.7
IQR	1.4-2.6	1.4-2.4	1.4-2.3
NO_X15_Y15_PM_K3_BT	2.2	2.1	1.8
IQR	1.6-2.9	1.5-3.1	1.4-2.7
NO_X20_Y20_P1_K3_BT	5.3	4.7	3.4
IQR	4-6	3.1-6	2.7-4.3
NO_X20_Y20_P2_K3_BT	3.1	2.7	2.7
IQR	2.5-3.6	2-3.5	2.1-3.5
NO_X20_Y20_P3_K3_BT	3	3	2.5
IQR	2.1-4	2.1-3.9	1.8-3.2
NO_X20_Y20_PM_K3_BT	3.1	3	2.9
IQR	2.2-3.6	2.2-3.2	2.2-3.6
NO_X24_Y24_P1_K3_BT	4.4	3.3	3.6
IQR	3.7-5.2	2.5-4.9	2.3-5
NO_X24_Y24_P2_K3_BT	3.6	3.6	3.1
IQR	2.7-4.3	2.8-4.6	2.5-3.9
NO_X24_Y24_P3_K3_BT	2.8	2.4	2.8
IQR	2-3.6	1.9-3.1	2-3.7
NO_X24_Y24_PM_K3_BT	3.4	2.7	2.7
IQR	2.1-4.2	1.9-4.1	2.1-3.8
NO_X26_Y26_P1_K3_BT	5.3	5.1	4
IQR	4.6-6.8	3.9-5.7	2.8-5.2
NO_X26_Y26_P2_K3_BT	3.8	3.5	3
IQR	2.8-4.8	2.9-4.3	2.4-3.4
NO_X26_Y26_P3_K3_BT	3.9	3.8	3.3
IQR	3.2-4.6	2.9-4.4	2.7-4.2
NO_X26_Y26_PM_K3_BT	3	3.3	2.8
IQR	2.5-3.8	2.4-3.7	2.2-3.4
NO_X28_Y28_P1_K3_BT	4.7	4.5	3.4
IQR	4.2-5.7	3.9-5.5	2.8-5.1
NO_X28_Y28_P2_K3_BT	4.3	3.7	3.9
IQR	3.3-5.1	3-4.7	3.3-4.5
NO_X28_Y28_P3_K3_BT	3.2	3.7	3.4
IQR	2.5-4.1	2.8-4.5	2.6-4
NO_X28_Y28_PM_K3_BT	3	3.2	3.2
IQR	2.6-3.9	2.3-4	2.5-4.2
NO_X30_Y30_P1_K3_BT	4.4	3.6	3.2
IQR	3.5-5	2.7-4.9	2.3-4.4
NO_X30_Y30_P2_K3_BT	3.5	3.5	3.2
IQR	2.9-4.6	3-4.2	2.8-4
NO_X30_Y30_P3_K3_BT	3.3	3.4	3.1
IQR	2.9-4	3.1-4.2	2.6-3.7
NO_X30_Y30_PM_K3_BT	3.6	3.4	3.4
IQR	2.9-4.4	2.3-4.4	2.7-4.4

Table B.10: Raw values of different instances of the IGD+ indicator. Shown are the median and the IQR values below.

B.5.4 IGDX Values - Minimum Approach

Instance Name	DTW-MIN	FD-MIN	HD-MIN
CH_X10_Y10_P1_K3_BT	0.76	0.59	0.54
IQR	0.76-0.76	0.5-0.65	0.49-0.64
CH_X10_Y10_P2_K3_BT	0.63	0.78	0.62
IQR	0.62-0.82	0.53-1.1	0.62-0.63
CH_X10_Y10_P3_K3_BT	0.54	0.53	0.54
IQR	0.44-0.74	0.5-0.69	0.41-0.76
CH_X10_Y10_PM_K3_BT	0.8	0.7	0.69
IQR	0.66-0.8	0.58-0.97	0.61-0.81
CH_X15_Y15_P1_K3_BT	0.66	0.72	1.1
IQR	0.65-1.5	0.58-0.73	0.57-1.6
CH_X15_Y15_P2_K3_BT	1.1	0.79	0.7
IQR	0.52-1.1	0.69-0.92	0.7-0.79
CH_X15_Y15_P3_K3_BT	0.63	0.44	0.55

Instance Name	DTW-MIN	FD-MIN	HD-MIN
IQR	0.6-0.81	0.44-0.56	0.5-0.62
CH_X15_Y15_PM_K3_BT	0.47	0.42	0.72
IQR	0.41-0.52	0.42-0.54	0.58-0.73
CH_X20_Y20_P1_K3_BT	0.27	0.27	0.54
IQR	0.26-0.59	0.26-0.51	0.33-3.2
CH_X20_Y20_P2_K3_BT	0.29	0.48	0.6
IQR	0.2-0.42	0.4-0.54	0.44-1.4
CH_X20_Y20_P3_K3_BT	0.48	0.66	0.43
IQR	0.15-3.2	0.45-3.2	0.41-0.49
CH_X20_Y20_PM_K3_BT	0.3	0.51	0.45
IQR	0.27-0.45	0.42-0.75	0.27-0.55
CH_X24_Y24_P1_K3_BT	0.51	0.63	0.47
IQR	0.48-0.53	0.4-0.72	0.27-0.88
CH_X24_Y24_P2_K3_BT	0.44	0.3	4.5
IQR	0.32-0.67	0.24-0.48	4.5-4.5
CH_X24_Y24_P3_K3_BT	0.34	0.21	0.56
IQR	0.31-0.45	0.16-0.4	0.37-0.93
CH_X24_Y24_PM_K3_BT	1.9	0.43	0.57
IQR	0.23-1.9	0.31-0.46	0.38-1.9
CH_X26_Y26_P1_K3_BT	0.35	0.28	0.27
IQR	0.27-0.69	0.25-0.33	0.21-0.39
CH_X26_Y26_P2_K3_BT	0.42	0.42	0.43
IQR	0.36-0.51	0.35-0.47	0.36-0.51
CH_X26_Y26_P3_K3_BT	0.39	0.42	0.25
IQR	0.34-0.46	0.31-0.48	0.18-0.41
CH_X26_Y26_PM_K3_BT	0.45	0.49	0.5
IQR	0.39-0.55	0.42-0.53	0.41-0.58
CH_X28_Y28_P1_K3_BT	0.88	0.29	0.3
IQR	0.34-3.8	0.24-3.8	0.26-0.42
CH_X28_Y28_P2_K3_BT	0.37	0.5	0.5
IQR	0.28-0.53	0.46-0.55	0.29-0.55
CH_X28_Y28_P3_K3_BT	0.6	0.46	0.41
IQR	0.33-4.1	0.33-0.72	0.33-0.57
CH_X28_Y28_PM_K3_BT	0.22	1.5	0.41
IQR	0.18-0.3	0.43-8	0.33-0.52
CH_X30_Y30_P1_K3_BT	0.31	0.99	0.73
IQR	0.21-0.66	0.83-3	0.72-2.7
CH_X30_Y30_P2_K3_BT	0.41	0.34	0.34
IQR	0.34-0.63	0.27-0.59	0.25-4.5
CH_X30_Y30_P3_K3_BT	0.42	0.37	0.34
IQR	0.33-0.56	0.31-0.44	0.32-0.42
CH_X30_Y30_PM_K3_BT	0.37	0.33	0.32
IQR	0.29-0.42	0.29-0.46	0.19-0.41
LA_X10_Y10_P1_K3_BT	0.85	0.59	0.48
IQR	0.58-1.1	0.5-0.74	0.48-1.1
LA_X10_Y10_P2_K3_BT	0.44	0.97	0.49
IQR	0.44-0.49	0.97-0.97	0.42-2
LA_X10_Y10_P3_K3_BT	0.87	0.53	1.4
IQR	0.73-0.94	0.53-0.53	1.4-1.4
LA_X10_Y10_PM_K3_BT	0.45	0.74	0.65
IQR	0.33-1.5	0.51-1.5	0.63-0.7
LA_X15_Y15_P1_K3_BT	0.24	0.27	0.39
IQR	0.21-0.33	0.22-0.57	0.25-0.52
LA_X15_Y15_P2_K3_BT	0.48	0.89	0.87
IQR	0.38-0.71	0.68-1.1	0.39-1
LA_X15_Y15_P3_K3_BT	0.43	0.51	0.77
IQR	0.41-0.77	0.43-0.77	0.44-0.79
LA_X15_Y15_PM_K3_BT	0.48	0.32	2.2
IQR	0.48-0.8	0.32-0.33	0.52-2.2
LA_X20_Y20_P1_K3_BT	0.51	0.5	0.51
IQR	0.51-0.52	0.24-0.51	0.26-0.52
LA_X20_Y20_P2_K3_BT	0.42	0.44	0.35
IQR	0.37-1	0.37-1	0.26-0.45
LA_X20_Y20_P3_K3_BT	1.3	0.5	0.95
IQR	0.65-2.9	0.41-1.5	0.26-1.1
LA_X20_Y20_PM_K3_BT	0.2	0.47	1.5
IQR	0.18-0.43	0.42-1.3	0.8-1.5
LA_X24_Y24_P1_K3_BT	0.37	0.5	0.56
IQR	0.32-1.8	0.29-3.5	0.33-0.59
LA_X24_Y24_P2_K3_BT	0.43	0.46	0.37
IQR	0.26-0.48	0.24-0.89	0.24-0.53
LA_X24_Y24_P3_K3_BT	0.42	0.42	0.42
IQR	0.42-0.88	0.42-0.49	0.29-0.45

Instance Name	DTW-MIN	FD-MIN	HD-MIN
LA_X24_Y24_PM_K3_BT	1.6	0.5	1.3
IQR	0.45-1.6	0.4-1.6	1-4.5
LA_X26_Y26_P1_K3_BT	2.3	2.3	2.3
IQR	0.4-2.3	0.38-2.3	0.37-2.3
LA_X26_Y26_P2_K3_BT	0.44	0.44	4.7
IQR	0.35-0.62	0.34-0.62	0.42-4.7
LA_X26_Y26_P3_K3_BT	0.29	0.25	0.25
IQR	0.25-0.45	0.18-0.43	0.23-0.43
LA_X26_Y26_PM_K3_BT	0.32	0.46	1.1
IQR	0.26-0.39	0.4-0.5	0.74-2.1
LA_X28_Y28_P1_K3_BT	0.87	0.14	0.38
IQR	0.21-0.9	0.12-0.19	0.14-0.47
LA_X28_Y28_P2_K3_BT	3.2	3.2	0.59
IQR	0.47-3.2	1-3.2	0.47-3.2
LA_X28_Y28_P3_K3_BT	0.55	0.37	0.36
IQR	0.31-0.64	0.3-0.56	0.28-0.58
LA_X28_Y28_PM_K3_BT	0.71	1.3	0.45
IQR	0.29-1.3	0.68-2.7	0.36-0.62
LA_X30_Y30_P1_K3_BT	0.89	2.2	3.2
IQR	0.27-2.2	0.32-2.2	1.6-4.2
LA_X30_Y30_P2_K3_BT	0.78	0.53	0.35
IQR	0.57-1	0.37-0.78	0.28-0.47
LA_X30_Y30_P3_K3_BT	1.8	1.8	1.1
IQR	1.8-5.9	1.8-6.2	0.32-1.8
LA_X30_Y30_PM_K3_BT	0.55	0.73	0.56
IQR	0.35-0.69	0.27-1	0.44-0.85
NO_X10_Y10_P1_K3_BT	0.68	0.35	0.81
IQR	0.32-0.68	0.3-0.93	0.81-0.81
NO_X10_Y10_P2_K3_BT	0.34	0.34	0.5
IQR	0.31-0.41	0.3-0.39	0.37-0.5
NO_X10_Y10_P3_K3_BT	0.3	0.38	0.3
IQR	0.24-0.33	0.32-0.89	0.24-0.35
NO_X10_Y10_PM_K3_BT	0.43	0.45	0.42
IQR	0.41-0.5	0.4-0.6	0.39-0.52
NO_X15_Y15_P1_K3_BT	0.41	0.27	0.26
IQR	0.24-0.41	0.22-0.41	0.21-0.41
NO_X15_Y15_P2_K3_BT	2.2	0.39	0.51
IQR	0.45-2.2	0.32-0.5	0.43-0.51
NO_X15_Y15_P3_K3_BT	0.76	1.1	0.41
IQR	0.39-0.76	0.41-1.1	0.37-0.44
NO_X15_Y15_PM_K3_BT	1.3	0.31	1.3
IQR	0.25-1.3	0.24-1.3	0.24-1.3
NO_X20_Y20_P1_K3_BT	4.5	0.2	0.25
IQR	1.5-4.5	0.18-0.24	0.21-0.36
NO_X20_Y20_P2_K3_BT	0.28	0.44	0.36
IQR	0.24-0.31	0.31-0.67	0.3-0.44
NO_X20_Y20_P3_K3_BT	0.47	0.27	0.41
IQR	0.28-0.86	0.24-0.33	0.3-0.79
NO_X20_Y20_PM_K3_BT	0.46	0.35	1.3
IQR	0.4-0.57	0.18-0.41	0.45-2.9
NO_X24_Y24_P1_K3_BT	0.43	1.8	0.37
IQR	0.38-0.55	0.49-4.1	0.32-0.44
NO_X24_Y24_P2_K3_BT	0.17	0.33	1.8
IQR	0.11-0.21	0.27-0.5	1.6-4.1
NO_X24_Y24_P3_K3_BT	0.38	0.47	0.21
IQR	0.29-0.48	0.21-2.1	0.18-0.89
NO_X24_Y24_PM_K3_BT	0.19	6.3	0.34
IQR	0.17-0.26	0.83-6.3	0.18-0.39
NO_X26_Y26_P1_K3_BT	2.4	0.35	0.27
IQR	0.15-2.4	0.13-1.1	0.21-0.52
NO_X26_Y26_P2_K3_BT	0.26	0.26	0.23
IQR	0.21-0.31	0.19-0.37	0.18-0.49
NO_X26_Y26_P3_K3_BT	0.18	0.17	0.23
IQR	0.17-0.21	0.15-0.19	0.19-0.52
NO_X26_Y26_PM_K3_BT	0.25	0.3	0.4
IQR	0.22-0.36	0.25-0.41	0.27-0.53
NO_X28_Y28_P1_K3_BT	0.12	0.18	0.89
IQR	0.11-0.35	0.11-0.26	0.87-0.91
NO_X28_Y28_P2_K3_BT	0.44	0.37	2.2
IQR	0.37-0.55	0.31-0.47	0.26-2.2
NO_X28_Y28_P3_K3_BT	0.22	0.23	0.31
IQR	0.2-0.51	0.18-0.25	0.28-2.9
NO_X28_Y28_PM_K3_BT	0.16	0.18	0.2

Instance Name	DTW-MIN	FD-MIN	HD-MIN
IQR	0.15-0.34	0.16-0.27	0.16-0.27
NO_X30_Y30_P1_K3_BT	0.62	0.37	0.33
IQR	0.28-1	0.11-0.57	0.25-0.57
NO_X30_Y30_P2_K3_BT	0.77	0.37	3
IQR	0.52-3.2	0.29-0.55	0.24-3
NO_X30_Y30_P3_K3_BT	2.7	1.1	0.22
IQR	1.1-2.7	1.1-1.2	0.2-0.6
NO_X30_Y30_PM_K3_BT	0.38	0.21	3.6
IQR	0.22-1.8	0.18-1.5	3.6-4.9

Table B.11: Raw values of different instances of the IGDX indicator. Shown are the median and the IQR values below.

Ehrenerklärung

Ich versichere hiermit, dass ich die vorliegende Arbeit ohne unzulässige Hilfe Dritter und ohne Benutzung anderer als der angegebenen Hilfsmittel angefertigt habe; verwendete fremde und eigene Quellen sind als solche kenntlich gemacht. Insbesondere habe ich nicht die Hilfe eines kommerziellen Promotionsberaters in Anspruch genommen. Dritte haben von mir weder unmittelbar noch mittelbar geldwerte Leistungen für Arbeiten erhalten, die im Zusammenhang mit dem Inhalt der vorgelegten Dissertation stehen.

Ich habe insbesondere nicht wissentlich:

- Ergebnisse erfunden oder widersprüchliche Ergebnisse verschwiegen,
- statistische Verfahren absichtlich missbraucht, um Daten in ungerechtfertigter Weise zu interpretieren,
- fremde Ergebnisse oder Veröffentlichungen plagiiert,
- fremde Forschungsergebnisse verzerrt wiedergegeben.

Mir ist bekannt, dass Verstöße gegen das Urheberrecht Unterlassungs- und Schadensersatzansprüche des Urhebers sowie eine strafrechtliche Ahndung durch die Strafverfolgungsbehörden begründen kann. Die Arbeit wurde bisher weder im Inland noch im Ausland in gleicher oder ähnlicher Form als Dissertation eingereicht und ist als Ganzes auch noch nicht veröffentlicht.

Magdeburg, den 14.10.2022

Jens Weise